



The
University
Of
Sheffield.

A Chemical Approach to Synthetic Quorum Sensing

By:

Jacob A. Lane

A thesis submitted in partial fulfilment of the requirements for the degree of
Doctor of Philosophy

The University of Sheffield
Faculty of Engineering
Department of Chemical and Biological Engineering

August 2019

Abstract

Quorum sensing is a biological phenomenon in which both stimuli and response are directly linked to population density. This process of collective behaviour is used by bacteria to regulate gene expression within bacterial colonies. This is achieved by the production and release and detection of signalling molecules known as autoinducers. Until very recently synthetic quorum sensing has been achieved by either; the 'splicing' of the quorum sensing machinery from one bacterial host to another; or chemically through derivatives of the oscillating Belousov-Zhabotinsky reaction. More recently there has been a shift to developing collective behaviour through the immobilisation of enzymes within polymer hydrogels.

This thesis is focused upon the development of a truly synthetic quorum sensing system. This is achieved by replicating the component technologies of biological quorum sensing with synthetic equivalents. A truly synthetic quorum sensing system requires; (i) the autonomous aggregation of particles; (ii) the generation of a signal by the particles; (iii) the detection of the signal; (iv) a response by the particles which only occurs when the population of the aggregate is above a threshold level.

In order to observe signal detection and response ratiometric imaging microscopy is retooled and used for the first time to observe continuous diffusion of a signal from its host. To meet the requirement of signal generation the enzyme glucose oxidase is used. This enzyme converts glucose to gluconic acid which results in the lowering of pH. To ascertain its suitability the action of glucose oxidase in solution was probed. Hydrogel particles of alginate were loaded with glucose oxidase and magnetite. The magnetite enables spontaneous aggregation to occur when the particles are placed within a magnetic field. The resulting signal generation and response of particle clusters of differing populations was observed with a ratiometric imaging setup. This results in the demonstration of a robust synthetic quorum sensing system.

Acknowledgements

Firstly I would like to thank my supervisor Dr Jonathan Howse, for his support and encouragement throughout my PhD. I would like to thank all the Howse group, with a special mention to Dr Daniel Toolan, for his support, development of the ratiometric set-up, upon which much of this body of work relies. I am truly in his dept.

I would like to give a special mention to Jade Rogers for her continued support throughout my PhD. Especially for putting up with my highs, lows, hanger and sleepless nights I have put her though during the write up process.

My thanks to Dr Richard Archer, Dr Daniel Wesley, Dr Sam Darby, Dr Lauren Platts, Dr Jordan Bye and Kimberley Anderson for taking me under their wings and creating a friendly working environment.

I am forever grateful to my family, especially my parents Hugh and Kay Lane for their continued support. I would also like to thank Andrew Sadler for introducing me to many different whiskies without which a paper could not have been read nor LabView VI's fixed. Finally, I would like to thank Steve Franklin and Jamie Rutherford for intervening when work would get the better of me and accompanying me on many runs.

This work was funded by the EPSRC

Innovations and Contributions

- Synthesis of quorum sensing bacteria inspired magnetite and glucose oxidase loaded alginate hydrogels, which exhibit autonomous aggregation and generate a shift in local pH.
- Setting up and calibration of an intricate ratiometric imaging microscopy unit, retooled for probing collective behaviour of hydrogels.
- Characterisation of signal molecule generation and diffusion, demonstrating an autocatalytic response, determination of diffusion parameters and demonstration of diffusive fickian behaviour.
- Demonstration of a dynamic quorum sensing response in clusters of glucose oxidase loaded alginate particles.

Abbreviations and nomenclature

A	Lewis base
AH	Lewis acid
AHL	acyl-homoserine lactone
AI	autoinducing signal molecule
AIP	autoinducing peptide
AMP	2-amino-2-methylpropan-1-ol
APMA	<i>N</i> -(3-aminopropyl) methacrylamide
APS	ammonium persulfate
<i>B</i>	Buffer strength
BA	<i>N, N'</i> -methylenebisacrylamide
BNC	Bayonet Neill-Concelman
BSA	bovine serum albumin
BZ	Belousov-Zhabotinsky
C_i	corrected image
CMT	critical micelle temperature ($^{\circ}\text{C}$)
CSTR	continuous flow stirred tank reactor
D	Diffusion coefficient ($\text{mm}^2 \text{s}^{-1}$)
DD	degree of deacylation (%)
DEAP	3 diethylaminopropyl
D_i	darkfield image
DOX	doxorubicin
DTT	dithiothreitol
DVB	divinyl benzene
ED	external diameter (mm)
EDTA	ethylenediaminetetraacetic acid
F_i	flat field image
G	α -L-gulonate
GCS	glycol chitosan
GDL	glucono- δ -lactone
G_i	gain image
GOx	glucose oxidase
GST	glutaraldehyde saturated toluene

Ia/Ib	emission intensity ratio of acidic and basic species of carboxy-SNARF-4F (excitation 640 nm)
ID	internal diameter (mm)
IEP	isoelectric point
IS	interstitial site
M	β -D-mannuronate
m	image averaged value
MAA	methacrylic acid
Mw	Molecular weight (kDa)
N	Number of particles
NADP ⁺	nicotinamide adenosine dinucleotide phosphate
NIPAAM	<i>N</i> -isopropylacrylamide
O/W	oil in water
PAA	poly(acrylic acid)
PCOC	palladium catalysed oscillatory carbonylation
PDMA	poly[(2-dimethylaminoethyl) methacrylate]
PDMAEMA	poly(dimethylaminoethyl methacrylate)
PEC	polyelectrolyte complex
PEGA	monoalkyne-terminated poly(ethylene glycol)
PISA	polymerisation-induced self-assembly
PMAA	poly(methacrylic acid)
QS	quorum sensing
R	ratio of emission intensities
r	radius (m)
RAFT	reversible addition-fragmentation chain transfer
R _h	hydrodynamic radius (nm)
R _i	Raw image
ROI	Region of interest
SA	Surface area (m ²)
SECOAS	Self-Organising Collegiate Sensors
SNARF	seminaphthorhodafuor
TEGDMA	tetraethylene glycol dimethacrylate
TEMED	<i>N,N,N',N'</i> -tetramethylenediamine
T _g	glass transition temperature (°C)
Tris	tris-(hydroxymethyl)-aminomethane

V	Volume (cm ³)
V _a /V _b	volumetric ratio of acid to base
W/O	water in oil
WANET	wireless ad-hoc networks
ZBKE	Zhabotinsky-Buchholtz-Kiyatkin-Epstein
α _n	concentration fraction of n-protic species
λ	wavelength (nm)
τ _c	fluorescence decay (ns)

Contents

Abstract.....	I
Acknowledgements.....	II
Innovations and Contributions	III
Abbreviations and nomenclature	IV
Aims and Objectives.....	XI
1. Introduction	1
1.1 Overview	2
1.2 Quorum Sensing.....	2
1.2.1 Quorum Sensing in Nature.....	2
1.3 Belousov-Zhabotinski Reaction.....	4
1.3.1 Synthetic Collective Behaviour Utilising the Belousov-Zhabotinsky Reaction.....	5
1.3.2 'Self-Oscillating' Gels.....	12
1.3.3 Conclusions on BZ oscillations	14
1.4 Palladium Catalysed Oscillatory Carbonylation	15
1.5 Enzyme loaded alginate particles	16
1.5.1 Particle synthesis.....	17
1.5.2 Programmed responses with enzyme loaded particles.....	17
1.6 Enzymes	20
1.7 Glucose oxidase	24
1.7.1 Sources.....	24
1.7.2 Applications.....	24
1.7.3 Structure and Physical Characteristics	26
1.7.4 Stability	26
1.7.5 Mechanism.....	27
1.8 Aliginate	31
1.8.1 Sources.....	31
1.8.2 Chemical structure	31

1.8.3	Gelation.....	33
1.8.4	Physical and Chemical Properties	33
1.8.5	Alginate modification.....	34
1.9	Chitosan	35
1.9.1	Sources.....	35
1.9.2	Chemical Structure.....	35
1.9.3	Gelation.....	35
1.9.4	Physical and Chemical Properties	36
1.9.5	Chitosan modification	37
1.10	pH Responsive Polymers.....	38
1.10.1	pH-Responsive Hydrogel Synthesis.....	42
1.10.2	Applications of pH responsive polymers.....	43
2.	Experimental Methods and Materials	45
2.1	Chemicals	46
2.2	Electrometric pH Measurements.....	46
2.2.1	pH Electrode Calibration	46
2.2.2	Aqueous Acid Base Titrations	47
2.2.3	Glucose oxidase in bulk phase titrations	47
2.3	Particle Synthesis	47
2.3.1	Alginate Particles.....	47
2.3.2	Chitosan Particles.....	48
2.3.3	Poly(methacrylic acid) particles	49
2.4	Ratiometric imaging.....	49
2.4.1	Experimental setup	49
2.4.2	Experimental Procedure	51
2.4.3	Calibration Experimental	51
2.5	Optical microscopy.....	52
2.5.1	Experimental	52

3.	Glucose oxidase in the bulk phase	53
3.1	Overview	54
3.2	Introduction	54
3.3	Results and Discussion	56
3.3.1	Achieving a near linear titration	56
3.3.2	Enzymatic Rate Profile Determination.....	68
3.3.3	Action of glucose oxidase in a bulk aqueous phase.....	70
3.4	Conclusions and Future Work.....	73
4.	Ratiometric Imaging.....	76
4.1	Overview	77
4.2	Introduction	77
4.3	Results and discussion	79
4.3.1	Tucam calibration with SNARF-4F.....	79
4.3.2	Image processing	83
4.3.3	Effect of SNARF-4F concentration.....	86
4.4	Conclusions and Future Work.....	87
5.	Particle Synthesis	88
5.1	Overview	89
5.2	Results and Discussion	89
5.2.1	Poly(methacrylic acid) Particles	89
5.2.2	Chitosan Particles.....	94
5.2.3	Alginate Particles.....	99
5.3	Conclusions and Future Work.....	101
6.	Glucose oxidase loaded particle analysis.....	103
6.1	Overview	104
6.2	Results and Discussion	104
6.2.1	Particle synthesis and characterisation	104
6.2.2	Ratiometric Imaging.....	104

6.2.3	Diffusion from a single particle	106
6.2.4	Increasing particle density	111
6.3	Conclusions and Future Work.....	123
7.	Conclusions and Future Work.....	124
7.1	Conclusions	125
7.1.1	Encorporating the component technologies	125
7.1.2	Ratiometric Imaging.....	127
7.2	Future Work.....	128
7.2.1	Stirred Reaction Media	128
7.2.2	Experiments using the Ratiometric Setup.....	130
7.2.3	Delivering a response.....	131
8.	References	136
9.	Appendices.....	1
9.1	Appendix: Aqueous Acid-Base Equilibria and Titrations.....	2
9.1.1	Concentration fractions	4
9.1.2	Titrations	8
9.1.3	Buffers.....	10
9.1.4	Buffer Strength.....	10
9.1.5	Activity Effects.....	12
9.2	Appendix: Diffusion.....	13
9.2.1	Fick's Laws of Diffusion	14
9.2.2	Time Dependent Diffusion Processes	16
9.2.3	Diffusion in a plane	17
9.2.4	Diffusion from a point source	18
9.2.5	Diffusion from a continuous source.....	19
9.3	Appendix: References	20

Aims and Objectives

Quorum sensing is a stimuli-response mechanism utilised by bacteria and social insects such as bees and ants to instigate population wide responses based on population density. The long reaching goal is to create a wholly synthetic quorum sensing system, allowing individual particles to act *en masse* and enabling the spontaneous delivery of a chemical payload. To date most chemotherapy agents cannot differentiate between non-cancerous and cancerous cells. As such the methods of site-specific drug delivery have been developed where the drug is entrapped within a particle that is drawn to a cancerous site. The drug then leaches out of the particle and destroys some of the cells it encounters. The drawback of current techniques is that they rely on the drug leaching from the particle. This is a relatively slow process resulting in a low concentration of the drug being present for a long period of time.

Synthetic quorum sensing has the potential to revolutionise the delivery of the therapeutic agents in cancer therapy, since the particles that carry the agent can determine their population density. When the particles are drawn to a tumour the population density increases. Upon reaching a threshold density a response is triggered resulting in a burst release of the therapeutic agent from the particles. A burst release means that a much higher concentration of the therapeutic agent is present to destroy the cancerous cells. This high concentration release is achievable since the therapeutic agent is delivered in unison by the carrier particles directly at a target site. This would not only increase the efficacy of the drug, but also lower the dosage required to obtain a therapeutic effect. As such the use of a synthetic quorum sensing drug delivery system would also decrease the side effects experienced with some therapeutic agents, in particular current chemotherapy agents for cancer treatment which attack both cancerous and healthy tissue.

Although it would be ideal to create a complete *in vivo* system, it is beyond the scope of this thesis, instead what is focused upon here is the *in vitro* recreation of the component technologies found in biological quorum sensing systems. However, the *in vivo* potential does guide this work in choices of chemicals and routes chosen as highlighted throughout the thesis. The component technologies of biological quorum sensing direct the aims of each chapter as they are addressed. These components are; (i) the autonomous aggregation of particles; (ii) chemical communication between aggregated particles enabling them to count their population; (iii) a triggered response by the particles upon the population reaching a threshold density, resulting in the coordinated release of a chemical cargo.

To date no quorum sensing experiments have demonstrated quorum sensing by locally changing the population density, rather they rely on a global change. With the concentration of particles being increased throughout the reaction vessel. However, a drug delivery system would require oral or

intravenous administration and then aggregation at a specific site. Therefore, making localised changes in population density far more important.

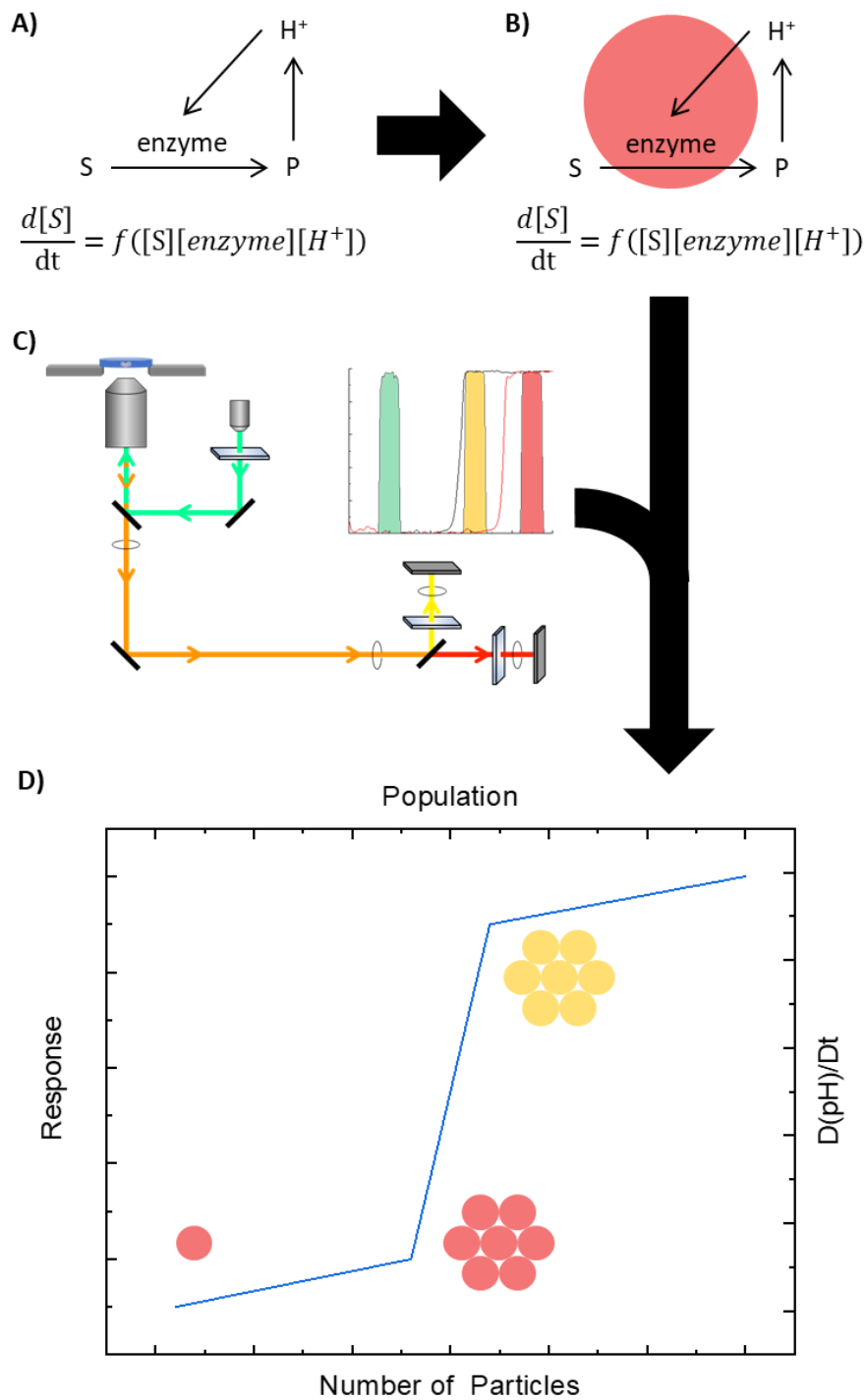


Figure 0-1-1 Scheme of work showing the proposed bringing together of component technologies to demonstrate quorum sensing. A) an understanding of autocatalytic feedback loops in enzymes that produce acid/base in bulk aqueous phases; B) Compartmentalisation of the autocatalytic reaction through the synthesis of enzyme loaded particles; C) Use ratiometric imaging to observe particle response; D) characterisation of the collective behaviour and the response demonstrated.

Most synthetic quorum sensing analogues utilise a colour change in the particle to observe a response. This is then used to model the concentration flux in the autocatalyst. By using a ratiometric imaging setup and H^+ as the autocatalyst it will be possible for more in-depth discussion to occur over theory and practice. Furthermore, it would be possible to probe dynamics of individual particles as well as clustered groups.

Currently synthetic quorum sensing has utilised inorganic reactions such as the Belousov-Zhabotinsky reactions or genetic splicing of quorum sensing genes into a new host. Recently enzyme loaded alginate particles have been used to exhibit a bistable switch in single particles. It is thought that using this emerging technology it is possible to gain further insights into quorum sensing.

Chapter one, provides the background theory and literature reviews required to fully comprehend the project.

Chapter two, contains all the experimental and analytical methods that were used in this body of work.

Chapter three, presents the results of generating a chemical signal through the use of glucose oxidase (GOx). By studying GOx in the bulk phase it is possible to understand its autocatalytic behaviour, whilst exposing it to environmental stresses (Figure 0-1 A)).

Chapter four, addresses the current void in understanding of calibration of ratiometric imaging setups and is a continuation/expansion of chapter two (Figure 0-1 C)).

Chapter five, sets about the creation of a 'host' particle (Figure 0-1 B)) to contain the component technologies, several synthesis techniques and materials are explored before introducing ferrous magnetite enabling the particles to aggregate in the presence of an external magnetic source.

Chapter six, presents the behaviour of GOx loaded particles, addressing single particle and aggregated group dynamics (Figure 0-1 B) and D) respectively).

Chapter seven, draws together the conclusions made in previous chapters and highlights possible directions for future work.

1.Introduction

1.1 Overview

This thesis sets out to quantitatively investigate synthetic quorum sensing in a system using glucose oxidised loaded alginate particles. Here in this chapter the fundamental information is laid out to inform the reader, not only of the principles explained in the process, but also to provide literature that have informed the decisions made throughout this thesis.

1.2 Quorum Sensing

Quorum sensing is the ability of a single organism to detect and respond to variations in its population, by exhibiting a response. Since each individual's measure of the threshold is approximately the same the entire population will demonstrate the response *en masse*. Since quorum sensing describes a form of communication enabling self-organisation of individuals within a population it falls under the umbrella term of collective behaviour. Collective behaviour also covers synchronisation and the formation of chimera states. Of these the synchronisation of oscillations in organisms to display a rhythmical production of chemicals is the simplest and most common example. Chimera state is the simultaneous existence of both coherent and incoherent states and is relevant to understanding activity in neural pathways, and disorders that arise from their disruption such as epilepsy, Parkinson's and Schizophrenia.¹ The emergence of collective behaviour can be observed at a whole organism level, for example fireflies exhibit periodic flashing², or at a cellular level, such as the production of light by *alvibrio fischeri* when above a threshold population density.³

1.2.1 Quorum Sensing in Nature

Quorum sensing (QS) is a stimuli-response process that is correlated to population density. QS is utilised in decision making of a decentralised system. In which individuals can assess the number of other components they interact with, and have a standard response when a threshold number of components is detected. As such quorum sensing is utilised; in computing;⁴⁻⁶ by social insects such as ants⁷, honey bees⁸; and by bacterial colonies.⁹

Bacteria use quorum sensing (QS) to regulate the expression of specific genes, so that they are only expressed at high cell densities allowing the resulting phenotypes to occur only when most beneficial to the bacterial colony. Quorum sensing was first observed in the regulation of bioluminescence within *Alivibrio fischeri* and *Vibrio harveyi* colonies.³ QS has since been shown to regulate nitrogen fixation¹⁰, sporulation¹¹, biofilm formation¹², virulence factor expression^{13,14} and motility¹⁴ in both gram-positive and gram-negative bacteria.⁹

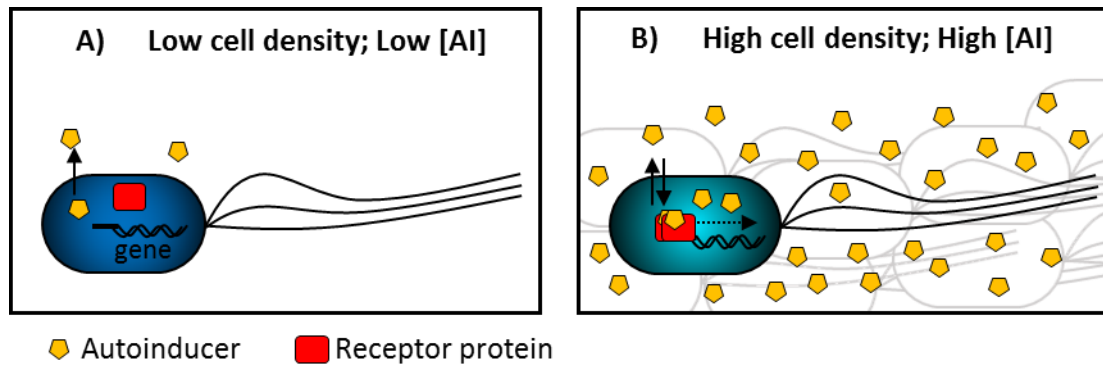


Figure 1-1 quorum sensing in bacteria is a population density dependent process. Bacteria continually produce an autoinducing signal molecule (AI). But it is only at high population density when the [AI] is above a threshold that a response occurs.

QS in bacteria occurs through the secretion of an autoinducing signal molecule, the concentration of which varies as a function of population density (Figure 1-1). Upon detection of this signalling molecule gene transcription occurs as a direct response. This Mechanism of QS is highly dependent upon the diffusion of the autoinducer (AI) molecule. The AI molecule is produced and secreted at low concentrations by individual bacteria. When the population density of the bacteria is low the AI just diffuses away. However, at high population density the local concentration of AI can exceed a threshold level, thereby triggering a change in gene expression.

Social insects are in essence the definition of a decentralised system, since no single individual is responsible for the decision making within the colony. Honey bees (*Apis mellifera*) exhibit QS decision making when looking for new nesting sites during a swarm.⁸ When a Queen leaves the nest to start a new colony she takes a small proportion of worker bees with her and leaves the remaining worker bees to congregate around the old nest as a swarm. A small proportion of workers then leave this swarm in search of a new nesting site, they do this individually. After assessing the quality of possible site, the worker returns and recruits other workers to come see the possible site with a 'waggle dance'. The number of repetitions the bee repeats of the dance directly corresponds to the quality the site. Once a quorum number of bees have visited the site they return to the swarm and begin a new method of recruitment known as 'piping'.⁸

Rock ants (*Temnothorax albipennis*) also utilise QS during the decision-making process when looking for a new nesting site. When a nesting site is destroyed, a small portion of the ants leave the nest to search for a new site. On returning to the colony the ant waits for a short period to recruit other workers to follow them to the potential new site through a process known as 'tandem running'. The waiting period is inversely proportional to the quality of the potential site. The newly recruited ants that visit the potential site make their own assessment on its quality and the number of ants that visit

the site increases. During this process any single ant may visit several different potential sites. However, due to the difference in waiting times, it is the best potential site that has fastest increases in number of ants visiting it. Eventually the ants sense that the rate at which they are visiting the best site has exceeded a threshold, indicating the quorum number has been reached.⁷ Upon sensing a quorum has been reached the ants destroy the old nest transferring all materials and eggs to the new nest site.

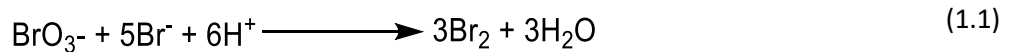
Both the honey bee and the rock ant utilise quorum sensing to determine the location of a new nesting site. In both instances a single individual never visits all of the available sites, enabling rapid decision making for the benefit of the whole colony. One example of QS in computing is self-organising networks like the SECOAS's (Self-Organising Collegiate Sensors) within environmental monitoring systems. Which have an inbuilt QS function that enables individual nodes to sense that there is a population of other nodes with similar data to report. The population then nominates a single node to report the data for all nodes, this enables the system to decrease power usage when possible.⁵ Peysakhov and Regli⁶ demonstrated how wireless ad-hoc networks (WANET) can utilise quorum sensing behaviour to find the optimal number of services required to achieve a desired effect whilst exhibiting emergent stability and resilience to possible disturbances. This is achieved by mimicking the action of QS behaviour of rock ants, an artificial ant is generated to manage the number of services that are deployed within the WANET. The 'ant' is preprogrammed to randomly visit a number of hosts within the network in a desired time interval, this time interval resets every time a service on a host is shutdown or restarted. As the 'ant' moves across the network it logs the elapsed time since last visiting host with an active service, if the time interval drops below a threshold the 'ant' restarts the service on its current host. However, if the 'ant' exceeds an upper threshold it will shut down the service on that host.

1.3 Belousov-Zhabotinski Reaction

The BZ reaction was developed by its namesakes as a inorganic analogue of the Krebs cycle, this involves the metal ion catalysed oxidation of an organic species by acidified bromate in aqueous media.^{15,16} The reaction can be monitored either electrochemically or optically, since oscillations are accompanied by a change in the oxidation state and colour of the metal catalyst (red to blue as the iron catalyst goes from its reduced (III) to oxidised (II) state). The BZ reaction can exhibit a wealth of behaviour, from chemical patterns and waves to chaos behaviour. A key advantage of the BZ reaction over many biological oscillators is its simplicity to model, often only two or three variables are required to reproduce most experimental feature. Such facile modelling makes the BZ reaction the most studied chemical oscillator if not the most studied chemical reaction.¹⁷

In a typical BZ reaction potassium bromate, sulphuric acid and potassium bromide are mixed in a stoichiometric ratio of 6:6:1. This instantaneously produces an orange solution due to the production of bromine (see Eq 1.1). An excess of an organic acid such as malonic acid is then added to the solution and it is mixed until the reaction mixture becomes colourless. Finally the metal catalyst such as ferroin is added to the solution (typically molar ratio 1:20 ferroin:potassium bromide). The resulting oscillatory reaction can then proceed for several hours.

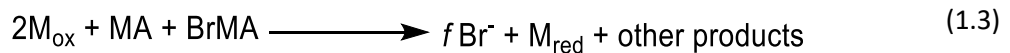
From the Field, Körös and Noyes reaction mechanism¹⁸ the BZ reaction has two key intermediate species: the inhibitor Br^- and the auto catalyst HBrO_2 . The inhibitor is removed in process A:



The production of the autocatalyst is accompanied by the oxidation of the metal catalyst (M) in process B:



The bromine from process A brominates the malonic acid. The effect of autocatalysis from process B diminishes as disproportionation of HBrO_2 . Finally, the inhibitor Br^- is regenerated in tandem with the reduction of the metal ion complex, in process C:



Where f is a stoichiometric factor, dependent upon the initial concentrations of bromate and malonic acid. The size of f dictates which process dominates. When f is high (typically $> 18 \times 10^{-6} [\text{BrO}_3^-]$)¹⁸ the reduced form of the metal complex is favoured. The oxidised form of the metal complex is favoured when f is low ($< 5 \times 10^{-6} [\text{BrO}_3^-]$)¹⁸ since process B dominates. When the stoichiometric factor is at an intermediate sweet spot, oscillations between these two-states occur via process C.

1.3.1 Synthetic Collective Behaviour Utilising the Belousov-Zhabotinsky Reaction

Initial forays into synchronised behaviour using the BZ reaction were carried out by Stuchl and Marek in 1975.¹⁹ This was achieved by connecting two continuous flow stirred tank reactors (CSTRs) with a perforated plate. As a result, each reactor was shown to be capable of displaying its own oscillatory dynamics. These dynamics were dictated by the inflow rate of the reactants and the temperature. The perforated disk enabled mass transfer to occur between the two reactors, under certain conditions synchronisation of the reactors occurred whilst under other conditions more complex behaviours could also be observed, such as rhythm splitting. The CSTRs have also been used to couple redox oscillations using electrical perturbation rather than mass flow.

Mimicry of collective behaviour through the utilisation of the multiple CSTRs is not only expensive but spatially impractical. To overcome this spatial issue one of two methods of miniaturisation can be used. The first is to create a water in oil emulsion so that only the organic reagent and product can partition into the oil phase.²⁰ The second method immobilises the catalyst onto ion exchange beads which are then suspended in an aqueous media which contains the remaining BZ reagents. Of the two methods it is the latter system which has been utilised most frequently on investigations into collective behaviour in chemical oscillators.^{21,22} This is in part due to increased complexity of the reaction kinetics for the emulsified system, due to malonic acids hydrophobic-lipophilic balance being pH dependent. Furthermore, the catalytic bead method allows multiple coupling methods to be explored, since the reaction mixture can be stirred or not. Without fear of coalescence of the micro-reactors.

A stirred reaction medium, results in rapid dissolution of the key intermediates HBrO_2 and Br^- . This allows the surrounding solution to be considered spatially uniform throughout and only dependent upon the contribution of all the 'micro-reactors'. This is referred to as global or all-to-all coupling. The strength of global coupling is affected by the transfer rate of the key intermediate species, which in part is related to the stir-rate.

Whereas, in static reaction mixtures the rate of transfer between a micro-reactor, the bulk solution and other reactors is diffusion limited. Since both key intermediates can also decay in the surrounding solution through process A and disproportionation, the strength of coupling is dependent on the distance between the micro-reactors and their relative size compared to the reaction timescale.^{23,24} This form of coupling is known as 'nearest neighbour' or 'local coupling', since only adjacent beads can influence one another.

More complex non-local coupling behaviour can be achieved by using a light sensitive catalyst like ruthenium bipyridyl ($\text{Ru}(\text{bipy})_3^{2+}$) which only becomes catalytically active when irradiated with light corresponding to a wavelength of 450 nm.²⁵ By increasing the intensity of the light on a specific microreactor the catalytic activity and coupling strength can be increased, this allows certain micro-reactors 'signals' to be felt further away than just its neighbours.

1.3.1.1 Catalytic Beads

The metal ion catalyst typically ferroin (iron phenanthroline) is loaded on to sulfonated polymer beads (40 μm – 1.2 mm) to produce the catalytic beads. Loading is typically around the order of 1×10^{-5} moles of catalyst per gram of beads.²⁶ The beads are then immersed in a solution of the remaining BZ reagents: bromate along with malonic and sulphuric acids (typically [0.1 M]). Since the uncatalyzed reaction is relatively slow and large volumes are used the pool chemical approximation stands. When the beads are sufficiently small enough compared to the reaction diffusion length scale, each

individual bead can be considered a uniform micro-reactor, whose intermediate concentrations vary as a function of both the reaction kinetics and the rate of transfer to the surrounding solution.²⁷

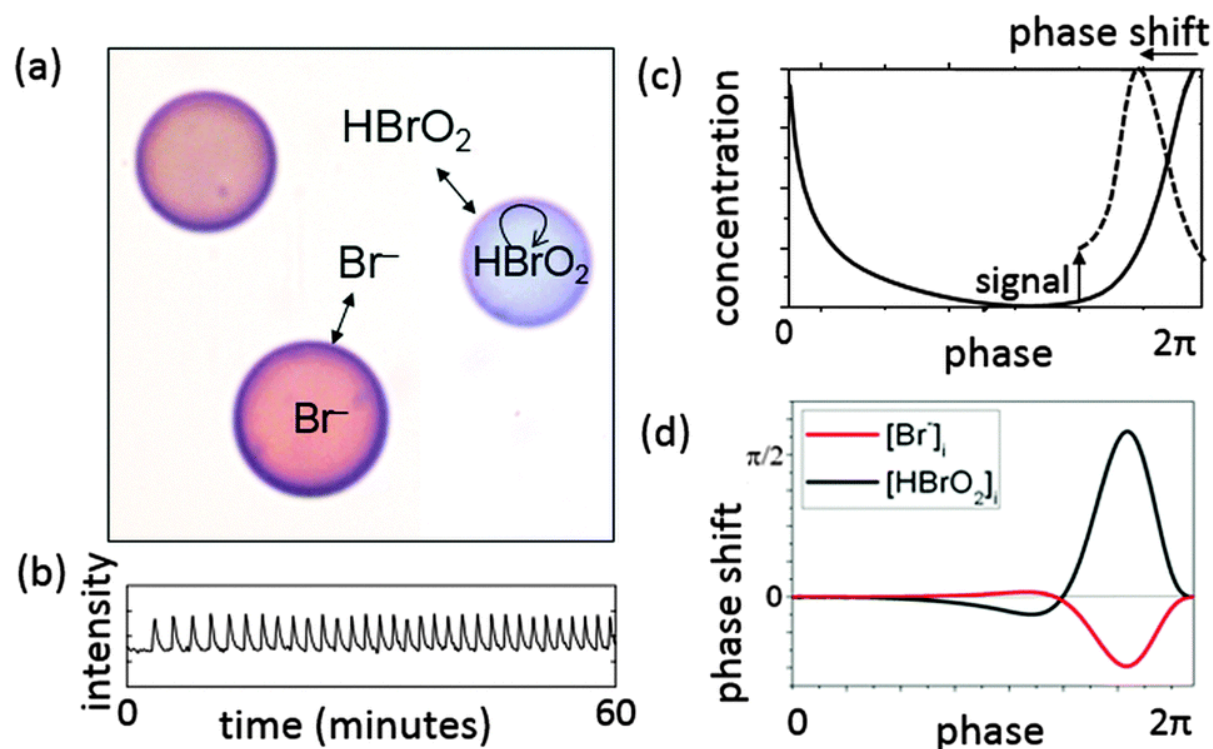


Figure 1-2 (a) Experimental image of ferroin-loaded catalytic beads in catalyst free BZ solution. The field of view is approximately 1 mm x 1 mm. The reduced catalyst is red (low intensity) and the oxidised catalyst is blue (high intensity). (b) Light intensity-time plot obtained from a series of images of a bead. (c) Sketch of peak to peak oscillation in concentration and corresponding phase of the cycle. Dotted line shows the oscillation after a phase shift in response to a signal. (d) Phase response curve constructed from simulations of the ZBKE model of the BZ reaction²⁸ showing the phase shift after perturbations in HBrO_2 or Br^- at different phases of the cycle. Figure replicated with permission from reference²⁹

The oscillatory state of the reaction between the oxidised and reduced states for the catalysed beads can last for hours with the beads exhibiting hundreds of oscillations before either the bromate or the malonic acid becomes depleted. The frequency of oscillations is typically in the order of minutes. However, this is dependent upon several factors including the reaction temperature, initial reactant concentrations, catalyst loading on the bead and the rate of intermediate species transfer between the beads surface and the bulk solution (Figure 1-2 (a)). Yoshikawa et al.³⁰ showed that using smaller beads resulted in faster loss of intermediate species from the bead than larger beads. When the temperature is kept constant a slight increase in the oscillatory frequency can be observed as the reaction proceeds, however, for most instances this is considered negligible.

The amplitude, period and phase of the oscillations can simply be determined from time-intensity plots which can be obtained from images of the beads. Low transmitted light intensity correlated to the reduced form of the metal catalyst, when process B (discussed earlier equation (1.2)) dominates

a rapid increase in the light intensity occurs to coincide with the shift from reduced to oxidised metal complex. The intensity then gradually decreases as process C takes place. The reaction's concentration-time profile of Br^- is like the metal catalysts. Meanwhile, the production of H_2BrO typically spikes through the time frame that is attributed to process B.

The method used to determine the period and phase of the reaction depends on the complexity of the time series.³¹ Alternatively the phase can also be defined by linearly scaling the time between sequential peaks from 0 to 2π .

The BZ micro-reactors (catalytic beads) can be considered coupled when they interact with one another, resulting in the oscillations to shift in amplitude, period and/or phase. This is driven by a change in the rate of production of the key intermediate species. This interaction is often characterised through the resulting phase shift. A phase advance is deemed to have occurred when there is a positive phase shift resulting in the oscillation to jump to a later point in the cycle (as shown in Figure 1-2 (c)), thereby reducing the period of the oscillation. A phase delay results in the oscillator returning to a previous point in the phase cycle, increasing the period of the oscillation. Figure 1-2 (d) is simulated using the Zhabotinsky–Buchholtz–Kiyatkin–Epstein (ZBKE) model of the BZ reaction.³² It shows the phase shift following an increase in either Br^- or HBrO_2 during a single cycle. Initially there is little variation and the reaction is deemed to be refractory. However, when the phase of the cycle is greater than π an increase in the inhibitor concentration leads to a phase delay, whereas, an increase in the autocatalyst predominately leads to a phase advance.

1.3.1.2 Modes of Collective Behaviour Demonstrated by the BZ Reaction

1.3.1.2.1 Synchronisation

Cellular Biological systems utilise the synchronisation of chemical oscillations in a variety of ways, for example pacemaker cells in the sinoatrial node dictate the electrochemical rhythm of cardiac cells to give a uniform contract of the heart.³³ A loss of synchronisation in pacemaker cells can lead to arrhythmias or tachycardia. The loss of synchronisation can occur through defects or heterogeneities, leading to spirals (supraventricular tachycardia) or complete loss of coordinated action.

Slime moulds like *Dictyostelium discoideum* utilise propagating reaction-diffusion waves of cAMP to trigger chemotactic aggregation of starving cells, with the cells move toward sources of cAMP. Lee, Cox and Goldstein³⁴ noted the mould cells produces that both target waves and spiral waves, the latter occurring at high cell density. Furthermore, modelling carried out by Lauzeral et al.³⁵ suggest that spirals occur through slow variation in the cells dynamics, with cells switching between excitable and spontaneous oscillatory states before returning to an excitable state.

In 1972 Winfree³⁶ demonstrated how the diffusion of the autocatalyst HBrO_2 in thin layers of the BZ solution resulted in target waves, with the highest frequency source entraining the solution to a single common rhythm. Moreover, introduction of a defect, by the dragging of a pipette through the solution lead to the formation of spirals.

The Showalter group³⁷⁻³⁹ utilised the BZ catalytic beads to investigate the synchronisation of locally coupled oscillators, both pre and post coupling. They showed that synchronisation is dependent upon the initial bromate concentration, which dictates the natural period of the beads. When the initial bromate concentration is low (0.3-0.42 M), a uniform layer of beads can be synchronised to a pacemakers oscillatory rhythm which is faster than the other beads natural frequency. Likewise, a spiral source entrains the bead's oscillations to have the same period. As the reaction waves move out from the core neighbouring beads remain phase locked, with a fixed phase difference. Increasing the bromate concentration (> 0.42 M) results in multiple spiral sources forming within the layer. These compete with one another to give an irregular wave pattern; such behaviour is referred to as spiral overcrowding. Furthermore, regions that are permanently unexcitable can play a role in this behaviour.⁴⁰ The group showed that uncoupled beads that were exposed to increasing bromate concentration exhibited more frequent oscillations. Such oscillations increased the likelihood of refracting the propagating wave and causing spirals to form.³⁹

A stirred reaction medium can be used to probe how population density can affect cellular dynamics, as demonstrated by Taylor et al.^{26,41} In a typical reaction the oxidation state of beads ($1-10 \times 10^4 \text{ cm}^{-3}$) was monitored by image processing of the stirred solution. The intermediate species concentration in the bulk solution phase was obtained electrochemically using a platinum electrode.

As the density of the beads increased the amplitude of the 'signalling' intermediate species proportionally increased. However, varying the stir rate of the reaction mixture resulted in two different transitions, the first is discussed here, for the second see section 1.3.1.2.2 page 10. At low stir rates (300 rpm) the electrochemical signal exhibited a large amount of noise when the particle density was low ($< 0.01 \text{ g cm}^{-3}$). However, increasing the particle density resulted a gradual growth in the amplitude of the electrochemical oscillation. Image processing of the reaction media allowed the fraction of blue, oxidised beads to be determined as a function of time. Upon exceeding a threshold density, regular oscillations were observed. With the fraction of oxidised beads increasing from 20 % to 80 % as the density increased from 0.01 to 0.035 g cm^{-3} . Experimental data and simulations of the reaction indicate that the increasing amplitude in of the oscillations at low stir rates occur through gradual synchronisation of the chemical oscillators as opposed to a change in the individual dynamics. When the reaction mixture is experiencing low shear a bead's autocatalyst concentration [HBrO_2] is

dependent on both the reaction kinetics and the rate of exchange between the bead and surrounding solution.

In a typical low stir rate reaction increasing the concentration of the autocatalyst in the solution results in an increase in the production of the auto catalyst by the bead. When a group of beads become oxidised at the same time a spike in the concentration of the autocatalyst in the solution occurs, this phase advances several other responsive beads. By increasing the particle density the magnitude of the autocatalytic spike increases causing more oscillators to synchronise.

In the 1960s Winfree developed a phase model of globally coupled oscillators.⁴² For such a model to work a critical coupling strength (K_c) for the emergence of synchronisation was added by Kuramoto,⁴³ K_c depends on the heterogeneity of the population, i.e., the distribution of natural frequencies of the population. In low stir rate BZ bead reactions, increasing the number density results in increased global coupling strength. The gradual synchronisation of beads is due to the beads having a wide range of natural frequencies. As such, synchronisation in this manner occurs through an internal force generated by the beads. Only the timing of a beads oscillation changes.

1.3.1.2.2 Dynamic Quorum Sensing

Quorum Sensing (QS) in bacteria is a population-wide activity that occurs in response to an increase in their density above a threshold.⁹ Changes in the cells density affects the gene regulation of the bacteria, resulting in phenotypic expression such as chemiluminescence and biofilm formation. Bacteria that demonstrate QS behaviour produce autocatalytic 'autoinducers' into the surrounding solution, this provides a means of chemical communication between cells. The parallel increase in cell density and autoinducer concentration is thought to coordinate activity across the population. This action of chemical communication by a chemical agent is analogous to the catalytic bead BZ reaction.

In large cultures of starving yeast cells oscillations of glycolytic intermediates have been observed, these oscillations have a period of minutes.⁴⁴ Cell cultures below a threshold population exhibit no such behaviour. However, mixing of the two, or of two out of phase populations results in the gradual reappearance of a global rhythm. This suggests that the cells synchronise their behaviour through intercellular communication.⁴⁵ This communication is believed to occur through acetaldehyde which acts as an autoinducer.

Taylor et al.²⁶ showed by increasing the stir rate (600 RPM) in their catalytic bead system (described previously) a similar behaviour could be observed in individual catalytic bead dynamics as their number density was increased. At low number densities the electrochemical signal corresponding to the concentration of the key intermediates was virtually flat. However, on crossing a threshold

density, large amplitude oscillations were observed. Furthermore, image analysis when the density was below the threshold showed none of the beads to become oxidised (blue), but when the density was above this critical limit almost all of the beads became oxidised and oscillations were observed.

The key to this behaviour in such a system is the increased stir-rate since this increases the shear of the solution, increasing the transfer rate of the intermediate species from the beads to the bulk solution. When the density is low the HBrO_2 (autocatalyst) is stripped from the beads surface before the ferroin can catalyse the reaction. As such the ferroin remains in its reduced (red) state. As the beads density is increased above the threshold the concentration of the autocatalyst in the surrounding solution becomes high enough to trigger oscillations en masse.

In a second experiment the Showalter group³⁹ showed how dynamic quorum sensing overcomes population diversity. The local kinetics of each particle can vary according to how much ferroin is loaded onto it, this results in a distribution. The threshold density for oscillations to occur is governed by this distribution. Mixing batches of beads with degrees of catalysts loading demonstrated that the distribution of oscillatory frequency could be varied. In such instances the threshold at which the beads became oscillatory corresponded to the mean of the distribution. As such an en masse transition was observed, irrespective of each bead's individual dynamics.

Work primarily done by Tinsley of the Showalter group demonstrated how dynamic quorum sensing can be observed using catalytic beads in non-stirred systems where the beads are spatially distributed.^{38,39} For such phenomena to be observed the loading of the beads with the iron catalyst has to be sufficiently low that an individual beads or even small clusters of beads in solution exhibits no oscillatory behaviour. However, the probability of an oscillation occurring increased as the number of adjacent neighbours increased and upon reaching a threshold a target or spiral wave source occurred. A bead was as an adjacent neighbour when it was within 200 μm (average diameter of the beads) of the edge of another bead.⁴⁶ Typically, this threshold was when a bead had six adjacent neighbours and was in a quasi-circular cluster of 100 beads, loaded with 1.7×10^{-5} mol/g of ferroin. Furthermore, modelling of the reaction suggests that the emergence of such activity was due to steric crowding of the cluster which reduces the diffusion of the autocatalyst (HBrO_2) from the beads into the solution, rather than the concentration of the autocatalyst increasing beyond a threshold concentration in the surrounding solution.

1.3.1.2.3 Other Modes of Collective Behaviour

This section talks briefly about multi-stability within clusters, oscillator death and chimera states. They are included for completeness however a detailed description is considered beyond the scope of this thesis, for further reading the author suggests the review article by Taylor, Tinsley and Showalter.²⁹

Multi-stability of globally coupled oscillators is the formation of two or more synchronised groups of particles that are separated by a phase difference despite being surrounded by the same solution. An analogy is the Ying and Yang symbol from Chinese philosophy, where the entire circle is the solution, but the dark and light portions describe the phase in that region. Such behaviour was initially modelled by Hansel et al.^{47,48} before being experimentally demonstrated using a gas phase variation of the BZ reaction and CO-Pt systems.^{49,50} Furthermore, simulations of the BZ reaction using the ruthenium catalyst show that coupling occurs through the inhibiting bromide ion rather than the autocatalyst.

Oscillator death is associated with the apparent disappearance of oscillation through the coupling of oscillatory reactors.^{51,52} However, this behaviour is not expected to be observed with catalyst loaded beads since models suggest that for such a phenomena to occur the metal catalyst would have to move from one bead to another.

Chimera states describes two co-existing groups within a population one that is synchronised and another that is not. For such states to exist oscillators must be nonlocally coupled. To demonstrate this Tinsley et al nonlocally coupled beads loaded with catalytic ruthenium via light.^{53,54} this resulted in a portion of the beads synchronising with the remainder being asynchronous.

1.3.2 'Self-Oscillating' Gels

In this section work carried out by the Yoshida group into self-oscillating polymer gels is discussed. Such gels can be used; to create function fluids that undergo a viscosity oscillation; in autonomous mass transport systems, through the use of polymer brushes and tubular structured gels; as biomimetic actuators that demonstrate self-propelled motion. However, herein particular attention paid to 'self-oscillating' crosslinked particles and micelles since these have the ability to be used to demonstrate collective behaviour that results in a volumetric transition. For a complete review of all functions demonstrated by 'self-oscillating' polymer systems reader should read 'Evolution of self-oscillating polymer gels as autonomous polymer systems' by Yoshida and Ueki.⁵⁵

Initially pH-responsive gels were coupled with a pH-oscillating reaction by soaking the gel in the self-oscillating reaction media and placing it in a CSTR.⁵⁶ The oscillating reaction was the oxidation of hydrogen sulphite by hydrogen peroxide in the presence of ferrocyanide. The pH would oscillate between pH 4.7 and 6.9. When coupled with the pH responsive poly(*N*-isopropylacrylamide-co-acrylic acid-co-butyl methacrylate) gel autonomous, periodic swelling and deswelling occurred.^{57,58} Such a system only demonstrates that the volumetric state of the gel only follows the oscillation in pH of the bulk media, which is controlled by the CSTR. Therefore, to develop a truly self-oscillating polymer gel Yoshida et al. incorporated an oscillating reaction into polymer system.⁵⁹ This was achieved by incorporating the BZ catalyst $[\text{Ru}(\text{bipy})_3]^{2+}$ into a responsive polymer backbone like poly(NIPAAm) (N-

isopropylacrylamide) by copolymerisation to create poly(NIPAAm-co-Ru(bipy)₃). When immersed in a solution that contains the remaining BZ reagents (malonic acid, sodium bromate and nitric acid) the pendant catalytic groups can undergo redox changes from reduced Ru(II) to oxidised Ru(III). This shift in redox state changes the temperature at which a volumetric transition occurs, through judicious selection of the reaction temperature the swelling ratio can also shift as a function of redox state. This is due to the ruthenium complex increasing the hydrophobicity of the polymer chain as it oxidises from Ru(II) to Ru(III).⁵⁹

In 2000 Yoshida et al.⁶⁰ demonstrated fine control of their 'self-oscillating' poly(NIPAAm-co-Ru(bipy)₃) gel. Through changes in the initial concentration of non-catalytic BZ reagents and the reaction temperature. As previously mentioned decreasing the initial reagent concentration of BZ reagents increases the period of the oscillation, slowing the frequency. However, the frequency of the oscillation can be increased by raising the temperature of the reaction. Reaction temperature also affects the amplitude of the volumetric transition. Moreover, it was demonstrated that a reduction in oscillation frequency resulted in a larger volumetric transition due to a greater portion of the catalyst becoming oxidised, thereby increasing the hydrophobicity of the gel.

As previously mentioned the utilisation of 'self-oscillation' in microgels is of the greatest relevance to this thesis since it demonstrates an en masse volumetric response to a shift in the concentration of an autocatalytic signal. Work carried out by Suzuki and Yoshida⁶¹⁻⁶⁴ demonstrated how microgels of poly(NIPAAm-co-Ru(bipy)₃) prepared by surfactant free aqueous precipitation polymerisation, could be used to demonstrate colloidal stability at low temperatures during which oscillations resulted in a change in the optical transmittance. However, when the temperature was raised to within a few degrees of the volumetric transition temperature (31 °C) of the reduced (Ru(II)) microgel, a shift in redox state of the ruthenium complex caused flocculation (reduced) or dispersion (oxidised) to occur. Further work on microgels published in 2012 crosslinked microgels oscillating microgels, to replicate the hierarchical structure of muscles that generates macroscopic displacement through microscopic cellular movement.⁶⁵ This was achieved by the crosslinking (using glutaric dialdehyde) of microgel 'self oscillators' fabricated by the copolymerisation of APMA (*N*-(3-aminopropyl) methacrylamide hydrochloride), NIPAAm and Ru(bipy)₃. This resulted in a covalently crosslinked porous macrostructure that exhibits large volumetric displacements through the oscillations initiated by the change in redox state of the ruthenium complex.

In 2013 Ueki and Yoshida demonstrated how BZ oscillations could reversibly control the self-assembly of micelles from unimers.⁶⁶ This was achieved by creating a block copolymer consisting of permanently hydrophilic polyethylene oxide and a self-oscillating block of NIPAAm randomly

polymerised with the BZ catalyst $\text{Ru}(\text{bipy})_3$. To generate this copolymer the group employed reversible addition-fragmentation chain-transfer (RAFT) polymerisation; a living radical polymerisation technique that enables fine control over the end polymers chain length. For a full explanation of RAFT polymerisation see Moad et al. *Polymer* 2005.⁶⁷ In brief the coblock polymers were formed by randomly copolymerising NIPAAm with vinyl $\text{Ru}(\text{bipy})_3$ in the presence of a polyethylene oxide based macro-chain transfer agent. The catalytic ruthenium groups resulting from block copolymer were then reduced $[\text{Ru}(\text{bipy})_3]^{2+}$ or oxidised $[\text{Ru}(\text{bipy})_3]^{3+}$ under constant ionic strength and the aggregation behaviour was probed by dynamic light scattering at constant temperature. Below 25.6 °C both the reduced and oxidised polymer chain solutions were stable as unimers exhibiting a hydrodynamic radius (R_h) of 7-10 nm. Above 28.1 °C both redox forms of the coblock polymer were above the critical micelle temperature (CMT), resulting micelle formation due to the NIPAAm- $\text{Ru}(\text{bipy})_3$ block becoming hydrophobic this results in the R_h increasing upto 100 nm. When between 25.6 °C and 28.1 °C only the reduced Ru^{2+} form of the polymer is above the CMT, the oxidised polymer remains in dissolution.

Furthermore, the group went on to show that this reversible micelle formation in the presence of the BZ reaction. By adding the remaining BZ reagents (NaBrO_3 , HNO_3 and malic acid) to a solution of the block copolymer (0.5 % w/w block copolymer, 26 °C) it is possible to observe the micelle formation through time-resolved dynamic light scattering. As the BZ reaction proceeds oscillations are observed in colour, the Tyndal effect (light scattering due to colloid formation) and R_h . When the $\text{Ru}(\text{bipy})_3$ catalyst is reduced ($\text{Ru}(\text{II})$) the solution is orange in colour and the degree of light scattering from the incidence laser is high. Therefore, the block copolymer is forming micelles. However, when the catalyst is oxidised ($\text{Ru}(\text{III})$) the solution turns green and the degree of light scattering decreases, implying the polymer chains are in dissolution.

1.3.3 Conclusions on BZ oscillations

Work on utilising BZ microreactors such as that carried out by Showalter, Taylor and Tinsley demonstrate how collective behaviour can be replicated utilising the immobilisation of the metal catalyst onto microbeads.²⁶ Furthermore, work by Yoshida shows how the BZ reaction can be coupled with smart polymers to demonstrate volumetric 'self-oscillations'.⁵⁵ However, to date no one has demonstrated collective behaviour with a 'self oscillating' gel. This could be due to the two technologies being incompatible with one another. Since Tinsley demonstrated that to obtain collective behaviour beyond that of synchronisation the loading of catalyst had to be reduced so that below a threshold population density either process A or B predominates, and the beads are kinetically locked to one redox state. While Yoshida showed that to achieve a 'self oscillating' gel, its composition requires a minimum concentration of catalyst for its redox state to alter the hydrophobicity of the gel.

It is noteworthy that this concentration could be reduced if the period of the oscillation is sufficiently long enough.

The spontaneous reversible micelle formation block copolymer created by Ueki and Yoshida demonstrates the action in which a hydrophobic cargo may be encapsulated within a micelle transported to a target site and be released. Finally, it should be noted that the reagents of the BZ reaction are not readily available in vivo, as such it is not a viable oscillatory system to drive collective behaviour in a drug delivery system.

1.4 Palladium Catalysed Oscillatory Carbonylation

Another oscillatory reaction that is of growing interest is palladium catalysed oscillatory carbonylation (PCOC). Very recent developments in polymeric substrate⁶⁸ and catalyst support⁶⁹ have highlighted it as an alternative oscillatory system to probe collective behaviour. PCOC occurs through the PdI₂/KI catalysed carbonylation of an alkyne (originally phenylacetylene) to a range of products when in the presence of CO was first described by the Temkin group.^{70,71} The reaction demonstrates oscillations in both redox potential and pH over a wide temperature range (0-40 °C).

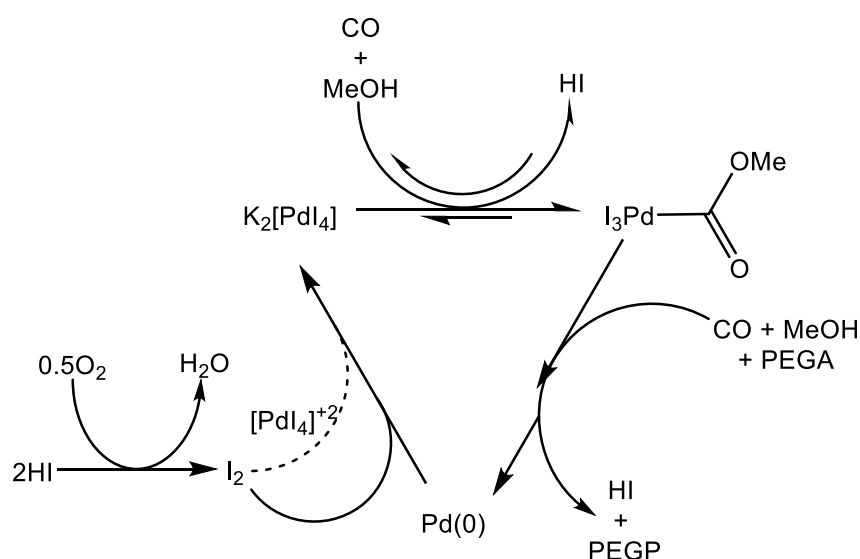


Figure 1-3 reaction scheme for palladium catalysed oscillatory carbonylation of acetylated poly(ethylene glycol).

In 2014 Donlon and Novakovic reported that monoalkyne-terminated poly(ethylene glycol) (PEGA) could be used as the alkyne substrate.⁶⁸ Figure 1-3 shows the cycling of active Pd(II) to its initial complexed form, through a multistep process of carbonylation of PEGA to 'PEGP' alongside depletion of the catalyst to insoluble Pd (0) and acid (HI). The oxidation of HI synthesises molecular iodine which reacts with the spent Pd (0) to reactivate the catalyst. This reactivation step can occur by itself, however, the rate constant is 14 orders of magnitude faster when catalysed by the Pd(II) product.⁶⁸

Furthermore, it was reported that pH oscillations were accompanied with an increase in turbidity due to the Pd (0) dropping out of solution. The major advantage of using PEGA is oscillatory behaviour is exhibited using a 100-fold decrease in both alkyne substrate (2.0 mmol dm^{-3}) and palladium catalyst ($40 \text{ } \mu\text{mol dm}^{-3}$).

In 2018 the Novakovic group reported the immobilisation of the Pd catalyst onto a chitosan hydrogel.⁷² Two methods of immobilisation were employed, the first bound the palladium catalyst to the polymer as a crosslinker joining two chitosan chains together. The second method reacted proline with the pendent amine groups of chitosan to form an imine. This provided a binding site for a portion of the palladium, with the remainder crosslinking the chitosan as before. The resulting hydrogels were then used in PCOC reactions with dialkyne functionalised poly(ethylene glycol). Although both hydrogels initially demonstrated oscillatory behaviour only the proline functionalised hydrogels were reusable generating oscillations in multiple reactions.⁷²

The palladium catalyst was also immobilised onto an imine functionalised chitosan backbone cross-linked with genipin.⁶⁹ The resulting macrogels were then used to catalytic carbonylation reactions, when the bulk phase was neat ethanol, oscillatory behaviour was observed. However, when a 1:1 volumetric ratio of water:methanol was used a step wise increase in pH was observed. Although direct volumetric transition was observed in the gel (due to its size) the oscillatory and stepwise pH shifts were accompanied by pulsatile releases of a fluorescein dye that had also been included in the macrogel.

Due to these being very recent developments PCOC wasn't considered as an alternative system to probe collective behaviour at the outset of this body of work. However, it has been included for completeness.

1.5 Enzyme loaded alginate particles

Urease (see section 1.6) has the potential to be utilised as a source of signal generation since it catalyses the production of ammonia from urea. As such, there has been recent interest in urease loaded alginate particles and their ability to demonstrate collective behaviour.⁷³ Experimental work by the Bon group has demonstrated synchronisation of particles and 'programmable' responses. Such responses include colour change⁷⁴, particle disintegration⁷⁵ and enzymatic activity inhibition⁷⁶ have been demonstrated. Meanwhile, Taylor and Bánsági^{73,77} have modelled and experimentally shown alginate particles containing urease to exhibit bistability and quorum sensing behaviour. In this section we review the recent advancements in the demonstration of collective behaviour using urease loaded alginate particles.

1.5.1 Particle synthesis

Both Taylor and Bon groups use physical methods of bioconjugation to generate urease loaded alginate particles. However, Taylor et al achieve this by absorption whereas Bon et al use a single step entrapment process.

In brief the method of absorption⁷⁷ is as follows, a homogenous aqueous solution containing sodium alginate (2.5 % w/v) and cresol red indicator (10 mg dm⁻³) is extruded through an 18G needle into a crosslinking solution of calcium chloride (6 % w/v). The resulting particles are approximately 3 mm in diameter. These are filtered and washed in DI water, then placed in an aqueous solution of urease (20 units cm⁻³). The particles are kept in the enzyme solution overnight at 5 °C, this allows absorption to take place whilst reducing the loss of enzyme activity. The enzyme loaded particles undergo an immersion in a cross-linking bath of CaCl₂ for 10 mins at room temperature, finally being separated by filtration and washed with DI water before use in further experiments. The second crosslinking is used to reduce leaching of both the indicator and the enzyme from the particles. It has been show that reducing the time the loaded particles spend in the crosslinking solution increases there activity but reduces enzyme retention within the particle.^{78,79}

Gel particle beads with entrapped urease^{74,76} can be synthesised by the simple mixing of an aqueous sodium alginate solution (typically 1-4 % w/w) with an indicator bromothymol blue (2 mg cm⁻³) and urease (0.008-10 g dm⁻³; activity 100,000 units/g). The solution is then extruded through a syringe, the resulting droplets fell into a gelation bath of calcium chloride (0.1 mol dm⁻³) for 10 minutes before separation by filtration and washing with DI water.

Jaggers and Bon have used stereolithography laser printing to create more complex shapes with regions of specific enzyme concentration.⁷⁵ Furthermore, the group have also utilised microfluidic devices for the fabrication of core-shell type particles and 'strings'.⁷⁴

1.5.2 Programmed responses with enzyme loaded particles

Both Taylor^{73,77} and Bon⁷⁴ groups have used pH responsive dyes loaded into alginate particle to demonstrate hydrogels switching between 'off' and 'on' states as the pH increases. Jaggers and Bon⁷⁴ used bromothymol blue (pK_a 6.5) and urease in alginate beads (5 % w/w) to demonstrate synchronisation of between locally coupled beads. In their experiment an 'on' (indicated its blue colour) particle with high urease concentration (1000 units cm⁻³) was placed adjacent to an 'off' particle of lower urease concentration (0.8 units cm⁻³; pH 3.5) for 240 s before being removed. This temporary contact accelerated the clock time of the lower concentration particle from 900 to 725 s (pH 3.5-6.5). This acceleration of clock time is analogous with, how target waves in thin layer BZ solutions emanate from the highest frequency source as previously discussed in section 1.3.³⁶

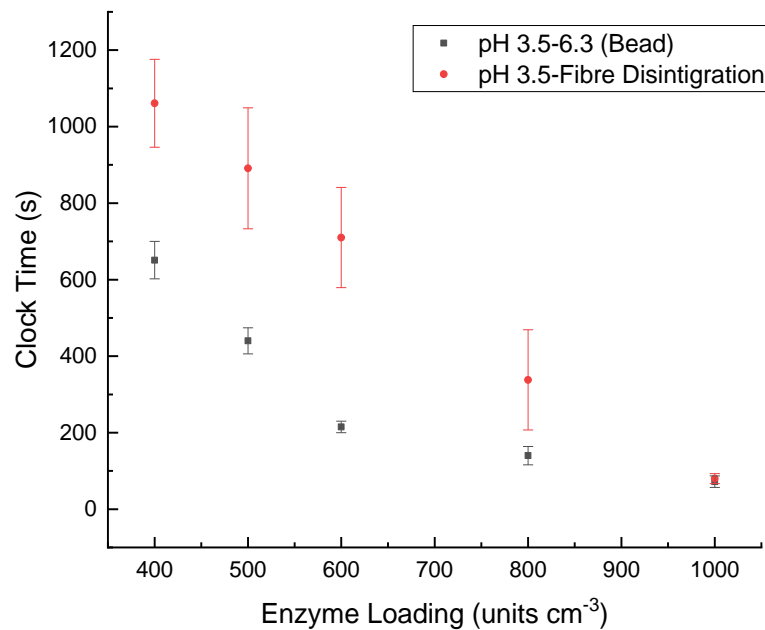


Figure 1-4 Graphical representation of clock times as a function of enzyme loading in alginate fibres. Showing how decreasing enzyme loading increases the clock time of both 'dormancy' (Grey; increasing the pH from 3.5 to 6.3) and fibre disintegration (red). Data from reference⁷⁴

Jaggers and Bon achieved 'programmable' alginate disintegration^{74,75} using ethylenediaminetetraacetic acid (EDTA) a pH responsive Ca²⁺ chelator which transitions into its protonated chelating form as the pH increase above 7.5. When at pH 3.5 calcium-alginate structures can exist in a 0.1 mol dm⁻³ EDTA solution for up to 5 days.⁷⁴ However, when fibres of urease loaded Ca-alginate (measuring approximately 112 x 4 mm; loading 400-1000 units cm⁻³) are exposed to both EDTA and urea (0.1 and 0.45 mol dm⁻³ respectively) at pH 3.5, the urease hydrolyses the urea increasing the pH, protonating the EDTA and enabling fibre disintegration. It was shown that clock time for complete fibre disintegration from pH 3.5 had near linear dependence on urease loading, decreasing from 1061 s (400 units cm⁻³) to 72 s (1000 unit cm⁻³; see Figure 1-4). However, the clock time for increasing the pH from 3.5 to 6.3 and the onset of fibre disintegration was shown rapidly decrease between 400 and 600 units cm⁻³ (from 651 to 215 s) at which point clock time plateaus only decreasing to 61 s when loading is 1000 units cm⁻³.

Further disintegration studies by the Bon group⁷⁵ used large (cm length scale) structures that had been made by stereolithographic laser printing and increasing the enzyme loading to between 2500 and 10000 units cm⁻³. In this instance the clock times from pH 3.5 to both the onset of and complete

disintegration showed non-linear dependence in enzyme loading. However, it should be noted that the clock times were significantly slower than that of the fibres. This could be due to several reasons including; increased activity of urease resulting in competition of urea; urea diffusion is inhibited due the larger structures having a smaller surface-to-volume ratio; enzyme denaturation due to the laser printing process exposing the enzyme to external stresses such as increases in temperature or ionic strength.

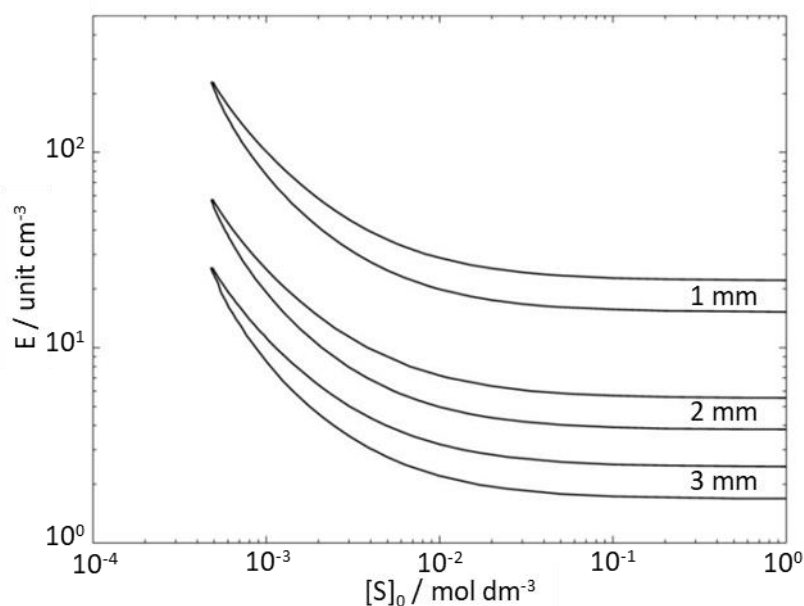


Figure 1-5 Modelled regions of bistability with as a function of enzyme activity (E) per unit volume of the gel and substrate concentration (S) in the surrounding solution for different enzyme-loaded beads with different diameter. The upper region of bistability is defined as between pH 5 and 9. Graph reproduced with permission from the supplementary information provided by Muzika et al.⁷⁷

The Taylor group⁷⁷ used a dye (cresol red; pK_a 8.3) was entrapped in the particles in order to observe a switch in state as the particle went from a low pH ('off'; yellow) to high pH ('on'; red). Particles (3 mm diameter) were loaded with urease by absorption as such accurate loading difficult to determine. The group showed that the clock time (pH 4.7-8.3) to have an inverse relationship with the initial urea concentration, increasing from 420 s (0.01 mol dm^{-3}) to 1038 s ($0.004 \text{ mol dm}^{-3}$) to 1542 s ($0.003 \text{ mol dm}^{-3}$). Further reducing the urea concentration to $1 \times 10^{-4} \text{ mol dm}^{-3}$ resulted in no transition in colour, as expected from their modelled simulations (see Figure 1-5). Moreover, the model Figure 1-5 shows how decreasing the size of alginate particles increases the degree of urease loading required to obtain a region of bistability. The region of bistability is defined as the region in which a particle may either be 'on' or 'off' the upper and lower bounds of which are defined by pH (9.0 and 5.0 respectively). Below this region of bistability the particle remains 'off' and above the region the particle is remains 'on'.

Further modelling by Bánsági and Taylor⁷³ looked at quorum sensing within three-dimension clusters of hexagonal close packed 100 µm diameter alginate particles. They showed that it is theoretically possible for these particles to undergo a switch and even oscillate. Upon reaching a threshold population the cluster would undergo a rapid pH shift from 4 to 9 and then under certain conditions oscillate between the two.

Jagers and Bon⁷⁶ set out the frame work of a second oscillatory system using silver cations to inhibit urease activity. These cations could then be sequestered by dithiothreitol (DTT) re-activating the urease. At present the sequestration of silver ions by DTT is irreversible, however, if reversibility were achieved through flow-cycling to remove excess inhibitors oscillation of dye and urease loaded alginate beads may be achieved.

1.6 Enzymes

Enzymes are globular proteins, which act as biological catalysts. They have a high degree of regio- and stereoselectivity.⁸⁰ This selectivity is due to their three-dimensional globular structure.⁸¹ However, enzymes do not have to be large to have a three dimensional structure, the smallest is just 62 amino acid residues long,⁸² but they can also be in excess of 2500 residues.⁸³ Enzymes act just like catalysts by providing an alternative low energy route for the conversion of substrate(s) to one or more products.

Naturally occurring enzymes are around three orders of magnitude faster rates of reaction than there artificial counterparts.⁸⁴ Additionally, enzymes relatively easily produced through the manipulation of bacteria. Whereas the synthesis of artificial enzymes and in particular catalysts often require an oxygen and water free environment with high purity reagents making them expensive and hard to produce. As such naturally occurring enzymes still have many applications from the everyday (washing detergents, dairy and brewing) through to the medicinal⁸⁵ (drug delivery, patient monitoring) and onto niche and emerging industries like biofuel cells and logic gates in microfluidic reactors.^{86,87}

Enzymes can be split into six distinct classes that are defined by the type of chemical reaction they catalyse. Those classes are; oxidoreductase, transferase, hydrolase, lyase, isomerase and ligase.⁸⁸ Oxidoreductase type enzymes like glucose oxidase catalyse the oxidation or reduction of the substrate. Transferase (e.g. acetate kinase) provide a pathway for the movement of a functional group from one molecule to another. Urease, lipase and beta-galactosidase are all hydrolase type enzymes that facilitate the addition of water to urea, lipids and lactose respectively. The hydrolysis of urea by urease is utilised by *Helicobacter pylori* to generate ammonia which raises the local pH allowing the bacteria to survive in acidic conditions. To aid the transfer of fat through the gut wall lipase hydrolyse the ester bonds of triglycerides this results in diglycerides and fatty acids which are more water soluble

allowing them to pass through the gut wall. People who suffer from lactose intolerance can take supplements that contain beta-galactosidase which catalyses the hydrolysis of the disaccharide lactose to its constituent monosaccharides galactose and glucose. Lyase is the term given to enzymes like isocitrate lyase which enable the elimination of small molecule or atoms without hydrolysis occurring. Isomerase catalyse structural rearrangement of a molecule. Ligase help generate new bonds between two large molecules (often nucleic acids). This process often requires the breakdown of adenosine triphosphate to generate the energy required in bond formation.

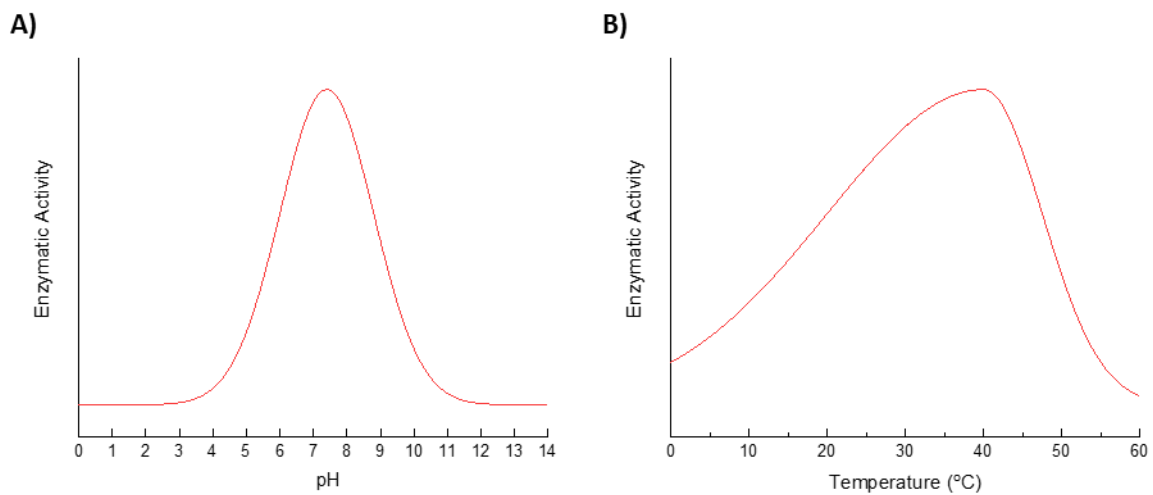


Figure 1-6 Typical intracellular mammalian enzymatic activity profiles as a function of A) pH which exhibiting Gaussian behaviour and B) temperature which exhibits Gaussian behaviour with a strong negative skew.⁸⁹

Enzymes often have a finite tolerance to changes in pH⁹⁰ and temperature⁹¹ (Figure 1-6). Activity as a function of pH and temperature exhibit Gaussian behaviour. The reversible reduction in enzymatic active at low temperature is due to the enzyme becoming inactive. The rapid and irreversible loss in activity above an enzymes maximum activity is due to the denaturation of the enzyme. Besides temperature and pH, enzymes are affected by stresses like salts, solvents and poisons. These stresses are exacerbated when an enzyme is in it native hydrated state as such enzymes are often stored as solids at low temperatures.

Perhaps counterintuitively there are enzymes whose products can cause a change in a systems pH. Such enzymes are of great interest, since pH can change an enzymes activity. Therefore, it can be utilised as an autocatalytic feedback loop (Figure 1-7 A)).^{92,93} this is due to the Gaussian behaviour of enzymatic activity with pH. Enzymes like glucose oxidase, urease and lipase catalyse acid/base production thereby generating a feedback loop when in non/weakly-buffered enviroments.⁹²

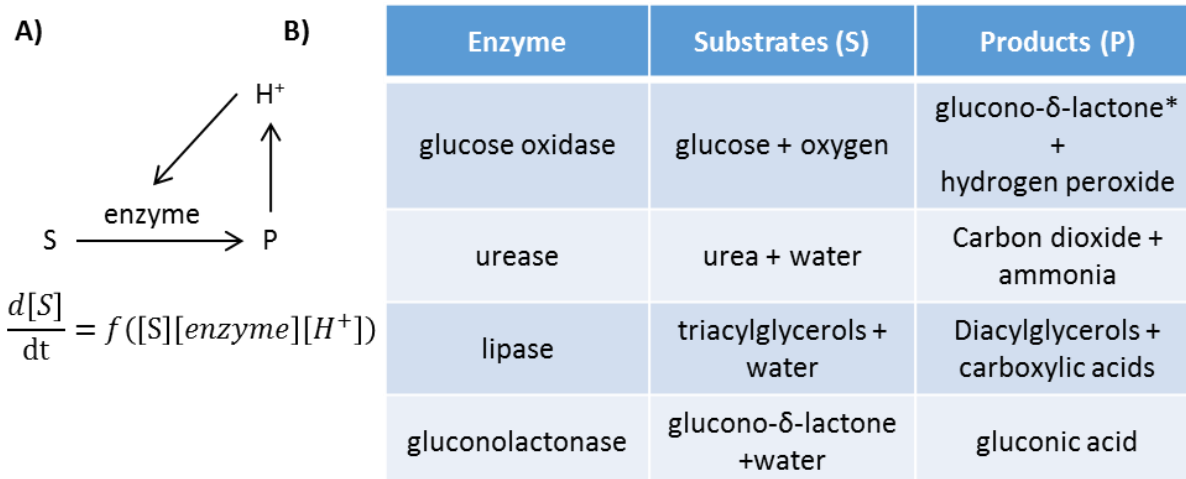


Figure 1-7 A) the autocatalytic feedback loop which changes enzymatic activity the shows how the rate of substrate ($[S]$) utilisation is dependent upon the $[S]$, $[enzyme]$ and $[H^+]$. The latter is generated by the product (P). B) A table of enzymes which have the potential to generate an autocatalytic feedback loop, their substrates and products. *glucono- δ -lactone undergoes rapid ester hydrolysis to gluconic acid.

Enzyme's whose products can induce a shift in pH include lipase, urease and glucose oxidase and gluconolactonase. Lipase enzymes are a subclass of esterases, responsible for catalysing lipid hydrolysis.⁹⁴ Lipases can be found in the small intestine where they catalyse the conversion of triacylglycerols into diacylglycerols and carboxylic acids which can be absorbed through the intestinal wall. Lipases have commercial applications in biological washing powders,⁹⁵ cheese production⁹⁵ and more recently in the production of biofuels.^{96,97}

Urease is found in *Helicobacter pylori* a bacteria linked to gastric ulcers. These bacteria utilise the urease to convert urea to ammonia and carbon dioxide. The former elevates the local pH protecting the bacterium from the stomachs acidic conditions.⁹⁸

Glucose oxidase is a well-documented enzyme whose ability to alter a systems pH is secondary to its primary use in nature.^{99,100} Glucose oxidase catalyses the reduction of glucose to glucono-D-lactone and hydrogen peroxide, the latter is used by fungi, insects and bees in antibacterial and antimicrobial applications.¹⁰¹ It is the subsequent rapid hydrolysis of glucono-D-lactone to gluconic acid that induces a shift in pH.¹⁰⁰ Glucose oxidase and the formation of gluconic acid has medical applications in the monitoring of blood sugar levels.¹⁰⁰

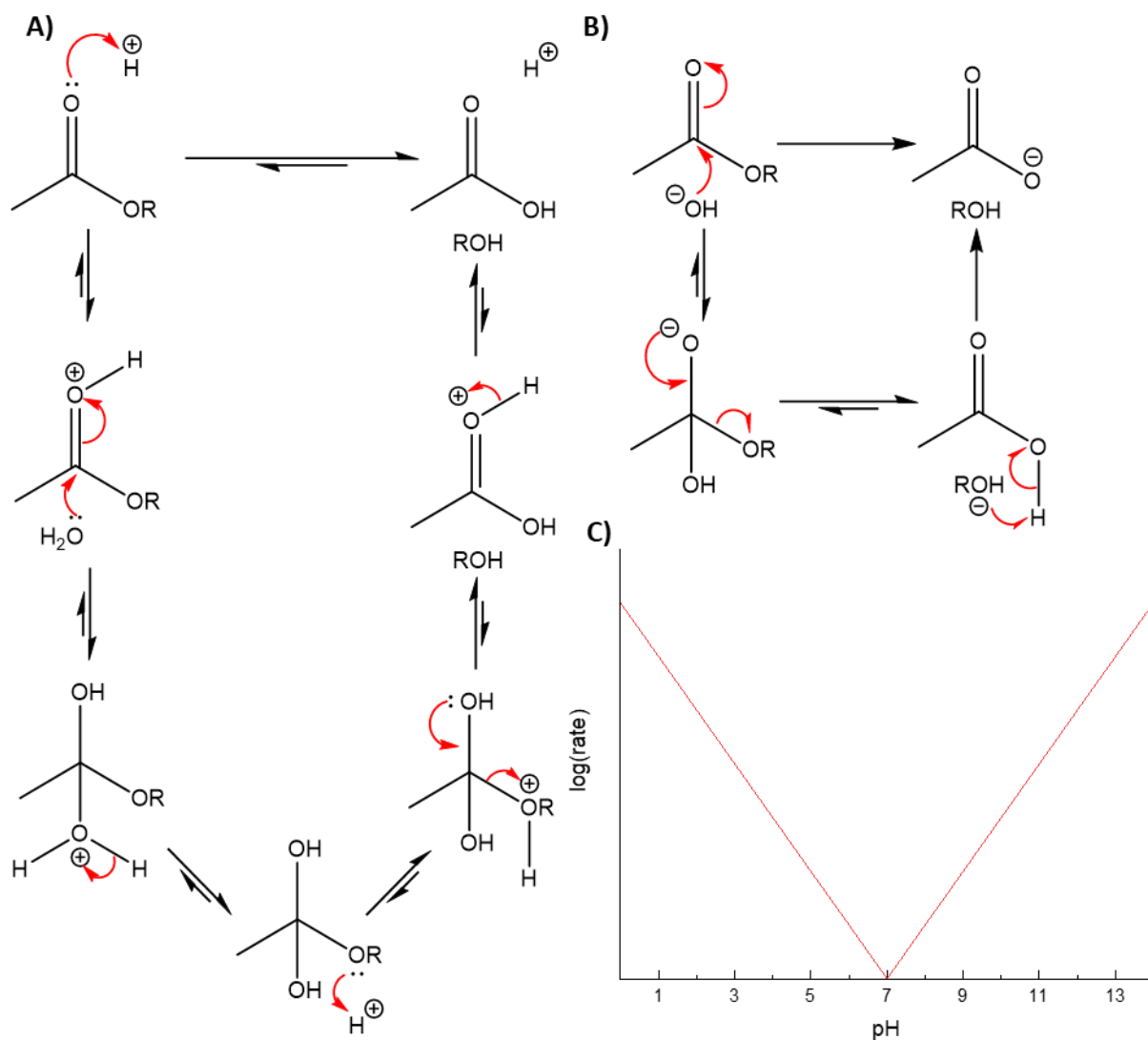


Figure 1-8 A) The mechanism for reversible acid catalysed ester hydrolysis, equilibrium lies to the right hand side, assuming there is an excess of water. B) the mechanism of base catalysed ester hydrolysis. C) $\log(\text{rate})$ as a function of pH for ester hydrolysis, showing how the rate slows as the pH tends toward neutral conditions.

One of the more unusual enzymes that has the potential to exhibit autocatalytic behaviour is gluconolactonase, which catalyses the hydrolysis of glucono- δ -lactone to gluconic acid. A process that is also catalysed by acidic and basic conditions yet exhibits a minimum in rate in neutral conditions (Figure 1-8). This is due to such conditions having tiny concentrations of hydroxide or protons, available to catalyse the reaction. Gluconolactonase has the potential to accelerate the hydrolysis of glucono- δ -lactone at such pH ranges, especially in buffered solutions. However, due to two, possibly three mechanisms occurring for at once the reaction dynamics of a system involving gluconolactonase could be hard to follow.

Of the enzymes discussed urease and glucose oxidase seem the most facile to incorporate into a synthetic quorum sensing system. Both convert a substrate that is commonly found in living organisms. Neither having complex reaction dynamics with the substrate being used in other pH dependent reactions like gluconolactonase. Furthermore, the substrates are hydrophilic. This allows them to diffuse throughout an aqueous system. Whereas a system that utilises triacylglycerol as a substrate would be heterogenous. Therefore, the enzymatic action only occurs at the interface, between the substrate oil phase and hydrogel loaded enzymes.

Ultimately glucose oxidase is the enzyme that is used in this study, due to urease exhibiting a relatively short reactive lifetime. However, very recent work by Jagers and Bon has utilised urease loaded alginate particles and chelation agents to show time dependent and population dependent behaviour.⁷⁴⁻⁷⁶ This is close to giving a complete synthetic quorum sensing system.

1.7 Glucose oxidase

There are four enzymes that oxidise glucose; glucose dehydrogenase; quinoprotein glucose dehydrogenase; glucose-1-oxidase; and glucose-2-oxidase (also known as pyranose oxidase). All convert glucose to glucono- δ -lactone apart from glucose-2-oxidase which converts it to glucosone. Both the dehydrogenases are specific to β -D-glucose with a high turnover, however, glucose dehydrogenase^{102,103} requires NADP⁺ (nicotinamide adenosine dinucleotide phosphate) as a cofactor to be present in the reaction mixture and quinoprotein glucose dehydrogenase^{104,105} is relatively unstable. Both forms of glucose oxidase utilise molecular oxygen (O₂) in the oxidation of glucose and produce hydrogen peroxide as a byproduct. Glucose-2-oxidase^{106,107} is less substrate specific oxidising xylose and gluconolactone. Herein only glucose-1-oxidase (GOx) is discussed.

1.7.1 Sources

Glucose oxidase can be isolated from several sources including red algae, citrus fruits and insects. Bees utilise GOx to produce hydrogen peroxidase as a bactericide to increase the lifetime of their honey. The most prevalent source of GOx is its isolation from bacteria and mould, the most common of which are *Aspegillus niger* and *Penicillium notatum*.

1.7.2 Applications

GOx is one of the more commercially viable enzymes, since it has applications in the medicinal sciences and biotechnology as well as the food and beverage industries. GOx's most notable use is as an analytical reagent in the determination of blood glucose concentration as used by diabetic to monitor their blood glucose level. GOx is also used in the food and beverage industry as a preservative and colour stabiliser, the use of GOx has prevailed due to its relative low cost and good stability. Glucose

oxidase is often paired with horseradish peroxidase or catalase either in solution or immobilized onto a matrix, this improves stability, and the use of solid or gel matrix enables reuse of the enzyme as well as the possibility of continuous chemical processing.¹⁰⁸

Diabetics can monitor their blood glucose levels to detect fluctuations in glucose minimising the risk of hyper/hypoglycaemia. The most prevalent method of monitoring is achieved by using a finger-prick blood sample and a portable glucose monitor. The blood sample is placed on a test strip which contains GOx. The enzyme produces hydrogen peroxide which along with other components in the strip produces ferrocyanide. This enables a current to pass through the strip, the strength of which is directly proportional the glucose level in the sample.¹⁰⁹

The application of GOx in biosensors is an area of ongoing scientific interest. These biosensors can be colourmetric^{110,111} or electrometric.^{112,113} Colourmetric sensors utilise the intrinsic fluorescence of GOx⁹⁹ Electrometric measurements occur through the immobilisation of GOx to an electrode and measuring the resultant charge. Glucose oxidase has been utilised in biosensor design for the monitoring of glucose in both the food^{111,114} and medical industries.^{110,112,113,115} Furthermore, GOx's optical properties lend itself to inline monitoring.¹¹⁴

As with Bees, the food and beverage industry use GOx to generate hydrogen peroxide as a bactericide. Resulting in a longer product shelf live. Moreover, GOx is used to remove residual glucose and oxygen from products thereby preventing colour and flavour loss.¹¹⁶ GOx is often used in conjunction with catalase, the latter converts' hydrogen peroxide to oxygen and water. Egg white and egg powder often have these two enzymes added to remove glucose, not only to improve the shelf life but also the aesthetics of the product.¹¹⁷ Furthermore, the addition of GOx and catalase is thought to improve the crumb properties in breads and pastries.^{116,118} Rheological studies on the effect of GOx addition to bread dough show a strengthening in the dough and an improvement in bread quality. However, excessive amounts of GOx can have adverse effect in the proving process since it competes with yeast for the glucose.¹¹⁹

This competition over the oxidative substrate between GOx and yeast has been highlighted as a potential application to produce low alcohol wine, since a portion of the glucose is converted to glucono- δ -lactone. It has been shown that not only does this reduce the alcohol content by around 2 % but the addition of GOx inhibits the growth of both lactic and acetic acid bacteria which can spoil wine during the fermentation process.¹²⁰ The alcohol level has been shown to be lowered further by combining the use of GOx and catalase with a base like calcium carbonate, which is used to raise the pH to increase the enzymatic lifetime of GOx.¹²¹

GOx remains the primary synthetic route to gluconic acid, which is rapidly produced by the hydrolysis of glucono- δ -lactone. Gluconic acid (pK_a 3.86^{122,123}) is used within the food industry as an acidity regulator as well as in bleaching and sterilisation agent. The low toxicity, of gluconic acid and its conjugate bases see them used in pharmaceutical formulations, it is commonly found in mouthwash as a counter ion to the antiseptic agent chlorhexidene.¹²⁴ Furthermore, gluconic acid and its salts are used in therapeutic solutions that contain proteins to increase their shelf life by contributing to ionic strength and pH that the proteins experience in vivo.^{116,124–126}

Gluconate salts also has uses in civil engineering as an additive to cement. Gluconate salts are added to Portland cement mixtures that are being used in large construction projects since gluconates retard the setting of the cement. This retardation stops the formation of cold joints and discontinuities which can allow water to penetrate the structure and damage it through freeze thaw action.¹²⁷ The addition of gluconates to cements also reduces the amount of water required to set the cement.¹²⁸

Additionally, both GOx and gluconic acid have rolls to play in the textile industry, gluconic acid as an acidulant used in tanneries. Whilst GOx is often immobilised onto alumina or silica supports and the hydrogen peroxide that GOx produces is used as a bleaching agent.¹²⁹ The immobilisation of GOx onto such substrates makes for facile processing also the gluconic acid produced in this process acts as a stabilising agent.¹³⁰

1.7.3 Structure and Physical Characteristics

GOx is a dimeric globular protein, formed of two identical sub-units. A study into GOx isolated from *A. niger* showed the protein to have a slightly elongated shape with an axial ratio of 2.5:1¹³¹ and an average diameter of 8 nm.¹³² Molecular mass for GOx varies depending on its source but is typically determined to be 155 ± 5 kDa¹³³ but can be as large as 186 kDa.¹³⁴

1.7.4 Stability

Lyophilised GOx is an extremely stable enzyme and exhibits little to no loss when stored at room temperature for up to 3 days. Lowering the storage temperature to 0 °C increases the lifetime to 2 years, and at -15 °C lyophilised GOx can be stored for 8 years with insignificant loss to its activity.¹³⁵ When in solution GOx rapidly denatures when exposed to temperatures in excess of 40 °C, complete denaturation of the protein moiety occurs at 72.5 °C. This lack of thermal stability is due to GOx having a relatively low enthalpy of denaturation ($450 \text{ kcal mol}^{-1}$).¹³¹

pH also effects the stability of GOx, it is most stable at around pH 5, which corresponds well with the slightly acidic nature of glucose (5 % w/w solution pH 5.5-6.5). Catalytic activity of GOx is lost when exposed to alkali conditions in excess of pH 8 and strongly acidic conditions (below pH 2).¹³⁶ Keilin and

Hartree¹³⁷ showed that if GOx, is stored in a solution at pH 8.1 that within 10 minutes only a tenth of its activity was retained. However, the addition of glucose to the solution was shown to perturb activity loss. This is thought to be due to gluconolactone undergoing rapid ester hydrolysis to gluconic acid which effectively lowers the pH around the active site of the enzyme.

This relatively low tolerance for alkaline conditions is thought to be due to GOx containing a protein-bound orthophosphate close to the surface of the protein.¹³⁸ Under basic conditions hydrolysis can occur removing the phosphate group from the enzyme thereby changing its structure.¹³⁸

The presence of surfactants can also inhibit GOx catalytic activity. A study by Jones, Manley and Wilkinson¹³⁹ showed anionic enzymes such as sodium dodecyl sulphate to increasingly inhibit activity at lower pH ranges, whilst cationic surfactants like hexdecyltrimethylammonium bromide deactivate GOx at high pH. On the other hand, non-ionic surfactants (span and tween) have no effect of enzymatic activity.

GOx has an isoelectric point between 3.9 and 4.3.¹⁴⁰ As such in most solutions GOx is extremely anionic. Therefore, polyamines like putrescine have been shown to alter the ionic environment of the amino acids within the active site thereby inhibiting activity.¹⁴¹ Bently¹³⁵ showed that millimolar quantities of other nitrogen rich amines and azines such as hydroxylamine and phenylhydrazine partially inhibits GOx activity. It is noteworthy that, some sugars like D-arabinose¹⁴² and 2-deoxy-D-glucose¹⁴³ have also been shown to perturb enzymatic activity by competing with β -D-glucose to occupy GOx's active site.

GOx activity can be inhibited by ions when exposed to certain conditions. More specifically, halides only inhibit GOx activity when in the solution is sufficiently acidic.¹⁴⁴ Weibel and Bright¹⁴⁵ showed that GOx become completely inactive when exposed to a 0.1 mol dm⁻³ potassium chloride solution at pH 3.

1.7.5 Mechanism

The reaction mechanism of glucose oxidase (GOx) is cyclical and can be split into two distinct processes (Figure 1-9). Firstly the GOx is reduced to GOx-H₂ in the oxidation of glucose, this is followed by the reforming of the active GOx by the oxidation with an oxidising agent (typically oxygen or quinones¹⁴⁶). In the subsequent two sections the catalytic cycle is discussed with attention given to the effect of changing reducing and oxidising substrates.

Glucose in solution exists in 2 cyclic states either as a 5 membered furanose ring or 6 membered pyranose ring (Figure 1-10). Formation of the cyclic state makes C₁ chiral, with four bonds leading to a -H, -OH, -C₂ and the ring bound oxygen. As such S and R conformers exist and are referred to as α and β forms respectively. All 4 ring structures can convert to one another by the intermediate aldehyde form of glucose in a process known as mutarotation as shown in Figure 1-10. This process of mutarotation can be accelerated by presence of mutarotase, an epimerase which catalyses the conversion from α- to β-D-glucopyranose.¹⁴⁷

Under standard atmospheric conditions the pyranose form of glucose is significantly more stable than furanose form. Of the pyranose isomers the β isomer with its equatorial hydroxyl group at the C₁ position is the more stable despite the anomeric effect. Unsurprisingly GOx has the greatest selectivity and activity for β-D-glucopyranose.^{142,148,149} Keilin and Hartree¹⁴⁸ found that GOx can also oxidise α-D-glucopyranose but at a significantly slower rate (1:625 α:β molar ratio). As a considerable amount of the α form will undergo mutarotation to the β form. A study by Stults, Wade and Crouch¹⁵⁰ showed that phosphate anions and buffers which contain them can also accelerate mutarotation. Allowing the equilibrium state to be reached in a few hours rather than days.

Although GOx is highly selective toward D-glucose it is capable of oxidising other aldohexoses,¹⁴⁸ as well as a variety of other compounds.¹⁵¹ In particular α-hydroxy compounds such as glyceraldehyde and furoin¹⁵² have been shown to undergo oxidation in the presence of GOx, nitroalkanes can also act as the reducing substrate for flavoprotein base oxidases.^{153–155}

1.7.5.2 Oxidising substrates

GOx in nature tends to rely upon molecular oxygen (O₂) or quinones to act as their oxidising substrate.¹⁴⁶ Quinones are produced by the biodegradation of lignin. This is a reversible process. Since the quinones may re-polymerise if they are not reduced to hydroquinone.^{146,156} oxygen acts as an oxidising agent resulting in the production of hydrogen peroxide. This is utilised by *P. notatum* to act as a bactericide.¹³⁶ The production of hydrogen peroxide was thought to be GOx's primary function.¹⁵⁷ However, numerous studies in the 1960's and 1980's^{108,158,159} show that hydrogen peroxide deactivates GOx especially when in its oxidised form.¹⁵⁹ This susceptibility to inactivation when in the oxidised form is thought to be due to GOx undergoing a conformational change as it switches from one state to another, this change in conformation exposes different amino acid residues some of which (e.g. methionine) are sensitive to oxidation by the hydrogen peroxide.⁹² For processes where hydrogen peroxide is a by-product it may be advantageous to remove it with catalase, however, this can cause competition for O₂ and could as much as halve the rate of conversion of glucose to GdL by

GOx. A study by Keilin and Hartree¹⁶⁰ showed that catalase preferentially utilises ethanol over O₂ as an oxidising substrate.

As well O₂, GOx can be oxidised by a large number of electron acceptors.^{161,162} These fall into 4 distinct groups that are based on pH dependent rate curves as shown in Figure 1-11.

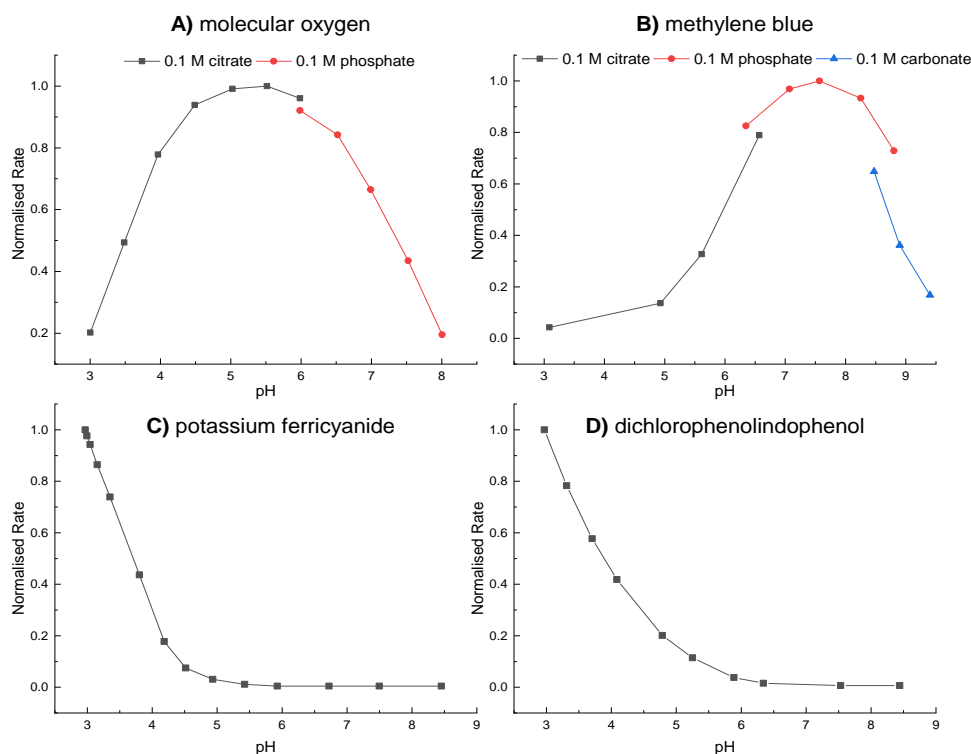


Figure 1-11 Plot of rate as a function of pH for the oxidation of glucose by GOx with; A) molecular oxygen as the electron acceptor in the presence of 0.1 M citrate, and phosphate; B) methylene blue as the electron acceptor in the presence of 0.1 M citrate, phosphate and carbonate; C) potassium ferricyanide as the electron acceptor; D) dichlorophenolindophenol (DCPIP) as the electron acceptor. Data from ref. ⁹⁹

The first type of oxidising substrate has a pH dependent rate profile that is Gaussian and uniform with a maxima at 5.6 in a citrate buffer, (Figure 1-11 A)) such substrates include O₂ and quinones. The second type of oxidising agent (Figure 1-11 B)) also exhibits Gaussian behaviour, however, the region of maximum activity is much more narrow (maximum at pH 7.6). The profile often has a slight negative skew. These substrates are based around either an amine/azine adjacent to an aromatic centre or an aromatic heterocycle, where the hetero atom is nitrogen. Examples include methylene blue (as shown above), wurster's blue, ferrocenes and benzylviologen. The third category of oxidizing substrates are those with high charge density such as ferricyanide (Figure 1-11 C)) these require strong to mild acidic conditions and exhibit very little/no activity above pH 5. The final form of oxidising substrate is those

with a low charge density like the indophenol dichlorophenolindophenol (DCPIP) (Figure 1-11 D)) again these require acidic conditions to function as an oxidising substrate for GOx.

1.8 Aliginate

In this section we focus on the polymeric matrix that will make up the bulk of our particle. Keeping in mind that in the long term we would like to develop this system into a route of drug delivery the polymer needs to be non-toxic. Since the polymer matrix is going to entrap the enzyme the gelation method needs to be relatively mild. Which will minimise the risk of denaturing the enzyme during the gelation process. The gelation needs occur relatively quickly, again to minimise the risk of denaturing the rehydrated enzyme. The polymer also needs to be able to generate a response to pH or be simply modified to exhibit pH responsive behaviour. These parameters rapidly narrow the available polymers. One of which is alginate, a naturally occurring polymer that has many applications across a wide range of industries varying from the molecular gastronomy¹⁶³ of the food industry to wound dressings¹⁶⁴ for trauma units, whilst remaining relevant and widely used in scientific research.^{74,75,77}

1.8.1 Sources

Alginate is commonly harvested from three species of brown seaweed: *Laminaria hyperborean*, *Ascophyllum nodosum* and *Macrocystis pyrifera*, where it exists as a mixed salt containing Mg^{2+} , Sr^{2+} , Ba^{2+} and Na^+ which the seaweed absorbs from the sea. Seaweed is the most common source of alginate as it makes up around 40 % of the seaweeds dry weight.^{165,166} Alginate can also be isolated from various bacteria including *Azotobacter vinelandii* and several *Pseudomonas* species.¹⁶⁷

1.8.2 Chemical structure

Alginate is an anionic water soluble linear polysaccharide formed of 1-4 linked linked β -D-mannuronate (M) and α -L-guluronate (G) residues that can be found in blocks as well as alternating structures across the polymer.¹⁶⁸ The physical properties of alginate are dictated by its composition, molecular weight and extent of sequencing. The ability of alginate chains to bind comes from the geometry and modes of linking along the polymer. The M-block regions exhibit an extended ribbon type structure (Figure 1-12 (below)) whilst the G-block regions have a buckled structure. When G-block regions of two alginate chains overlap a diamond shape hole that is negatively charged is formed. The dimensions of this void lends itself cooperative binding of divalent cations. Due to the size of the cavity affinity and binding characteristics of the alkali earth metals increases as you go from Mg^{2+} to Ba^{2+} .

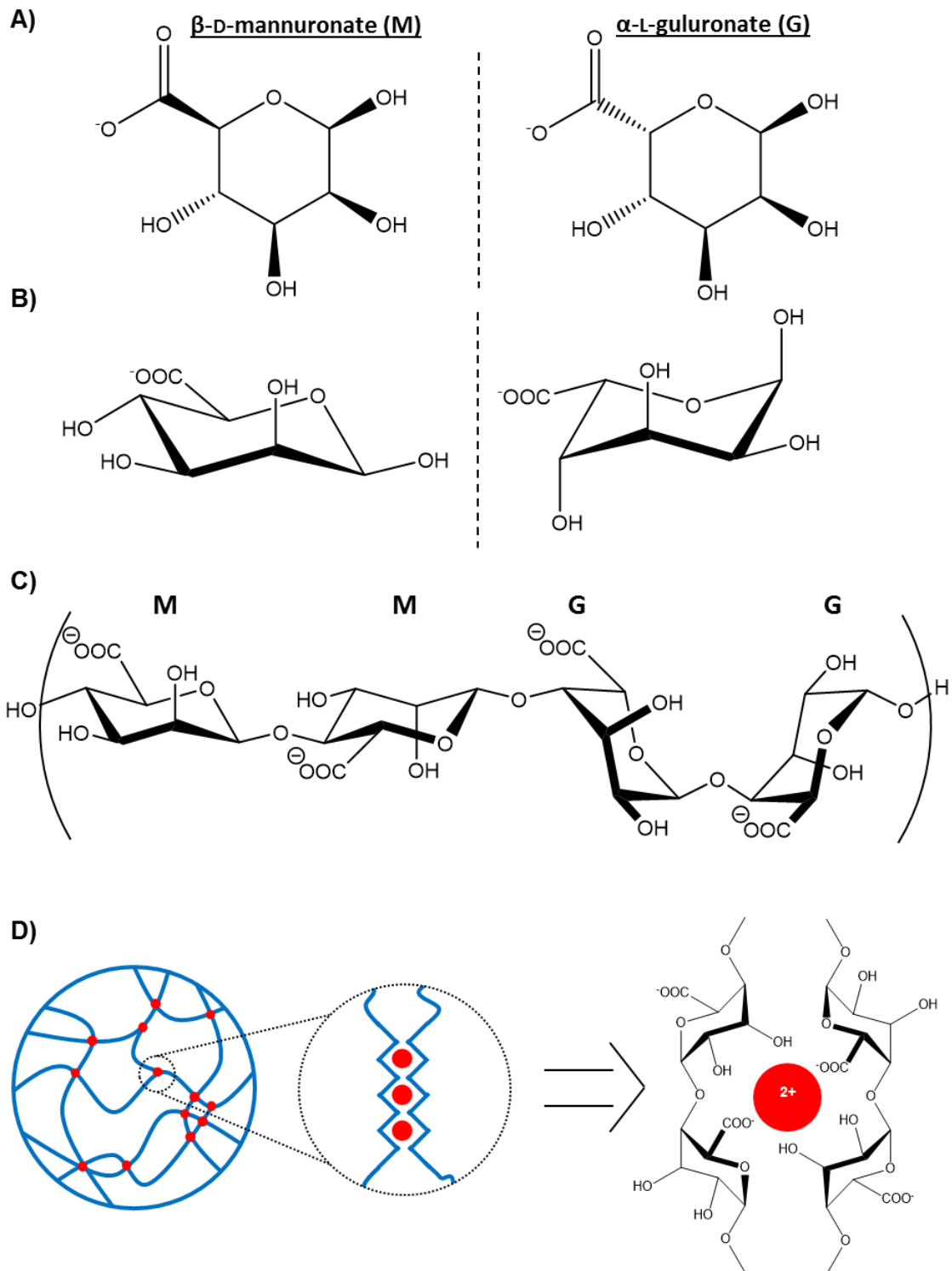


Figure 1-12 A) The chemical structure of the subunits β -D-mannuronate (M) and α -L-guluronate (G) that form the anionic polysaccharide alginate. B) Chair-conformers of M and G. C) alginates structure showing how the sub-unit order imparts structure on the polymer, both M-M and M-G regions result in an extended polymer chain where as G-G regions result in a buckled structure. D) crosslinking mechanism of alginate with a divalent cation to acting as an 'egg' to fill alginate G-block's 'box'.¹⁶⁹

1.8.3 Gelation

Gelation of alginate is a facile affair utilising the anionic cavity formed by aligned G-blocks and alkali earth metals affinity for the cavity. As such gelation occurs under extremely mild conditions using non-toxic reagents. Alginate beads and colloids are often prepared by the extrusion of a solution of sodium alginate solution into a solution of divalent cations (commonly from calcium chloride; 5-10 % w/v). The sodium alginate solution (typically 1-2 % w/v) can be mixed with any components that are to be incorporated into the gel can be added. Common additives include pigments¹⁷⁰ and dyes, magnetite,¹⁷¹ vaccines,^{172,173} or biological material such as proteins^{174,175} and enzymes.^{74-77,176}

The crosslinking occurs through the ionic exchange of Na⁺ for the divalent cation with along the G-block. The stacking of multiple alginate groups on top of one another forms a characteristic egg box structure with the divalent cations acting as eggs, sitting in the cavity.¹⁷⁷ Typically a single chain requires a G-block formed of 20 monomeric units in order to form a cooperative unit.¹⁶⁶

The resultant gel typically consists of 99-99.5 % water, which can pass in and out of the polymer matrix via its pores. These pores typically vary in size from 5 to 200 nm.¹⁷⁸ Furthermore the surface of the gel particle is thought to have narrower pores than the core due to gelation occurring from the outside toward the centre and alginate having a high affinity for divalent cations.¹⁷⁹

1.8.4 Physical and Chemical Properties

Both sodium alginate and alginate gels are used extensively in the food industry either as thixotropic agents or to form gels and membranes.¹⁶³ Alginate biodegrades and is non-toxic when taken orally.¹⁸⁰ Furthermore sub-dermal alginate exhibit little to no immunoresponse by the host.¹⁸¹ However, intravenous use of alginate require purification, otherwise a foreign body reaction or fibrosis can occur in the patient.¹⁸²⁻¹⁸⁴

Being an anionic polymer, alginate beads can collapse in sufficiently low pH media, however, alginates have a typical pK_a between 1.5 and 3.5,¹⁸⁵ as such only exhibit such a collapse in strongly acidic media such as gastric acid. Theoretically alginate can therefore, be used as a protective agent for an orally administered drug that is sensitive to low pH environments and needs to be released in the gut.¹⁸⁶ An area of growing interest is the use of alginate gels with an agent like ethylenediaminetetraacetic acid (EDTA) which exhibit pH dependent chelation properties with divalent cations. Competition for the cations results in the alginate particles disintegrating as the pH is increased.⁷⁶ This mechanism of particle disintegration could be utilised in a drug delivery system. Furthermore, the disintegration of the particle would ensure complete drug release and would aid metabolism and excretion of the alginate.

As previously mentioned enzymes and biological material can be entrapped within alginate particles. It is noted that positively charged proteins, enzymes and small drug molecules may compete with divalent cations for available COO⁻ pendant groups off of the alginate's backbone.¹⁸⁷ Such actions can result in the loss of protein/enzymatic activity. However, by including additives such as poly(acrylic acid) in the hydrogel Sundan et al. prevented deactivation of their protein TGA-β1.¹⁸⁰ the inclusion of the weak polyelectrolyte additive is thought to provide a preferential site for the TGA- β1 to bind within the gel and is able to cooperatively bind to any free cations that may lead to deactivation of the protein. Furthermore, Åsberg and Inganäs¹⁸⁸ showed how the inclusion of bovine serum albumin (BSA) protected GOx from denaturation by poly(4-vinylpyridine). However, the mechanism of this protective action is unknown.

Despite an alginate particle's surface pores being of a smaller order than its internal unwanted diffusional release of material through the pores can occur.¹⁸⁹⁻¹⁹¹ Such a release mechanism can be advantageous of implants and drug delivery, however, it is not ideal for the proposed enzyme loaded particles since release of the enzyme from the particle would result in a reduction in the particles ability to shift pH. Fortunately, the diffusion process is not merely molecular weight dependent but is also influenced by the net charge of the material. Cargo that has a net positive charge interacts with the negatively charged alginate thereby inhibiting diffusion. On the other hand, negatively charged material can be released more rapidly from the matrix. Loss through diffusional leaching is common during the gelation process.^{192,193} One method to overcome this is the use of aldehydes as crosslinking agents.¹⁹⁴⁻¹⁹⁶

1.8.5 Alginate modification

Alginate gels can be modified or combined with other polyelectrolytes to change a particles behaviour.¹⁹⁷ alginate can be made amphiphilic by the addition of pendant alkyl chains that form esters with the carboxylic acid groups along the polymers backbone. The resulting hydrogels have been used to encapsulate urease.¹⁹⁷ Another favoured method is the formation of polyelectrolyte complexes (PECs), these are formed by combining two polymers of opposite charge. This influences both the pore size and network complexity. Mixing of alginates with preformed polymer like eudragit,^{198,199} or natural polymers such as gum,¹⁹⁸ pectin,¹⁹³ and chitosan²⁰⁰ reduces the leaching of encapsulated material.

The PEC of the greatest interest is that which combines chitosan and alginate since it retains pH responsive behaviour.²⁰¹ Such complexes have been used in the controlled release of drugs and other substances.²⁰²⁻²⁰⁴ Properties of the alginate/chitosan capsules can be changed by not only the

molecular weight of the two polymers but also their composition. For alginate this is the ratio and ordering of G and M units whereas for chitosan it is the degree of deacylation.^{202–204}

1.9 Chitosan

1.9.1 Sources

Chitosan is derived from chitin the second most abundant naturally occurring polymer after cellulose. The primary source of chitin is from the exoskeleton of crustaceans. Common crustacean sources include crab and shrimp shells where it accounts for up to 70% of the organic material present. Chitin can also be obtained from molluscs, insects and fungi.

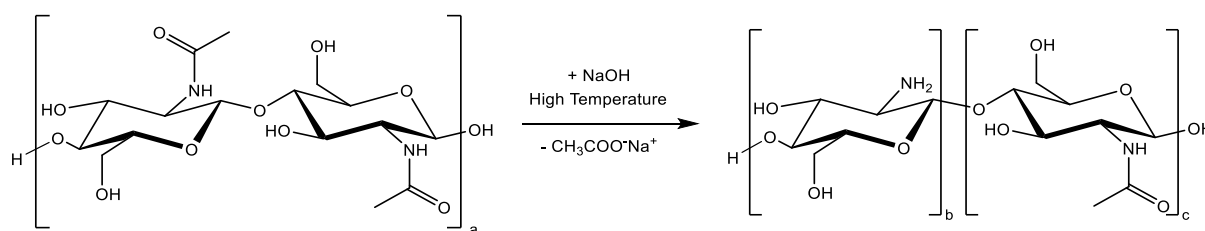


Figure 1-13 Reaction scheme for the conversion of chitin to chitosan by high temperature alkaline hydrolysis. This process hydrolyses a portion amide groups to amines and carboxylates

Chitin is separated from the shells by sequential alkali and acid treatment which demineralises and deproteinates the chitin. The resulting purified chitin is then deacylated by high temperature alkaline hydrolysis to form chitosan (Figure 1-13).

1.9.2 Chemical Structure

Chitosan is the term given to a series of linear copolymer polysaccharides. They are formed of β (1-4)-linked D-glucosamine and N-acetyl-D-glucosamine (Figure 1-13). The composition of the copolymer is described by the average molecular weight (Mw; typically 10-1,000 kDa) of the polymer and its degree of deacylation (DD; typically 70-95 %). The DD is proportion of the repeat units that contain primary amines, this is often given as a percentage.

1.9.3 Gelation

As with alginate (1.8.3) a chitosan hydrogel can be formed under relatively mild conditions, by the mixing of the polymer with an anionic crosslinking agent. Commonly a solution of chitosan (1-4 % w/v) is added dropwise to a crosslinking solution containing a polyanion such as tripolyphosphate.²⁰⁵ Electrostatic interactions between chitosan and the polyanion result the formation of ionic cross-linked networks. The formation of ionic cross-links is rapid and facile making it an attractive technique for the gelation of chitosan. However, the strength of the crosslinks formed is proportional to ionic strength of the polyanion.^{206,207} Tripolyphosphate's pK_a's are 0.9, 1.9, 5.3 and 7.7²⁰⁷ therefore the ionic

strength of the crosslinker is proportional to the pH. As such an ionically crosslinked chitosan gel would be relatively weak in acidic conditions since the anion would be in a neutral protonated form. The gel strength would increase as the solution becomes more basic and the crosslinking agent becomes deprotonated.

Alternatively, Chitosan can be covalently crosslinked.²⁰⁸ This produces a strong, stable gel since the crosslinks are permanent. However, common crosslinkers such as glutaraldehyde^{209–211} and glyoxal^{212,213} bind through the primary amines of chitosan to form an imine this can result in a reduction in the pH sensitivity of the gel particle since the new amide bond can be stabilised by resonance structures via a Schiff reaction.²¹⁴ The formation of chitosan particles by covalent crosslinks with dialdehydes is relatively simple. The most commonly reported method is by water in oil (W/O) emulsion.²¹⁵ The aqueous phase of which is typically made up of 1-4 % w/v chitosan in 1-4 % v/v acetic acid this is mixed with an oil phase containing a non-ionic surfactant to make a 10 % v/v W/O emulsion. The crosslinker can then be added either as a second water in oil emulsion or in a saturated oil solution.²¹⁵ The cross-linking process is relatively fast only taking a couple of hours at room temperature. An alternative crosslinking agent is genipen.²¹⁶ As with the dialdehydes, genipen crosslinks through the primary amine groups of chitosan. However, genipen is a less reactive crosslinking agent as such it takes longer for the crosslinks to form. Furthermore, genipen is biocompatible this makes gels crosslinked with genipen simpler to process for use in living cells than other crosslinking agents like dialdehydes which can bind to DNA making it unreadable.²¹⁷

1.9.4 Physical and Chemical Properties

As a weak polyelectrolyte chitosan exhibits some pH sensitivity through high quantity of amino groups the chain. These amino groups (pK_a 6.2)²¹⁸ make chitosan soluble at pH's lower than 6.5 due to the amines electrostatically repelling one another as they become charged through protonation.²¹⁹ When the pH is greater than 6.5 chitosan chains deprotonate and collapse making it insoluble. The process of hydration is enthalpically driven by the electrostatic interaction. Whereas, the dissolution of the chains is entropically driven since the water molecules that hydrate the chain lose intermolecular structure as the amino groups are deprotonated. This hydration at low pH has lead chitosan to be a commonly used delivery agent for chemical drugs into the stomach.²²⁰

Chitosan has been an approved food additive in Japan since 1986 and is commonly used in 'over-the-counter' formulations for slimming and lowering cholesterol.²²¹ Since it is believed that chitosan interacts binds to fats when in the intestine, due to their cationic nature and hydrophobicity at higher pH.²²¹ Chitosan is also biocompatible as such can be used for biomedical applications such as implants.²²¹ Additionally, implants formed of chitosan are biodegradable, since chitosan can be broken

down by human enzymes, in particular lysozyme. Which hydrolyses chitosan's sugar backbone at the C₁ and C₄ positions, breaking it down into its monomeric units which can then be expelled from the body.

Furthermore, commercially available chitosan has been shown to have good mucoadhesive properties.²²² This has been demonstrated by the in vitro binding of chitosan coated particles to porcine gastric mucosa.²²³ This property of bioadhesion could be utilised to create a site-specific drug mechanism throughout the gastro-intestinal tract, from the stomach^{223,224} to the small intestine.^{222,224,225} Lehr et al²²² have shown that swollen hydrogels form of chitosan can repeatedly bind with mucus with little loss in the adhesion strength. this suggests that adhesion occurs by the formation of hydrogen bonds between the positively charged chitosan and the negatively charged mucus, as well as ionic and electrostatic interactions.^{226,227} Work by He et al²²⁵ show that adhesion strength is greatest when the solution pH is either strongly or mildly acidic. Moreover, they showed that the number of adhering chitosan microparticles decreased as the crosslinking of chitosan increased. Schnürch et al²²⁸ showed a similar affect when decreasing the degree of deacylation of the chitosan. This suggests that the adhesion strength correlates with the number of free primary amine groups in the chitosan.

Since the mid 1990's chitosan has been seen as a potential absorption enhancer.²²⁹ Junginger et al.^{222,230,231} reported that chitosan can increase the absorption of peptide based drugs through mucosal epithelia by interacting with the cells tight junctions. It has been shown that this permeation enhancement occurs through the interaction of the positive charges along chitosan's backbone interacting with the cell membrane results in structural reorganisation the tight junction's proteins.²³² This permeation enhancement coupled with chitosan's mucoadhesive-ness can increase drug absorption at a specific site when compared to using a low molecular weight enhancer.²³³

1.9.5 Chitosan modification

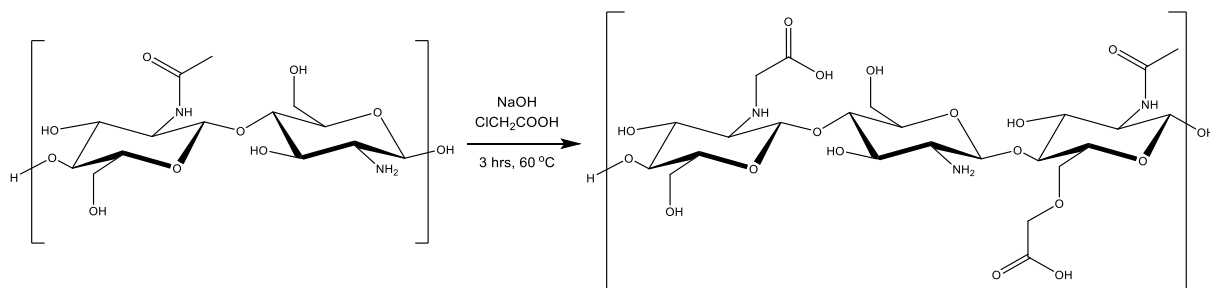


Figure 1-14 Reaction mechanism for the formation of N,O-carboxymethyl chitosan by a basic alkylation reaction.

The primary amine groups of chitosan allow chemical modifications to the polymer through the formation of covalent bonds to be made very simply. The mucoadhesive properties of chitosan can be

improved by either the addition of thiol groups²³⁴ or the trimethylation²³⁵ of chitosan. However, of greater interest to the scope of this thesis is the formation of carboxymethyl chitosan (Figure 1-14), which exhibits enhanced pH responsive behaviour.^{236,237} By introducing -CH₂OOH groups to hydroxyl groups along the polymer backbone chitosan becomes an amphoteric polyelectrolyte. Hydrogels of carboxymethyl chitosan have been formed and used to study the release characteristics of a model protein drug (BSA).²³⁶ Furthermore, it was shown that the particles were smallest when the pH was equal to the isoelectric point (IEP). The particles would then swell as the pH deviated from the IEP, with the degree of swelling proportionally increasing as the deviation increased. By increasing the degree of deacylation particles polyampholytic nature became more cationic. Conversely increasing the degree of substitution made the particles more anionic. Additionally, it has been reported that carboxymethyl chitosan is more susceptible to biodegradation than chitosan.¹⁸⁶

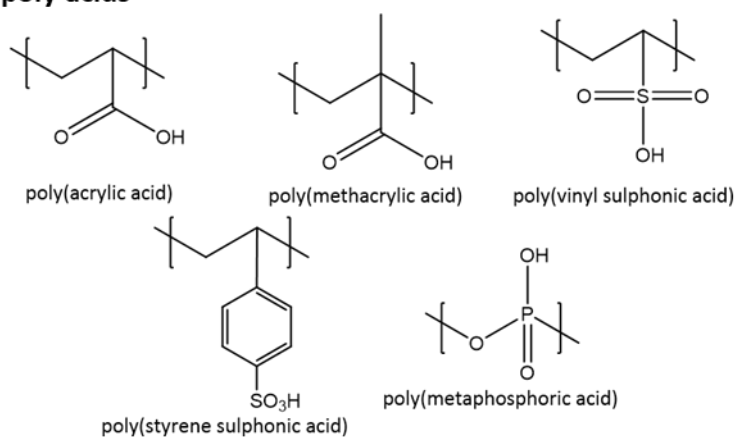
As with alginate, chitosan can be incorporated into PECs. The mixing of chitosan with alginate has been discussed previously (section 1.8.5). However, PECs can also be formed by mixing chitosan with pectin,^{238,239} carrageenan,²⁴⁰ and collagen.²⁴¹ Complexes of chitosan and carrageenan are often used as a comparative drug delivery matrix to chitosan-alginate complexes.²⁴⁰ Since alginate and carrageenan are both high molecular weight, anionic polymers. However, the use of carrageenan resulted in a more rapid release of its diltiazem clorhydrate cargo due to carrageenan holding more water by weight than alginate.²⁴⁰

1.10 pH Responsive Polymers

pH responsive polymers exhibit a physical volumetric response to their environment. Commonly the polymers are polyelectrolytes based on poly acids/bases and their derivatives. All of these have ionisable pendent groups which accept and donate protons. The degree of ionisation is linked to the environmental pH dramatically shifting when the pH corresponds to the polymers pK_a. This rapid change in net charge instigates a shift in the polymer chains' hydrodynamic volume. Poly acids (Figure 1-15 A)) act as proton acceptors at low pH, however, at neutral and high pH they donate the protons of their pendent groups, which become negatively charged and repel one another causing the polymer to swell.²⁴² Whereas, polybases become charged and expand at low pH (Figure 1-16).²⁴³

The collapsed state occurs when the polymers are in a non-ionised state. This is because the polymer hydrophobic making its interactions between it and the aqueous bulk of the solution unfavourable. The polymer remains in a hyper-coiled state to minimise the intrafacial energy between the polymer and the water. This entropically driven action is aided by attractive intramolecular forces of the polymer.

A) poly acids



B) poly bases

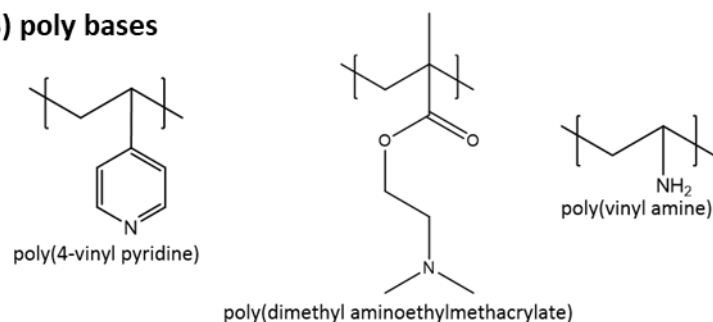


Figure 1-15 examples of poly acids (A) and poly bases (B) which are weak enough acids/bases respectively to be utilised in smart response systems.

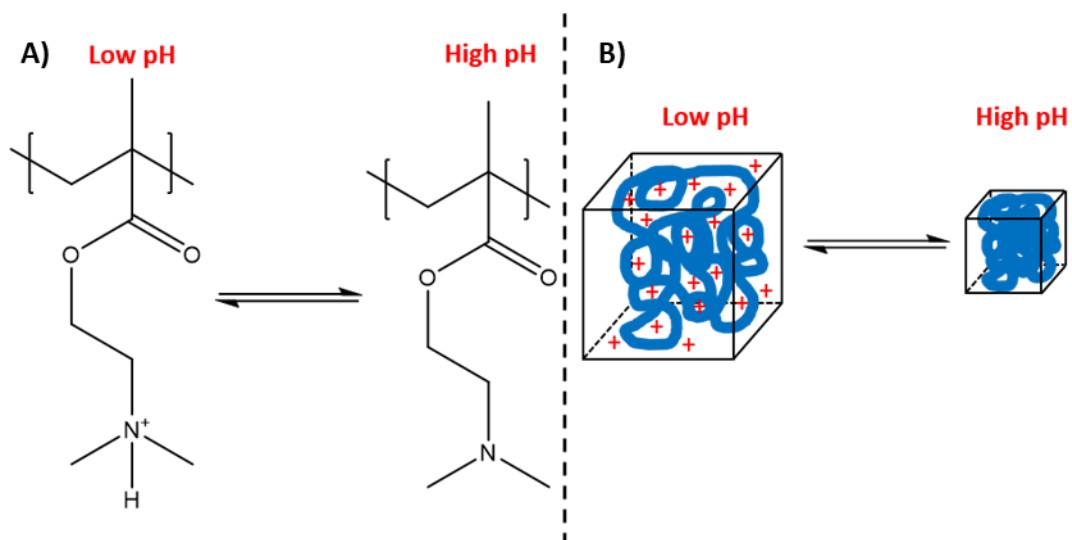


Figure 1-16 A) shows the reversible ionisation of poly(dimethyl aminoethylmethacrylate) with pH. An increase in the pH causes protonation of the tertiary amine on the pendant group. Formation of these ions cause electrostatic repulsion which initiates volumetric changes of the polymer (A).

The collapsed state occurs when the polymers are in a non-ionised state. This is because the polymer is hydrophobic making its interactions between it and the aqueous bulk of the solution unfavourable. The polymer remains in a hyper-coiled state to minimise the interfacial energy between the polymer and the water. This entropically driven action is aided by attractive intramolecular forces of the polymer.

The polymer enters the expanded state when the polymers pendant groups become ionised. This leads to electrostatic repulsions along the polymer the polymer chain. Formation of such ions makes the polymer hydrophilic increasing the polymers compatibility with water thus allowing the polymer to expand. This expansion is enthalpically driven, in contrast the collapse is of a pH responsive polymer is entropically driven. This is due to swollen polymers ionically charged backbone imposing order on the hydrating water, whereas the collapsed particle is uncharged. Thereby, imparting no constraints the bulk aqueous phase.

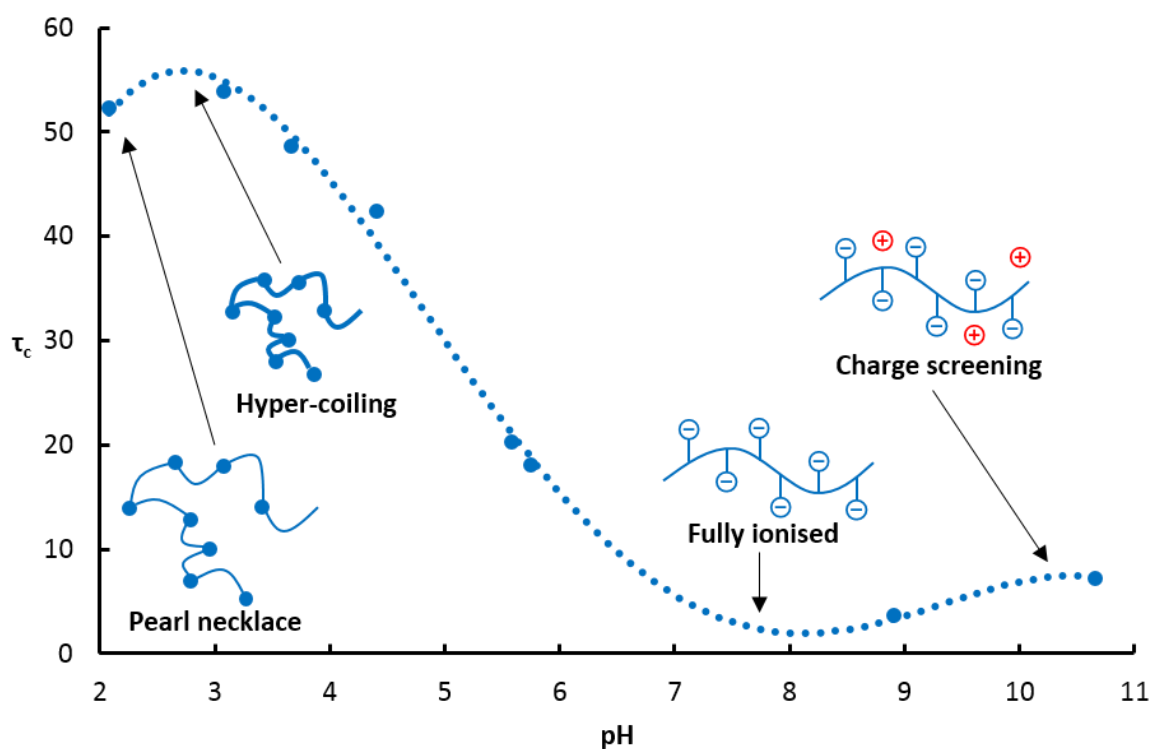


Figure 1-17 time resolve anisotropy measurements of poly(methacrylic acid) copolymerised with 1 % acenaphthylene results in the fluorescence decay (τ_c) which is plotted against pH (data from soutar and swanson ²⁴⁴).

When a weak acid is titrated with a strong base (or vice versa) the midpoint to equivalence (i.e. transition from protonated to ionised acid) occurs when the pH is equal to the pK_a . The pK_a of methacrylic acid (MAA) is 4.65 at 20 °C.²⁴⁵ Although the pK_a of a monomer is a good indicator to its polymer, the actual pK_a depends on several contributing factors including comonomers, counter ions

and polymer architecture, not only linear or branched but the degree of mixing of comonomers along the backbone (homopolymer < block < statistical < alternating).

When the pendent groups of polyelectrolytes are uncharged the polymer is hydrophobic. Placed in water the polymer chain collapse in on itself to form a 'pearl necklace'.²⁴⁶ This is where the polymers backbone forms globules (pearls) of polymer minimising the unfavourable interactions between the polymer and the solvent. These globules are connected by segments of coiled polymer chain (Figure 1-17).²⁴⁷ Initially a theory, evidence from light scattering²⁴⁸ (radius of gyration of the coil), X-ray scattering (globule size)²⁴⁹, and NMR²⁴⁶ studies gives physical validity to this effect.

Fluorescence studies by Soutar and Swanson²⁴⁴ on poly(methacrylic acid) (PMAA) labelled with 1% acenaphthylene in aqueous solutions, highlighted this anomalous behaviour of PMAA when titrated with base (Figure 1-17). For comparison poly(acrylic acid) (PAA) chains smoothly expand with increasing pH.²⁵⁰ The string of pearls that PMAA forms initially contracts (by hypercoiling), as the pH increases upto pH 3. Beyond which the degree of neutralisation reaches a critical point, at which the polymer undergoes rapid swelling due to the formation of anions along the polymer which repel one another. This expansion continues until the polymer is fully ionised. However, once this is achieved if pH continues to increase the hydrodynamic radius of the polymer decreases this is due to the increased concentration of cations in solution, which when in close proximity with the polymer chain screen the negative charge of the pendent groups from one another, thereby reducing the repulsion.

Crosslinking of pH-sensitive polymers forms hydrogels. Such pH-sensitive polymeric hydrogels have been highlighted as a potential drug carrier since 1955.²⁵¹ However, it was not until 1996 that a pH responsive nanogel was developed as a biomedical drug carrier.²⁵² Typically pH-responsive hydrogels contain one or more of the following; poly(methacrylic acid) (PMAA), poly[(2-dimethylaminoethyl) methacrylate] PDMA, poly(acrylic acid) PAA, chitosan. Peppas et al²⁵³, synthesised a nanoparticle hydrogel of poly(methacrylic acid-grafted-ethylene glycol) for oral delivery of the protein chemotherapeutic interferon alpha. By judiciously combining the a chemotherapeutic with a complementary hydrogel they were able to improve the agents permeation through model epithelium gastrointestinal cells.

Islam, Tan, Kwok and Tam²⁵⁴ recently probed the hydrophobic drug release from pH responsive microgels with different glass transition temperatures (T_g). Using methacrylic acid (MAA) based hydrogels they determined that drug release was dependent upon both chain relaxation and diffusion. With increasing T_g drug release exhibited greater chain relaxation dependence. Furthermore, drug release was diffusion dominated in swollen low T_g microgels.

1.10.1 pH-Responsive Hydrogel Synthesis

Hydrogels are polymer networks whose crosslinks allow the polymer to swell to a physical limit at which point they hold their 3-dimensional structure.²⁵⁵ In this way they differ from a gel which describes an equilibrium state of a polymer network that is entangled and swollen to an equilibrium. Exceeding the equilibrium causes dissolution as the entanglements break apart.²⁵⁶ The polymer chains of a hydrogel are commonly covalently crosslinked by co-polymerising the pH responsive polymer with a multifunctional monomer such as divinyl benzene (DVB)²⁵⁷, *N, N'*-methylenebisacrylamide (BA)²⁵⁸ or tetraethylene glycol dimethacrylate (TEGDMA).²⁰⁶ However, pre-formed polymer chains can also be used to form a hydrogel by either crosslinking the chains with low molecular weight crosslinking agents such as glutaraldehyde²⁵⁹, genipen²⁶⁰ and ethylenediaminetetraacetic acid (EDTA).²²⁸ Alternatively interpenetrating networks of complementary polymers can be formed by single or two step reactions.

Dispersion, emulsion and precipitation²⁵⁷ polymerisations are typically employed in to synthesise hydrogels for drug delivery. Precipitation reactions typically result in a narrow distribution of particles < 10 µm diameter.²⁵⁷ This is due to the reaction mechanism, the monomers are soluble in the reaction solvent. However, as the polymer proceeds the propagating polymer chain becomes insoluble dropping out of solution. the upper size limit is dictated by the colloidal stability of the growing particles. Dispersion polymerisations are similar to precipitation polymerisations, the monomer is soluble and the polymer insoluble.²⁶¹ However, in a dispersion the polymerisation predominantly occurs within the particle rather than the bulk solvent phase as it is with precipitation reactions.

Emulsion polymerisation is the most commonly used method of hydrogel synthesis due to its flexibility in solvent, monomer and narrow particle size distribution.^{262,263} Typically oil soluble monomers are emulsified in water and the presence of a surfactant, however, the system can be inverted to form hydrophilic polymer particles in a continuous oil phase. Emulsion polymerisations utilise monomers that are immiscible with the bulk solvent, the resulting polymer is also insoluble in the bulk phase. The initiator freely partitions from one phase to another.

Surfactants are also required in emulsion polymerisations to stabilise the droplets as the polymerisation proceeds, these can be anionic (sodium dodecyl sulphate)²⁶⁴, cationic (lauryl dimethyl amine oxide)²⁶¹, zwitterionic²⁶¹ or non-ionic such as polysorbates like tween™ or span™.^{265,266} All surfactants have water soluble portions formed of either an ionic head or hydrophilic group and an oil soluble portion often an alkyl chain. This causes the surfactant to sit at the water oil interface of the emulsion. Ionic surfactant's charged head groups stabilise the interface through electrostatic interactions whereas non-ionic surfactants stabilise by sterically crowding the interface.²⁶¹

Emulsion polymerisation is high yielding giving rise to long chained hydrogels in a relatively short time frame. Typical particle's diameter vary between 150 nm and 100 μ m depending on the degree of emulsification and amount of surfactant used.²⁶¹

Recent advances in polymerisation-induced self-assembly (PISA) using reversible addition fragmentation chain-transfer polymerisation (RAFT) has utilised pH responsive macro-RAFT agents formed from either acrylic acid or poly(dimethylaminoethyl methacrylate) (PDMAEMA) to act as a stabilising hydrophilic polymer in surfactant-free emulsion polymerisations.²⁶⁷

1.10.2 Applications of pH responsive polymers

The use of pH responsive polymers has been highlighted in the areas of biotechnology, nanotechnology, chromatography, membranes and coatings.^{268,269} In particular focus has been on gene delivery systems,²⁷⁰ controlled drug release,²⁷¹ drug carriers,²⁷⁰⁻²⁷² biosensors,^{270,272} stabilizers²⁶⁷ and viscosity modifiers.²⁶⁷ With the exception of the gastro-intestinal tract physiological pH values of extracellular fluid around healthy tissues and blood is kept constant at pH 7.4 and the intracellular pH is maintained at 7.2.^{273,274} Moreover, the measured extracellular pH of most tumours is lower than that of healthy cells ranging between pH 6.5 and 7.2.^{275,276} This difference in pH has driven the development of responsive, targeted drug delivery.

pH initiated drug release from pH responsive polymers occurs through one of two methods. Firstly, and most simply hydrogels that exhibit swelling/deswelling behaviour or degradation with shifting pH enable the leaching of their cargo. Alternatively a cargo can be immobilised onto a polymeric structure through pH-labile bonds. As the pH decreases the drug is cleaved form the backbone enabling the drug to diffuse out of the polymeric matrices. Polymeric structures can be covalently bound to its cargo through pH-labile bounds such as; hydrazine^{277,278}, acetal/ketal²⁷⁹, cis-acotiny²⁸⁰, imine²⁸¹ and others.²⁸²

pH-responsive micelles and hydrogels can be used to store and release of not only drug compounds but also; proteins, genes and enzymes. Furthermore, multiple compounds can be immobilised within a pH-responsive hydrogel. Hydrogels formed of pH responsive polymers have proven very promising as a method of drug delivery since they have inherently high loading capacities, high stability and undergo a sharp transitional response to changes in environmental pH.²⁸³ The Kabanov group²⁸⁴ have reported loading of < 30 % w/w of a poly(ethylene glycol)-polyethyleneimine nanogel with antisense phosphorothioate oligonucleotides.

A pH responsive nanogel of glycol chitosan (GCS) grafted with 3-diethylaminopropyl (DEAP), demonstrated pH dependent dissolution.²⁸⁵ At physiological pH (7.4) the hydrogel self-assembled to

give nano-structures with a hydrophobic DEAP core and hydrophilic GCS shell. These structures were loaded with the chemotherapeutic doxorubicin (DOX; 78 % w/w of polymer). When the environment pH was lowered to 6.8 the DEAP becomes partially ionised, causing a change in structure and enabling drug-release. Decreasing the pH further to 6.0 results in full ionisation of the polymer and dissolution of the polymer.

Another novel, multifunctional nanoogel was developed by Wu, Shen, Gai et al..²⁸⁶ A magnetic core of silver coated nickel had a shell of pH responsive poly(ethylene glycol-co-methacrylic acid) grafted to it. The silver coating enables fluorescent imaging of the nanoparticles. The swelling of the pH responsive grafts mediates the particles magnetic susceptibility of the gels. Furthermore, these hydrogels were loaded with the anticancer drug 5-fluorouracil to demonstrate pH responsive drug delivery.

2. Experimental Methods and Materials

2.1 Chemicals

All chemicals were purchased from Sigma Aldrich (Gillingham, UK), were of analytical grade and used as received unless stated otherwise.

Calibration buffers tablets, phthalate (pH 4.00), phosphate (pH 7.00) and borate (pH 9.20) purchased from Alfa Aesar (Heysham, UK). Acids, conjugate bases and salts used for titrations are listed below, phosphoric acid, trisodium phosphate, hydrochloric acid, ammonium hydroxide, glucono- δ -lactone, citric acid (Alfa Aesar, Heysham, UK) trisodium citrate, 2-amino-2-methylpropan-1-ol (AMP), sodium hydroxide (Alfa Aesar, Heysham, UK) and potassium chloride (Alfa Aesar, Heysham, UK).

Further chemicals used solely in the synthesis of particles; sodium alginate, calcium chloride, ferrous magnetite (<5 μm diameter), *N,N,N',N'*-tetramethylenediamine (TEMED), ammonium persulfate (APS), xylene, chitosan (medium molecular weight (190-310 kDa); 82 % deacylted), glutaraldehyde, ethanol and *N,N'*-methylenebisacrylamide (BA; Thermo Fischer Scientific, Loughborough, UK). Other chemicals for particle synthesis namely; methacrylic acid, petroleum ether 60/80 and span 80 were all purchased from Alfa Aesar (Heysham, UK). Signal generation utilised glucose oxidase from *Aspergillus niger* (GOx; activity 19290 units g^{-1}) with glucose as the substrate. The ratiometric dye SNARF 4F 5- (and 6-) carboxylic acid was purchased from Thermo Fischer Scientific (Loughborough, UK).

2.2 Electrometric pH Measurements

The electrometric pH measurements were made using a micro pH combination electrode (Sigma Aldrich, Gillingham, UK). When not in use the electrode was stored in a 3 M potassium chloride solution. The electrode was rinsed with deionised water prior to and after being in any solution. The probe was fitted with a BNC (Bayonet Neill-Concelman) connector and is connected to a NI-9025 module in an NI cDAQ-9172 cradle (both purchased from National Instruments). Custom programs written in LabView enables pH measurements to be determined from the voltage. The LabView script written for aqueous acid base titrations allowed controlled addition of the titrant through automation of an Aladdin AL-2000 syringe pump in unision with pH measurement being taken.

2.2.1 pH Electrode Calibration

The electrode was placed in a buffer of known pH, upon reaching thermal equilibrium the voltage was logged 6 times a second for 60 seconds, from this an average and standard error could be determined. This procedure was repeated for three buffers all of know pH; phthalate (pH 4.0), phosphate (pH 7.0) and borate (pH 9.2). Plotting of the pH as a function of voltage enabled a calibration plot to be drawn. A calibration plot would be generated immediately preceding any titration.

2.2.2 Aqueous Acid Base Titrations

Titrations were carried out on various acids and bases. In a typical titration 40 cm³ of the analyte (0.01 mol dm⁻³) was placed in a reaction vessel along with a magnetic flea and pH electrode. The analyte was stirred at 300 rpm and left for typically 1 minute to reach thermal equilibrium. The titrant (40 cm³; 0.02-0.04 mol dm⁻³) was added by syringe pump at a rate of 40 cm³ hr⁻¹. pH measurements were logged every second starting 1 minute before the titration and continuing for 5 minutes after the syringe pump had ceased.

2.2.3 Glucose oxidase in bulk phase titrations

In a typical experiment an aqueous solution of glucose (9 cm³; 19.3-0.193 mmol) and base (typically sodium hydroxide (40 μmol)) were added to a reaction vessel fitted a pH electrode and magnetic flea. The reaction mixture was stirred at 300 RPM and left for one minute to reach thermal equilibrium. An aliquot of freshly made glucose oxidase solution (0.5-5 mg cm⁻³; in deionised water) was added to the reaction mixture and the change in pH was measured. pH measurements were logged every second starting one minute prior to the addition of the glucose oxidase solution and typically for 180-240 minutes after addition.

2.3 Particle Synthesis

2.3.1 Alginate Particles

Alginate particles were synthesised by the facile extrusion-dripping method. In a typical reaction a sodium alginate solution (3 % w/w) was prepared from sodium alginate in demineralised water (15 Ω cm) and stirred for 24 hours at room temperature. the resulting solution could then be used immediately or stored at 5 °C for up to 30 days. A fresh glucose oxidase solution (2 mg cm⁻³) was prepared by dissolving glucose oxidase demineralised water, a 0.375 cm³ aliquot was added to a portion of the sodium alginate solution (2.0 cm³) along with a ferrous magnetite solution (< 5 μm diameter; 0.03 % w/w; 0.625 cm³) and aqueous SNARF-4F (1 mg cm⁻³; 0.081 cm³). The resulting pre-gel solution mixed and loaded into 6, 1 ml syringes, the syringes were stored for up on month at -18 °C. The syringes loaded with the pre-gel solution were allowed to warm up to room temperature for 20 minutes prior to gelation.

A fresh solution of CaCl₂ (10 % w/w) was prepared from calcium chloride dihydrate. The pre-gel solution was extruded from the syringe through a needle (32G) using a syringe pump (Aladdin AL1000; 0.35 ml min⁻¹). The pre-gel dripped from the syringe tip into the crosslinking CaCl₂ solution, creating gel particles approximately 2 mm in diameter. The particles were gently mixed in the crosslinking

solution for 10 minutes to reduce the risk of enzyme leaching.⁷⁸ The particles were separated by filtration and washed with demineralised water prior to immediate use.

The pre-gel was altered for characterisation studies (non-ratiometric) of alginate particles, such as size measurements and determining the proportion of ferrous magnetite. The ratiometric dye carboxy-SNARF 4F, and glucose oxidase was left out of the pre-gel mixture. In such studies rhodamine 6G (alfa aesar; 0.01 % w/w of pre-gel) was added to the pre-gel solution to enhance the contrast between the resulting particle and the bulk aqueous phase. Typical proportions of solutions in the pre-gel are summarised in the table below.

Table 1 summary of stock solutions and typical proportions for sodium alginate pre-gel solutions

Ratiometric studies pre-gel		Characterisation pre-gel	
Alginate solution (3 % w/w)	2 cm ³	Alginate solution (3 % w/w)	4 cm ³
Magnetite solution (0.03 % w/w)	0.625 cm ³	Magnetite (0.03 % w/w) + Rhodamine 6G (0.03 % w/w) solution	0-2 cm ³
Glucose oxidase solution (2 mg cm⁻³)	0.375 cm ³	Rhodamine 6G solution (2 mg cm⁻³)	0-2 cm ³
SNARF-4F solution (1 mg cm⁻³)	0.081 cm ³		

2.3.2 Chitosan Particles

Chitosan particles were formed by a 10 % v/v water in oil emulsion. A stock solution of glutaraldehyde saturated toluene (GST) was prepared by mixing 1:1 glutaraldehyde (25 % w/v) with toluene stirred at 600 RPM overnight. The resulting mixture was stored at -18 °C for up to 3 months. GST would be brought up to room temperature 1 hour prior to use. Stock chitosan solution (2 % w/v) was prepared by dissolving chitosan (molecular weight 190-310 kDa; 82 % deacylated; 3 g) in acetic acid solution (3 % v/v; 100 cm³) by stirring at 300 RPM for 24 hours. The resulting chitosan solution was stored for up to 1 month at 5 °C. The oil phase consisted of hexane and paraffin oil (volumetric ratio 5:7) and span 80 (1 % v/v of oil phase).

In a typical reaction (300-800 RPM) particle synthesis, 1 cm³ of the chitosan solution was added to the oil phase (9 cm³). The reaction mixture was stirred using a cross shaped magnetic flea and a stirrer hot plate (IKA RCT basic) at a given stir rate for 30 minutes. the stir rate was then lowered to 300 RPM and

GST (2 cm^3) was added over the course of one hour in four equal aliquots. The reaction was then left stirring for 2 hours. The resulting particles were separated by vacuum filtration using a Buchner funnel. They were then washed three times with hexane and then demineralised water.

2.3.3 Poly(methacrylic acid) particles

Poly(methacrylic acid) particles were synthesised by a water-in-oil free-radical emulsion polymerisation employing a thermal redox initiator using the method described by Zhang et al.²⁵⁸ In a typical reaction the bulk phase of xylene (100 cm^3) and span 80 (0.32 g; 0.4 % w/w of bulk phase) were homogenised and purged with nitrogen for 1 hour in 250 cm^3 round bottomed flask fitted with a magnetic flea, over a stirrer hotplate (RPM 400). The reagents of the aqueous phase; methacrylic acid (2 cm^3 ; 29 mmol), sodium hydroxide (8 cm^3 ; 1.56 mol dm^{-3}), *N, N'*-methylenebisacrylamide (45 mg; 0.29 mmol), rhodamine 6G (0.20 g) and ammonium persulfate (APS; 108 mg; 0.47 mmol) were mixed in a separate vessel. Before being added to the continuous phase and purged for a further 20 minutes. Finally *N, N, N', N'*-tetramethylethylenediamine (TEMED; 0.5 cm^3) was added to the reaction mixture, which was then held at $40 \text{ }^\circ\text{C}$ for 2 hours, whilst maintaining the stir rate (400 RPM). The resulting particles were separated by filtration and washed 3 times with hexane and acetic acid (0.1 mol dm^{-3}).

2.4 Ratiometric imaging

2.4.1 Experimental setup

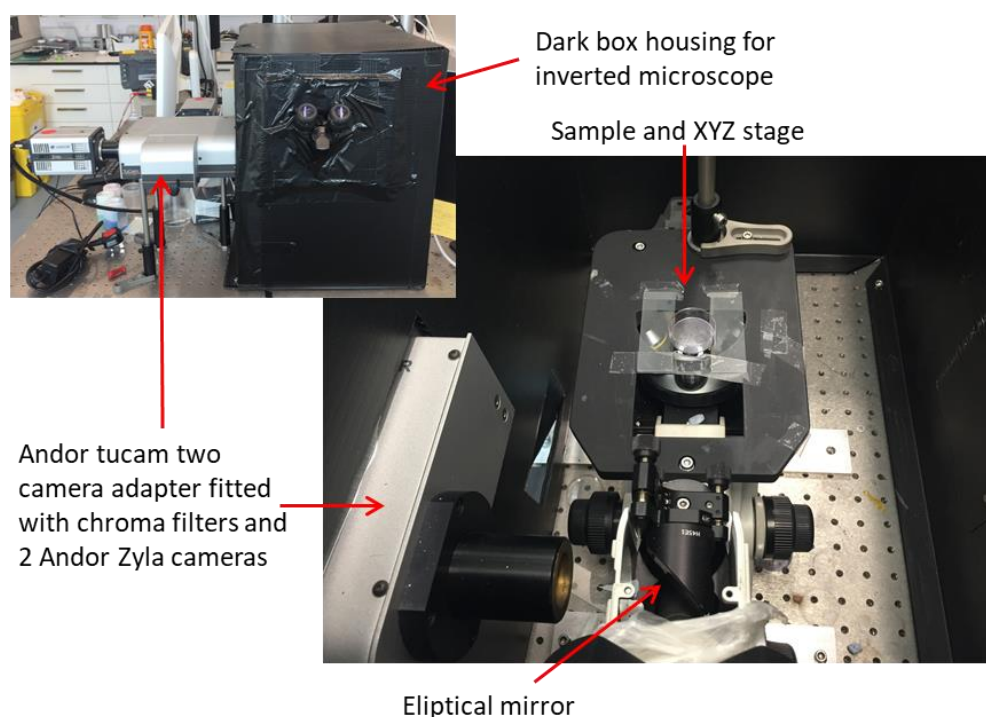


Figure 2-1 images of the ratiometric microscopy imaging setup.

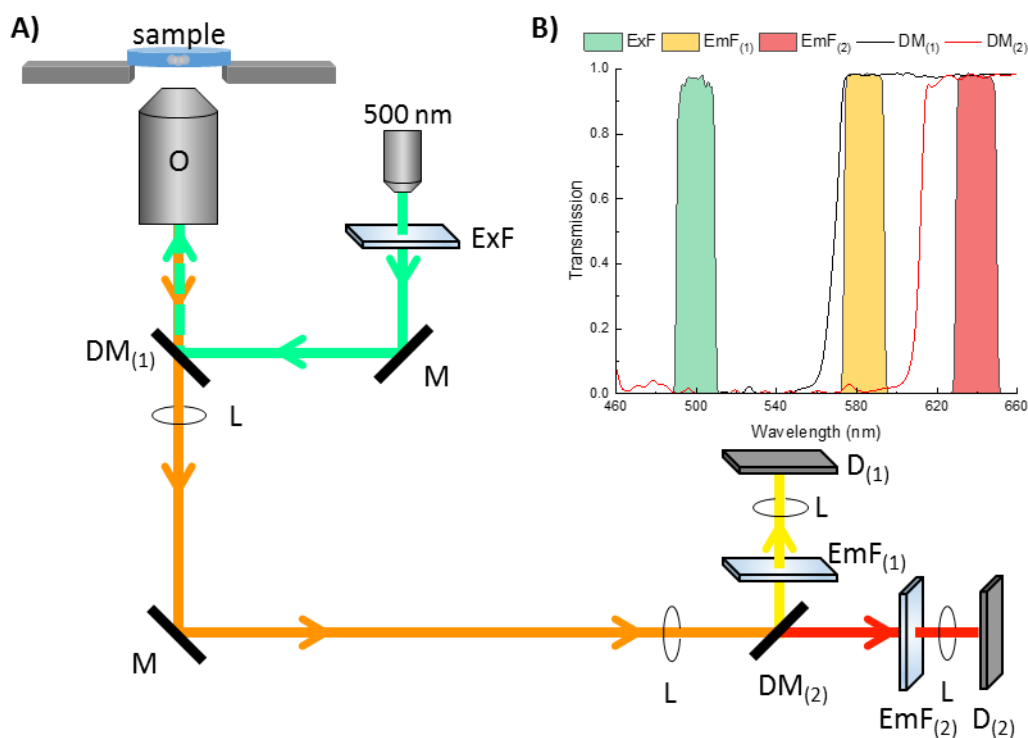


Figure 2-2 A) inverted microscope setup for ratiometric imaging, where; $D_{(n)}$ camera n 's detector; $DM_{(n)}$, dichroic mirror n ; $EmF_{(n)}$, emission filter n ; ExF , excitation filter; L , lens; M , mirror; O , objective. B) transmission spectra for the filter sets and dichroic mirrors used for carboxy-SNARF-4F, where; ExF , chroma ET500/20x; $EmF_{(1)}$, chroma ET585/20m $EmF_{(2)}$, chroma ET640/20m; $DM_{(1)}$, chroma T70lpxr; $DM_{(2)}$, chroma T612lpxr-UF1.

Figure 2-1 and Figure 2-2 A) shows the set up for ratiometric imaging in the experiments. Light from a blue-green LED (Green-Cyan laser; RS-online) passed through an excitation filter (500±10 nm; ET500/20x; Chroma Technology). The light was directed into an air immersion objective (1x; NA 0.04; Nikon) of an inverted microscope (Nikon Eclipse Inverted Microscope) by a dichroic mirror (T70lpxr; Chroma Technology). The fluorescent emission from the sample was collected by the same objective and transmitted through the dichroic mirror and by way of another mirror into a two-camera imaging adapter (Tucam; andor). In the adapter the beam was split by a dichroic mirror (T612lpxr-UF1; Chroma Technology) allowing two-channel detection by refocusing the beams through lenses onto the active areas of two cameras (zyla 5.5 mega pixel camera; employing 4x4 pixel binning; Field of View 540 x 640 pixels, 14.46 x 17.13 mm with the x 1 objective; exposure 4 s; Andor). Two emission filters were placed in front of the cameras (ET585/20m and ET640/20m; Chroma Technologies). This further discriminates the fluorescence emission, and selectively collects the shorter wavelength of the emission spectrum (due to the protonated form of carboxy-SNARF-4F) on camera 1's detector. The longer wavelength of the emission spectrum (due to the deprotonated form of carboxy-SNARF-4F) on camera 2's detector. Data acquisition was performed on a PC with a programme written in LabView by Dr Dan Toolan.

2.4.2 Experimental Procedure

Stock solutions of glucose (0.01 mol dm^{-3}) and sodium hydroxide (1.0 mol dm^{-3}) were prepared in demineralised water ($15 \text{ } \Omega \text{ cm}$). The reaction vessel was a Perspex petri dish (Thermoscientific Diameter 35 mm) and filled with 2.5 cm^3 of the stock glucose solution, carboxy-SNARF-4F solution (0.064 cm^3 ; 1 mg cm^{-3}) and mixed. The pH was adjusted to near neutral pH (7.0-7.4) using the sodium hydroxide solution. 1-25 of newly synthesised glucose oxidase loaded alginate particles were placed in the reaction vessel. A neodymium magnet and 16G needle were used to move the particles into clusters. The reaction vessel was placed on the viewing platform of the inverted microscope, the particles were held in place by the neodymium magnet and surface contact of the particle with the water-air interface of the reaction mixture. The reaction was imaged with a 4 s exposure with the ratiometric setup for up to 3 hours, employing 4x4 pixel binning.

2.4.3 Calibration Experimental

An aqueous solution of sodium hydroxide (5 cm^3 ; 100 mmol dm^{-3}) was mixed with carboxy-SNARF (0.128 cm^3 ; 1 mg cm^{-3}). A second solution of hydrochloric acid (3.0 cm^3 ; 100 mmol dm^{-3}) was mixed with carboxy-SNARF (0.077 cm^3 ; 1 mg cm^{-3}). A 2.5 cm^3 aliquot of the hydroxide solution was placed in a reaction vessel with fitted with a calibrated micro-pH electrode. A length of peristaltic tubing (1.02 mm internal diameter (ID)) led from the main reaction vessel through a peristaltic pump (Watson Marlow 101U; 32 RPM) to a glass capillary (World Precision Instruments Inc.; 100 mm Length; 0.52 mm ID; 1.00 mm external diameter (ED)). Which was secured to the XYZ stage of the inverted microscope of the ratiometric setup. A second length of tubing led back from the capillary tube to the reaction vessel. The solution was cycled through the peristaltic pump (flow rate $2.5 \text{ cm}^3 \text{ min}^{-1}$). The pH was adjusted with small aliquots of the HCl solution ($<0.1 \text{ cm}^3$), until $\text{pH} < 4$. After each addition of acid the reaction was left for 5 minutes to allow the pH to equilibrate. The pH was then increased by the addition of the remaining NaOH solution in small aliquots ($<0.1 \text{ cm}^3$). The pH was recorded with the micro probe through a programme written in LabView. The capillary tube was imaged (0.25 s^{-1} ; 4x4 binning) throughout the reaction. the images were combined by a programme written with LabView to give a ratiometric image. The resulting ratio from the ratiometric image was plotted against the pH value from the electrode. The resulting plot was fitted with the rearranged Grynkiewicz equation (Eq. (2.2)) or the modified concentration fraction equation:

$$R = \frac{R_{max} 10^{\frac{\text{pH} - \text{p}K_a - \log\left(\frac{I_a}{I_b}\right)}{c}} + R_{min}}{1 + 10^{\frac{\text{pH} - \text{p}K_a - \log\left(\frac{I_a}{I_b}\right)}{c}}} \quad (2.2)$$

$$R = \alpha_1(R_{max} - R_{min}) + R_{min} = \frac{10^{-pK_a}(R_{max} - R_{min})}{10^{-pH} + 10^{-pK_a}} + R_{min} \quad (2.3)$$

Where; R is the ratio of the emission intensities for the two images; R_{max} and R_{min} are the upper and lower limits of the ratio; I_a/I_b is the intensity ratio for the acidic and basic species of carboxy-SNARF-4F at 640 nm; C is a constant that that indicates the relationship between the ratio (R) and pH, tends to be around -1.

2.5 Optical microscopy

2.5.1 Experimental

Optical microscopy was performed with a Cannon EOS 5Ds fitted with a MP-E 65 mm f/2.8 1-5x macro lens. The camera was connected to a computer running EOS utility, this enabled live imaging. Analysis of the images were carried out using ImageJ.

3. Glucose oxidase in the bulk phase

3.1 Overview

In this chapter we set out to find a simple way of observing glucose oxidase activity as it was believed that auto catalytic behaviour of glucose oxidase effects the rate of pH change. To do this we set out to design a buffer system that when titrated gave a near linear progression curve between pH 8 and 3. Once several systems had been developed the action of glucose oxidase in solution was looked at. It was found that the rate limiting step of pH change was not the action of glucose oxidase but the subsequent ester hydrolysis.

3.2 Introduction

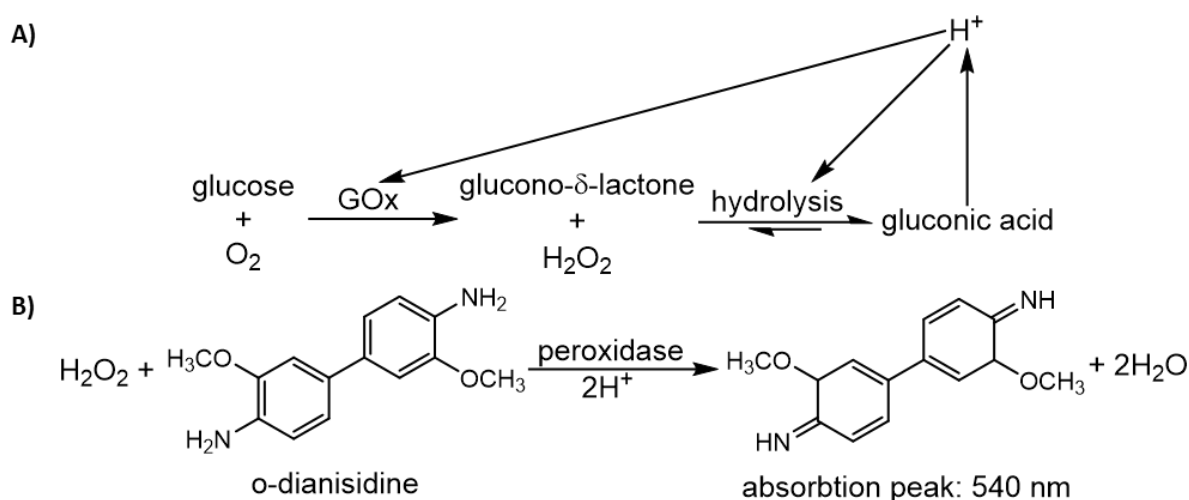


Figure 3-1 A) reaction scheme of glucose oxidase catalysed oxidation of glucose to glucono- δ -lactone and hydrogen peroxide, the former undergoes ester hydrolysis to form gluconic acid, resulting in a shift in pH. Any change in pH initiates a feedback loop on both the oxidation and hydrolysis steps. B) Reaction scheme of a typical glucose oxidase activity kit, hydrogen peroxide is reduced by peroxidase in the presence of acid and an electron donor (o-dianisidine). The oxidised electron donor has an absorption peak at 540 nm which can be used by UV-vis spectroscopy to determine enzymatic activity.

The activity of GOx is commonly determined by UV-vis spectroscopy. A by-product of the oxidation process is hydrogen peroxide, which when oxidised by peroxidase in the presence of o-dianisidine (an electron donor) and acid results in the formation of water and dianisidine quinonediimine which has an absorption peak at 540 nm (Figure 3-1 B).²⁸⁷ This reaction is carried out at a static pH in presence of a buffer like sodium acetate. Since the proposed signalling molecule for our quorum sensing system is H⁺ which is produced by the oxidation of glucose by glucose oxidase to form glucono-d-lactone and the subsequent ester hydrolysis to gluconic acid. Due to [H⁺] affecting both enzyme activity and ester hydrolysis (Figure 3-1 A) conventional GOx activity assays (Figure 3-1 B) become less useful as they would only tell half the story.

Buffers are often used when wishing to maintain a stable pH and probe enzyme kinetics.^{288,289} A typical monoprotic buffer has a buffer range of $pK_a \pm 1$ pH unit. However, enzymes function over a much wider pH range. Mammalian enzymes can be exposed to a broad range of pH (typical physiological range; $6.1 \leq pH \leq 10.4$).²⁹⁰ Furthermore, enzymes such as GOx (Figure 3-1 A)) and urease²⁹¹ demonstrate a broad pH dependent rate bell curve, maximum activity at pH 5.5 and 7.0 respectively. To observe enzymatic activity over such a broad pH range several buffers have to be incorporated creating a 'universal' buffer. Universal buffers not enable a broad pH range to be covered with a single system they can also give rise to a linear titration profile.²⁹² Several universal buffer systems have been developed over the years (see Table 2) covering a range of physiological pH's.

Table 2 universal buffer systems, their chemical constituents and effective pH range

Buffer	Chemicals	pH Range
Mcllvain ²⁹³	Disodium phosphate and citric acid	2.2-8
Michaelis ²⁹⁴	Sodium barbitone and sodium acetate	6.8-9.2
Britton Robinson ²⁹⁵	Sodium hydroxide, boric, phosphoric and acetic acid	2-12
Modified Universal Buffer (MUB) ²⁹⁶	Sodium hydroxide, tris-(hydroxymethyl)-aminomethane, maleic, citric and boric acids	2-8
Cacodylate ²⁹⁷	Sodium cacodylate and sodium hydroxide	5-7.4

Although several buffer systems exist each has its own inherent issues. Mcllvain²⁹³ buffer uses citric acid which has been reported to bind some proteins inhibiting their activity.²⁹⁸ Michaelis buffer utilises sodium barbitone which has been a controlled substance since 1978²⁹⁹, moreover, it is not particularly effective at low pH ranges (<7). Buffer systems that contain inorganic compounds such as borates, cacodylates and bicarbonates are generally not avoided in enzyme solutions since they are not considered to be inert. Thereby, inhibiting enzymes and interacting with enzyme substrates.^{300,301} For example borates are known to bind to mono- and oligo- saccharides.³⁰¹ Maleic acid should be avoided in systems that are used in colourmetric experiments due to it absorbing UV light.³⁰² Finally, the pK_a (hence pH) of tris-(hydroxymethyl)-aminomethane (Tris) has a strong temperature dependence ($d(pK_a)/dT = -0.028$).¹²² Since no single universal buffer system is without its flaws no it would be beneficial to observe enzymatic activity in a couple of buffering systems.

3.3 Results and Discussion

3.3.1 Achieving a near linear titration

3.3.1.1 Titrations with a strong acid

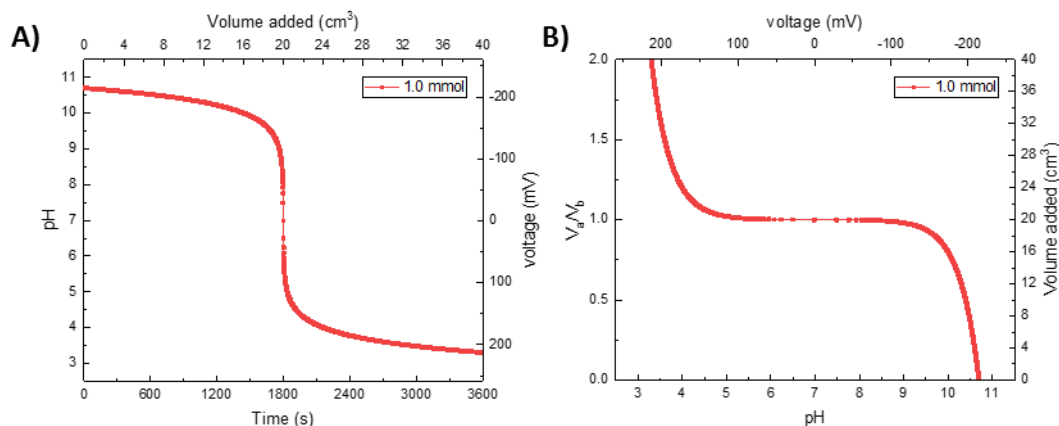


Figure 3-2 titration of sodium hydroxide (1.0 mmol dm⁻³; 20 cm³) with hydrochloric acid (1.0 mmol dm⁻³; 40 cm³), y-axes the linear relationship between pH and the voltage measured by a calibrated pH probe. A) shows how the data is collected, pH as a function of the volume of acid added. B) shows the transposing of data and the use of the ratio of volumes which facilitate the drawing of comparisons between data sets and other pH dependent properties.

In order to observe the full titration curve of initially titrations were carried out with hydrochloric acid, since it completely dissociates between pH 0 and 14. Whereas, gluconic acid is a weak acid (pK_a 3.86³⁰³) as such it does not fully dissociate in normal pH ranges. All titrations explore the change in pH as a function of the volume of titrant added or more precisely the ratio of the volume of titrant to the volume of sample. In the case of this body of work that is the volume of acid to the volume of base V_a/V_b . As such titration data is collected as a function time or volume added (Figure 3-2 A)). On the other hand, it is advantageous transpose the data, plotting V_a/V_b as a function of pH (Figure 3-2B)). This enables data sets to be easily compared to other pH dependent properties such as, ionic strength, concentration fractions and buffer strength.

Titration of a strong base like sodium hydroxide (pK_a 13.8³⁰⁴) with HCl results in a sharp transition when the concentration of acid is equal to the concentration of base (Figure 3-3 A)). This is due to both NaOH and HCl being fully dissociated throughout the titration. A further artefact of this full deprotonation of both the acid and the base is the shifting of the starting and finishing pH by a whole pH unit toward pH 7 as the molarity of the starting solutions is decreased ten-fold. The shape of the titration can be attributed to the buffer strength (B) of the system (Figure 3-3 B)). For strong acids and bases the buffer strength is merely sum of hydroxide and proton concentrations, since both the acid and base are fully dissociated. The buffer strength exponentially decreases to a minimum at pH 7, assuming the dissociation constant of water (pK_w) is 14.

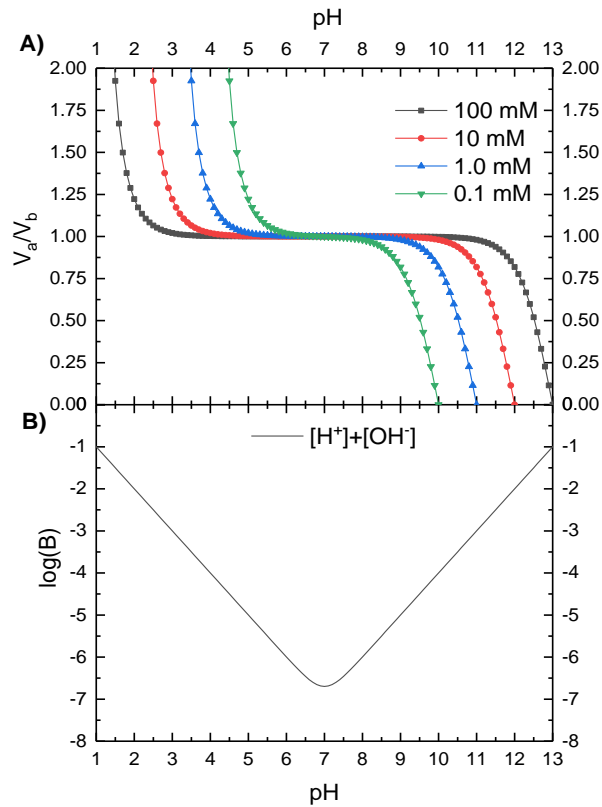


Figure 3-3 Titration of sodium hydroxide with equimolar hydrochloric acid; A) the change in pH as a function of the ratio of the volume of acid to the volume of base (V_a/V_b); B) logarithmic buffer strength ($\log(B)$) as a function of pH

As the buffer strength tends toward its minimum the profile of the titration curve shallows to a point at which a large pH shift can be achieved by an infinitesimal change in V_a/V_b . Therefore, to obtain a near linear titration curve the buffer strength of the system requires regions where the variation in buffer strength is minimal as a function of pH. To change the buffer strength a weak acid or base is required. Since buffer strength is dependent upon the product of an acid's or base's concentration fraction.

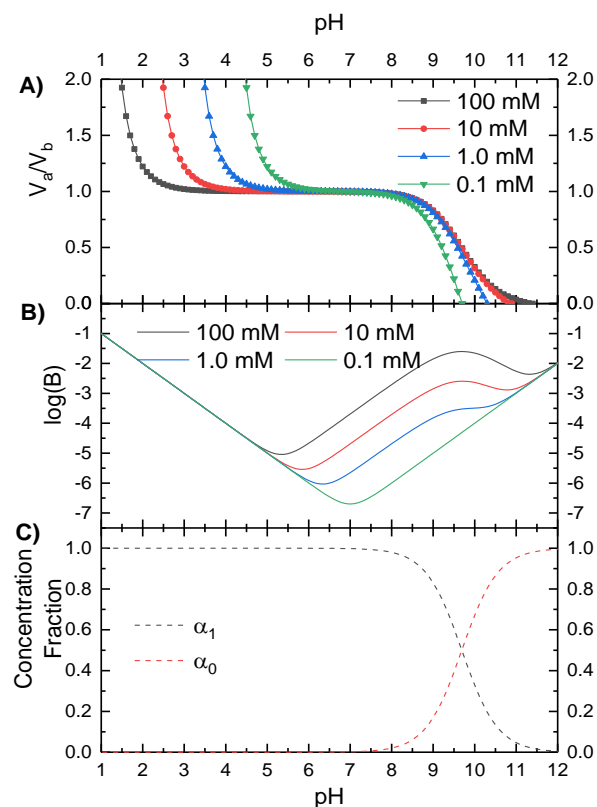


Figure 3-4 Titration of 2-amino-2-methylpropan-1-ol (AMP) with equimolar hydrochloric acid; A) the change in pH as a function of the ratio of the volume of acid to the volume of base (V_a/V_b); B) logarithmic buffer strength ($\log(B)$) as a function of pH; C) concentration fraction of both the protonated (α_1) and deprotonated (α_0) forms of AMP as a function of pH.

A weak base such as 2-amino-2-methylpropan-1-ol (AMP; pK_a 9.69^{122,123}) can exhibit some linear behaviour when between pH 8.7 and 10.4. AMP can be used as an effective buffer for biological material in that pH range as it does bind to or inhibit a proteins activity.³⁰⁵ On the other hand AMP only works as a buffer when used in millimolar concentrations. Higher concentrations ($>10 \text{ mmol dm}^{-3}$) result in a narrowing of the linear region. This is due to the increased concentration raising the pH but lowering the buffer capacity (Figure 3-4 B)). When the concentration is sufficiently high enough rather than creating a shoulder in the buffer strength plot a second peak is generated the pH equal to the electrolytes pK_a (Figure 3-4 B) and C)). This is due to the product of the electrolytes concentration fractions being greatest when they are equal. Lower concentrations ($<0.1 \text{ mmol dm}^{-3}$) result in the buffer strength of the system being dominate by the hydroxide and proton concentration.

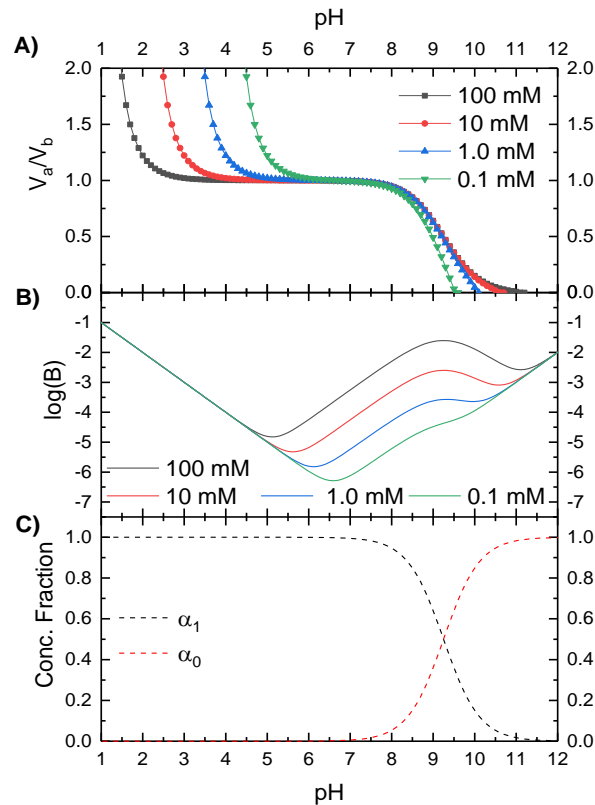


Figure 3-5 Titration of aqueous ammonia with equimolar hydrochloric acid; A) the change in pH as a function of the ratio of the volume of acid to the volume of base (V_a/V_b); B) logarithmic buffer strength ($\log(B)$) as a function of pH; C) concentration fraction of both the protonated (α_1) and deprotonated (α_0) forms of ammonium hydroxide as a function of pH.

Initially both glucose oxidase and urease were considered for use as the signal generating enzyme for the quorum sensing system. Urease convert to urea to carbon dioxide and ammonia. As such the titration profile for aqueous ammonia is included for completeness (Figure 3-5), despite ammonia having a similar pK_a to AMP, 9.25 and 9.69 respectively.^{122,123} Furthermore, ammonia demonstrates a little more control over the titrations progress at low concentrations ($<1.0 \text{ mM dm}^{-3}$; Figure 3-5 A) and B)). The $\log(B)$ plot demonstrates this through the residual of a shoulder for the 0.1 mM dm^{-3} curve. Both AMP and ammonia are great buffers for alkali conditions between pH 8.2 and 10.7. But, as previously discussed GOx denatures when held above pH 8 for an extend period of time.¹³⁷ Therefore, the lowering of buffer strength when going from alkali to neutral pH is advantageous when working with GOx. As only a small amount of acid is required to move an alkali solution of GOx to a near neutral pH ($\text{pH } 7 \pm 0.5$). Thereby, retaining GOx's activity. As such rather than looking for a weak base it would perhaps be more advantageous to look at the conjugate base of a weak acid. This would shift the shoulders and peaks generated by the weak electrolyte from the alkali, $[\text{OH}^-]$ dominated region of the $\log(B)$ plot to the acidic region.

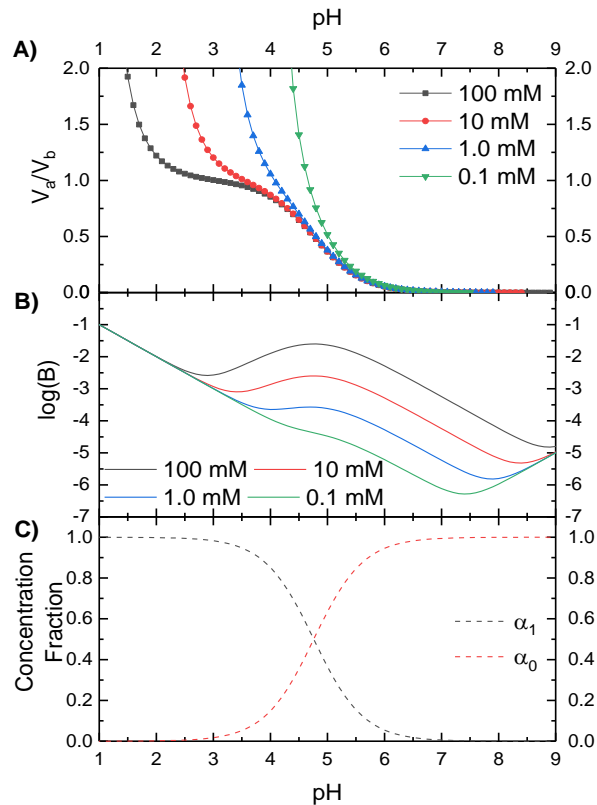


Figure 3-6 Titration of sodium acetate with equimolar hydrochloric acid; A) the change in pH as a function of the ratio of the volume of acid to the volume of base (V_a/V_b); B) logarithmic buffer strength ($\log(B)$) as a function of pH; C) concentration fraction of acetic acid (α_1) and acetate (α_0) as a function of pH.

One such conjugate base is sodium acetate, which has a pK_a of 4.76.^{122,123} The low pK_a gives acetate a functional buffering range, between pH 3.7 and 5.7, down to millimolar concentrations. When the concentration is less than millimolar the ratio of acid to base required to shift the pH becomes impractical (Figure 3-6 A)). The titration curve is also near linear through the acetate buffered regions, when the buffer concentration is millimolar or greater.

The aversion to requiring buffer concentrations greater than 1.0 mMol dm^{-3} stems from the target of using the buffering system with GOx. Where the GOx converting glucose to gluconic acid thereby causing the pH to change. This throws up two problems, the primary scientific argument is that the reaction requires oxygen. Due to the reaction occurring in water the molecular oxygen required for the reaction must be dissolved in the water. For a stirred reaction this oxygen can simply be replaced by bubbling air through the reaction media. However, such a method would facilitate the stripping of acid from an enzyme loaded particle, generating a 'global' shift in pH rather than a local one. Therefore, we are reliant upon oxygen absorption through the surface of the reaction media alone. This limits the maximum amount of glucose oxidase we can use. If the buffer strength is too high the time taken to see a significant change in pH will be in the order of hours or even days. Enzymatic

activity is described in units which is the liberation of 1 μmol of substrate (glucose) per minute per unit mass of enzyme. Typically, enzyme activity is between 2 and 250 units mg^{-1} with the cost of purchase being proportional. Therefore, to obtain short reaction times low strength buffers are required.

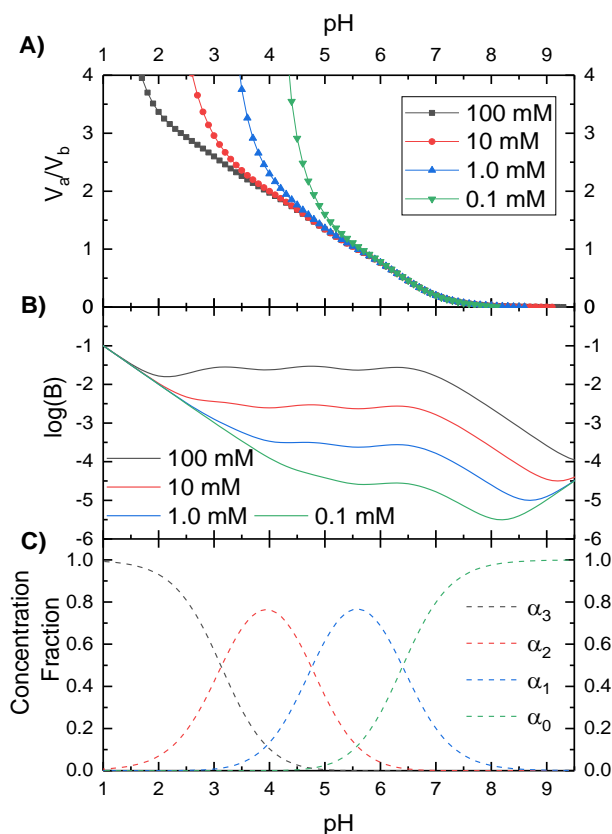


Figure 3-7 Titration of trisodium citrate with equimolar hydrochloric acid; A) the change in pH as a function of the ratio of the volume of acid to the volume of base (V_a/V_b); B) logarithmic buffer strength ($\log(B)$) as a function of pH; C) concentration fraction of all citrate species (α_n where n denotes the number of dissociable protons bound to the citrate) as a function of pH.

A drawback of monoprotic acids is that their buffering capacity is limited to a pH range where the $pH = pK_a \pm 1$. To extend this range either multiple monoprotic acids or polyprotic acids could be used. One of the most common polyprotics is citric acid and its conjugate bases of mono-, di-, or trisodium citrate. Citrate can be used as a biological buffer. However, it can bind to some proteins, inhibiting their activity.³⁰⁶

The titration of trisodium citrate (pK_{a1} 3.13, pK_{a2} 4.76, pK_{a3} 6.40)^{122,123} exhibits a broad linear region between pH 7.2 and 2.2 (Figure 3-7 A)). This is due to the pK_a 's being close enough to interfere with one another (Figure 3-7 C)). This causes the buffer strength to plateau over several units (Figure 3-7 A)). It is noteworthy that the linear portion of the titration curve shortens by a pH unit every time

there is a 10 fold decrease in concentration. On closer examination of the $\log(B)$ plot it becomes apparent that this is due to the buffering strength of the $[H^+]$ coming to the fore earlier as the concentration is increased. This highlights one drawback of working with low concentration systems. The lower the concentration the smaller the obtainable pH range. This should be taken into consideration when trying to generate a response in quorum sensing system.

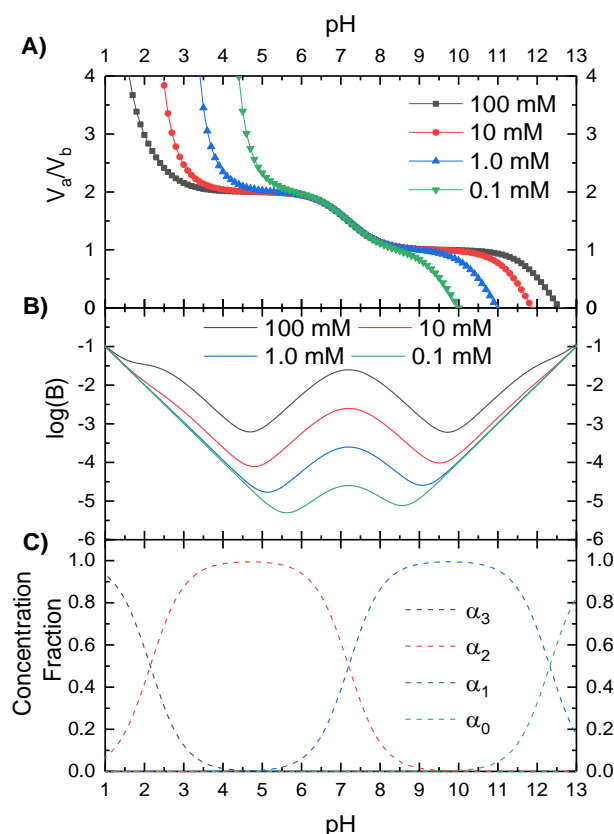


Figure 3-8 Titration of trisodium phosphate with equimolar hydrochloric acid; A) the change in pH as a function of the ratio of the volume of acid to the volume of base (V_a/V_b); B) logarithmic buffer strength ($\log(B)$) as a function of pH; C) concentration fraction of all citrate species (α_n , where n denotes the number of dissociable protons bound to the citrate) as a function of pH.

Another biologically relevant triprotic electrolyte is phosphoric acid and its phosphate conjugated bases. Moreover, phosphate buffered saline (PBS) is often used to recreate in vivo pH, osmolarity and ionic concentrations in vitro. The relevance of phosphate is demonstrated in the titration of trisodium phosphate (Figure 3-8 A)). The interaction of the concentration fractions α_2 and α_1 (H_2A^- and HA^{2-} respectively) around phosphate's pK_{a2} (7.20)^{122,123} results in a broad linear region in the titration curve between pH 6.5 and 8.0 for all concentrations. Furthermore, phosphate's dissociation constants (pK_{a1} 2.15, pK_{a2} 7.20, pK_{a3} 12.33)^{122,123} are spaced sufficiently far part from one another for only two species of phosphate to be of consequence at any pH value. At millimolar concentrations and below only the

pH values around the second dissociation constant offer any extra buffer strength. However, there is the potential for extending the buffer strength. This can be done through the judicious combination of phosphate a second buffer. Such a buffer would require a pK_a of around 5 ± 0.3 .

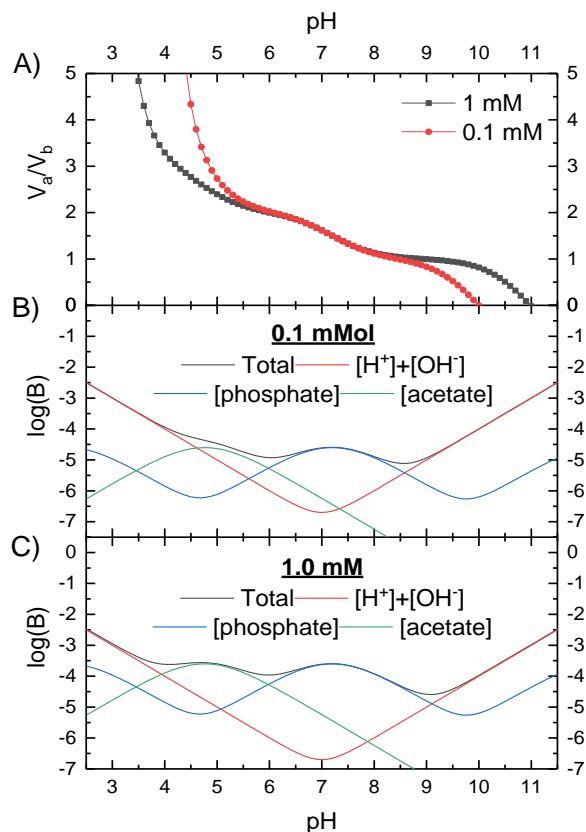


Figure 3-9 Titration of equimolar trisodium phosphate and sodium acetate with equimolar hydrochloric acid; A) the change in pH as a function of the ratio of the volume of acid to the volume of base (V_a/V_b); B) logarithmic buffer strength ($\log(B)$) of each individual species and the sum total strength, as a function of pH; C) logarithmic buffer strength ($\log(B)$) of each individual species and the sum total strength, as a function of pH.

The action of sodium acetate has been discussed previously (Figure 3-6). The combination of sodium acetate with trisodium phosphate was titrated with hydrochloric acid (Figure 3-9). This resulted in a near linear titration curve between pH 8 and 5 for solutions that are less than $\leq 1 \text{ mmol dm}^{-3}$. Before the amount of acid required to cause a significant shift in pH perturbs the continued titration. The effect of acetate had less of an effect than expected in extending the titration curve at 0.1 mmol dm^{-3} concentrations. This is due to the buffer strength of acetate only partially overlapping the buffer strength associated to $[H^+]$ and $[OH^-]$ (Figure 3-9).

We have explored several systems to obtain a near linear titration curve. So far we have only studied the systems with HCl. To ascertain as to whether or not they are suitable for use with glucose oxidase it would be beneficial to perform the titrations with gluconic acid since it is a weak acid (pK_a 3.86).^{122,123}

3.3.1.2 Using gluconic acid as the analyte

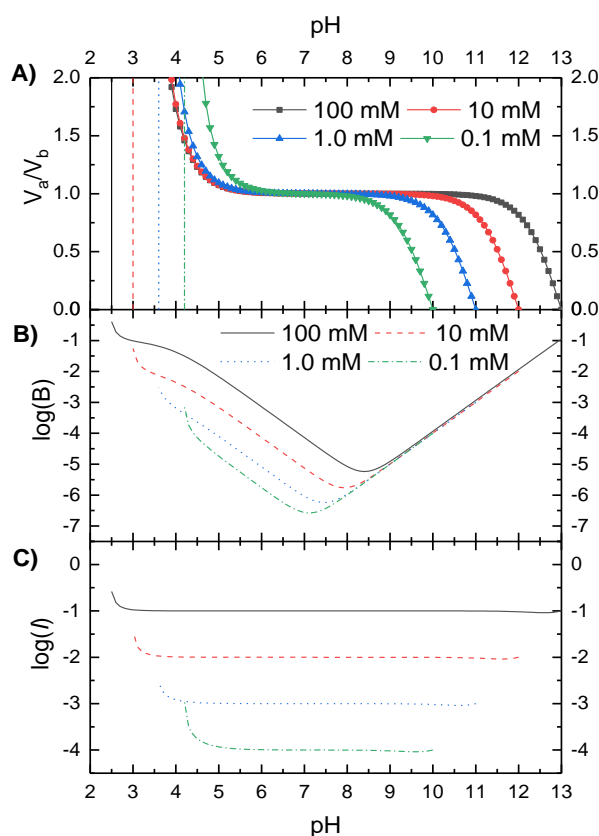


Figure 3-10 Titration of NaOH with equimolar gluconic acid; A) the change in pH as a function of the ratio of the volume of acid to the volume of base (V_a/V_b), vertical lines at pH's 2.5, 3.0, 3.6 and 4.2 indicate the lowest achievable pH by 100, 10, 1.0 and 0.1 mmol^{-3} gluconic acid respectively; B) logarithmic buffer strength ($\log(B)$) of the titration; C) logarithmic ionic strength ($\log(I)$) of the titration.

It is advantageous to observe gluconic acids behaviour as a function of pH, without the interference of other constituents changing the conditions of the reaction. As such the titration of sodium hydroxide with gluconic acid is included (Figure 3-10), as sodium hydroxide is fully dissociated throughout the titration. The titration curve is like that of NaOH with HCl. However, the resulting final pH of the titration is greater than that of HCl. Examination of the buffer strength shows that gluconic acid is the mirror image of alkali systems ammonia and AMP through pH 7. The ionic strength of the system remains approximately constant throughout, only showing a dramatic increase when the pH corresponds to V_a/V_b more than 2.

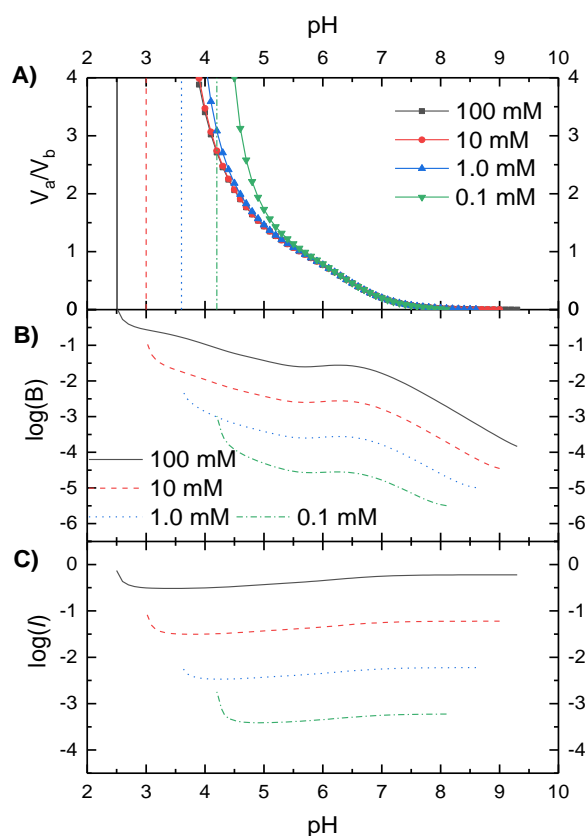


Figure 3-11 Titration of trisodium citrate with equimolar gluconic acid; A) the change in pH as a function of the ratio of the volume of acid to the volume of base (V_a/V_b), vertical lines at pH's 2.5, 3.0, 3.6 and 4.2 indicate the lowest achievable pH by 100, 10 1.0 and 0.1 mmol dm^{-3} gluconic acid respectively; B) logarithmic buffer strength ($\log(B)$) of the titration; C) logarithmic ionic strength ($\log(I)$) of the titration

The action of citrate was explored in a titration with gluconic acid (Figure 3-11). Initially the progression curve of the titration identical to that of citrate with HCl. The starting pH of the titration is directly proportional to the [trisodium citrate]. A large shift in pH is observed with little acid added, until the pH is lowered to 7.5, when the system becomes relatively well buffered. This results in a linear decrease in the pH between 7 and 5.5 as V_a/V_b increases from 0.2 to 1.0, which equates to a 1:1 molar ratio of gluconic acid to citrate. As the molar ratio is increased further there is little variance between concentrations and the pH achieved, the exception being 0.1 mmol dm^{-3} . This is attributed to the buffer strength of water exceeding that of citrate by pH 5, this does not occur until lower pH ranges as the concentration increases. However, at these low pH ranges the gluconic acid (pK_a 3.86)^{122,123} is also starting to act as a buffer. The ionic strength of titration involving citrate species have a maximum at pH values greater than 7 due to much of the citrate being in its trivalent anionic state (Figure 3-11). As the pH is lowered the citrate becomes di- and then mono-valent causing the

ionic strength to decrease. In the case of the more concentrated titrations some of the citrate will become neutral since $pK_{a1} = 3.13$ (citrate).

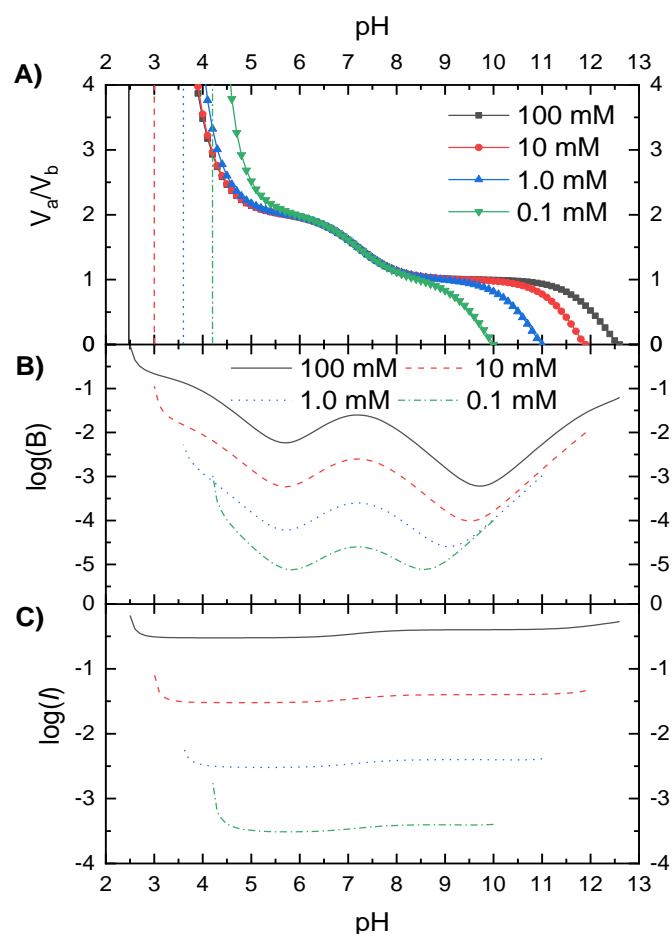


Figure 3-12 Titration of trisodium phosphate with equimolar gluconic acid; A) the change in pH as a function of the ratio of the volume of acid to the volume of base (V_a/V_b), vertical lines at pH's 2.5, 3.0, 3.6 and 4.2 indicate the lowest achievable pH by 100, 10 1.0 and 0.1 mmol dm^{-3} gluconic acid respectively; B) logarithmic buffer strength ($\log(B)$) of the titration; C) logarithmic ionic strength ($\log(I)$) of the titration

Again, tri-sodium phosphate exhibits a similar progression curve with gluconic acid as it does with hydrochloric acid. Variation occurs at from around pH 5.5 and below. This is due to the decreasing proportion of gluconic acid being deprotonated. At lower concentrations (0.1 mmol dm^{-3}) this make the progression curve of the titration closely resemble the acetate phosphate titration with HCl. This suggests that the addition of acetate may not be required to achieve a near linear titration. The ionic strength exhibits similar behaviour to that of the citrate titration previously discussed.

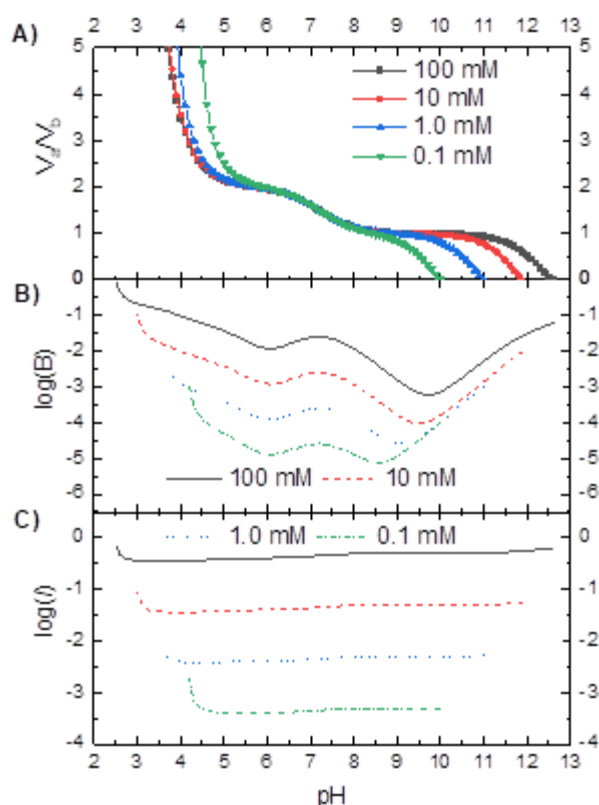


Figure 3-13 Titration of trisodium phosphate and sodium acetate (molar ratio of 1:1) with equimolar gluconic acid; A) the change in pH as a function of the ratio of the volume of acid to the volume of base (V_a/V_b), vertical lines at pH's 2.5, 3.0, 3.6 and 4.2 indicate the lowest achievable pH by 100, 10 1.0 and 0.1 mmol dm^{-3} gluconic acid respectively; B) logarithmic buffer strength ($\log(B)$) of the titration; C) logarithmic ionic strength ($\log(I)$) of the titration.

It was expected that the addition of acetate (pK_a 4.76)^{122,123} to phosphate would extend the linear portion of the titration curve from pH 5.8-8.4 to 3.8-8.4. To test this hypothesis various equimolar solutions of trisodium phosphate and sodium acetate were made. These were then titrated with HCl (Figure 3-9). The resulting progression curves only showed marginal differences from a titration of just phosphate. However, the action of 0.1 mmol dm^{-3} solutions did look promising. As such the titrations were carried out again but with gluconic acid replacing hydrogen chloride as the acid. The resulting progression curves are shown in Figure 3-13. On comparison of the progression curves with the progression curves for the titration of trisodium phosphate and gluconic acid (Figure 3-12). Little difference can be seen. This is due to gluconic acid being a weak acid (pK_a 3.86)^{122,123} as such the proportion of acid that is deprotonated starts to show a significant increase as the pH is lowered from pH 5.

Ultimately since the analyte used in all future experiments is gluconic acid the addition of acetate to the buffer system is not required, due to gluconic acid and acetate having similar pK_a 's (3.86 and 4.76 respectively). As such when gluconic acid is used as the analyte with phosphate as the buffer a near

linear titration is observed without the addition of acetate. Moving forward, most promising systems for obtaining a linear titration profile in weakly acidic-neutral pH conditions are citrate and phosphate when titrated with gluconic acid.

3.3.2 Enzymatic Rate Profile Determination

Glucose oxidase as with any other enzyme displays a rate profile which is dependent upon variety of external stresses as discussed in Section 1.5.4. Herein we are interested in the enzyme's ability to produce gluconic acid in a system where the pH is ever changing. The determination of rate profile of glucose oxidase under specific conditions, is best shown in the example below.

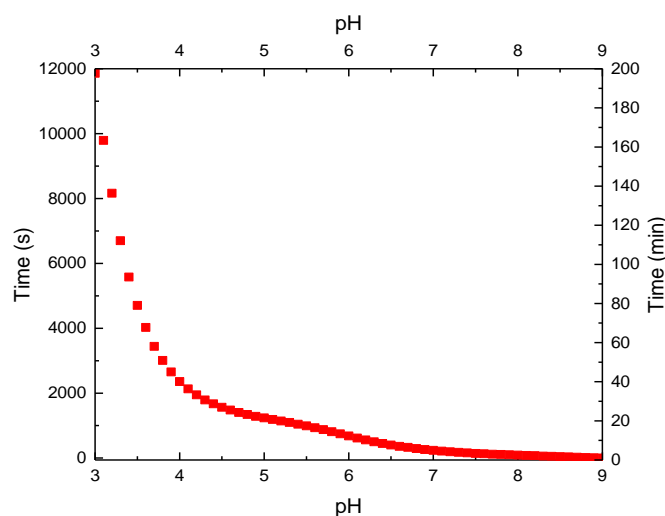


Figure 3-14 the change of pH as a function of time for the titration of sodium hydroxide (0.4 mmol dm^{-3}) by gluconic acid produced by the oxidation of glucose ($19.8 \text{ mmol dm}^{-3}$) by glucose oxidase (5 mg)

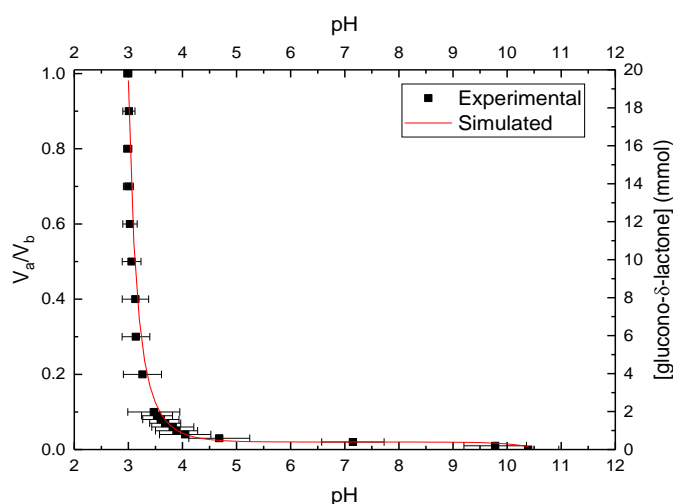


Figure 3-15. The change in pH as a function of the ratio of the volume of acid to the volume of base (V_a/V_b) for the titration of sodium hydroxide ($(C_b) 0.04 \text{ mmol dm}^{-3}$) by gluconic acid ($(C_a) 19.8 \text{ mmol dm}^{-3}$, $pK_a 3.86$). Fitting of equation (A-2.49) (red line) returned an R^2 value of 0.96.

The resulting titration curve for the conversion of glucose ($19.8 \text{ mmol dm}^{-3}$) into gluconic acid by glucose oxidase (0.5 mg cm^{-3}) in the presence of sodium hydroxide (0.4 mmol dm^{-3}) is shown below (Figure 3-14). Since the activity of glucose oxidase changes as a function of pH, time is not directly proportional to the concentration of acid present in the reaction mixture. Which is what is observed in a standard titration like those described in appendices 9.1.2.

If you consider the chemical components of the reaction mixture only the sodium hydroxide and gluconic acid can influence the pH. Therefore, mimicking the reaction by titrating sodium hydroxide (0.4 mmol dm^{-3}) with gluconic acid ($19.8 \text{ mmol dm}^{-3}$) can give the volume (and mass) of acid required to lower the pH (Figure 3-15).

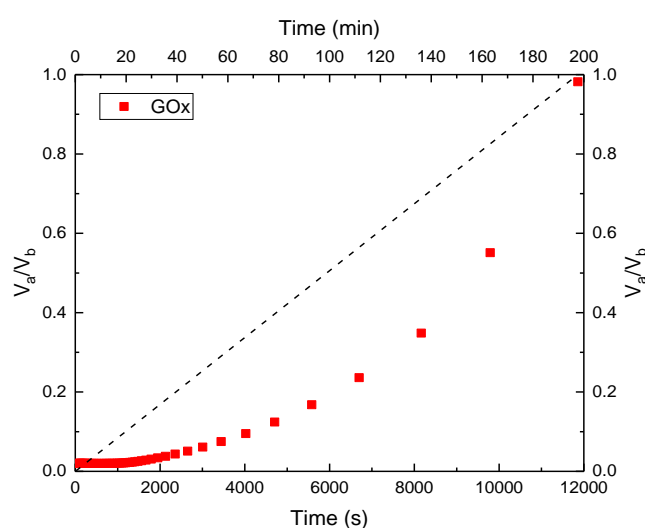


Figure 3-16. The change in time as a function of V_a/V_b , for the titration of sodium hydroxide by gluconic acid. The red data points show the production of acid by glucose oxidase and the black line is for the addition of acid by standard titration methods.

This enables the ratio V_a/V_b for any pH in the titration curve to be determined. Plotting of the V_a/V_b as a function of time (red data; Figure 3-16) shows how the titration does not occur in a linear fashion. However, this plot does show that there must be a variation if the rate as a function of time.

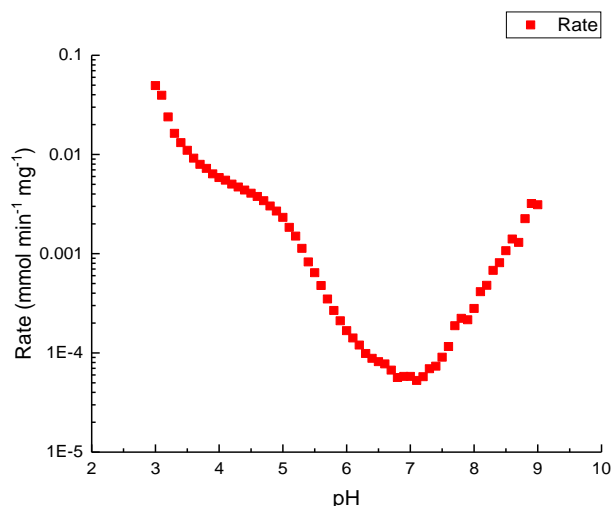


Figure 3-17 the rate of gluconic acid production as a function of pH for the titration of sodium hydroxide with gluconic acid which is produced by the hydrolysis of glucose catalysed by glucose oxidase.

The rate is determined by taking the differential of the data generated in Figure 3-16. This gives (V_a/V_b time⁻¹) the change in volumetric ratio as a function of time. Therefore, to find the rate of acid production as a function of enzyme mass the rate must be multiplied by the initial number of moles of glucose in the solution and divide by the mass of glucose oxidase in solution to give the rate (mol time⁻¹ mass⁻¹). This can then be expressed mathematically as;

$$\text{enzymatic activity (mol time}^{-1}\text{mass}^{-1}) = \frac{\text{rate (time}^{-1}) \times \text{glucose (mol)}}{\text{enzyme (mass)}} \quad (3.1)$$

The rate is then plotted as a function of pH (Figure 3-17).

3.3.3 Action of glucose oxidase in a bulk aqueous phase

3.3.3.1 Choice of buffer

From the titration of various buffers with known quantities of gluconic acid, citrate and phosphate were highlighted as systems which gave strong linear regions in neutral-weak acid conditions. Furthermore, sodium hydroxide gives a reference point to non-buffered systems.

Examination of the titration curves of various buffers (Figure 3-18 A). Of the buffers used trisodium citrate showed the smoothest curve, with little deviation from its progression curve of a normal titration. The action of phosphate also gave good correlation to that of normal titrations. On the other hand, the titration of NaOH exhibits a slowing between pH 7 and 6 followed by returning to the normal titration curve. Looking at the rate of these titrations shows a general trend of a minima in rate at pH 6-7 with rapid increases in rate either side. The rates appear to plateau when the pH decreases

below 5 or raises above pH 7.5-8. The rate of acid production reaches a higher maximum in basic conditions than in acidic ones. The rate was significantly faster for NaOH than for phosphate (by 2 orders of magnitude) and citrate. This could be due to the multivalent anions complexing to the active site glucose oxidase thereby inhibiting glucose oxidase activity.

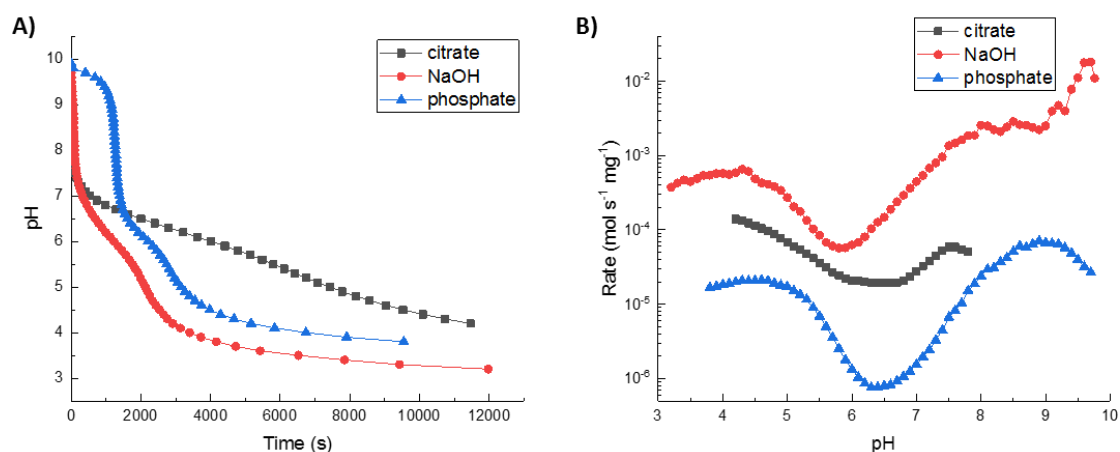


Figure 3-18 A) titration curve as a function of time for; trisodium citrate (black); trisodium phosphate (red); sodium hydroxide (blue) with gluconic acid generated by glucose oxidase's oxidation of glucose. B) Corresponding rate profiles for gluconic acid production as a function of pH. Experimental conditions; glucose oxidase (0.5 mg cm^{-3}); buffer ($100 \text{ } \mu\text{mol dm}^{-3}$); glucose ($1.98 \text{ mmol dm}^{-3}$) total volume 10 cm^3 .

Figure 3-18 A) shows that the use of a near-linear titration can mask the variation in rate that is occurring. Whereas using a base like NaOH to raise the initial pH of the solution enables variations in the progression curve to be spotted easily.

3.3.3.2 Glucose concentration

The concentration of glucose has no effect on the rate of pH change (Figure 3-19). All concentrations of glucose exhibit the same rate behaviour as a function of pH. As the pH decreases from alkali to neutral pH so does the rate. As the pH becomes acidic the rate steadily increases before starting to plateau around pH 5. The shape describe bears little resemblance the rate profile of GOx (Figure 1-11). As previously discussed, glucose oxidase catalyses the oxidation of glucose to glucono- δ -lactone. The lactone undergoes ester hydrolysis to form gluconic acid. Ester hydrolysis catalysed by acidic or basic conditions, (Figure 1-8). As such the rate of ester hydrolysis is dependent on $[\text{H}^+]$ and $[\text{OH}^-]$. Moreover, the pH dependent rate profile of ester hydrolysis is similar in shape to that of the buffer strength of water (Appendix 9.1.4 Figure 9-4 A)). When the pH is greater than 7, the rate of change in pH is proportional to the $[\text{OH}^-]$. This is because the rate limiting step is ester hydrolysis. Rather than glucose oxidase activity. The low rate of change at pH 6.5-7 is due to a shift in ester hydrolysis mechanism from base catalysed to reversible acid catalysed.

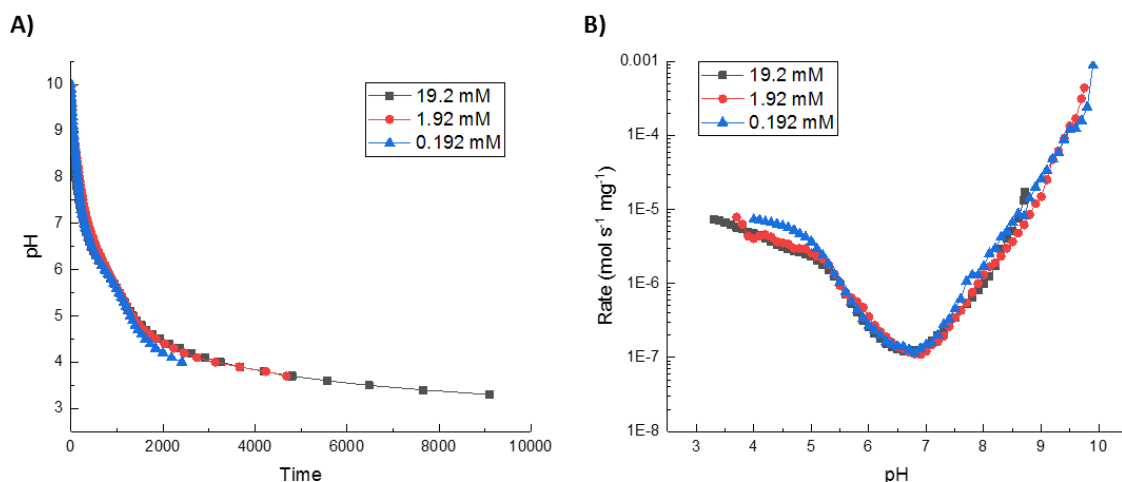


Figure 3-19 A) titration curve of NaOH with gluconic acid produced by the reaction of glucose oxidase with glucose as a function of time. Showing the effect of initial [glucose] on the rate of the titration. 19.2 mmol dm⁻³ (black); 1.92 mmol dm⁻³ (red); 0.192 mmol dm⁻³ (blue) with gluconic acid generated by glucose oxidase's oxidation of glucose. B) Corresponding rate profiles for gluconic acid production as a function of pH. Experimental conditions; glucose oxidase (5.0 mg cm⁻³); buffer (40 μmol dm⁻³); total volume 10 cm³.

Between pH 6 and 5 there is a 1 order of magnitude change in the rate, this due to the [H⁺] also shifting by one order of magnitude, again the rate limiting step is ester hydrolysis. Below pH 5 the rate starts to plateau. This is thought to be due to several factors. Firstly, the pK_a of gluconic acid is 3.86. Therefore, when the pH is greater than 4.86 almost all the acid is in a deprotonated form. When deprotonated the acid is unable to undergo base catalysed ester formation. As the pH decreases a larger proportion of the acid becomes protonated causing the rate to slow as an equilibrium forms between acid catalysed ester hydrolysis and ester formation. In Figure 3-19 all rates are independent of GOx and glucose concentration this since the enzymatic activity is faster than the rate of ester hydrolysis.

3.3.3.3 Mass of glucose oxidase

As with changing the [glucose] changing the mass of glucose oxidase has little effect on the shape of the rate of pH change (Figure 3-20). However, the minimum rate shifts from pH 7 to pH 6.2 as the GOx mass is decreased from 5 mg to 0.5 mg. This is possibly due to a slower initial rate. The rate of change is significantly slower for the 0.5 mg system. This is attributed less glucono-δ-lactone being produced resulting in a slower initial titration to pH 6.

It is noteworthy that, the rates for both titrations show minimum rates of the same order (Figure 3-21). Furthermore, the rate in weakly acidic conditions is very similar for high and low masses of GOx. This can be seen in Figure 3-20 A) where the time taken for the pH to decrease from 5 to 3.7 almost identical.

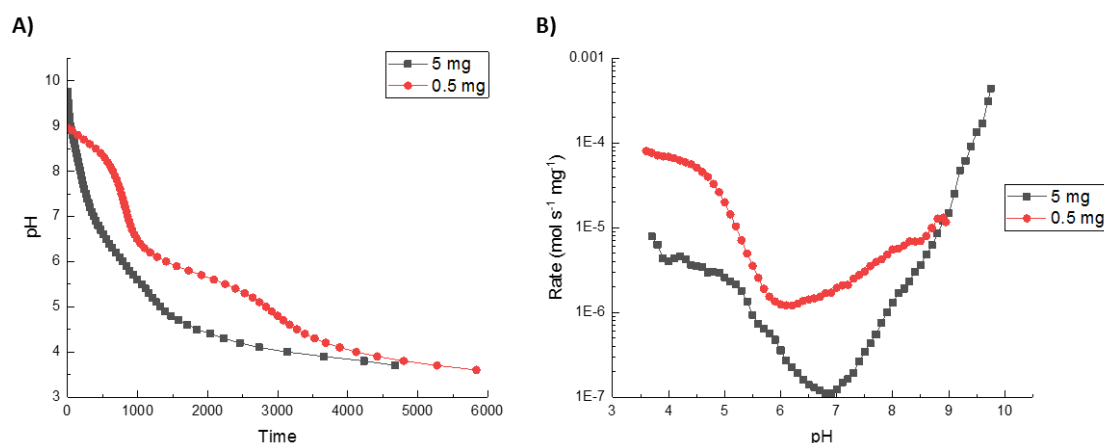


Figure 3-20 A) titration curve of NaOH with gluconic acid produced by the reaction of glucose oxidase with glucose as a function of time. Showing the effect of glucose oxidase mass on the rate of the titration. 5 mg cm⁻³ (black); 0.5 mg cm⁻³ (red) with gluconic acid generated by glucose oxidase's oxidation of glucose. B) Corresponding rate profiles for gluconic acid production as a function of pH. Experimental conditions; glucose (1.92 mmol dm⁻³); buffer (40 μmol dm⁻³); total volume 10 cm³

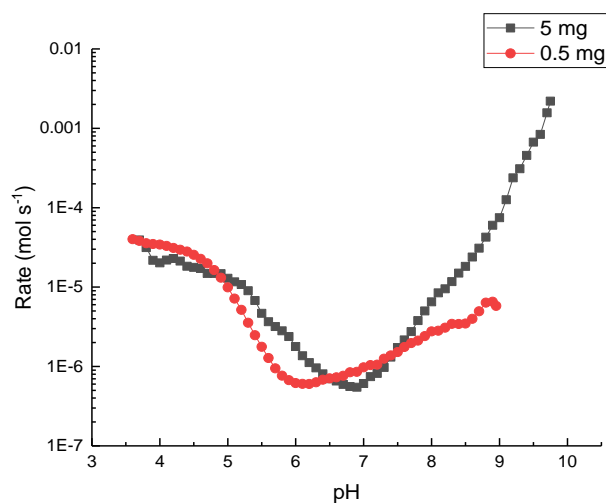


Figure 3-21 rate of acid production as a function of the entire reaction system, where the only difference between the 2 systems is the mass of glucose oxidase.

3.4 Conclusions and Future Work

In this chapter we set out to use a near linear titration curve to explore the action of glucose oxidase in solution. From initial titrations with hydrochloric acid the following buffer systems warranted further explorations; trisodium citrate; trisodium phosphate; trisodium phosphate combined with

sodium acetate. It was also decided that sodium hydroxide should be included as it does not alter the buffer strength of water.

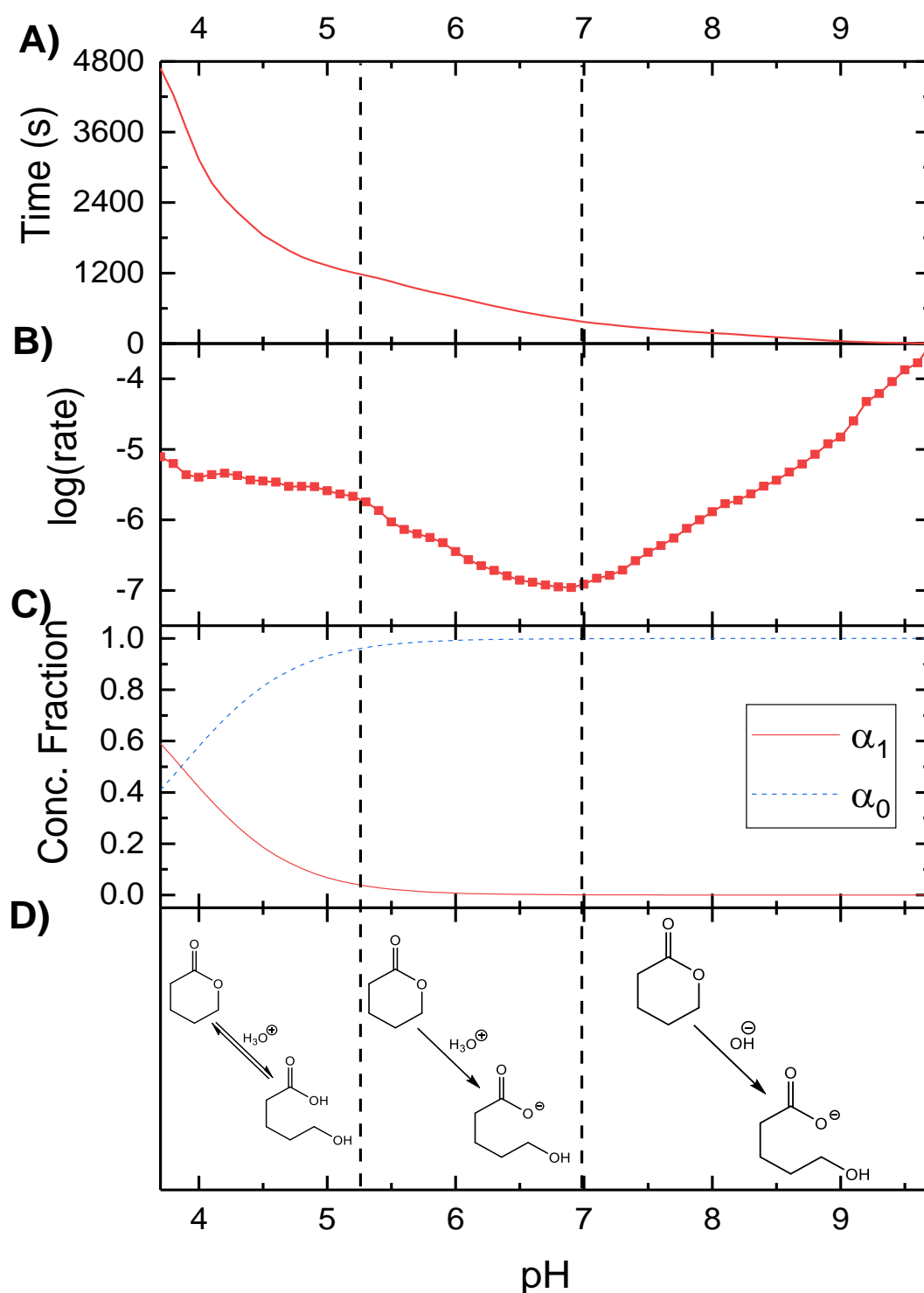


Figure 3-22 A) titration curve for NaOH with gluconic acid produced by the reaction of glucose oxidase with glucose; B) $\log(\text{rate})$ profile as a function pH; C) concentration fraction of gluconic acid; D) dominant catalysis method of ester hydrolysis of gluconic acid (alcohol groups omitted) as a function of pH.

On titrating these buffers with gluconic acid, the further use of the combined buffer system of acetate and phosphate was unnecessary. Due to gluconic acid having a pK_a of 3.86, which at sufficiently low concentrations cause the titration to tend toward a linear at around pH 5.5. Therefore, only the three remaining systems were used to observe the action of glucose oxidase in solution. These all showed similar rate profiles. However, it was only by examining the rate profiles that deviation from normal behaviour could be observed for the highly buffered systems. On the other hand, sodium hydroxide which is a notoriously poor buffer. Due to it being a strong base. Readily showed variation in titration profile for enzymatic acid production compared to a standard titration.

The rate of acid production by glucose oxidase was then explored as a function of pH. Due to the concentration of glucose being in excess the rate of glucono- δ -lactone production (and subsequent ester hydrolysis) was only dependent upon the turn over rate of GOx for the conditions used. A tenfold reduction in the enzyme concentration resulted in a reduction in acid production rate under basic conditions but not acidic ones. It was observed that the rate of acid production does not mimic glucose oxidase activity which reaches a maximum at around pH 5.1. Rather the rate of acid production is linked to catalysed ester hydrolysis (Figure 3-22). Ester hydrolysis is catalysed by acid and base. This explains the rate minimum at pH 7 since under neutral conditions the sum of hydroxide and protons in solutions is at its lowest. The rate of acid production was also shown to slow below pH 5.2. This was attributed gluconic acid nearing its pK_a as such more of the acid is protonated as the pH lowers. Protonated gluconic acid can undergo acid catalysed ester formation. This causes an equilibrium to form between glucono- δ -lactone and gluconic acid which slows the rate of acid formation.

In terms of signal generation, we have demonstrated a robust signal in generating a shift in proton concentration. Furthermore, generation of protons is autocatalytic, the lower the pH the faster the rate of production, when starting from a neutral pH.

Future work would be focused toward obtaining the rate profile for GOx. To achieve this glucono- δ -lactone would have to become the rate limiting step rather than ester hydrolysis. This could be achieved by either reducing the amount of GOx so that the production of the lactone is sufficiently slow. Alternatively, gluconolactonase could be used to increase the rate of lactone to acid conversion.

4. Ratiometric Imaging

4.1 Overview

In this chapter we look at ratiometric imaging, how to get high quality, reproducible images and data sets. Firstly, we compare methods of calibrating a ratiometric setup with carboxy-SNARF-4F. Before discussing the requirements that must be met to obtain clear images and what actions are involved in image processing. Furthermore, we investigate how image processing and experimental setup can reduce error.

4.2 Introduction

The role of pH and its importance in biological systems as well as in agricultural and environmental chemistry, food and pharmaceutical industries has been discussed previously. In the previous chapters bulk pH measurements have been carried out using pH-combination electrode, this method is fine for a system that is uniform (in chapter 3 uniform pH was achieved by stirring the reaction media).

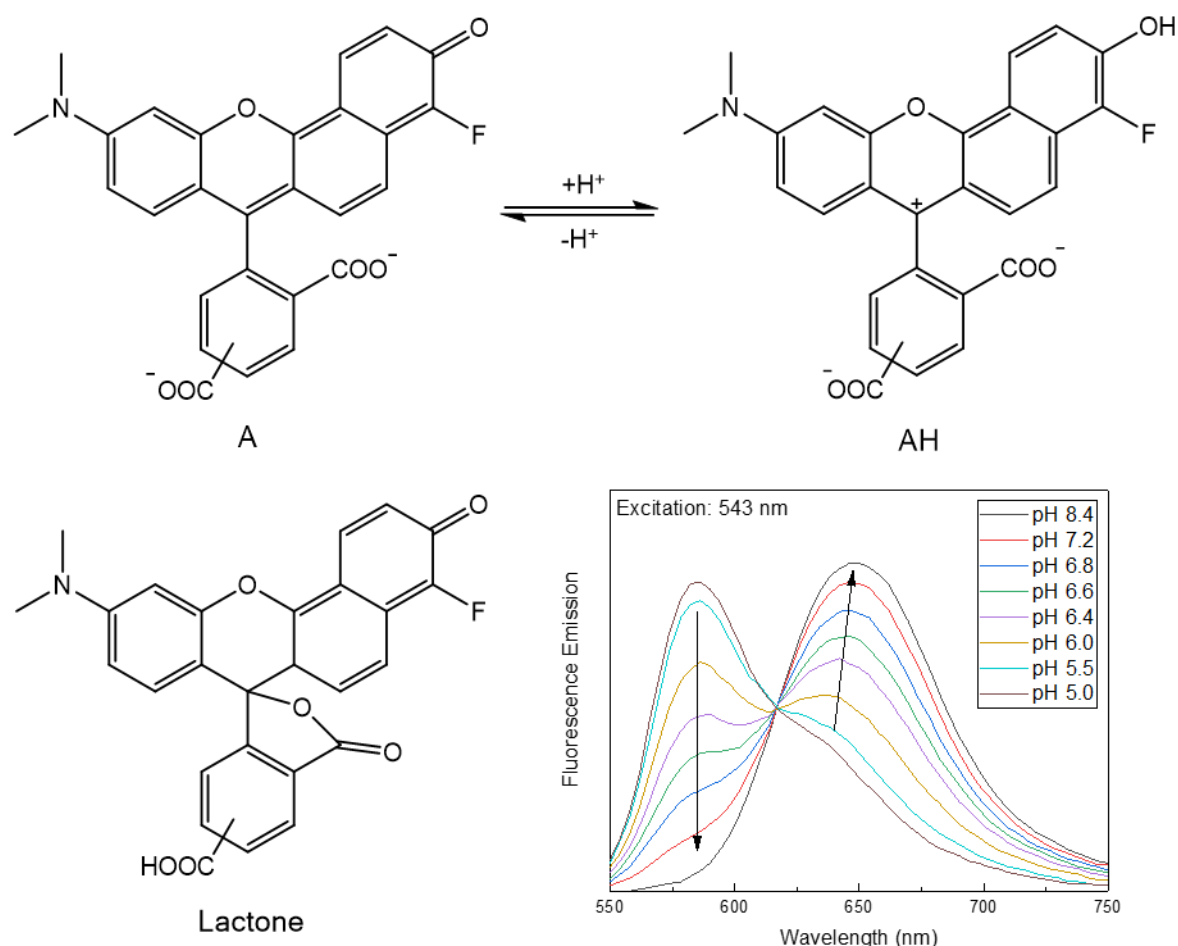


Figure 4-1 The equilibrium structures between the acid (AH) and base (A) form of the carboxy-seminaphthorhodafleur (carboxy-SNARF-4F; pKa 6.4) when in their ground state, the lactone form is the neutral structure of SNARF-4F and the fluorescence emission spectra of SNARF-4F (pKa 6.4) arrows highlight the shrinking peak at 587 nm with increasing pH and the peak that grows with increasing pH at around 645 nm

For a quorum sensing system each particle can be thought of as having a sphere of influence, this sphere is a region where the particle generates a shift in pH which can initiate autocatalytic behaviour. In this instance stirring the particles would disrupt the sphere of influence. As such a noninvasive method of monitoring pH is required. One such method is the use of fluorescent pH probes, these pH probes exhibit a shift in fluorescence upon the direct binding of a proton onto the dye.

There are two distinct classes of fluorescent pH probe, these can be identified by the photophysical properties of the neutral and charged forms of the probe.³⁰⁷ The first and most commonly used class of probe are the anthracene derivatives, fluorescein and pyrene. In these probes only one of the acidic/basic forms exhibits any significant fluorescence. As such the shift in pH is simply proportional to intensity of the fluorescent emission at a given wavelength, therefore they are dependent on concentration. This concentration dependence has implications when studying non-uniform systems or biological systems, since areas such as cell membranes, densely packed regions, lipophilic/hydrophilic regions can all cause shifts in the concentration of the pH probe, thereby shifting that regions dye emission intensity. This introduces a large degree of uncertainty into any pH measurement taken using single peak pH probes. SNARF dyes have primarily been used by microbiologist and physiologists in both single cell cultures³⁰⁸ and organs.³⁰⁹ the dual emission properties of SNARF makes it particularly effective in applications such as confocal laser-scanning microscopy,^{308,310} flow cytometry³¹¹ and microplate reader-based measurements.³¹²

The second class of probe addresses this concentration dependence issue since both the acidic (AH) and basic (A) (Figure 4-1) forms have specific fluorescence and/or adsorption bands. These probes respond to shifts in pH with shifts in their emission and/or excitation spectra.³¹³ The ratio of the fluorescence (emission or excitation) at two different wavelengths is independent of overall concentration, photobleaching, sample composition, as well as variations in optical setup such as path length, excitation intensity and detector sensitivity.³¹⁴ Applying, such an approach by taking two images at different wavelengths is the concept behind ratiometric imaging that enables quantitative 2-dimensional pH images to be obtained, circumventing the drawbacks associated with conventional pH indicators.³¹⁴

Calibration of ratiometric setup is essential. However, there is very little in the way of literature. One of the most commonly used methods is a linearized form of a derivative of Henderson-Hasselback equation known as the Grynkiewicz equation.³¹⁵⁻³¹⁸

$$pH = pK_a + C \log \left(\frac{R - R_{min}}{R_{max} - R} \right) + \log \left(\frac{I_a}{I_b} \right) \quad (4.1)$$

$$pH - \log\left(\frac{I_a}{I_b}\right) = pK_a + C \log\left(\frac{R - R_{min}}{R_{max} - R}\right) \quad (4.2)$$

Where; C is a constant that indicates the relationship between the ratio (R) and pH; R is the ratio of the 2 images with max and min indicating the limiting values; I_a/I_b is the ratio of the emission intensities for the fluorophore in basic and acidic conditions at 640 nm. The drawback of this technique is the calibration is highly dependent upon the number of data points that are collected in the transition regions.

A more robust use of the Grynkiewicz equation is to rearrange it to make R the subject.^{319,320}

$$pH = pK_a + C \log\left(\frac{R - R_{min}}{R_{max} - R}\right) + \log\left(\frac{I_a}{I_b}\right) \quad (4.1)$$

$$\frac{pH - pK_a - \log\left(\frac{I_a}{I_b}\right)}{C} = \log\left(\frac{R - R_{min}}{R_{max} - R}\right) \quad (4.3)$$

$$10^{\frac{pH - pK_a - \log\left(\frac{I_a}{I_b}\right)}{C}} = \left(\frac{R - R_{min}}{R_{max} - R}\right) \quad (4.4)$$

$$R - R_{min} = R_{max} 10^{\frac{pH - pK_a - \log\left(\frac{I_a}{I_b}\right)}{C}} - R 10^{\frac{pH - pK_a - \log\left(\frac{I_a}{I_b}\right)}{C}} \quad (4.5)$$

$$R - R_{min} + R 10^{\frac{pH - pK_a - \log\left(\frac{I_a}{I_b}\right)}{C}} = R_{max} 10^{\frac{pH - pK_a - \log\left(\frac{I_a}{I_b}\right)}{C}} \quad (4.6)$$

$$R \left(1 + 10^{\frac{pH - pK_a - \log\left(\frac{I_a}{I_b}\right)}{C}} \right) - R_{min} = R_{max} 10^{\frac{pH - pK_a - \log\left(\frac{I_a}{I_b}\right)}{C}} \quad (4.7)$$

$$R = \frac{R_{max} 10^{\frac{pH - pK_a - \log\left(\frac{I_a}{I_b}\right)}{C}} + R_{min}}{1 + 10^{\frac{pH - pK_a - \log\left(\frac{I_a}{I_b}\right)}{C}}} \quad (4.8)$$

4.3 Results and discussion

4.3.1 Tucam calibration with SNARF-4F

Calibrations were initially carried out using the rearranged Grynkiewicz equation

$$R = \frac{R_{max} 10^{\frac{pH - pK_a - \log\left(\frac{I_a}{I_b}\right)}{C}} + R_{min}}{1 + 10^{\frac{pH - pK_a - \log\left(\frac{I_a}{I_b}\right)}{C}}} \quad (4.9)$$

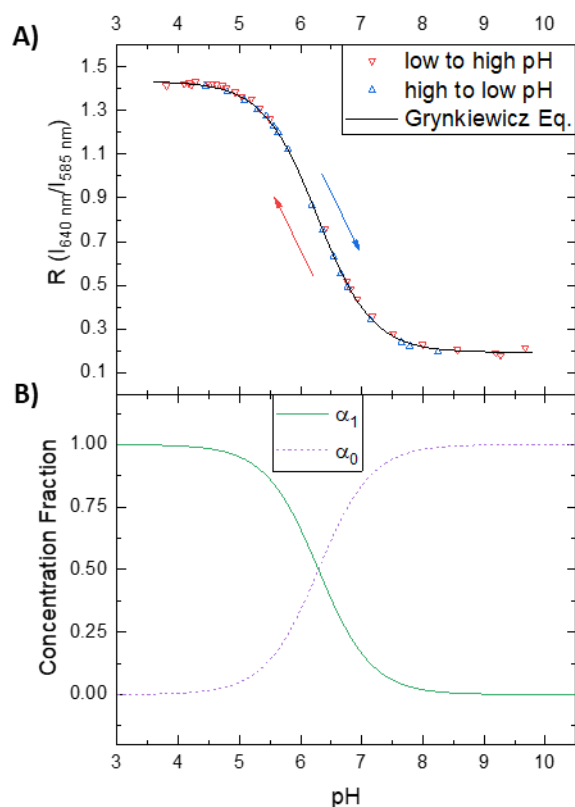


Figure 4-2 A) Calibration plot for carboxy-SNARF-4F using the rearranged Gryniewicz equation;³¹⁵ Red data is for the titration of 0.01 molar NaOH with 0.01 molar HCl, (decreasing the pH); blue data for the titration of 0.01 molar HCl with equimolar NaOH (increasing pH), calibration curve had an R^2 of 0.999. B) Concentration fraction diagram for the protonated (α_1 , black) and deprotonated (α_2 , red) form of carboxy-SNARF-4F $pK_a = 6.29$ from the Gryniewicz calibration curve.

Figure 4-2 A) (Above) shows that there is little to no hysteresis for the dye whether increasing and decreasing in pH. The fitted curve has an adjacent R^2 value of 0.9995 when using the Gryniewicz equation. However, as Table 3 (below) shows the derived values for the calibration curve have large associated errors the origin of which cannot be easily explained. Furthermore, the pK_a of the fitted equation ($pK_a = 5.87 \pm 3.74$) is significantly lower than the nominative pK_a (~ 6.4) given by Thermofischer.

Since the pK_a value of SNARF-4F is the pH at which the ratio of the protonated:un-protonated dye is 1:1 it is possible to determine the pK_a from the calibration data. The pK_a is equivalent to the pH at the midpoint of the calibration curve. This can be expressed mathematically as:

$$pK_a = pH \text{ at } \frac{R_{min} + R_{max}}{2} \quad (4.10)$$

R_{min} and R_{max} of the calibration data set were 0.179 and 1.433 respectively. From this the pK_a was determined to be 6.29. Defining these parameters significantly reduces the associated errors of the remaining parameters.

Table 3 derived values for the calibration of carbox-SNARF-4F using the Grynkiewicz equation.

Parameters	Non-defined pK_a	Defined pK_a
R_{max}	1.433 ± 0.006	1.433
R_{min}	0.194 ± 0.006	0.179
pK_a	5.87 ± 3.74	6.29
$\frac{I_{AH}}{I_A}$	2.546 ± 22.001	1.021 ± 0.012
C	-1.028 ± 0.116	-1.035 ± 0.006
<i>Adjacent R^2</i>	0.9995	0.9993

It is noteworthy that the shape of the calibration plot is indicative of the concentration fraction of protonated carboxy-SNARF as function of pH (Figure 4-2 B). Both are at a maximum at low pH before decreasing to a minimum at high pH. The mid-point of this transition coincides with the pK_a of dye. For these reasons it appears a strong starting point for a simpler calibration equation. Starting with the equation for the concentration fraction of a protonated monoprotic acid (as discussed in Appendix 9.1.1).

$$\alpha_0 = \frac{[H^+]}{[H^+] + K_a} = \frac{10^{-pH}}{10^{-pH} + 10^{-pK_a}} \quad (A1.33)$$

The concentration fraction varies between 0 and 1 depending on the pH. The ratio (R) of the peak intensities of SNARF's at 585 nm and 640 nm (corresponding to the protonated and deprotonated forms of SNARF-4F respectively) vary from a minimum (R_{min}) and maximum (R_{max}) this range can be built into equation 4.2, so that:

$$R = \alpha_0(R_{max} - R_{min}) = \frac{10^{-pH}(R_{max} - R_{min})}{10^{-pH} + 10^{-pK_a}} \quad (4.11)$$

Finally, R_{min} needs to be added to the equation to set the baseline.

$$R = \alpha_0(R_{max} - R_{min}) + R_{min} = \frac{10^{-pH}(R_{max} - R_{min})}{10^{-pH} + 10^{-pK_a}} + R_{min} \quad (4.12)$$

Where:

$$R = \frac{I_{585 \text{ nm}}}{I_{640 \text{ nm}}} \quad (4.13)$$

Or more generally

$$R = \frac{I_{AH}}{I_A} \quad (4.14)$$

Using this altered concentration fraction equation gave the value set out in Table 4. As with the Grynkiewicz the adjacent R^2 is near unity, R_{max} values differ by 0.005, but overlap when taking into account the error. R_{min} values to differ. None the less it is the pK_a values that show the most dramatic difference, more precisely the associated error. Decreasing from 3.47 to 0.008 when changing from the Grynkiewicz equation to the altered concentration fraction equation. Furthermore the latter has two fewer parameters that can affect the curve. One of which (the ratio of intensities) has a large associated error. Another added advantage of the altered concentration fraction method is that the inverse ratio can be fitted to with the deprotonated concentration fraction. Expressed mathematically as, when

$$R = \frac{I_A}{I_{AH}} \quad (4.15)$$

$$R = \alpha_1(R_{max} - R_{min}) + R_{min} = \frac{10^{-pH}(R_{max} - R_{min})}{10^{-pH} + 10^{-pK_a}} + R_{min} \quad (4.16)$$

The calibration was carried out in a capillary tube. This enabled the pixels could be overlapped to get a better camera alignment (camera alignment is discussed more in section 4.3.2). Calibration pH was determined by a pH combination electrode allowing multiple pH measurements to be taken at intervals that are closer together than if using a stock buffers of known pH.

Table 4 derived values for the calibration of carbox-SNARF-4F using the altered concentration fraction equation (4.3).

Altered Concentration Fraction Calibration Curve Parameters	
R_{max}	1.433 ± 0.003
R_{min}	0.197 ± 0.004
pK_a	6.279 ± 0.008
Adjacent R^2	0.99945

The calibration was carried out in a capillary tube. Which acts as a flow cell allowing direct measurement of the pH with a calibrated pH probe. Calibration pH was determined by a pH combination electrode allowing multiple pH measurements to be taken at intervals that are closer together than if using a stock buffers of known pH.

One issue that the calibration curve of carboxy-SNARF-4F does bring to the fore is that the area that exhibits the greatest shift in R occurs over a relatively narrow pH range, 1 pH unit either side of the derived pK_a (6.29) this is unsurprising considering pH is a logarithmic scale. Therefore, any error in the ratio (R) when the pH greater than 7.29 or less than 5.29 can result in a large error in pH. Such errors can be minimised using filters and optics with high transmission at the correct wavelengths and the use of pixel binning, all of which maximise the signal to noise ratio.

Pixel binning is the combining of pixels to make a larger pixel. Pixel binning is pay off between a loss of resolution for a reduction in noise. For the particles synthesised and discussed later (section 5.1) this loss of resolution is not an issue as they are of a millimetre length scale, as such 4x4 pixel binning could be employed.

4.3.2 Image processing

A flat-field correction removes artefacts in the image caused by variation between individual pixel sensitivities and by distortions/aberrations in the optical path. The process of flat-field corrections compensates for the dark currents within the camera’s detector and the gain which occurs throughout the microscope setup. The flat field correction can be expressed mathematically as;

$$C_i = \frac{m(R_i - D_i)}{(F_i - D_i)} = G_i(R_i - D_i) \quad (4.17)$$

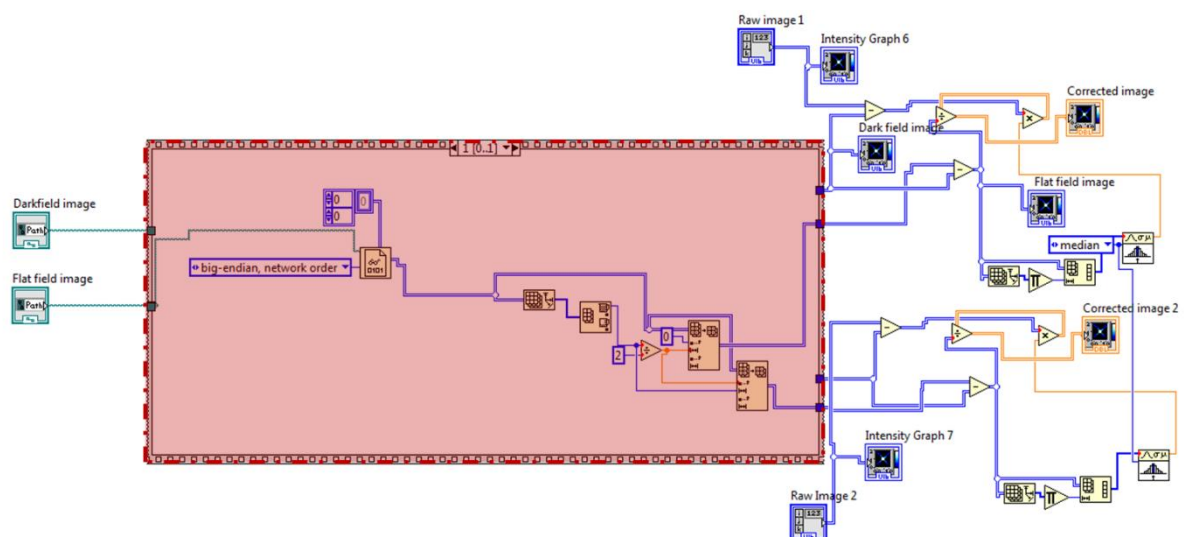


Figure 4-3 Image of the ‘block’ diagram of the flat-field correction sub-VI written in LabView, the section in red converts the image to an array of values the section to the right performs the mathematics of the flat-field correction and convert the array back to an image.

Where C_i is the corrected image, R_i is the raw image, F_i is the flat field image, D_i is the darkfield image and m is the image-averaged value of $F_i - D_i$. The gain is:

$$G_i = \frac{m}{(F_i - D_i)} \quad (4.18)$$

The flat-field correction of each image is carried out by a script written in LabView (Figure 4-3). In order to process data in real time the raw data for the darkfield image and flat-field image is written from its raw byte data form into a 1 dimensional array of data, it is then reshaped into a 2 dimensional array to form the image (highlighted area in Figure 4-3). The data from each camera is stitched together allowing it to be treated as a single entity. This inhibits any problems occurring when trying to separate the streams from two different cameras.

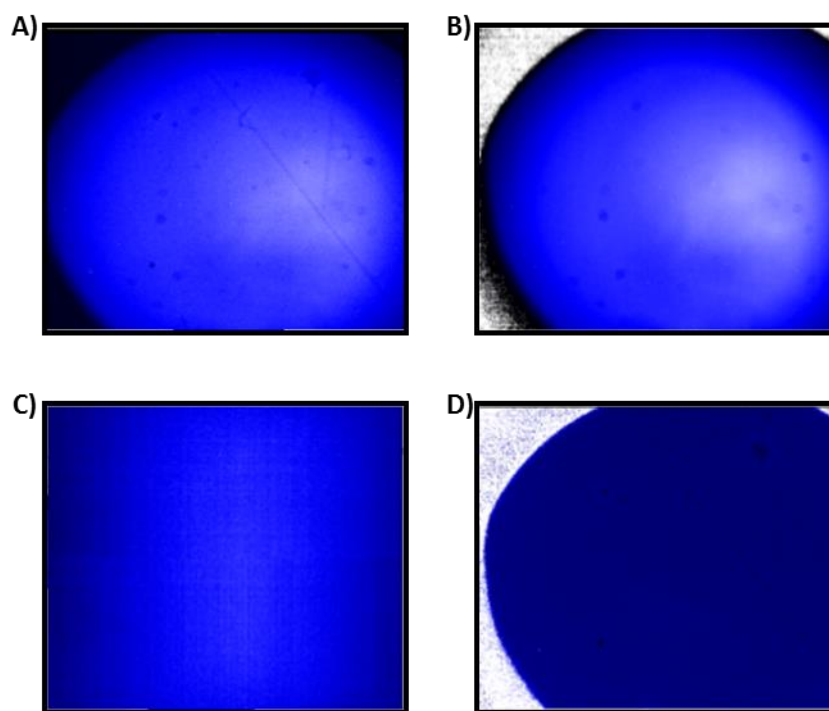


Figure 4-4 A) a raw image prior to flat-field correction B) composite image of the gain C) enhanced image of the dark field D) flat-field corrected image

A raw image (Figure 4-4 A)) shows up the scratches on the reaction vessel and what could be particles or dust. The gain image (Figure 4-4 B)) is a composite image of the reaction vessel in slightly different positions and accounts for dust on lenses, aberrations on the reaction vessel and non-uniform lighting. The gain image is akin to a background/blank sample used in UV-vis and IR spectroscopy. The dark field image (Figure 4-4 C)) accounts for the small electric current that flows through camera's chip even when no photons are entering the device, and is due to the random generation of electrons and holes. By applying the flat-field correction artefacts that could be

attributed to the apparatus are removed. The corrected image (Figure 4-4 D)) now shows near uniform pH across the entire image, however the peripheral 50-100 pixels do still show a slight variation in pH.

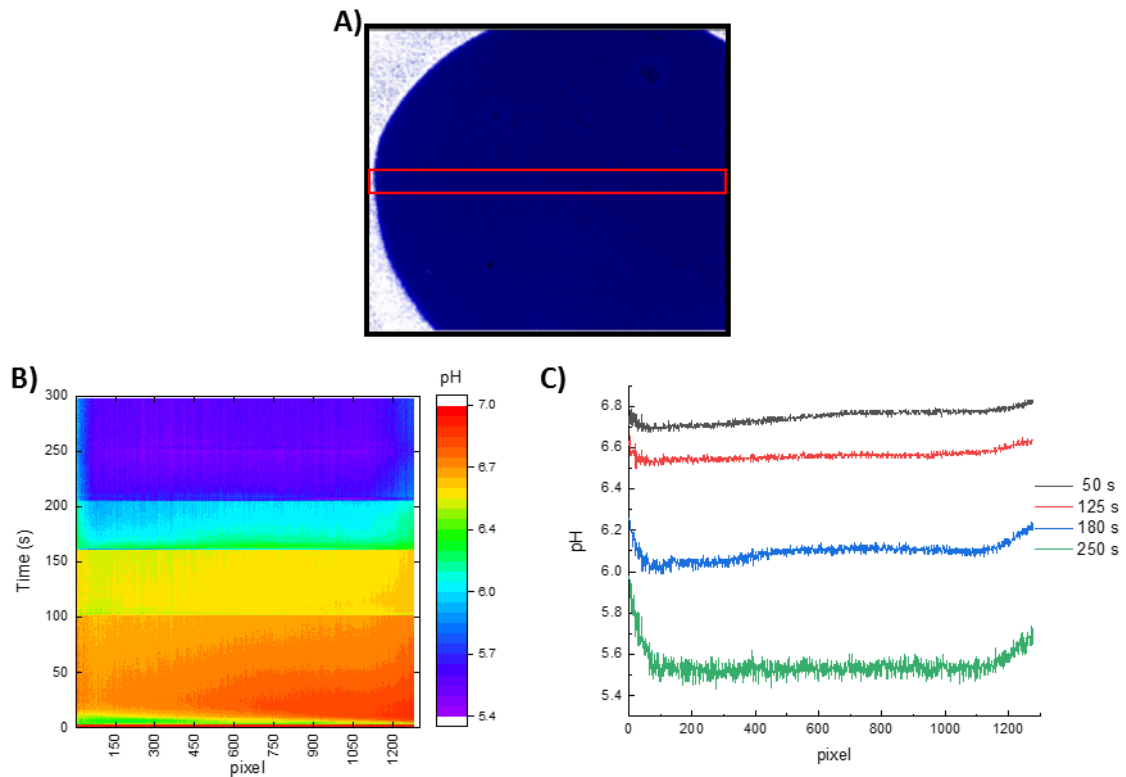


Figure 4-5 A) corrected image with the region of interest highlighted in red, the pH is an average of the y-axis for each position employing 2x2 pixel binning. B) a heat map of the change in pH as a function of the x-pixel against Time (s) C) pH as a function of x-pixel for a specific time.

This variation may be attributable to errors in camera alignment. However, the camera alignment was carried out with no pixel binning using a standard grid. It is more likely that this error is due to the use of an elliptical mirror to direct the light into the Tucam coupled with the large field of view. This results in the periphery of the image being prone to distortion. Employing 2x2 pixel binning as in Figure 4-5 results in a small signal:noise ratio at low pH (around pH 5.5). This error at pH 5.5 is due to the shallowing on the calibration curve. As such a small error due to noise can cause a significant shift in pH. Furthermore, Figure 4-5 shows that despite a flat-field correction being carried out at a single pH the correction can be applied to a range of pH values.

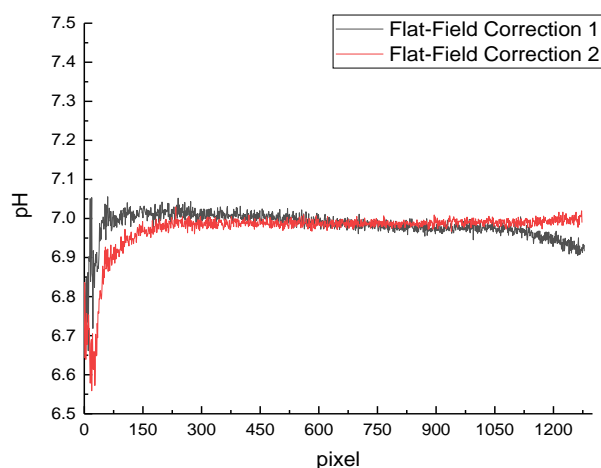


Figure 4-6 pH as a function of pixel position in the x axis for an initial flat field correction (black) and a second attempt (red) shows how taking more care in obtaining the flat-field image improve the overall flat-field correction. These flat field corrections use 2x2 binned data.

The quality of the flat-field image can have a dramatic effect on the quality of the flat-field correction. Figure 4-6 shows how the use of flat-field image that is comprised of more sample images diminishes the shift in pH for pixels toward the edge of the sensor. The shift at low end (0-100 pixels) is thought to be due a high degree of noise possibly due to the edge of the elliptical mirror distorting the light as it is reflected into the two camera imaging adapter.

4.3.3 Effect of SNARF-4F concentration

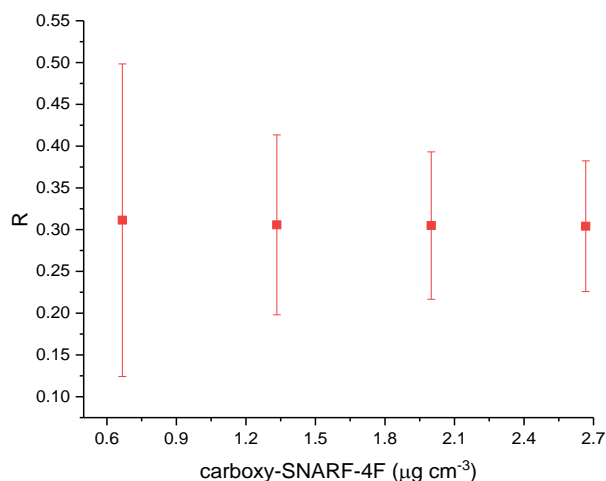


Figure 4-7 Graph showing the effect of increasing the concentration of SNARF-4F on the fluorescent ratio (R) for a pH 7.0 phosphate buffered solution

Increasing the concentration of SNARF-4F in solution has little effect on the fluorescent ratio value (Figure 4-7), decreasing from 0.311 to 0.304 as the concentration is increased four-fold. Increasing the concentration does, however, have a great effect on the standard error, increasing the concentration from $0.67 \mu\text{g cm}^{-3}$ to $1.33 \mu\text{g cm}^{-3}$ almost halves the error from ± 0.187 to ± 0.107 . Further increases in the concentration see a plateauing in the standard error as it decreases to a minimum of ± 0.078 when the concentration is increased to $2.67 \mu\text{g cm}^{-3}$. This decrease in standard error is due to the counts (intensity) increasing thereby increasing the signal to noise ratio in the signals favour. Due to the expense of SNARF-4F (£248 for 1 mg (price correct as of April 2017)) and only small gains being seen when increasing the concentration above $2.67 \mu\text{g cm}^{-3}$ all experiments unless specified use SNARF-4F at that concentration.

4.4 Conclusions and Future Work

In this chapter we have discussed the building and calibration of an intricate ratiometric imaging setup, which can be used for the probing of collective within pH shift inducing soft hydrogel objects. Within this setup a flatfield correction has been written in LabView and applied to the resulting images. This compensates for individual pixel sensitivities and distortions in the optical path, such as that caused by the edges elliptical mirror that directs the light into the two-camera image adapter. Furthermore, it has been shown that increasing the SNARF-4F concentration has little effect on the fluorescent ratio. However, the resulting standard error increases with dye concentration up to $2.00 \mu\text{g cm}^{-3}$ ($R_{std\ error} = \pm 0.089$). Increasing the dye concentration further has little effect on the further reduction the associated standard error. It has also been demonstrated that SNARF-4F shows little to no hysteresis when $\frac{dpH}{dt}$ is positive or negative. Two separate calibration equations (the rearranged Grynkiewicz equation (Eq. 2.2) and a manipulation of the concentration fraction equation (Eq. 2.3)) have been used on the calibration data both of which have a high degree of accuracy.

5. Particle Synthesis

5.1 Overview

In order to create a wholly synthetic quorum sensing system a host particle for the component technologies to be entrapped within was required. Initially pH-responsive hydrogels formed of either methacrylic acid or chitosan were synthesised and characterised. However due to rapid, facile synthesis and reported enzyme encapsulation Ca-alginate hydrogels were chosen instead. The addition of magnetite to meet the first key stage of autonomous aggregation is also explored.

5.2 Results and Discussion

5.2.1 Poly(methacrylic acid) Particles

5.2.1.1 Preparation of poly(methacrylic acid) particles

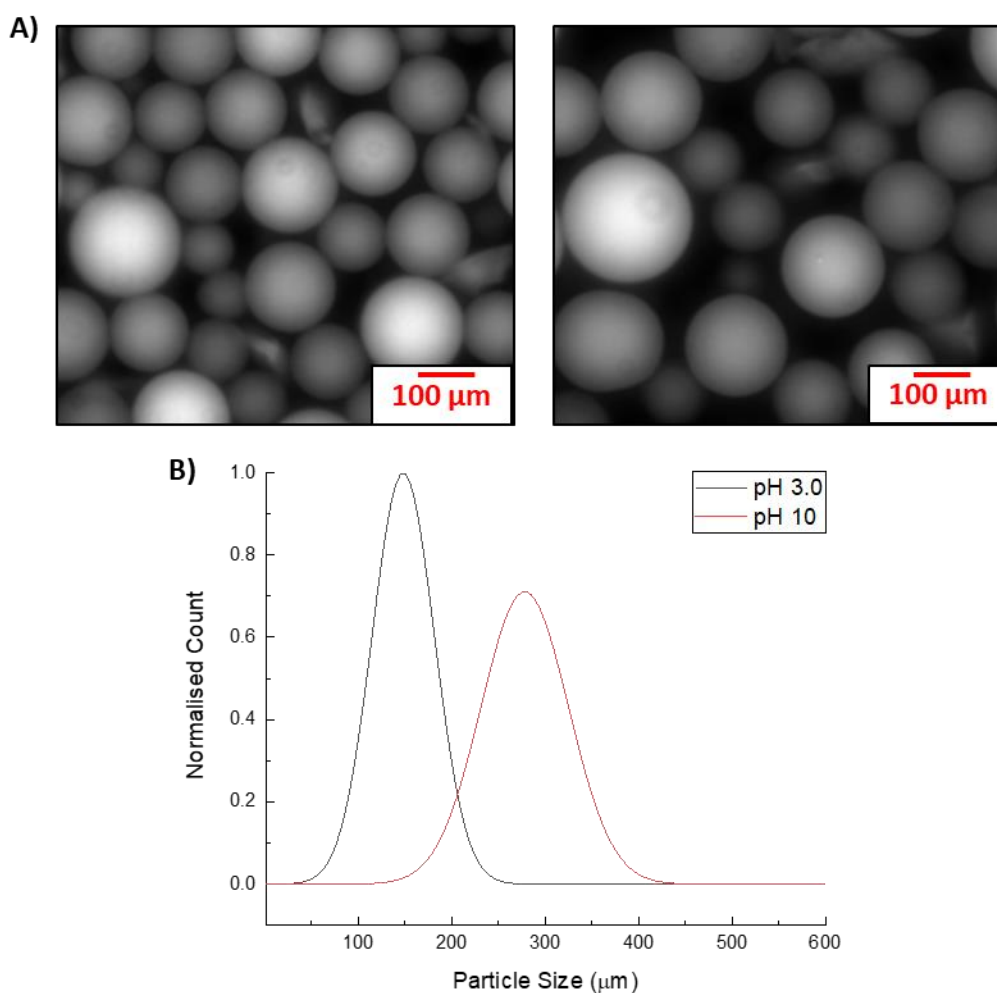


Figure 5-1 A) fluorescent microscopy images of rhodamine 6G loaded PMAA particles at pH 3.0 demonstrating their polydispersity. B) normalised size distribution plots for PMAA particles in their shrunken (pH 3.0; grey; $148 \pm 33 \mu\text{m}$) and swollen (pH 10; red; $278 \pm 47 \mu\text{m}$) $N = 2500 \pm 50$

A water in oil emulsion polymerisation was used to fabricate poly(methacrylic acid) (PMAA) particles. A thermal redox initiator of APS and the accelerator TEMED was used since APS has a half life time of 130 hours at 50 °C, pH 7.0.³²¹ Addition of the accelerator enabled the reaction to reach completion in 2 hours at 40 °C. A relatively quick reaction at a low reaction temperature would be required if GOx were to be included for a one-pot particle synthesis. Since GOx rapidly denatures when exposed to temperatures over 40 °C.¹³¹ Base (sodium hydroxide) is added to the aqueous phase to deprotonate the acid groups of the monomer, thereby stopping the monomer partitioning into the bulk oil phase.

The fluorescent dye rhodamine 6G ($\lambda_{\text{ex}} = 526 \text{ nm}$; $\lambda_{\text{em}} = 555 \text{ nm}$) was included in the synthesis to aid particle imaging and size analysis (Figure 5-1). The resulting PMAA particles were relatively polydisperse ($148 \pm 33 \mu\text{m}$ at pH 3.0) this can be attributed to a couple of factors, the use of a non-ionic surfactant and low shear mixing. The non-ionic surfactant, span-80, was used rather than an ionic surfactant such as sodium dodecyl sulphate due to the continuous phase being oil based rather than aqueous. Increasing the pH to 10 causes the particles to swell due to the deprotonation of the pendent acid groups along the PMAA backbone, the particles almost double in size to $278 \pm 47 \mu\text{m}$.

5.2.1.2 Reversibility of PMAA particle's pH response

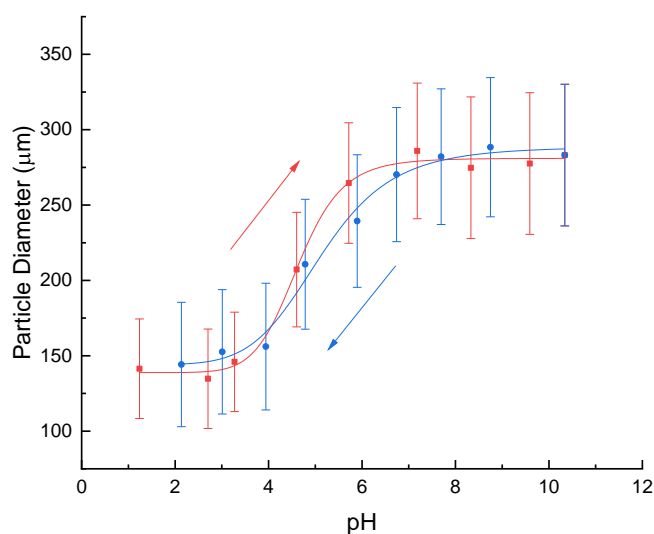


Figure 5-2 PMAA particle diameter as a function of pH, demonstrating hysteresis and slight loss of responsiveness. $N = 27$

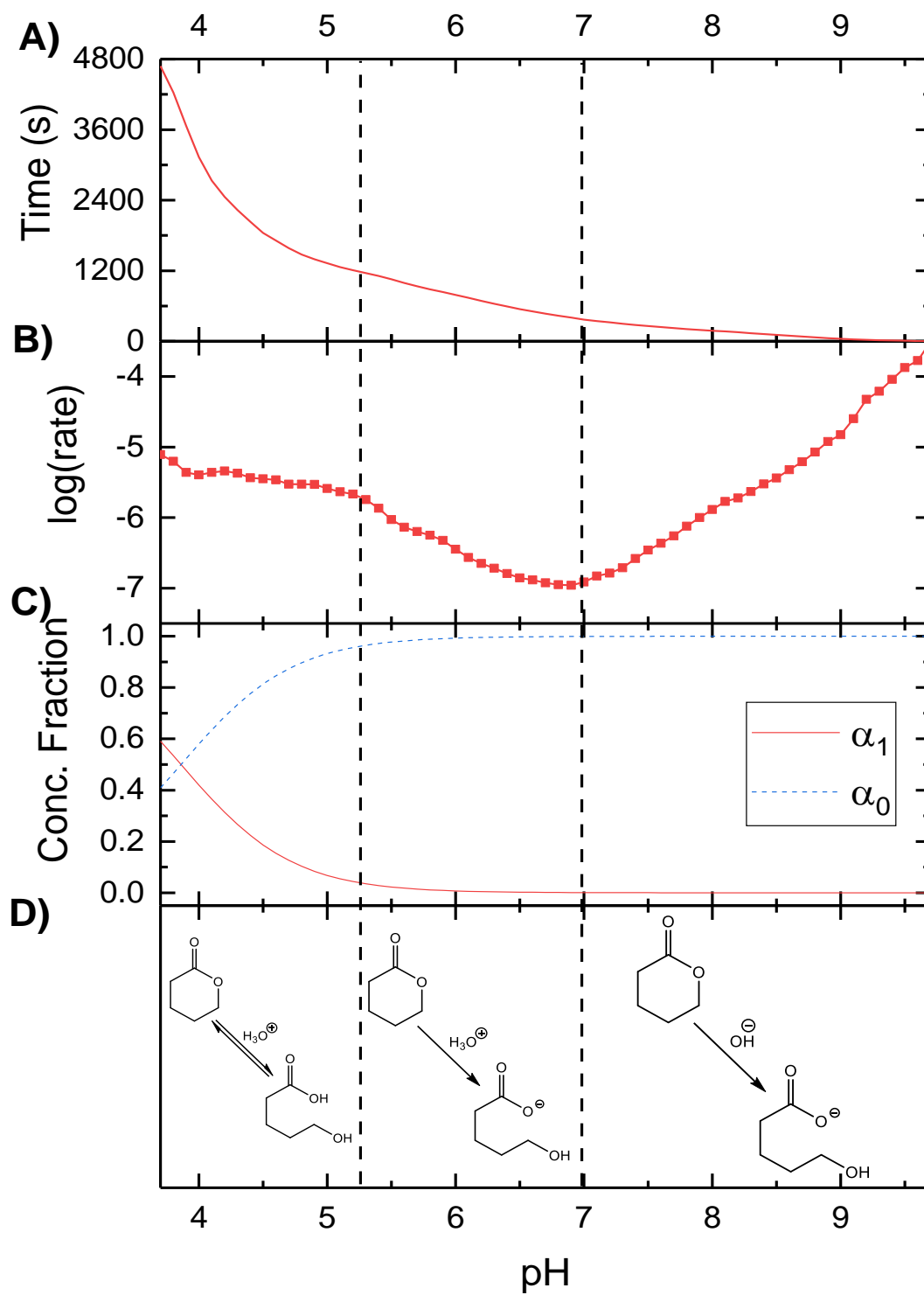
The action and reversibility of PMAA's volumetric response was investigated by a titrating hydrochloric acid (100 mmol dm^{-3}) with sodium hydroxide (100 mmol dm^{-3}) in a similar fashion to the calibration experimental of carboxy-SNARF-4F (see pages 51 and 79). In brief rhodamine 6G labelled PMAA particles were placed in a petri dish, HCl (100 mmol dm^{-3}) was placed in a separate beaker fitted with a calibrated micro-pH electrode. The solution cycled from the reaction vessel to the petri dish and

back through via a peristaltic pump and tubing (flow rate; $1 \text{ cm}^3 \text{ min}^{-1}$). The pH was increased by the addition of NaOH, after each addition the reaction mixture was left for 15 minutes for the pH to equilibrate. Upon reaching pH 10 the process was reversed with aliquots of HCl being added. The particles were imaged in fluorescence mode using an optical microscope see page 52. The resulting images were analysed using ImageJ to obtain the average particle diameter and standard deviation then plotted as a function of pH (Figure 5-2).

The PMAA particles exhibited some hysteresis as pH was increased and decreased. Furthermore, the cycling of pH shifted the midpoint of the transition from 4.6 (addition of base) to 5.1 (addition of acid). This is thought to be due to some of the pendent acid groups within the PMAA particles remaining deprotonated as the HCl is added. This theory is supported by the increase in size and standard deviation of the particles when the pH is less than 3.0 pre and post pH cycle ($138 \pm 33 \text{ }\mu\text{m}$ and $148 \pm 41 \text{ }\mu\text{m}$ respectively). During the decreasing pH cycle the steep volumetric response as a function of pH is slightly broader. Again, this can be attributed to the fewer of the pendant acid groups becoming protonated during the addition of acid.

Further investigation of PMAA particles was not carried out due to a combination of factors. A one-pot synthesis entrapping GOx in the PMAA particles would expose GOx to free radicals, that could denature the enzyme and some denaturation would occur at $40 \text{ }^\circ\text{C}$. Furthermore, sodium hydroxide is included in the aqueous phase of the emulsion polymerisation to stop the methacrylic acid partitioning into the oil phase. Since NaOH is a strong base, the pH of the solution can easily become basic due to minute variations in the volume acid to base. Coulthard et al demonstrated that GOx rapidly denatures when exposed to a pH in excess of pH 8.0.¹³⁶ The exposure of GOx to such stresses would therefore significantly change the enzyme activity between particle syntheses.

Adsorption of GOx into PMAA particles is an unfavourable technique as may give rise enzyme leaching which would inhibit observation of the collective behaviour since free enzyme could diffuse into the bulk of the reaction. Finally, from Chapter 3 (



Figure

3-22

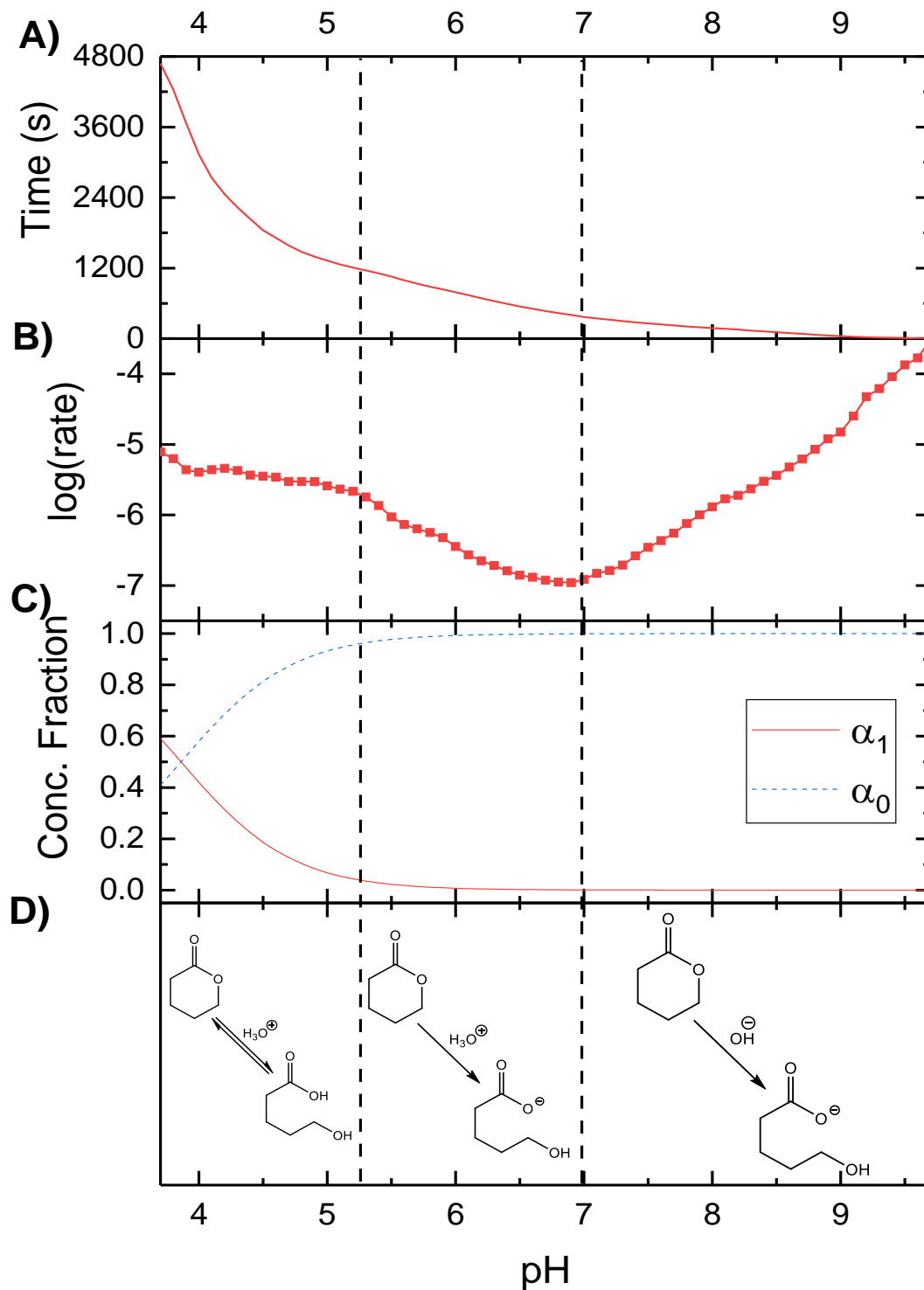


Figure 3-22) and work by Foss, Goto, Morishita and Peppas³²² into insulin delivery suggest that GOx loaded hydrogels can only lower the pH to a minimum around pH 5.0. Therefore, the volumetric shift of PMAA particles would be of little statistical significance.

5.2.2 Chitosan Particles

An alternative smart polymer to deliver a potential volumetric transition with a shift in pH is chitosan (pK_a 6.2).²¹⁸ As with the methacrylic acid particle synthesis a water in oil emulsion technique was employed. This was so that if an enzyme were to be incorporated in a one-pot synthesis there would be no loss of enzyme into the bulk phase.

5.2.2.1 Preparation of chitosan particles

Chitosan particles were synthesised by a water in oil emulsion (10 % v/v). The chitosan (190-310 kDa; 82 % deacetylated) requires an acid solution to dissolve. This was achieved by dissolving chitosan (2 %w/ v) in an acetic acid solution (3 % v/v). This results in the aqueous solution being slightly acidic. This is an advantage over the MAA particle since if GOx were to be included in a one-pot synthesis the pH it would be exposed to would not denature it. The aqueous solution was mixed with an oil phase of hexane and paraffin oil (volumetric ratio 7:5) and the non-ionic surfactant Span 80 (1 % w/w of oil phase). Wang, Ma and Su²¹⁵ reported that the volumetric ratio 7:5 hexane:paraffin oil resulted in a relatively narrow size distribution of chitosan particles due to the relatively low viscosity of the aqueous phase. Furthermore, particles synthesised in a mix of hexane and paraffin require less washings with hexane to remove the oil phase, than particles synthesised in paraffin oil alone.

The addition of the crosslinking agent glutaraldehyde saturated toluene (GST) took place over 1 hour. As the addition of the 2-6 cm³ of an oil phase (without an emulsifier) in a single step would decrease the proportion of surfactant at the particle interface resulting in coalescence of the aqueous phase and larger particles. It is thought that initial aliquots of GST crosslink a thin layer of the chitosan droplets, allowing them to hold their shape. With later aliquots and the residual 2 hours of stirring allowing the glutaraldehyde to partition into the particles and form cross links throughout.

After all the GST was added stirring was maintained and the emulsion was left for 2 hours. The resulting particles were separated by vacuum filtration followed by washing with hexane and then water three times.

5.2.2.2 Effect of Emulsifying Stir-Rate on Particle Size Distribution

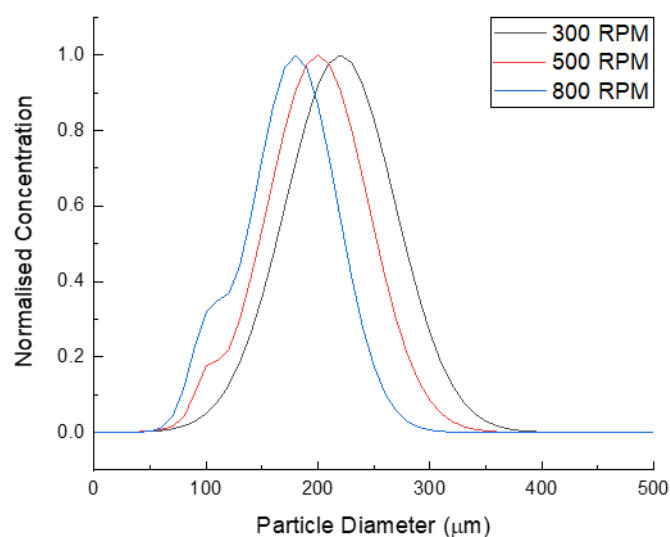


Figure 5-3 Particle size distribution of collapsed (pH 9.0) chitosan particles emulsified at different low shear stir rates. $N = 500 \pm 25$

Prior to the addition of GST, the water in oil emulsion was stirred (300-800 RPM) for 30 minutes. This emulsified the solution. The stir-rate was then slowed to 300 RPM and GST (1:2 volumetric ratio chitosan solution:GST) was added to the solution as previously described. The resulting particles were left to swell in a 0.1 mol dm^{-3} NaOH solution corrected pH 9.0 with hydrochloric acid (1 mol dm^{-3}) for 1 hour. Particles were imaged with a Nikon microscope fitted with a Pixelink camera. The resulting images were analysed using ImageJ. Particle size decreased with increasing stir-rate (Figure 5-3). However, only the lowest stir-rate (300 RPM) had a single peak ($220 \pm 49 \mu\text{m}$). Particles that had been emulsified at faster stir-rates had a smaller particle diameter, $199 \pm 46 \mu\text{m}$ and $176 \pm 42 \mu\text{m}$ at 500 and 800 RPM respectively. Furthermore, the faster stir rates gave rise to a shoulder at around $100 \mu\text{m}$. This shoulder grew with increasing stir rate and is thought to be due to a combination of factors. Firstly, slowing the stir-rate to 300 rpm prior to the addition of crosslinker decreases the shear in the reaction mixture allowing the droplets to coalesce. Secondly, since emulsion is of set volume the surface area of the water oil interface has a reciprocal relationship with the particle size;

$$SA = 3V_{aqueous}r^{-1} \quad (5.1)$$

Where SA is the surface area, $V_{aqueous}$ is the total volume of the aqueous phase and r is the mean radius of the particle. Therefore, the proportion of span-80 at the water oil interface is greater, as GST is added the concentration of emulsifier in the oil phase decreases. To compensate for this a portion of the emulsifier is stripped from the interface making the droplets unstable and increasing the probability of them coalescing. This is an artefact of using a non-ionic surfactant which stabilise the interface through steric crowding. Therefore, it could potentially be overcome by including an

emulsifier in the GST solution so that there is no change in the emulsifier concentration as the crosslinking solution is added. Alternatively, a non-ionic surfactant such as tween-80 could be added to the aqueous phase. The tween family of non-ionic surfactants more favourably partition into the aqueous phase of an emulsion due to the PEG side chains. A collaboration between the Mainwaring and Jackson^{265,266} used a combination of both span and tween emulsifiers to synthesis chitosan nano/microparticles. Increasing the proportion of tween-80 resulted in larger particle size when all other reaction conditions were kept the same. One drawback of using tween is that the emulsifier may remain in the chitosan particle even after several washings.

5.2.2.3 Degree of Crosslinking and pH responsiveness

The degree of crosslinking was altered by changing the volumetric ratio of the aqueous chitosan solution:GST from 1:1 to 1:3. GST was added in 4 aliquots over the course of one hour. Typical images of the resulting particles in there collapsed state (pH 7.5) and swollen state (pH 3.0) can be seen below (Figure 5-4). Increasing the volumetric ratio from 1:1 to 1:2 has little effect on the particle size or distribution. However, increasing the proportional volume of GST further to 1:3 generates a larger distribution of particles. This could be a result of the method of GST addition, since the neither the number of aliquots nor the crosslinker addition time is increased. As the volumetric ratio changes from 1:1 to 1:3 the volume of GST increases 3-fold.

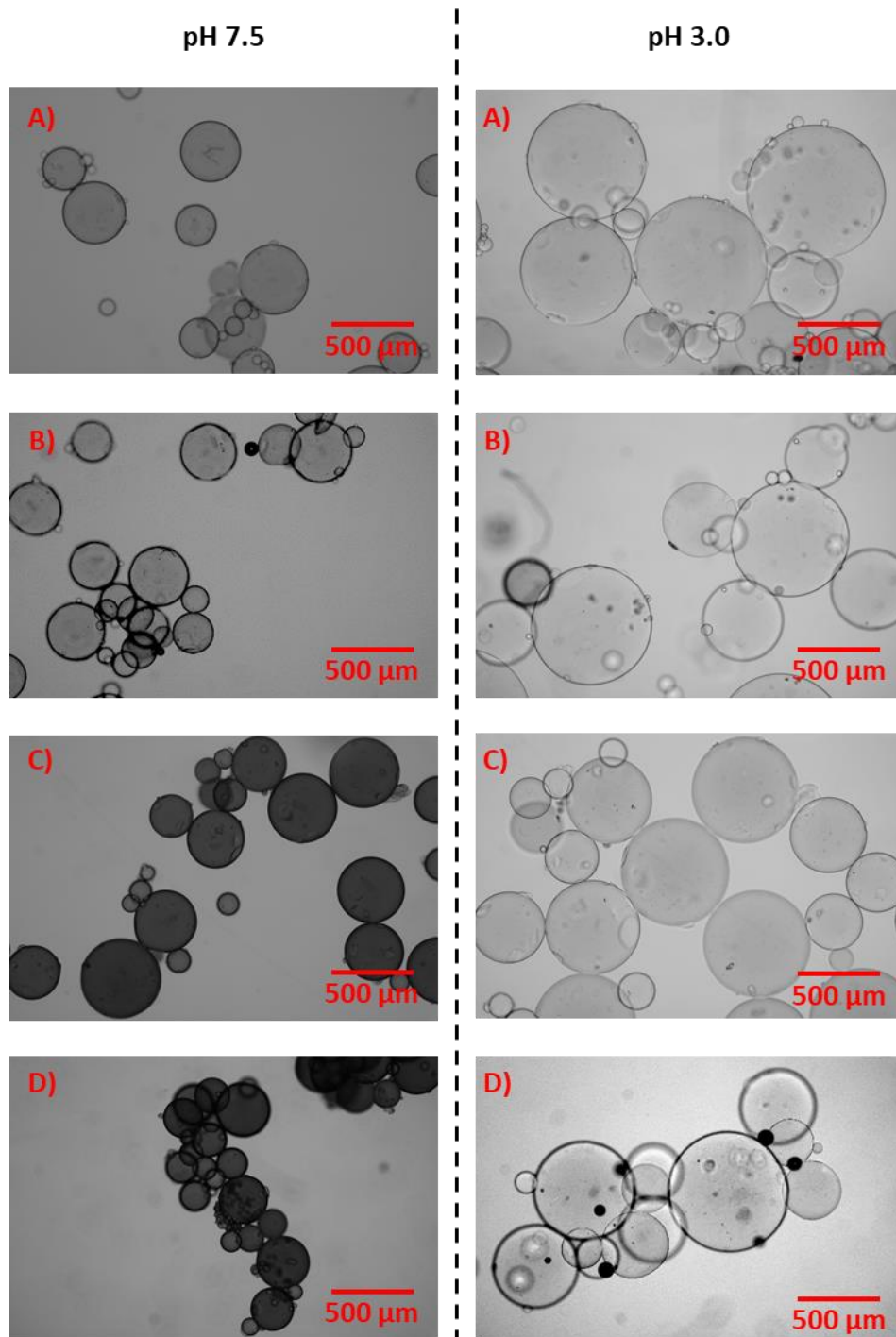


Figure 5-4 representative images of collapsed (pH 7.0) and swollen (pH 3.0) glutaraldehyde crosslinked chitosan particles. volumetric ratio of chitosan solution:GST is; A) 1:1; B) 2:3; C) 1:2; D) 1:3. Particles imaged with a Pixelink camera (PL-B742F) on an Nikon eclipse inverted microscope with a 4x zoom lens.

It is believed that in a reaction with 1:1 volumetric ratio of chitosan solution:GST, the initial particles thought to be smaller than the final average size and of a relatively uniform in size. As GST is added crosslinks start to form within the chitosan droplets. By the final addition of GST the % v/v of span 80:oil phase reduces from 1 to 0.9 % v/v. This reduces the concentration of span 80 at the oil water

interface resulting in unstable particles. These then collide with one another, due to only light crosslinks being formed at this point they coalesce to form larger particles. As the degree of crosslinking increases in the final stages of the reaction the particles no longer coalesce.

Whereas in a reaction with a volumetric ratio of 1:3 the opening addition of GST (0.75 cm³) is equivalent to the addition of the first 3 aliquots of GST of a 1:1 reaction. As such crosslinks form more rapidly as the reaction proceed a portion of the particles coalesce. However, some particles rapidly form a 'shell' of crosslinked chitosan and are unable to merge with one another. This results in the broader particle distribution that is observed.

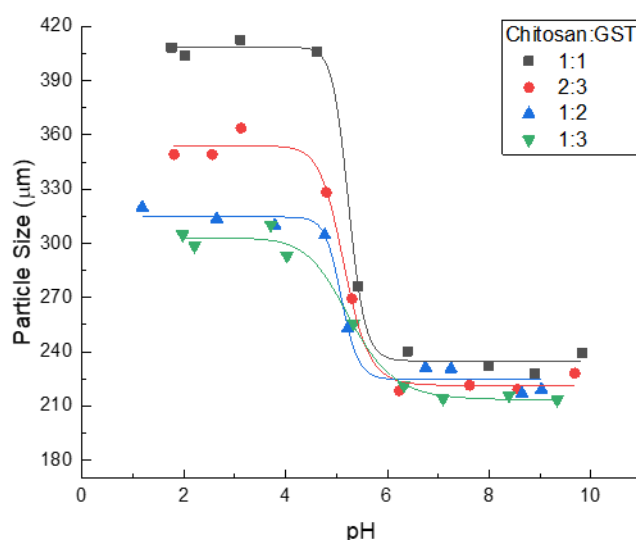


Figure 5-5 Chitosan particles diameter as a function of pH and crosslinking.

The volumetric response of glutaraldehyde crosslinked chitosan particles to shifts in pH was investigated by titrating sodium hydroxide (100 mmol dm⁻³) with hydrochloric acid in the presence of chitosan particles. The reaction was carried out in a similar fashion to the investigation of PMAA's volumetric response (section 5.2.1.2 page 90). However, due to the particles size they were imaged using a Pixelink camera (PL-B742F) on a Nikon eclipse inverted microscope with a 4 x lense. The resulting images were analysed with ImageJ to obtain the average particle diameter, and then plotted as a function of pH (Figure 5-5).

All chitosan particles exhibited a volumetric transition, from a collapsed state at pH > 6.2 to a swollen state under acidic conditions (< pH 5.1). However, the volumetric transition became less sharp, broadening from around 1 to 2.5 pH units as the volumetric ratio of chitosan:GST was increased from 1:1 to 1:3. This is due to glutaraldehyde forming crosslinks by reacting with the pendent amine groups

of the chitosan to form an imine. This increases the distance between charged species along the polymer chain, since there are fewer primary amines to protonate. This results in weaker charge repulsion and a broader region of response. Furthermore, increasing the degree of crosslinking reduces the degree of swelling from 1.8 to 1.4. Due to the glutaraldehyde crosslinks inhibiting water absorption and weaker charge repulsion along the polymer backbone.

Further investigation of chitosan particles was not carried out for several reasons. A volumetric transition response results in accelerated leaching unbound enzyme when the chitosan particle is in a swollen state.³²³ This can be overcome by either entrapping the enzyme within the polymer matrix during the particle synthesis. Alternatively, the GOx can be chemically immobilised through the formation of covalent bond between the polymer and enzyme. However, the latter can result in loss of enzymatic activity due to immobilisation blocking the enzymes active site or kinetically locking it into an unreactive conformer.^{324,325} Both chitosan and GOx are abundant with primary amines making immobilisation with glutaraldehyde facile. However, it would be difficult to control both the degree of crosslinking and number of covalent bonds between GOx and the polymer backbone. As such it was sought a hydrogel particle that could be rapidly synthesised, into which GOx could be physically entrapped preferably in a single pot synthesis. Furthermore, the resulting particle did not exhibit a volumetric response.

5.2.3 Alginate Particles

5.2.3.1 Alginate Particle Synthesis

Particles were left in the aqueous calcium chloride solution for 10 minutes allowing the divalent calcium cations to penetrate the whole of the particle, thereby hardening the particle by crosslinking through the egg-box model (section 1.8.2) with Ca^{2+} in the interstitial sites acting as the eggs. Particle synthesis resulted in near spherical particle with a diameter of 2.11 ± 0.05 mm (Figure 5-6) the variation in particle size is thought to be due to hysteresis of the contact angle between the propagating alginate droplet and the stainless steel needle.^{326,327} The slight non-spherical nature of the particles is attributed to the high viscosity of the alginate solution.^{328,329} Prüsse et al. have shown two effects that result in non-spherical beads both of which are driven by the inherent high viscosity of alginate solutions.³²⁸ Firstly the adhesion force of the alginate solution to the needle tip increases with increasing viscosity resulting in an elongated tear-shape.^{328,329} Secondly the increased viscosity slows droplet formation as such gravimetric effects stretch the droplet.³²⁹ On release from the needle tip the surface tension driven contraction of the droplet into a spherical shape is slowed by the high viscosity of the alginate solution, as such a greater distance between the needle tip and CaCl_2 bath would be required to allow the alginate droplets to become spherical.^{328,329}

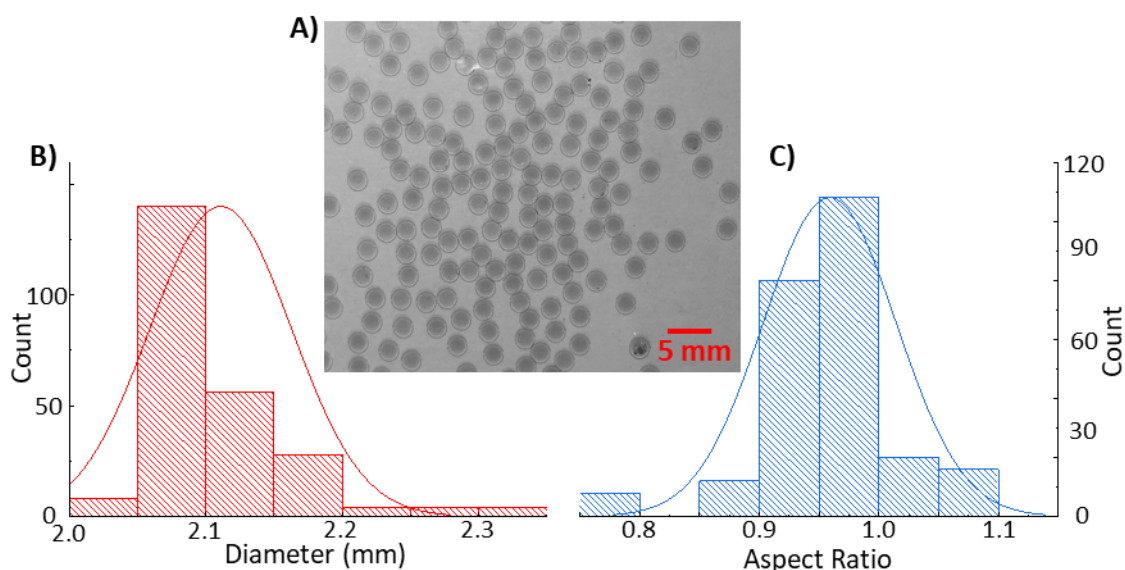


Figure 5-6 A) Image of 2 % w/w alginate particles containing 0.015 % w/w rhodamine B; B) Size distribution plot of alginate particles, mean diameter 2.11 ± 0.05 mm, $N=244$; C) Aspect Ratio histogram of the alginate particles, $N=244$. Image taken with a Canon EOS 5Ds fitted with a MP-E 65 mm f/2.8 1-5x macro lens.

5.2.3.2 Ferrous Magnetite Loaded Particles

The Hawaiian Bobtailed Squid (*Euprymna scolopes*) filters the bacteria *A. fisheri* from sea water and stores it in its light organ. When the bacteria population crosses a threshold, they fluoresce. The bobtailed squid can be described as acting as an aggregating agent. This action could be replicated by simply adding more particles to a petri dish. However, to have truly autonomous system it would be preferable to have a defined particle population within a reaction and draw them to a single point, thereby increasing the local population density. Such aggregation could be used for sight specific drug delivery. Magnetite containing ferrofluids and polymeric particles have been used to demonstrate sight specific drug delivery.^{330,331} Targeted chemotherapy can be simply carried out through the intravenous administration magnetic drug carriers to arterial blood supply of a tumour. Application of an external magnetic field then retains the carrier at the target site.³³⁰ The chemotherapeutic then leaches from the carrier and is delivered directly to the tumour sight.

Taking inspiration from this ferrous magnetite (0.0025-0.01 % w/v of the solution) was included in the pre-gel alginate solution the resulting particles were then placed in a petri dish (3.5 cm diameter) with DI water (2 cm³). Such that the particles were in a single plain, sandwiched between the surface of the petri dish and the water air interface. The particles were imaged in the both without and with a magnetic field present, brought about using and neodymium magnet (Figure 5-7). All degrees of magnetite loading exhibited a degree of aggregation. However, only when loading was ≥ 0.0065 % w/v did all particles aggregate to a single point in a pseudo-hexagonal arrangement. For particles with

magnetite loading < 0.0065 % w/v the meniscus formed between it and the water air interface inhibited aggregation of the particles.

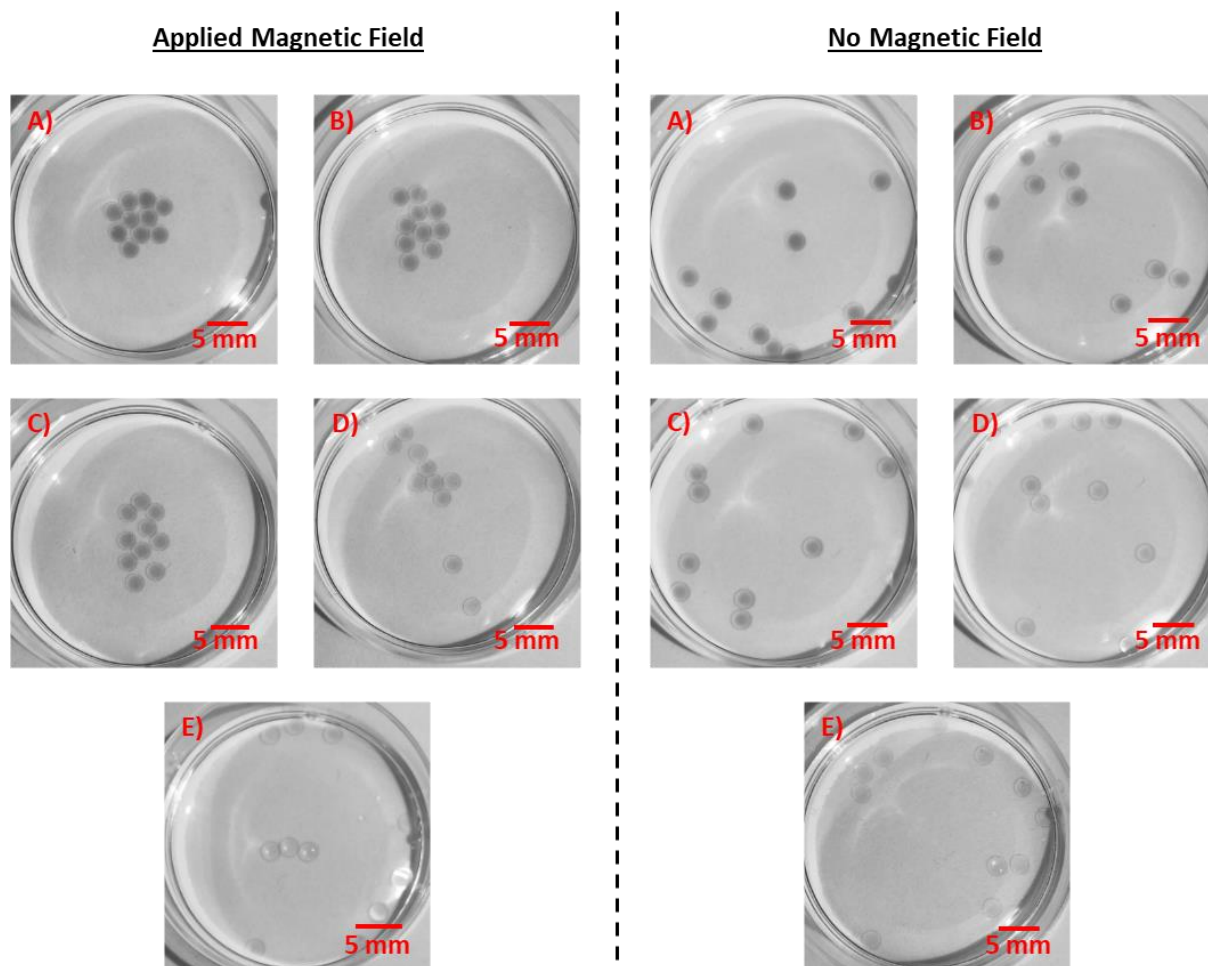


Figure 5-7 Images of 10 rhodamine labelled Ca-alginate particles loaded with 5 μm ferrous magnetite (A) 0.01; B) 0.0075; C) 0.00625; D) 0.005; E) 0.0025 % w/v of pre-gel solution) in and out of an applied magnetic field.

5.3 Conclusions and Future Work

Three particles formed by different methods have been investigated. Particles formed by the crosslinking of alginate by an extrusion-dripping method into a calcium ion gelation bath were found to have a narrow particle distribution and could be rapidly synthesised. Furthermore, such particles have been reported in physical entrapment and adsorption of urease.^{75,77} The addition of magnetite to the alginate particles enabled autonomous aggregation in the presence of a magnetic field to occur.

Particles that exhibited a volumetric response to changes in pH employed water in oil emulsion techniques to form the particles. The PMAA particles increased in size with pH with a midpoint of transition at around pH 4.8. Whereas, chitosan particles shrank with increasing pH with the midpoint

around 5.1. Although both PMAA and chitosan particles exhibited a volumetric response glucose oxidase was not immobilised within them since it was feared that the enzyme would be denatured. However, all particles synthesised could potentially be the carrier particle for the component quorum sensing technologies.

6. Glucose oxidase loaded particle analysis

6.1 Overview

So far, we have developed a consistent ratiometric setup with a calibration curve that involves no erroneous values. And we have studied GOx as method of signal generation by its conversion of glucose to glucono- δ -lactone and the subsequent ester hydrolysis to gluconic acid. This method of signal generation is autocatalytic, acid production increases as the pH is lowered from pH 7 to 5.2. In this section we look at the alginate particles which contain the signal generator GOx and magnetite. Once characterised we look at diffusion of the signal from a single particle through ratio metric imaging. Finally, cluster size is changed and in order to attain to gain a further understanding of group dynamics.

6.2 Results and Discussion

6.2.1 Particle synthesis and characterisation

As discussed previously (section 5.2.3.1) calcium alginate particles containing GOx (4.95 units cm^{-3}) and magnetite (0.00625 % w/w) were synthesised by a simple extrusion dripping method. The resulting particles were left in the crosslinking Ca^{2+} bath for 10 minutes to minimise the risk of enzyme leaching.⁷⁸ Finally, the particles were washed with DI water and immediately used in a reaction. GOx loading of 4.95 units cm^{-3} was judiciously selected with guidance from the supplementary information provided by the Taylor group.⁷⁷ Their modelling showed that urease loaded alginate particles measuring 2 mm in diameter exhibited bistable switching when the enzymatic loading was between 3.8 and 5.1 units cm^{-3} .

6.2.2 Ratiometric Imaging

Ratiometric data acquisition, processing, and analysis was carried out using software written in LabView in conjunction with Dr Dan Toolan. Data acquisition and processing (Figure 6-1) was carried out in a single programme. Acquisitions parameters such as pixel binning, frame rate, number of frames were set before initiating data acquisition. The parameters were saved as an array for reference. Upon initiating data acquisition, the two cameras were simultaneously triggered to image the reaction in unison. The resulting images then underwent a flat-field correction to remove aberrations and distortions caused by the ratiometric setup. Every corrected image (C_i) that records the fluorescence intensity at $\lambda = 585 \pm 10$ nm was then saved as a tiff file for use in data analysis. The image corresponding to the lower wavelength peak was used as it demonstrates the greatest intensity shift with pH (see Figure 4-1). A ratiometric image was then formed by dividing the individual pixel intensity values of C_i $\lambda = 640$ nm with the corresponding pixel from C_i $\lambda = 585$ nm. The resulting

ratiometric intensity (R) values of each pixel were then put into a 1D array. As each frame was processed a 2D array of R values was generated and saved as a temporary file.

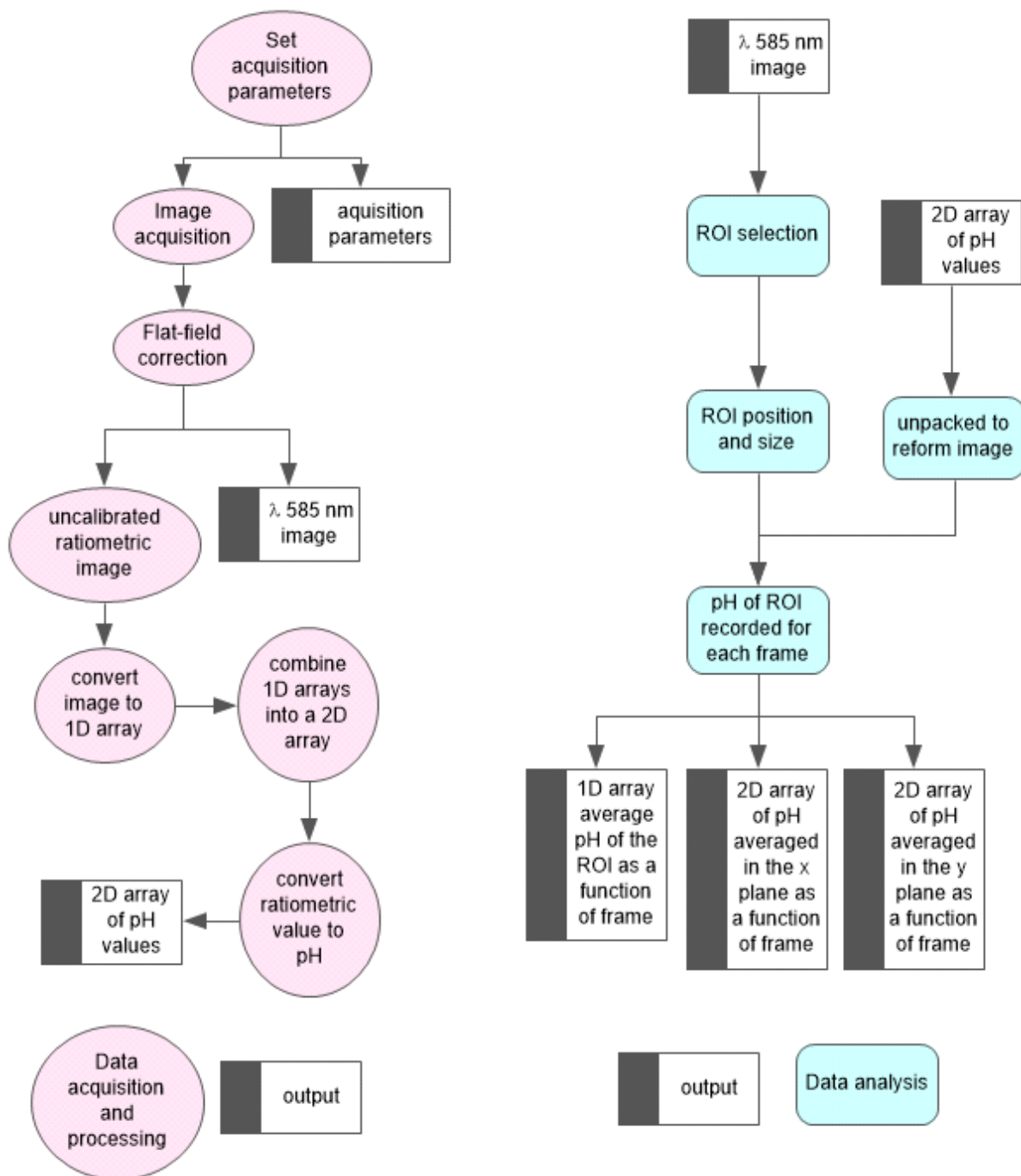


Figure 6-1 Flow diagrams of the software processes involved in ratiometric imaging data acquisition, processing and analysis

Once all the frames of the reaction had been taken the 2D array of R values was converted to a 2D array of pH values, by using either calibration plot described previously (4.3.1). The resulting pH values were reported to two decimal places then multiplied by 100 to remove the decimal point. As the lack of a decimal point reduces the processing power required in subsequent data analysis. Finally, the 2D array of pH values was spooled.

A separate data analysis programme written in LabView with Dr Dan Toolan, opened a selected tiff files of the C_i ($\lambda = 585$ nm) typically within the first 250 frames. Onto which multiple rectangular regions of interest (ROI's) could be marked. Such ROI's included particles and interstitial sites. The xy coordinates of the top left corner of the ROI along with its length in both x and y directions were logged. The 2D array of pH values for the corresponding reaction was then unspooled each column was sequentially converted back to its image and the ROI pH values collected. The ROI's in each frame had the overall average pH logged along with the 1D arrays of the pH averaged in each plane. This data was then collated to form a 1D array of average pH and 2D arrays of the pH averaged in each plane as a function of frame. The data was then saved as .csv files along with a marked up tiff showing the ROI's.

6.2.3 Diffusion from a single particle

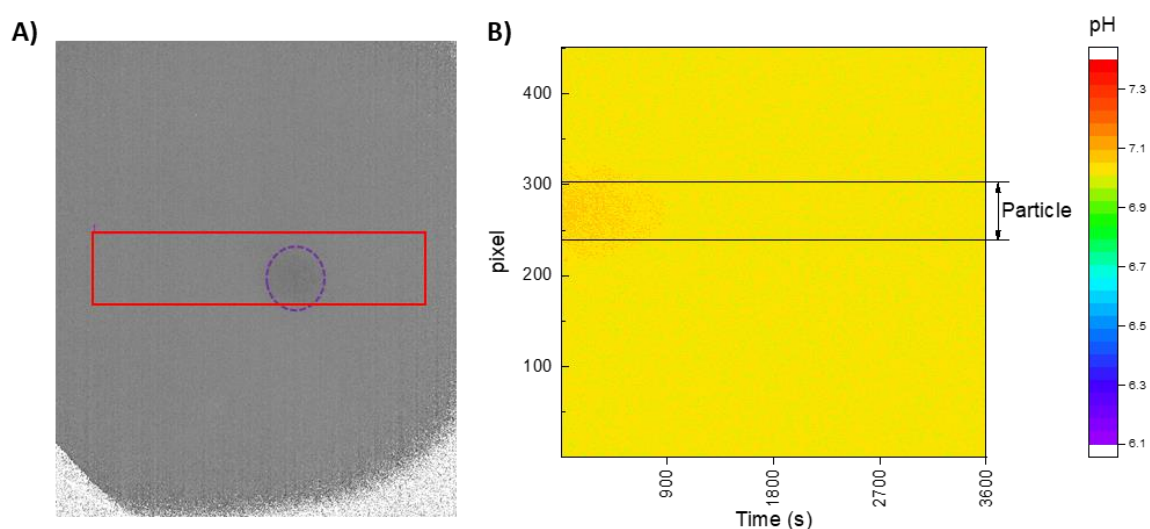


Figure 6-2. A single GOx loaded particle in DI water at pH 7 as a bench mark; A) image of a single particle (outlined in purple) and the region of interest (red box) B) heat map plot showing pH as a function of time and pixel the highlighted region of interest, demonstrating a lack of particle activity.

Both ratiometric imaging parameters and alginate particle synthesis are discussed in full in previously (Chapters 4 and 5 respectively). In brief 4x4 binning was used to lower the noise:signal ratio. Furthermore, a combination of binning and an exposure of 4 s allows a relatively high count to be obtained in each pixel well. The carboxy-SNARF concentration of $2.67 \mu\text{m cm}^{-3}$ was used to minimise the error in the ratio of the peaks, hence pH. Alginate particles were synthesised by a simple extrusion-dripping method. The resulting sodium alginate droplets were crosslinked by dropping into a Ca^{2+} bath (0.1 mol dm^{-3}) for 10 minutes to reduce the risk of enzyme leaching.⁷⁸ The alginate hydrogel contained SNARF-4F, GOx and ferrous magnetite, for ratiometric image, signal generation and facile particle placement respectively. The degree of GOx loading was determined from the modelling performed by

Taylor et al (Figure 1-5).⁷⁷ Which showed that 2 mm alginate particles loaded with 3.9-5.4 units cm^{-3} of urease could demonstrate a bistable switch.

A single GOx loaded particle was placed in a solution of DI water and SNARF-4F (pH 7). the solution was then imaged for 3600 seconds using the ratiometric setup previously described. Figure 6-2 A) shows a raw image from the camera that captures light with a wavelength (λ) of 585 ± 10 nm, the lack of contrast in the image is due to the particle being of similar pH to the solution. When no glucose is present in the solution the GOx within the particle has no substrate to react with as such there is no shift in pH as shown in Figure 6-2 B). The initial diffusion of pH from the particle observed in the initial 900 s is due to a slight variation in initial pH between the particle and its surroundings.

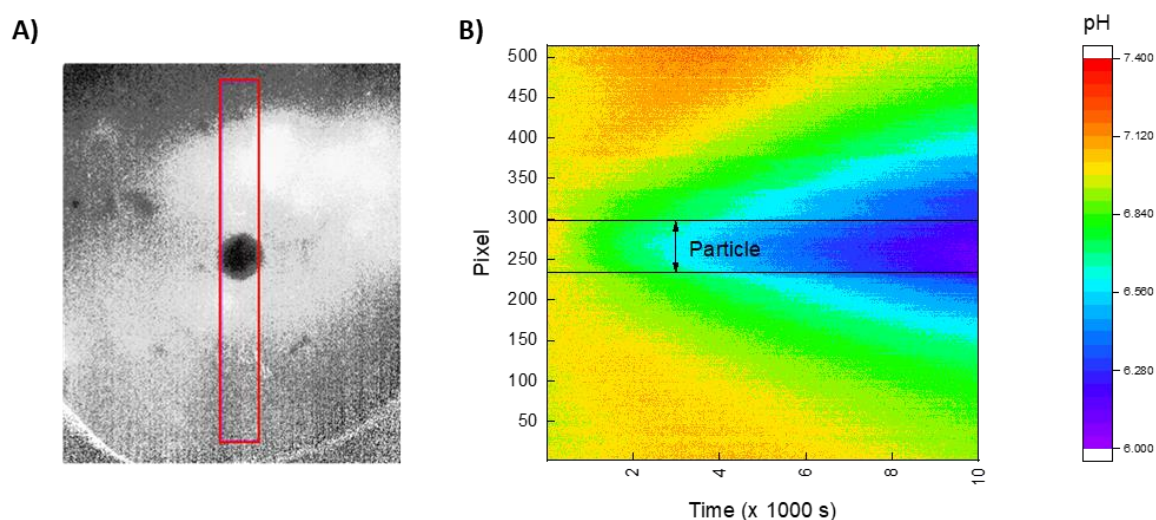


Figure 6-3 A) image showing the region of interest for diffusion from a single particle. B) pH as a function of time (s) and y axis pixel. Pixel pH is the average of the x-pixels, the black lines indicate the edges of the particle.

A single GOx loaded alginate particle is placed in a solution of glucose and was imaged for 10,000 s (Figure 6-3). initially the pH is uniform throughout the ROI. As the time progresses to around glucose penetrates the particle where it is converted by GOx to glucono- δ -lactone before undergoing ester hydrolysis to gluconic acid. After 3000 second the glucose has penetrated to the centre of the particle and the pH within is approximately uniform. External to the particle gluconic acid slowly diffuses away, thereby lowering the pH. However, this is not a uniform process. On one side of the particle the shift in pH diffuses further away than the other. This may be due to; one side of the particle being closer to the edge of the sample vessel which would inhibit diffusion; the particle has an imperfect structure resulting in diffusion being favoured from one side; or this is an artefact of the reaction and the particle is slowly migrating.

The pH profile as a function of time (Figure 6-4 A) below) shows the gradient of the pH profile to be uniform throughout the reaction. However, a shoulder can be observed on the right-hand side of the

of the particle. Despite this it is possible to obtain a diffusion coefficient for the proton concentration in the aqueous phase, but not in the alginate particle. This is because the pH profile is formed by the imaging of a 3-dimensional sphere in 2-dimensions. As such the pH profile of the alginate particle can be masked. The diffusion profile can be fitted using the equation for diffusion from a continuous source (appendix).

$$c(r,t) = \frac{q}{4\pi Dr} \operatorname{erfc}\left(-\frac{r^2}{\sqrt{4Dt}}\right) \quad (\text{A-2.81})$$

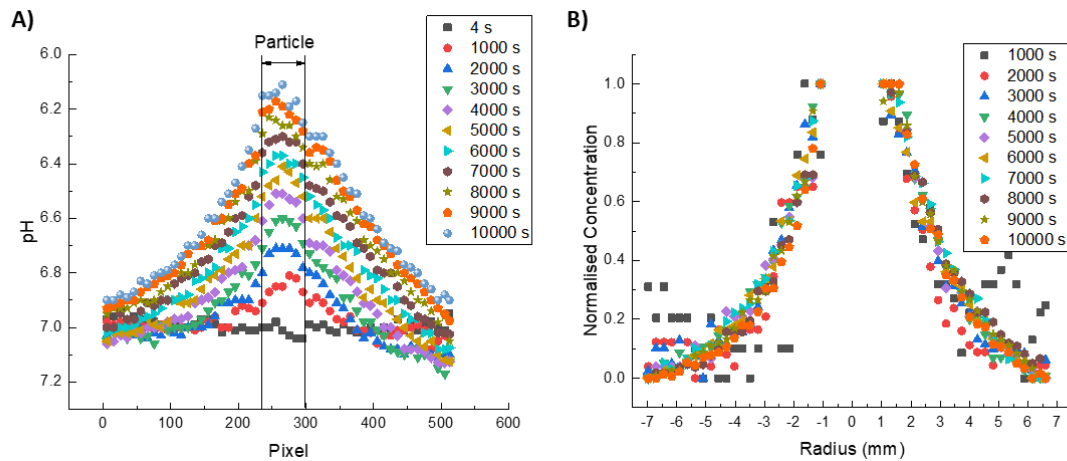


Figure 6-4 A) pH as a function y pixel for different times, the pH has been inverted to replicate $[H^+]$ the two black line identify the outer edge of the particle at t_0 . B) Normalised proton concentration profile in water the aqueous phase of the reaction

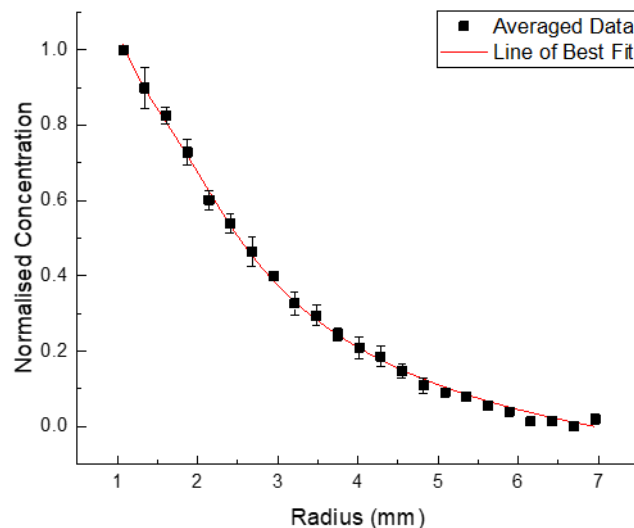


Figure 6-5 Average normalised concentration for 3000 s to 10000 s

Where q is the production of protons. However, there is a pH dependent variation in proton production (q) due to both the rates of enzymatic driven glucose oxidation and the subsequent ester hydrolysis being susceptible to changes in pH as previously discussed. As such it is advantageous to normalise the proton concentration thereby removing q from the equation (Figure 6-4 B)). Further

smoothing of the diffusion profile can be achieved by averaging the LHS and RHS data, negating the data for the first 2000s and averaging the remaining data points (Figure 6-5).

The normalised, averaged data was then fitted using a normalised form of the continuous diffusion equation:

$$c_{(r,t)} = \frac{\frac{1}{r} \operatorname{erfc}\left(-\frac{r^2}{\sqrt{4Dt}}\right) - \frac{1}{r_b} \operatorname{erfc}\left(-\frac{r_b^2}{\sqrt{4Dt}}\right)}{\frac{1}{r_p} \operatorname{erfc}\left(-\frac{r_p^2}{\sqrt{4Dt}}\right) - \frac{1}{r_b} \operatorname{erfc}\left(-\frac{r_b^2}{\sqrt{4Dt}}\right)} \quad (6.1)$$

Where subscripts p and b denote the edge of the alginate particle and the boundary of the region of interest (respectively) relative to the centre of the alginate particle. The parameters of the fitted curve are shown in Table 5 below.

Table 5 parameters of the normalised diffusion concentration profile

Parameters for the fitted normalised diffusion concentration profile	
Diffusion Coefficient (D; $\times 10^{-4} \text{ mm}^2 \text{ s}^{-1}$)	3.246 \pm 0.283
Time (t; s)	7000
Radius particle edge (r_p; mm)	1.101 \pm 0.014
Radius boundary limit (r_b; mm)	6.96
Adjacent R^2	0.9982

The derived particle size diameter ($2.20 \pm 0.03 \text{ mm}$) is slightly larger than that describe previously ($2.11 \pm 0.05 \text{ mm}$; Figure 5-6). The derived diffusion coefficient is of a magnitude akin to other similar chemicals aqueous diffusion coefficients under standard atmospheric conditions. Typical aqueous diffusion coefficients are between 10^{-4} and $10^{-3} \text{ mm}^2 \text{ s}^{-1}$. More specifically the diffusion coefficient of glucose³³² is $6.7 \times 10^{-4} \text{ mm}^2 \text{ s}^{-1}$ and organic weak acids are slight higher (salicylic acid³³³ $1.11 \times 10^{-3} \text{ mm}^2 \text{ s}^{-1}$). However, the derived diffusion coefficient is significantly lower expected, this likely due to a combination of factors including charge screening effects and hydrogen bonding between the acid and glucose substrate. The Stoke-Einstein equation describes the diffusion coefficient (D) as being dependent upon temperature, the particle size and the dynamic viscosity. The latter is composite function and is dependent upon the interactions of the diffusing species of the bulk solution as well as the solutions viscosity. The reference diffusion coefficients previously mentioned are for in demineralised water which has a slightly lower viscosity than the 0.01 M glucose solution that is used in this system, 0.89 and 0.91 mPa s respectively.³³⁴ As such the diffusion coefficient would be expected to be slightly smaller in the glucose solution.

A gaussian model of the diffusion in the of acid in the aqueous phase was generated from the data of Figure 6-5 (see Figure 6-6 A) below) using the gauss function

$$y = y_0 + \frac{A}{w\sqrt{\frac{\pi}{2}}} e^{-2\frac{(x-x_c)^2}{w^2}} \quad (6.2)$$

Where y_0 is the offset, x_c is the center, A is the area and w is the width of the curve. The values of the parameters are given in the table below.

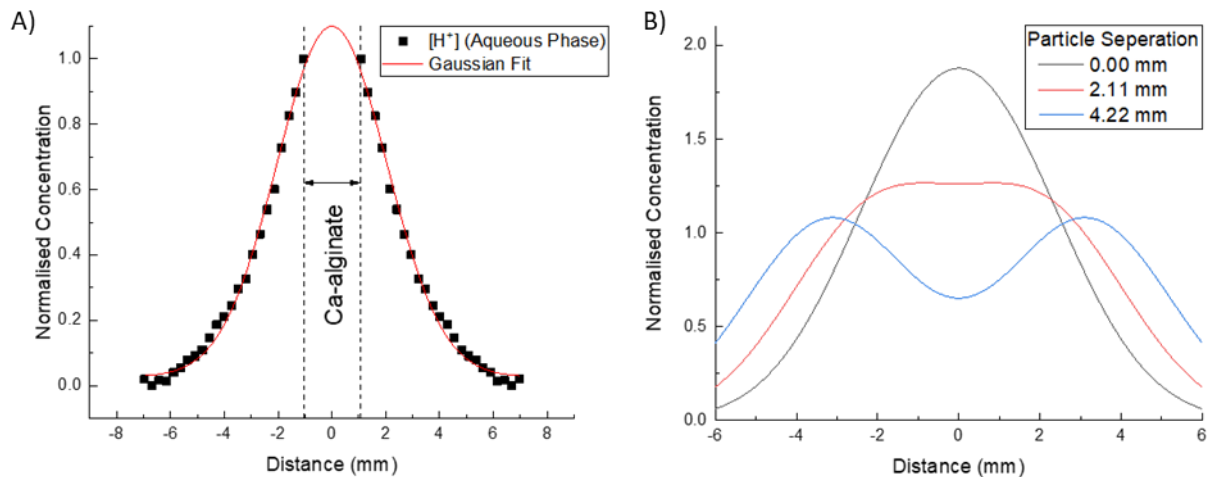


Figure 6-6 A) fitted gaussian distribution for the normalised concentration profile of protons in the aqueous phase. B) the modelled interaction of two particles normalised aqueous proton concentration, showing the interaction and cumulative effects as the particles are positioned closer together.

Table 6 Parameters of fitted gaussian curve (equation 6.2) for the data presented in Figure 6-6 A).

Parameter	Value
y_0	0.0274 ± 0.0068
x_c	0.000 ± 0.017
w	4.102 ± 0.061
A	5.510 ± 0.082
Adjusted r^2	0.9942

The resulting gaussian curve was then used to model when neighbouring particles diffusing ‘signalling’ concentrations would overlap to have a cumulative effect (Figure 6-6 B)). If the diffusion profile is the same in the alginate particle as the surrounding solution, it is shown that the particles start to strongly interact with one another when the distance between them is ≤ 2.11 mm (the average diameter of the alginate particle). This corresponds with the findings of the Sakamoto⁴⁶ group and later the Showalter^{38,39} group who demonstrated that complex oscillatory behaviour such as the formation of

spirals was dependent upon a particle having multiple adjacent neighbours. Where particles are adjacent neighbours when the distance between particles was \leq average particle diameter.

6.2.4 Increasing particle density

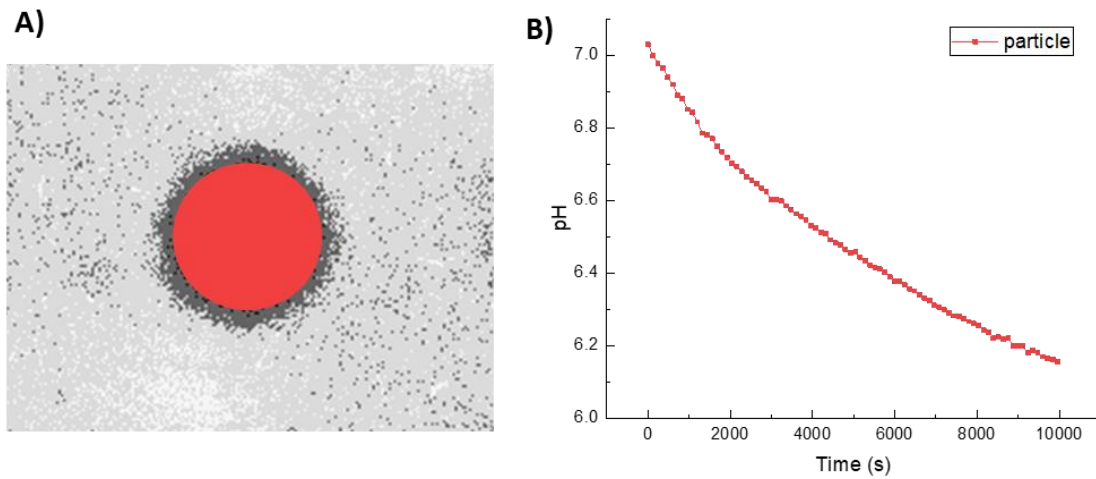


Figure 6-7 the change in pH as a function of time for a single particle loaded with glucose oxidase in 0.01 mol glucose solution: A) location of the Region of Interest (ROI) B) graphical representation of pH as a function of time for the ROI highlighted in A.

A single enzyme loaded alginate particle gradually lowers its pH from pH 7.0 to 6.2 over the course of 10,000 seconds (Figure 6-7). The non-linear behaviour of the rate is thought to be due to an increasing buffer strength with decreasing pH rather than a loss in enzymatic activity.

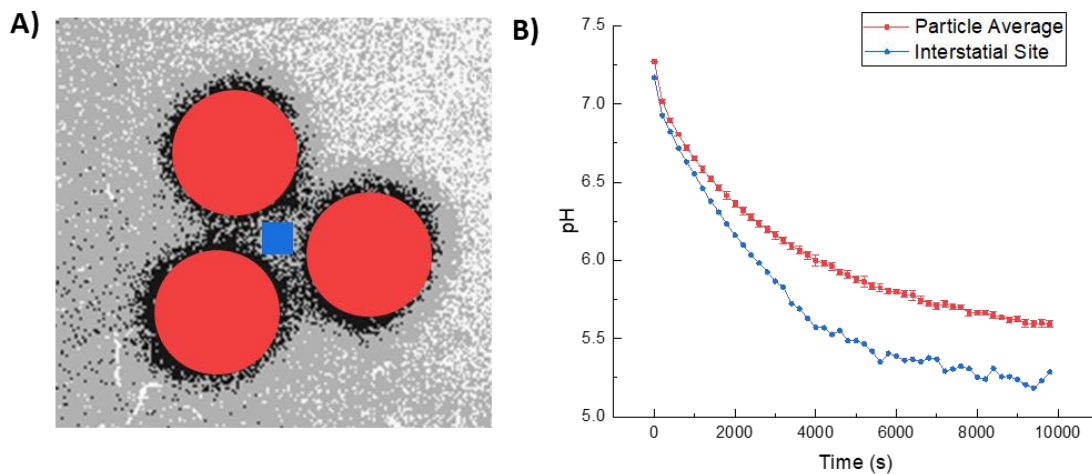


Figure 6-8 A) ROI's for a trio of GOx loaded alginate particles and the interstitial site; B) particle and interstitial site (IS) pH as a function of time showing that the pH shift at the interstitial site is significantly lower than that of the particle.

Increasing the number of particles to a cluster of three both lowers average final pH for the clustered particles from pH 6.1 to 5.6 and introduces interstitial sites between the particles. These sites exhibit a lower pH than the particles that boarder it. This is thought to be due to diffusion from the IS being hindered by the particles and alginate beads have a strongly ionic environment due to their chemical structure it is thought that this accelerates the diffusion of gluconic acid from the particle.

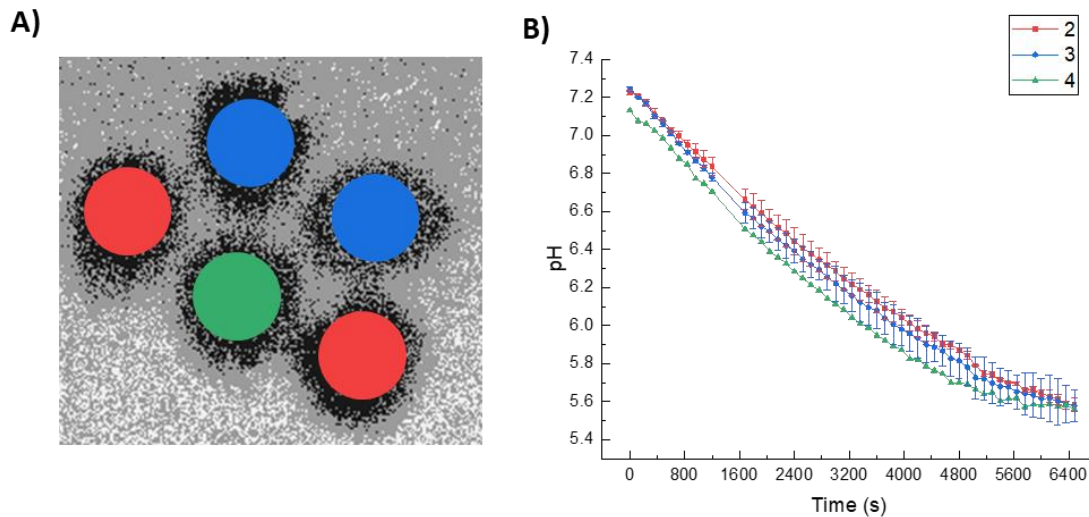


Figure 6-9 A) Image showing a cluster of 5 particles colour coordinated to show the connectivity between particles (connectivity of 2 (red); 3 (blue); 4 (green)) B) average pH as a function of time for particles of differing connectivity (2 (red); 3 (blue); 4 (green)) in a 5 particle cluster.

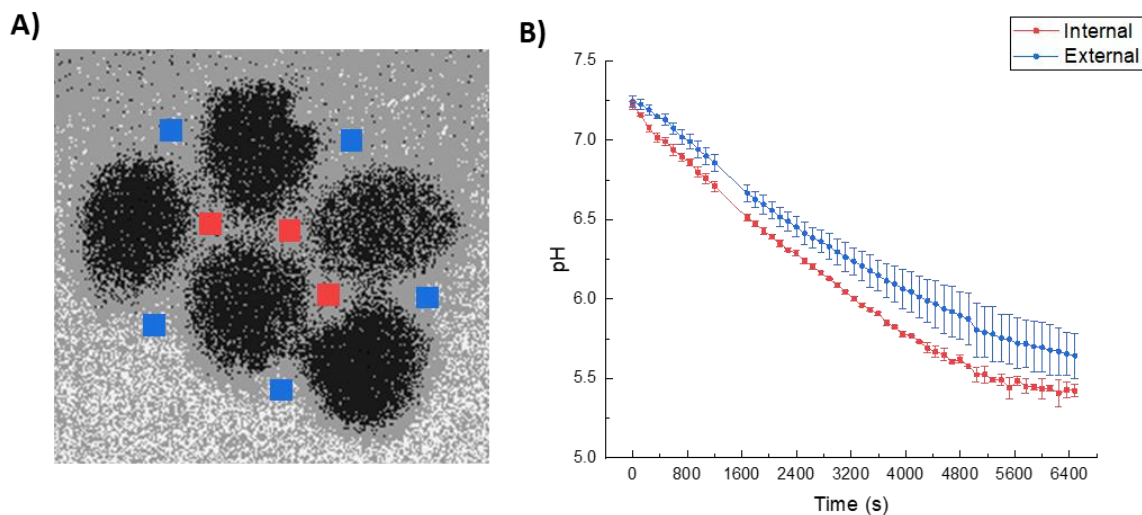


Figure 6-10 A) Image showing the interstitial sites (IS) that are internal (red) to the cluster and external (blue) B) pH as a function of time for the internal (red) and external (blue) interstitial sites showing that the internal diffusion limited sites have a much faster rate of change in pH.

Increasing the number of particles again to 5 particles shows that as the connectivity of the particle influences the rate of change in pH (Figure 6-9). Increasing the connectivity of the particle has a

proportion effect on the rate, however, as time progresses and the acid diffuses further away from the overlapping spheres of influence cause all the particles to obtain near uniform pH.

Examination of the interstitial sites (IS) show that the Internal IS have a near linear faster rate to around 70 mins at which point the pH starts to plateau at around pH 5.5 (Figure 6-10). The External IS have a slower rate of change in pH as one side of the site is open allowing the acid to diffuse away more easily.

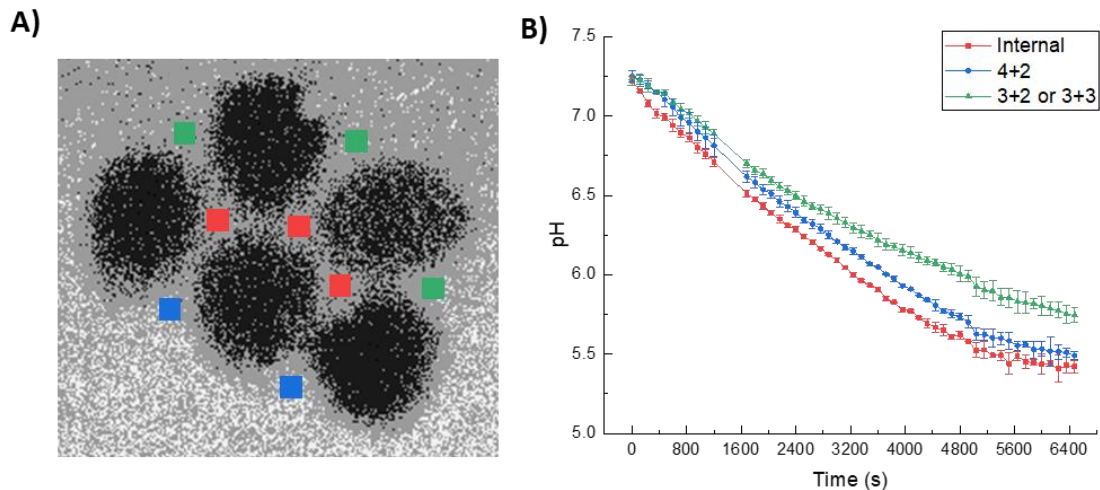


Figure 6-11 A) image of a cluster of 5 particles showing the interstitial sites (IS) that are internal (red) to the cluster and external to the cluster which border the particle which has a connectivity of 4 (blue) as well as those which border particles with a connectivity of 3 (green) B) pH as a function of time for the IS: internal (red) and external that border the particle with a connectivity of 4 (blue) and those that border at least one particle with a connectivity of 3 (green).

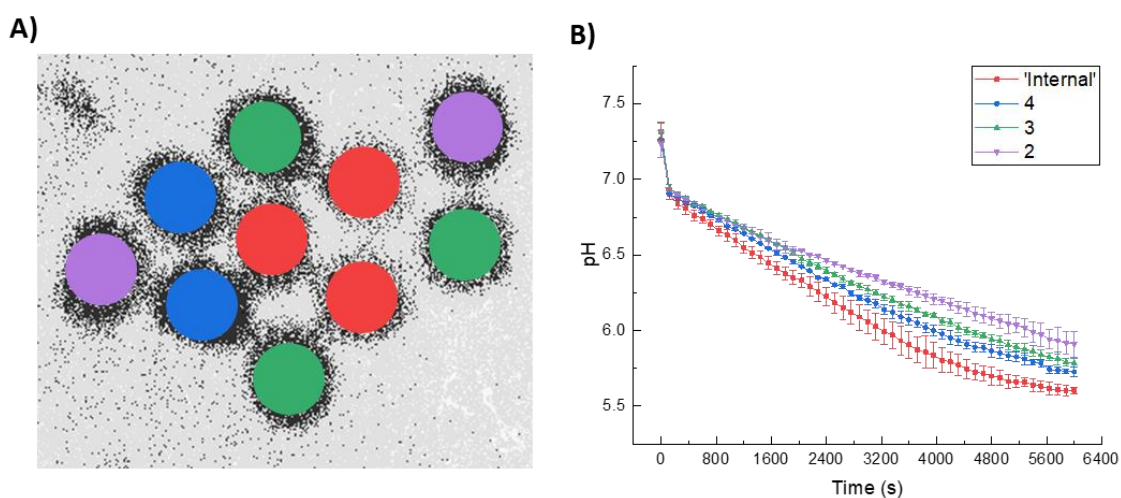


Figure 6-12 A) Image showing a cluster of 10 particles colour coordinated to show the connectivity between particles; internal/pseudo-internal, red; connectivity of 4, blue; connectivity of 3, green; connectivity of 2 purple B) average pH as a function of time for particles of differing connectivity; "internal", red; 4, blue; 3, green; 2, purple in a 10 particle cluster.

As the time increases and pH lowers the error associated to the external IS increases. On closer examination (Figure 6-11) Particles which have the greater connectivity lower the pH of its bordering IS faster and to a greater extent than those with a lower connectivity. This shows that the particles activity is not uniform but dependant on at least their connectivity as the more connected they are the lower the pH thereby increasing the glucose oxidase activity.

Figure 6-12 shows that particles in the core of the cluster (red) rapidly lower the pH near linearly before starting the plateau at around pH 5.75, this plateauing is due to pH being a logarithmic scale as such the acid required to lower the pH further diffuses from the particle faster than it can be produced. The ‘internal’ particles large error between pH 6.25 and 5.75 can be attributed to two of the have large regions exposed to exterior of the cluster. The growing influence of the truly internal particles sphere of influence eventually engulfs the other red particles eventually lowering the discrepancy between the particles. The exterior particles show near linear decreases in pH with little differences in pH for particles of with the same connectivity. The exception for the is the lowest connected particles i.e. those with a connectivity of two, however, as the image (coloured purple) in Figure 6-12 A) shows this can be explained by the fact that not only is one these particles closer to the ‘internal’ red particles, but the diffusive path from that region is less hindered than it is to other particle with a connectivity of two (located to the left hand side of the image).

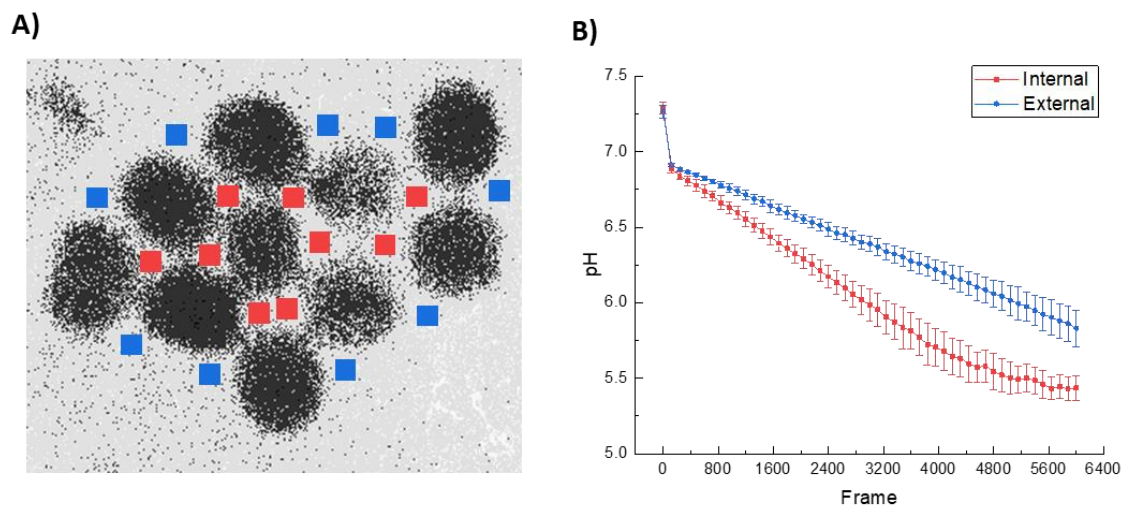


Figure 6-13 A) Image showing the interstitial sites (IS) that are internal (red) to the cluster and external (blue) B) pH as a function of time for the internal (red) and external (blue) interstitial sites showing that the internal diffusion limited sites have a much faster rate of change in pH.

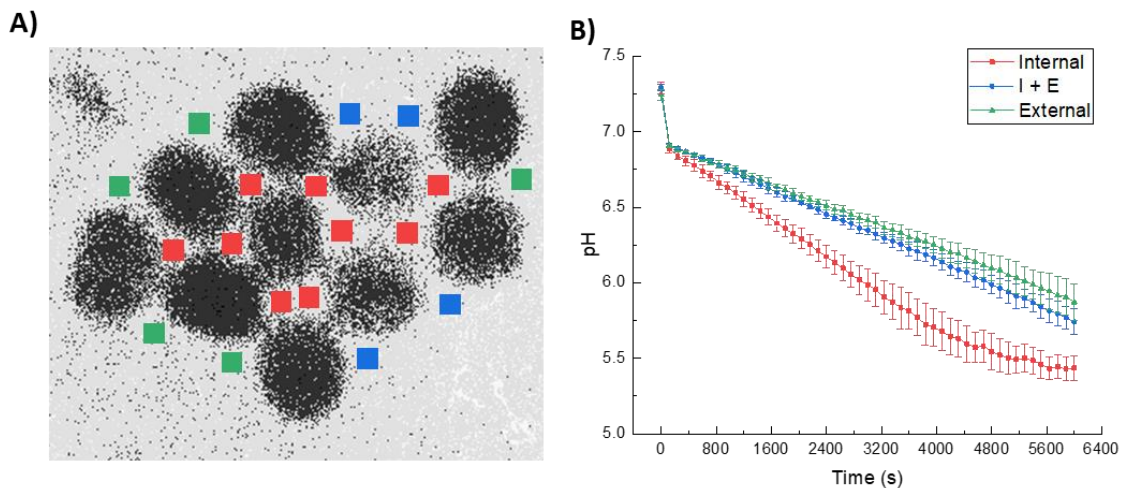


Figure 6-14 A) image of a cluster of 10 particles showing the interstitial sites (IS) that are internal (red) to the cluster and external to the cluster which border the pseudo-internal particles (blue) as well as those which just border 'low-connectivity' particles (green) B) pH as a function of time for the IS: internal (red); external that border pseudo-internal particles (blue); and external sites that border only external particles (green).

Figure 6-13 illustrates how the interstitial sites that are internal to the cluster decrease in pH much more rapidly than those that on the periphery of the structure, as observed in the 5 particle cluster. Furthermore, both the internal sites and the 'internal' particle both exhibit a plateauing in pH at the same time (4400 s). The external sites decrease in pH remains linear throughout, this mimics the other trend the non-internal particles pH (Figure 6-12 B)). Moreover, this retention of linear behaviour shows that merely doubling the number of particles in the cluster from 5 to 10 enhances the clusters ability to change pH. However, both set of particles exhibit a minimum pH around 5.5, despite this being significantly higher than the theoretic minimum of pH 3.0 (calculated using $\Delta = CF_a$), this could be due to enzymatic deactivation, environmental stresses or rate limitation of the diffusion of substrate (glucose) and product (gluconic acid) to and from the alginate entrapped GOx.

Closer examination of the external interstitial sites (Figure 6-14) shows that there are two types of site, those that border external particles only and those that are next to the pseudo-internal particles. The latter show accelerated lowering of the pH. Both external sites types continue to exhibit linear decreases in pH, this confirms that the cluster is not being affected by the walls of the vessel causing the propagating pH front to return to the centre.

Again increasing the cluster size to 15 particles (Figure 6-15) the internal particles initially exhibit a near linear lowering in pH before plateauing off to a minimum of pH 5.5. Externally the overall trend is similar to that of 10 particles, however, the final pH is lower 5.7 compared to 5.85. In those final 0.15 pH units the rate of pH shift decreases.

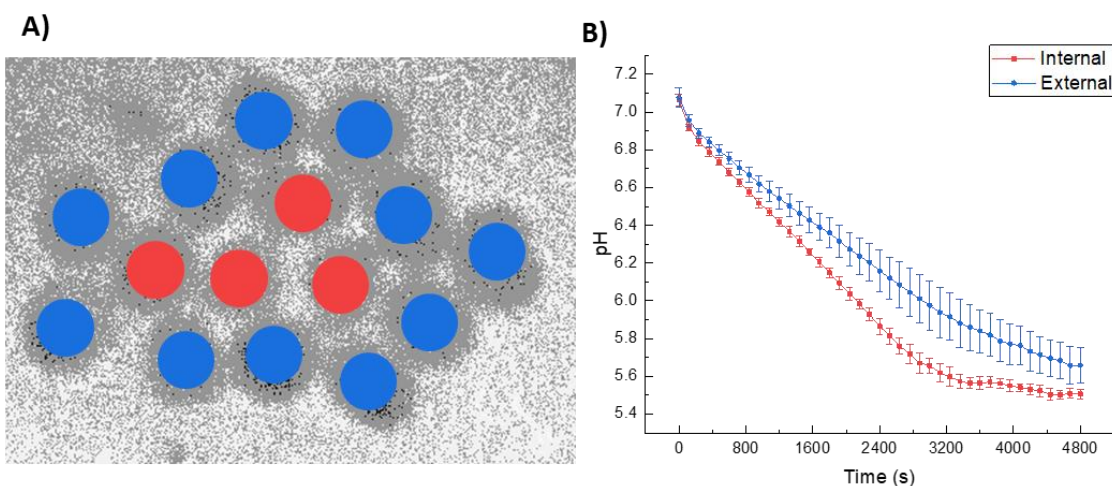


Figure 6-15 A) Image showing a cluster of 15 particles colour coordinated to show the particles that are internal (red) and external (blue) to the cluster. B) Average pH as a function of time for particles that are internal (red) or external (blue), within the 15 particle cluster (frame rate = 0.25 s^{-1}).

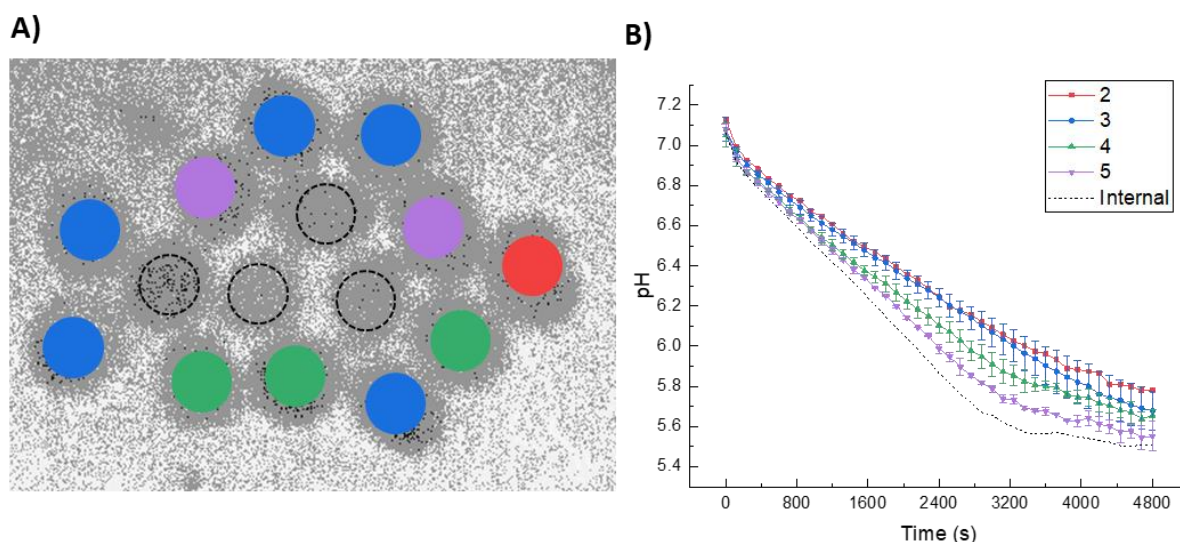


Figure 6-16 A) Image showing a cluster of 15 particles colour coordinated to show the connectivity between particles; internal are outlined in black; connectivity of 2, red; connectivity of 3, blue; connectivity of 4, green; connectivity of 5, purple B) average pH as a function of time for particles of differing connectivity; internal, black; 2, red; blue, 3; green, 4; purple, 5 in a 15 particle cluster.

Merely splitting the particles in the cluster to internal/external although giving an overall trend loses some of the intricacies in the variation in particles that are on the external shell of the cluster. By separating the particles by how many particles the particle is adjacent to a more succinct trend can be observed (Figure 6-16). The connectivity of a 15 cluster varies from 2 to 6, when considering the internal particles as the centre of a hexagonally packed structure. Increasing the connectivity of a particle final observed pH from to 5.8 down to 5.5. Furthermore, the onset of the levelling off of pH,

can be seen to occur earlier for particles that exhibit a higher order of connectivity and does not merely occur at the same pH.

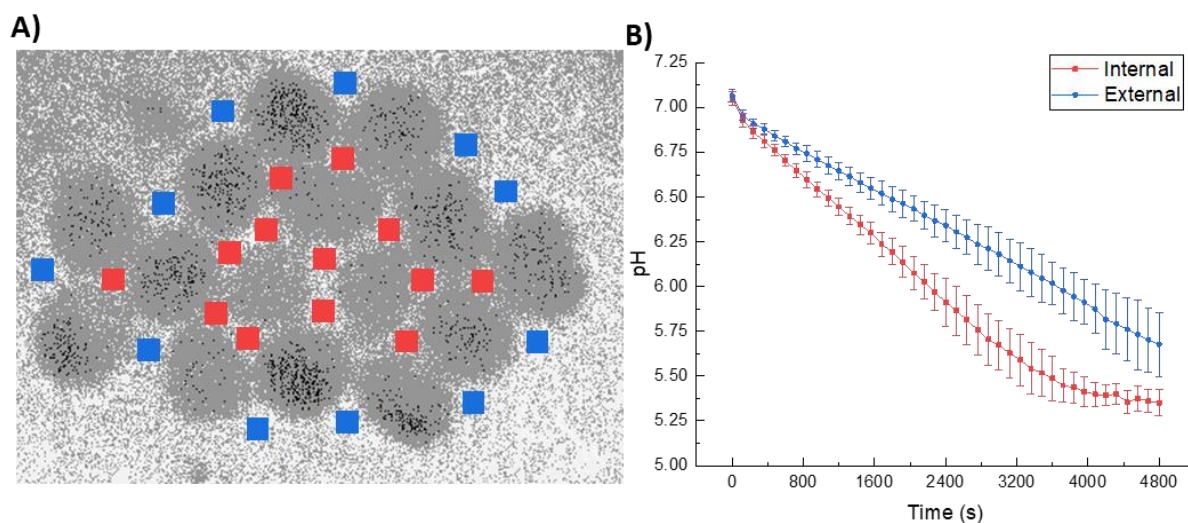


Figure 6-17 A) Image showing the interstitial sites (IS) that are internal (red) to a cluster of 15 particles and external to the cluster (blue) B) pH as a function of time for the internal (red) and external (blue) interstitial sites showing that the internal diffusion limited sites have a much faster rate of change in pH.

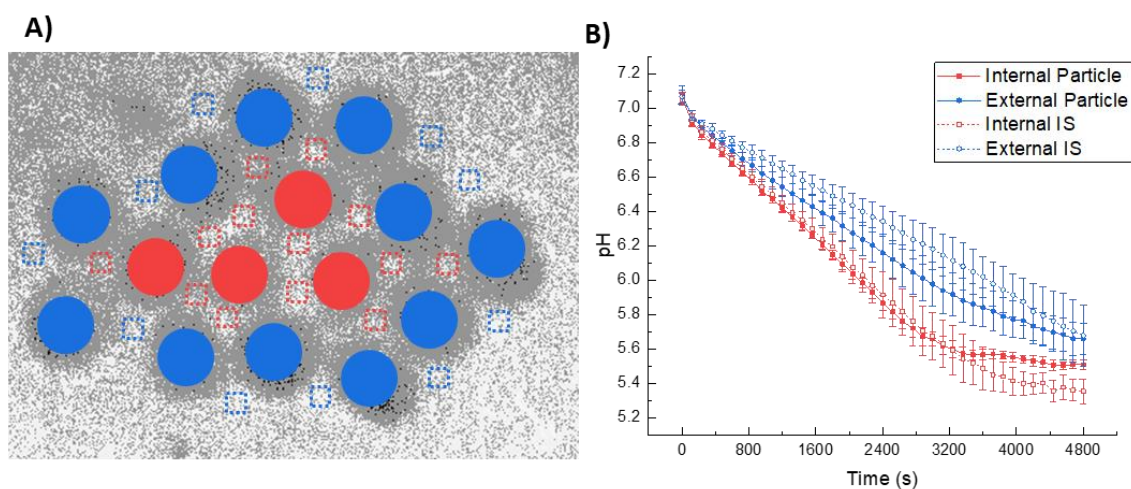


Figure 6-18 A) An image showing a cluster of 15 particles (solid) and interstitial sites (IS; dotted line) that are internal (red) and external (blue) to the cluster. B) pH as a function of time for the internal (red) and external (blue) particles (solids) and IS (open) of a 15 particle cluster.

A comparison of the internal and external interstitial sites of a 15 particle cluster (Figure 6-17) show the external sites to decrease pH linearly, however, as the reaction proceeds the standard deviation increases this is thought to be due to variations in the connectivity of the particles, that border the interstitial sites. As shown previously (Figure 6-13 B) and Figure 6-14 B)) the general linear trend for all external sites is hold when looking at the particles that border an external interstitial site, on the gradient changes. Internally located interstitial sites obey the same trend as internal particles.

Increasing the particle population of the cluster to from 5 to 10 to 15 has little effect on the final observed pH (~5.4). This is due to an equilibrium being reached in proton production and its diffusion away from the cluster.

Figure 6-18 shows that the external interstitial sites have the slowest rate of pH shift, due to diffusion not being limited by any boundaries. Although the initial rate of pH change is slowest at the external site it does not exhibit any slowing in rate. Whereas the external particles, has initially a faster rate before slowing at around 3200 s. Both the internal interstitial sites and internal particles exhibit near uniform lower of pH, both initially lower the pH linearly before levelling off. The particles rapidly cease decreasing pH after 800 s (pH 5.5), whereas, the internal interstitial sites continue to increase in proton concentration for a further 800 seconds before levelling off at pH 5.4. The difference in minimum pH between the interstitial site and the particles that are internal to the cluster is due to the alginate particles composition. The calcium alginate is formed of a polymeric backbone of 1-4-linked β -D-mannuronate and α -L-guluronate crosslinked by calcium cations (see section 1.8.2). The calcium cations cooperatively bound into the alginate structure, as such as the hydrolysis of glucono-d-lactone is either inhibited when in the alginate structure or once hydrolysed the protons being more mobile than the Ca^{2+} is rapidly ejected from the particle into the bulk aqueous phase.

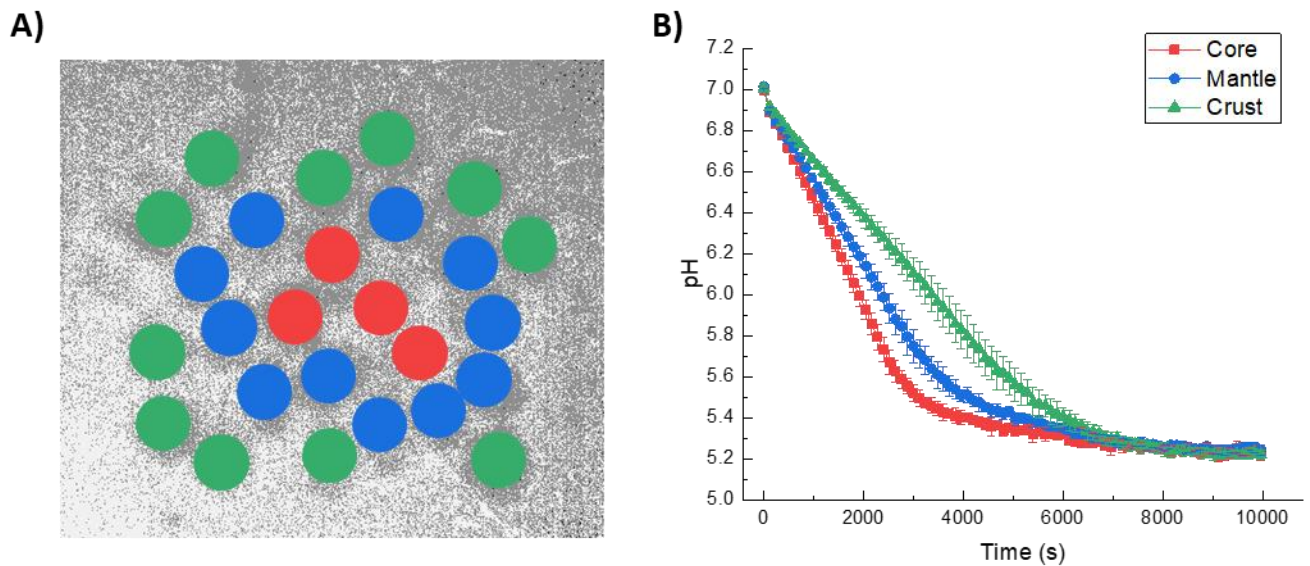


Figure 6-19 A) a cluster of 25 particles colour coordinated to their position within the structure; core, red; mantel, blue; shell, green. B) pH as a function of time a 25 particle clusters, particles grouped into the location within the cluster; core, red; mantel, blue; shell, green.

This interstitial pooling of acid is analogous to the stir rate behaviour observed in BZ beads by Taylor et al.²⁶ In low shear (300 RPM) situations they observed that ferriin loaded beads acted independently

of one another due to diffusion of the autocatalyst to the bulk solution being slower than the rate of autocatalysis. However, a two-fold increase in shear (600 RPM) increases the rate of diffusion, stripping the autocatalyst off the particles before it initiates the oxidation of ferriin. This causes the concentration of the autocatalyst to build up in the bulk phase, upon crossing a threshold concentration of autocatalyst the ferriin loaded particles are reduced en masse and enter an oscillatory state. In the static system we have developed diffusion of acid from single particles and small clusters is unhindered and rapid. However increasing the cluster size (Figure 6-11, Figure 6-14 and Figure 6-18) inhibits diffusion and causes interstitial pooling. Such pooling is thought to generate a feedback loop accelerating the production of acid (Figure 3-22). However, at present this has not lead to oscillatory behaviour.

A 25 particle cluster (Figure 6-19) shows not only how increasing the isolation of a particle from the bulk phase increases the rate at which the particle's pH is lowered to pH 5.4 when the proton concentration starts to plateau but each layer of particles exhibit a perceptible increase in rate of proton production around pH 6.2 as expected when referring back to the observed trends in glucose oxidase activity (Figure 1-11 A))⁹⁹ as it exhibits maximum activity at pH 5.5 and is at least 90% of maximum rate between pH 4.4 and 6.2. The plateauing of pH at 5.3 occurs for a variety of reasons. In part due to the buffer capacity of the system (Figure 3-10 B)) which increases by a factor of 10 per pH unit as the pH is lowered from pH 7.2 to 4.5, this contributes to the limiting of minimum pH that is obtained. Furthermore, as discussed in the previous chapter at pH >5.86 a growing proportion of gluconic acid is protonated, which initiates the forming of an equilibrium between glucono- δ -lactone and gluconic acid.

The similarity in shape of the pH curve of the 'core' and 'mantle' particles suggests phase locking emanating from the centre of the cluster. This is thought to be due diffusion from the particles making up the core being the most hindered, increasing the rate of interstitial pooling, initiating the feedback loop earlier. Eventually the concentration of acid in the core's interstitial sights 'bursts its banks' and starts to fill the mantle's interstitial sights initiating the feedback loop in the surrounding particles. The particles of the external 'crust' eventually reach the same pH as the interior particles. However, it takes almost twice as long as the core (around 6000 and 3000 s respectively) due to diffusion of the acid being less hindered.

The pH responsive behaviour of GOx loaded alginate particles in clusters of increasing size is summarised in Figure 6-20. Initially ($t=0$) in all instances the particle's pH matches the pH of the surrounding solution, as such there is no contrast between the particles and the surrounding solution and they appear to be as one. As the GOx entrapped within the particle initiates the production of

gluconic acid, there is a drop in the local pH so that by 10 minutes this shift can be observed emanating from the particles.

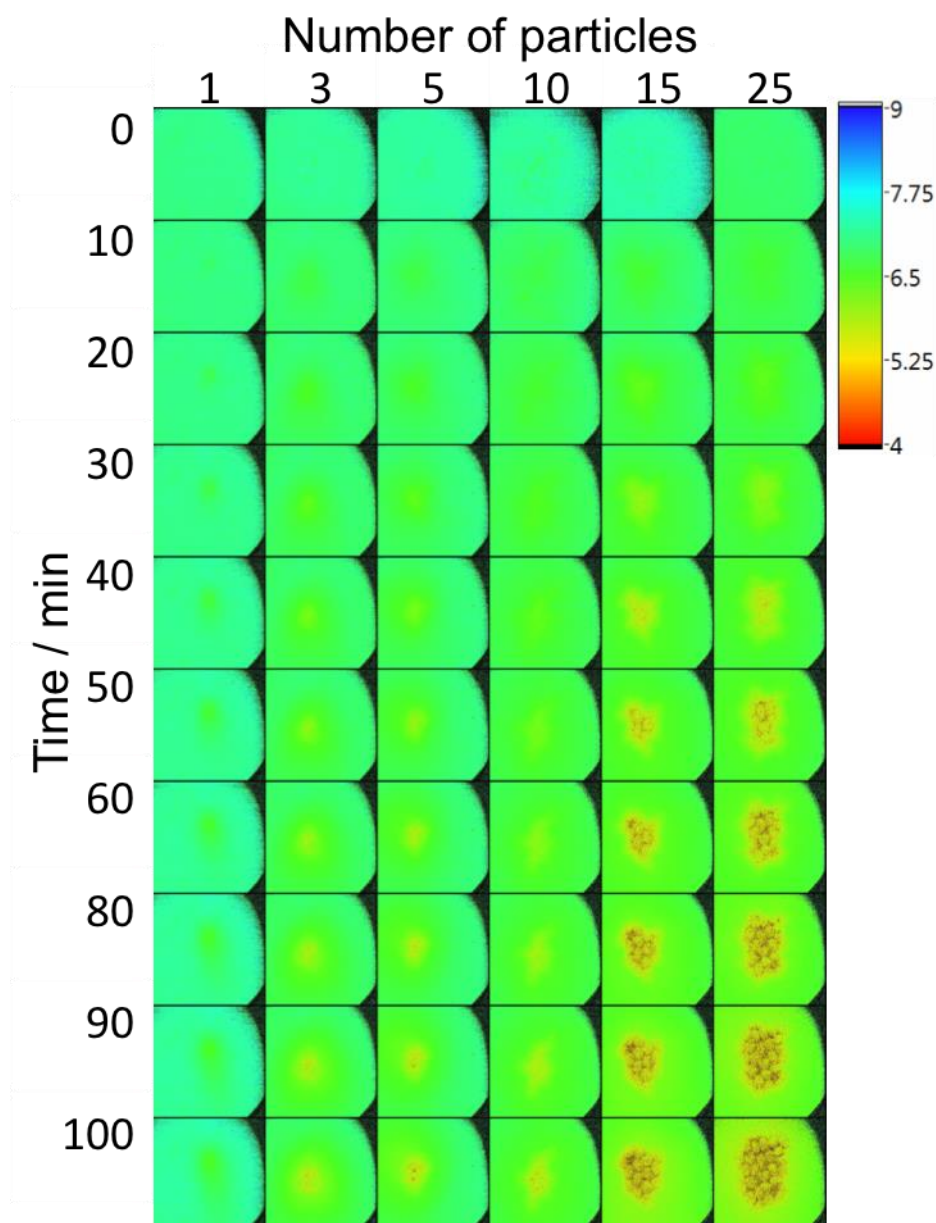


Figure 6-20 coloured ratiometric images of GOx loaded alginate particle clusters in 0.01 M glucose solution as a function of time. Showing the diffusion of acid from the particle and the attainment of QS for clusters of up to 25 particles.

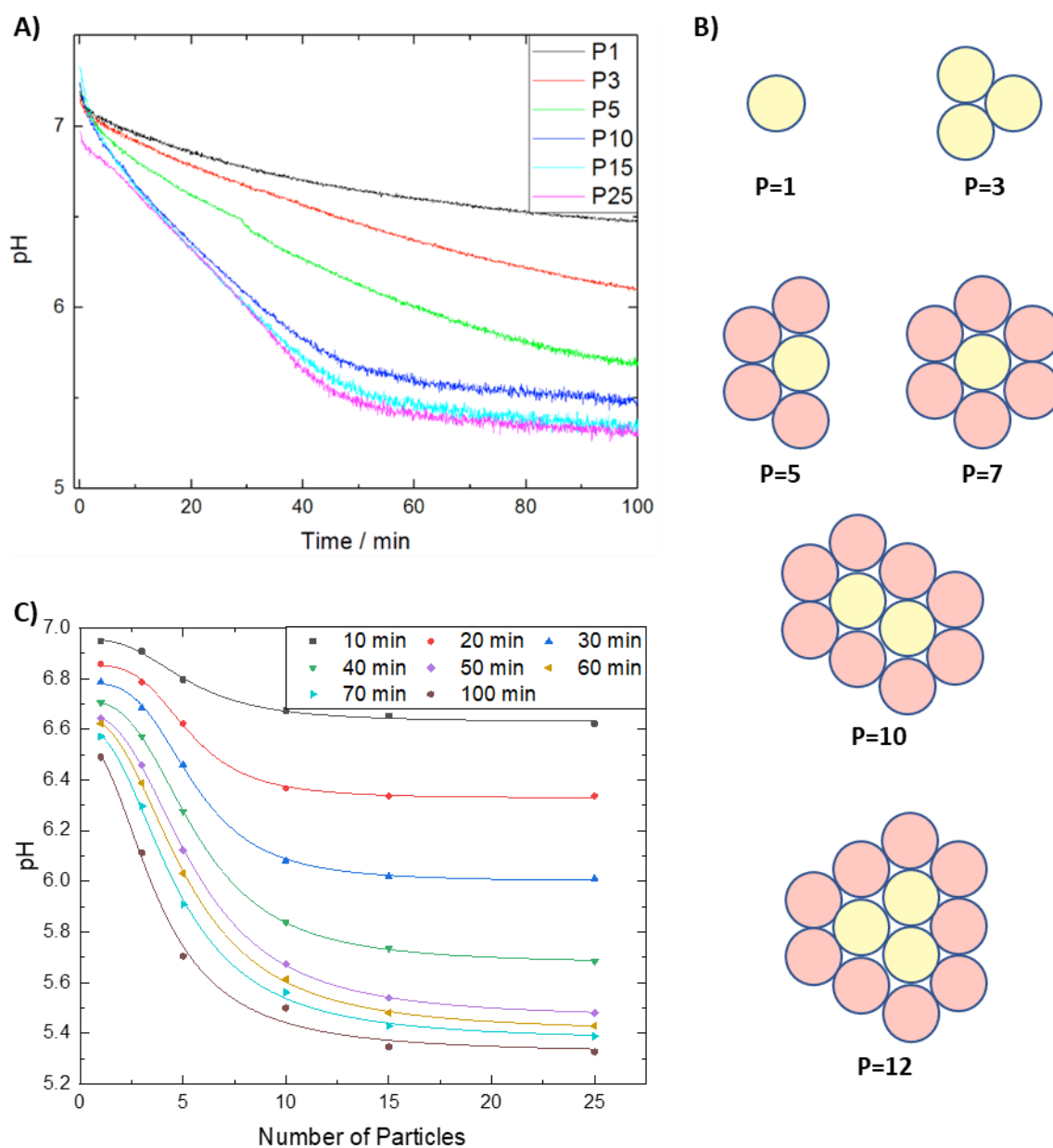


Figure 6-21 A) pH as a function of time for the particle with the highest activity within different cluster sizes. B) perfect packing of particles with the highest activity particles highlighted in yellow. C) pH as a function of the highest activity particle within a cluster at different times, demonstrating the presence of a threshold and plateauing of pH shift.

Figure 6-21 A) shows the pH profile for the most active particle in a given cluster over 100 minutes. This shows how increasing the cluster size causes a greater shift in pH, up to clusters of 10 particles. For clusters of 10 or there is a plateauing in pH shift. This can be explained by the packing of the particles, if packing is idealised to a hexagonal arrangement (Figure 6-21 B)) it is possible to see how particle diffusion from the most active particles (yellow) becomes inhibited causing a greater shift in pH. In small clusters the pH shift of the most active particle is used because an average pH of all particles would be skewed by the external particles which are proportionally greater in number and

exhibit a smaller pH shift (see Figure 6-9 and Figure 6-18). In a 2 dimensional arrangement of hexagonally packed particles the internal (more active) particles only become greater in number when the total number of particles ≥ 37 .

The effect of limiting the diffusion from a particle can be experimentally observed by plotting the pH at a give time for the most active particle within clusters of different sizes (Figure C)). By increasing cluster size from one to five there is a dramatic decrease in the pH of the most active particle. Furthermore, increasing the number of particles in the cluster further leads to a plateauing in the pH. The sigmodial change in pH with increasing cluster size can be modelled using the following equation:

$$pH_{t,Pn} = pH_{t,P1} + (pH_{t,P25} - pH_{t,P1}) \frac{Pn^c}{m^c + Pn^c} \quad (6.3)$$

Where, Pn is the number of particles in the cluster, m is the mid-point of the threshold and c is a parameter that is inversely proportional to the width of the threshold. The subscript t indicates the time. The parameters for the fitted curves are given in Table 7 (below).

Table 7 parameters for fitted curves of Figure 6-21 C) using equation (6.3)

t (min)	$pH_{t,P1}$	$pH_{t,P25}$	m	c	Adjacent R^2
10	6.95	6.63	5.2 ± 0.3	2.92 ± 0.51	0.9922
20	6.85	6.33	5.3 ± 0.1	3.65 ± 0.37	0.9979
30	6.78	6.00	5.5 ± 0.1	3.42 ± 0.25	0.9988
40	6.71	5.67	5.6 ± 0.1	2.91 ± 0.07	0.9998
50	6.66	5.46	5.5 ± 0.1	2.59 ± 0.09	0.9997
60	6.65	5.40	5.1 ± 0.1	2.46 ± 0.11	0.9995
70	6.61	5.37	4.6 ± 0.2	2.40 ± 0.26	0.9972
100	6.55	5.32	3.8 ± 0.4	2.27 ± 0.61	0.9856

The mid-point of the threshold is around 5 particles clustered together for reaction times up to 60 minutes. As the reaction continues further the mid-point lowers to ~ 4 particles. Furthermore, after 20 minutes the pH achieved by highly active particles in clusters of 10 or more particles is lower than that achieved by a single particle at after 100 minutes. This suggests that a quorum sensing triggered switch is observed. A sharper switch could be observed through the addition of a second pH dependent process (e.g. colour shift or volumetric transition) could be triggered between pH 5.4 and 6.5. It is also thought that reducing the enzyme loading of the particles would increase the mid-point of the transition.

6.3 Conclusions and Future Work

A bistable switch in pH was obtained in mm-sized GOx loaded alginate particles when immersed in a neutral glucose solution. In all instances the particles lowered the pH. However, the degree of pH shift was shown to be dependent on cluster size. A quorum sensing type response was observed a dramatic shift being observed in of 10 or more particles. Furthermore, the midpoint of the threshold was shown to be around 5 particles suggesting that diffusion kinetics of the acid play a key role in initiating the pH shift. Diffusion coefficient of the acid in the bulk phase emanating from a single particle was shown to be $3.24 \times 10^{-4} \text{ mm}^2 \text{ s}^{-1}$ which is of the same magnitude as molecules of a similar size. However, it is smaller than expected due to charge interactions and increased viscosity of the aqueous phase. The cluster of 25 particles was the only cluster large enough to have more than 1 row of particles that do not have an exposed edge to the bulk phase. This cluster demonstrated phase locking of the response emanating from the centre of the cluster.

To date only relatively small clusters of enzyme loaded particles have been used to probe collective behaviour. In part this is due to the ratiometric dye SNARF-4F being relatively expensive. This could be overcome by entrapping either methyl red (pK_a 5.1) or chlorophenol red (pK_a 6.0) in the alginate matrix. A colour change would then be observed when the particle switches states. Increasing the cluster size may initiate oscillations as predicted by the Taylor group in urease loaded particles.⁷³

In order to meet the blue skies aim of the project to be instigating a burst release of a drug cargo from quorum sensing particles some form of pH release or degradation is required. To obtain this there is two possibilities, the addition of preformed particle that undergoes a pH induced transition. Alternatively urease could be used instead along with the Ca^{2+} chelator EDTA as used by the bon group.⁷⁵ Of the two the former is the more attractive option if only from a point of vanity. There are at least two potential pH-responsive drug carrier that maybe used. Both the Langer³³⁵ and the De Geest³³⁶ groups have developed such carriers that exhibit little to no leaching under physiological conditions (pH 7.4), as the pH is lowered to carriers break down to release their cargo. Incorporation of such particles into the alginate matrix would be extremely facile. However, diffusion of a cargo from the alginate matrix may be slow. Therefore, may be beneficial to put the drug carriers in the interstitial sights to observe a release, if merely as a proof of concept.

7. Conclusions and Future Work

7.1 Conclusions

Increasing Functionality				
	Population Density Increase	Signal Generation (generator/signal)	Signal Detection	Response
<i>Alivibrio fischeri</i>	Harvested by <i>Euprymna scolopes</i>	LuxIR/acyl-homoserine lactone (AHL)	AHL binds to Lux operon	Accelerated AHL production and bioluminescence
<i>Staphylococcus aureus</i>	Reproduction and colonisation	Agr/autoinducing peptide (AIP)	AIP binds to kinase sensor AgrC	Secretion of proteases and toxin
Alginate particles (system reported)	Magnetic aggregation	glucose oxidase/H ⁺	Acid catalysed ester hydrolysis/dye protonation	pH decrease and dye colour change
Ideal pH responsive hydrogel	Magnetic aggregation ligand receptor interactions	glucose oxidase/H ⁺ urease/H ⁺	Volumetric response	Cargo release

Figure 7-1 Quorum sensing entities and the methods used to meet each key stage.

Overall aim of the thesis was to create a wholly synthetic QS entity that mimicked the key stages of quorum sensing communication between bacteria. These key stages were population increase, signal generation and detection, and a response (Figure 7-1). This was achieved by synthesising calcium alginate hydrogels loaded with ferrous magnetite and glucose oxidase moieties (Chapters 5 and 6). Thereby achieving the first two goals of generating population density increase and generating a signal. In order to observe the signal detection and response ratiometric imaging microscopy was employed using the ratiometric dye carboxy-SNARF-4F, a technique which until now has predominantly been used by biologists to observe pH differences at an inter and intracellular level. Upon retooling the ratiometric setup it was possible to not only observe pH driven responses of clustered particles but also observe the extent of a particle's 'adjacent neighbourhood'.

7.1.1 Incorporating the component technologies

Herein we draw conclusions from the thesis with regard to meeting the key stages of quorum sensing. From creation of a host particle to contain the component technologies through to each individual stage.

7.1.1.1 Synthesis and Characterisation of Host Particles

In chapter 5, two pH responsive hydrogels were initially synthesised. A poly(methacrylic acid) hydrogel crosslinked with *N, N'*-methylenebisacrylamide was formed by a redox initiated, water in oil emulsion polymerisation. The resulting particles measured $148 \pm 33 \mu\text{m}$ in their shrunken state at pH 3 but swelled to almost double the size at pH 10 ($278 \pm 47 \mu\text{m}$). Furthermore, the reversibility of the pH driven volumetric transition was explored. Although the particles demonstrated slight hysteresis the midpoint of the transition remained around pH 4.9.

The second hydrogel was formed by crosslinking chitosan with glutaraldehyde again in an water in oil emulsion. The resulting particles also exhibited pH-dependent swelling, collapsed above pH 6.0 and rapidly swelling to a maximum when the pH was less than pH 4.0. Although varying the degree of crosslinking had an effect on the size of the volumetric transition it had little effect on the mid-point of the transition.

At this time neither pH-responsive hydrogel was followed up as a host particle. This is due expected difficulties in loading and retaining the signal generating enzyme within the hydrogel without loss of activity. Furthermore, using a pH-responsive hydrogel could complicate the reaction dynamics with substrate and product diffusion rate changing depending on the hydrogel's degree of ionisation. Therefore, an alternative non-responsive hydrogel was sought.

Due to its well reported, facile, rapid, synthesis Ca-alginate gels were selected as an ideal host particle.^{77,328–330} Moreover, there has been recent interest in using such gels to immobilise enzymes.⁷⁷ Hydrogels of Ca-alginate were formed by a simple extrusion dripping method of Na-alginate into a calcium ion bath. The resulting particles were relatively monodisperse (2.11 ± 0.05 mm) and spherical (aspect ratio 0.96).

7.1.1.2 Increasing Population Density

In nature quorum sensing bacteria increase their population 'by hook or by crook'. *A. fischeri* are harvested from the sea by the Hawaiian Bobtailed Squid and stored in its light organ, through continued harvesting and cell division the bacteria increase their population density above a threshold and initiate a response. Bioluminescence along the sea shore is caused by tidal currents and waves pushing such bacteria and their secreted autoinducers toward the sea shore where the perceived population density crosses a threshold and the bacteria become bioluminescent. As synthetic particles can be either 'harvested' increasing the population of particles within a reaction vessel. Alternatively, the local population of particles can be increased by the application or removal of an external force.

In section 5.2.3.2 autonomous aggregation alginate particles was achieved by including ferrous magnetite particles (0.0025-0.01 % w/w) in the Na-alginate pre-gel. Although all explored loading parameters demonstrated a degree of magnetic response when a magnetic field was applied. At least 0.00625 % w/w magnetite was required for all of the particles to overcome the opposing drag forces of the meniscus. This meniscus comes from the pseudo-2D reaction conditions, which were imposed due to the subsequent ratiometric reaction.

7.1.1.3 *Signal Generation*

From the outset enzymes whose product induces a shift in pH had highlighted as a potential source of signal generation. These enzymes would breakdown a substrate present in the solution converting it to an acid or base. The enzyme glucose oxidase was chosen as it not only generates glucono- δ -lactone which undergoes subsequent ester hydrolysis to form gluconic acid. But it also has a bell-shaped pH-dependent activity profile with a maximum at pH 5.1.⁹⁹ In chapter 3 the activity of glucose oxidase was probed. It was shown that the rate of pH change was dependent upon both the amount of glucose oxidase and the subsequent rate of ester hydrolysis. At high GOx concentrations (96.45 units cm^{-3}) the rate limiting step was ester hydrolysis. However, at lower a GOx concentration (9.65 units cm^{-3}) it is hypothesised that the production of the lactone by GOx is the limiting factor between pH 6.0 and 7.0. however, this requires further investigation (see section 7.2.1.2 page 128)

GOx was immobilised within Ca alginate gels by incorporating it in the pre-gel solution. Ratiometric imaging of a single particle in a static glucose solution demonstrated how the acid diffused away from the particle in a Fickian manner. Furthermore, the limit of particle's 'adjacent neighbourhood' was shown to be 2.11 mm (the average particle diameter) from the edge of the particle.

7.1.1.4 *Signal Detection and Response*

Signal detection in bacterial systems is accompanied by an increase in autoinducer production.⁹ From chapter 3 it was shown the production of gluconic acid mediated by the glucose oxidase catalysed oxidation of glucose demonstrated strong pH dependence under physiologically relevant pH's (5.0-7.4). Due to both the bell-shaped rate profile of glucose oxidase (maxima at 5.1) increasing the production of the lactone intermediate, and subsequent acid catalysed ester hydrolysis increasing with decreasing pH. As such any decrease from an extracellular pH (7.4) results in an increased production of lactone and acid by GOx.

Ratiometric imaging and analysis of clusters varying from one to twenty-five particles demonstrates a population dependent response. With a midpoint of the transition around five particles. particles that are in clusters smaller than the threshold population are unable to significantly lower their pH.

7.1.2 *Ratiometric Imaging*

Ratiometric imaging microscopy has predominantly been used by biologists to probe differences in pH both inter and intra cellularly. In chapter 4 page (76) the retooling of a ratiometric setup for use in probing interparticle dynamics and collective behaviour of cluster is set out and discussed. Calibration of the ratiometric setup with carboxy-SNARF-4F, used the rearranged Grynkiewicz equation. Table 3 (page 81) demonstrated the importance of experimentally pre-determining the dyes pK_a . Treating the dye as a weak acid and the calibration as a titration enabled an alternative equation to be used for the

calibration. This equation was based on the concentration fraction equation (Eq. A-1.24), the reduced number of parameters made for fast, facile calibrating. Chapter 4 also defined the reaction parameter such as dye concentration and pixel binning. Furthermore, the importance of image processing was demonstrated by carrying out a flatfield correction.

Use of the ratiometric system enable reaction parameters such as diffusion coefficients to be determined. Moreover, ratiometric imaging of GOx loaded particles demonstrated the importance of cluster packing to inhibit diffusion enabling a large pH shift to be observed. Simple modelling used experimental data gained from the ratiometric imaging of single particles demonstrated how the particle obeyed Fickian diffusive behaviour.

7.2 Future Work

7.2.1 Stirred Reaction Media

Stirred reaction media could be used to probe glucose oxidase activity further and to demonstrate global coupling of particles. In brief GOx loaded particles would be prepared by the method described previously (Section 2.3.1; page 47). With carboxy-SNARF-4F either omitted or replaced by a pH responsive dye such as methyl red (pK_a 5.1) or chlorophenol red (pK_a 6.0). The particles would then be placed in a reaction vessel fitted with a magnetic stirrer containing a glucose solution corrected to between pH 7 and 8. The pH of the bulk aqueous phase would be logged using a pH electrode and LabView code (as described in section 2.2.3; page 47). Image analyses of the stirred reaction media would enable a quantifiable colorimetric pH response to be observed.

7.2.1.1 Global Coupling

Using the reaction protocol laid out above, it would be possible to replicate the seminal work of Showalter et al.²⁶ In which they demonstrate global coupling of ferriin loaded beads in stirred uncatalyzed BZ reaction media. By adjusting the stir rate of the reaction media, the acid produced by GOx would be stripped from the alginate particle into the bulk solution causing a global shift in pH. This would cause an en masse colour shift of the pH responsive dye. Further parameters such as GOx loading and the mixing of particles at different degrees of loading could also be explored.

7.2.1.2 Glucose Oxidase Activity

From Chapter 3 it was shown that the rate of pH change was limited by the ester hydrolysis of the lactone to acid rather than the rate of glucose oxidation (Figure 7-2). However, as shown by Wilson and Turner⁹⁹ the action of glucose oxidase is pH sensitive. Furthermore, two assumptions were made firstly that the enzymatic activity with changing pH is uninhibited by encapsulating GOx in alginate. Secondly leaching of GOx from within the particles is negligible. By taking aliquots of the bulk solution

at set time or pH intervals of the protocol described above. The change enzymatic activity could be measured by the growth of the absorption peak at 540 nm when the hydrogen peroxide is broken down by peroxidase in the presence of o-dianisidine.²⁸⁷ The resulting enzymatic activity could be plotted as a function of pH or time. It is thought that the former would give the indicative bell-shaped activity profile (Figure 7-2). It is hypothesised that under the right conditions the time dependant enzymatic rate profile would demonstrate a sigmoidal growth. With the enzymatic rate increasing as the reaction proceeds.

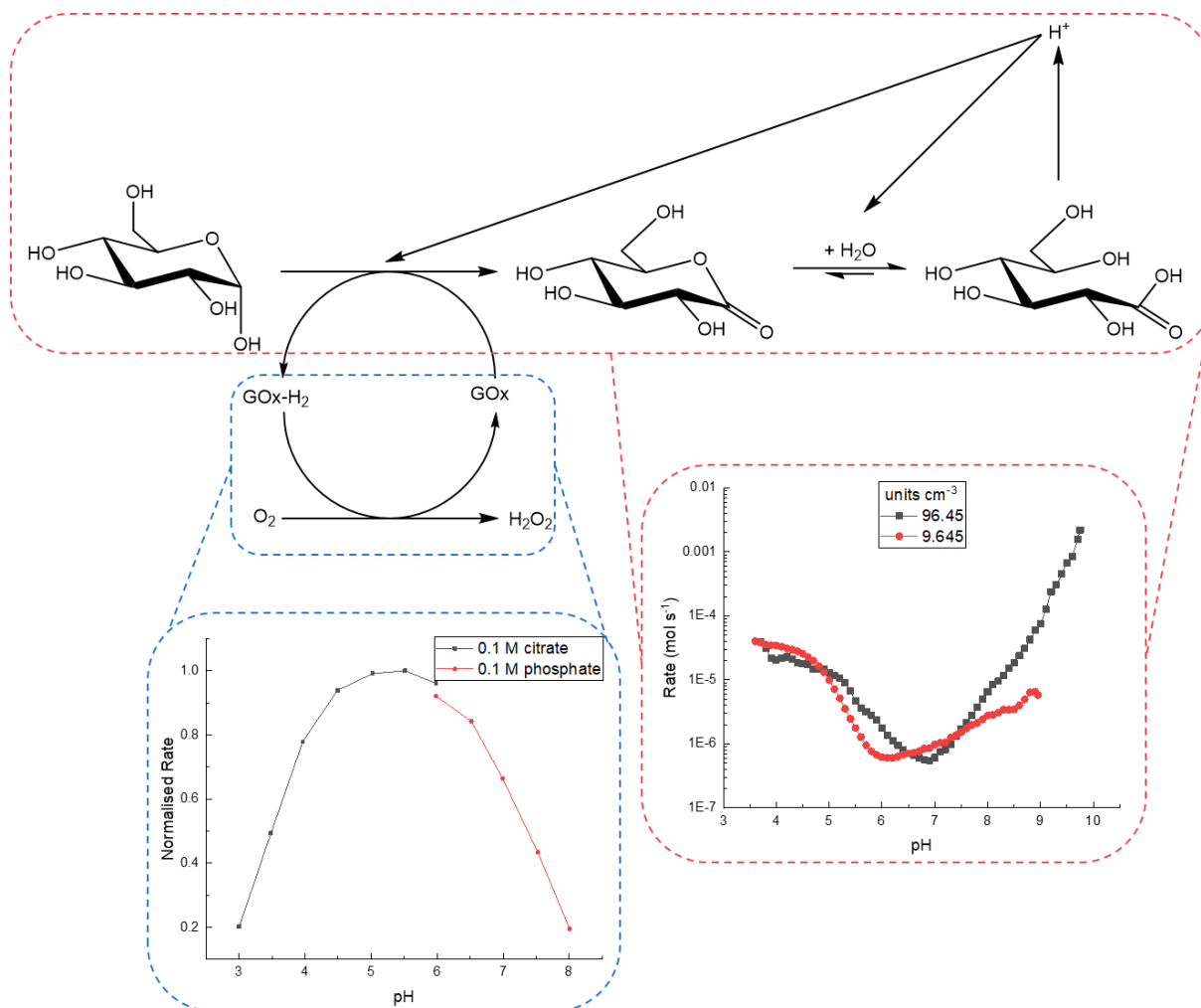


Figure 7-2 reaction mechanism for the glucose oxidase catalysed oxidation of glucose to glucono- δ -lactone accompanied by the reduction of oxygen to hydrogen peroxide. The glucono- δ -lactone then undergoes pH dependent ester hydrolysis to form gluconic acid. The enzymatic rate of GOx as a function of pH is highlighted in blue from reference ⁹⁹. The overall rate profile of GOx in a solution of glucose (1.92 mmol dm⁻³) and NaOH (40 μ mol dm⁻³) highlighted in red.

Enzyme leaching from the particle could also be explored. If GOx leaches into bulk solution and an aliquot is taken. The GOx present will continue to produce hydrogen peroxide causing a shift in intensity in the absorbance peak at 540 nm.

7.2.2 Experiments using the Ratiometric Setup

Using the protocols described in the experimental chapter it would be possible to explore several parameters further. Such parameters include enzymatic loading and a series of spatial studies to determine the effect of both particle packing density and diffusion dependence.

7.2.2.1 Enzyme Loading

As discussed previously (section 1.3.1.2) synchronisation and quorum sensing are relatively similar phenomena. With one key difference in a synchronising system of BZ catalytic beads is any individual particle has the ability to oscillate by entering an autocatalytic state. Individual particles synchronise their oscillations to the particle which demonstrates the most rapid auto-catalytic behaviour through it's the frequency of its oscillations. Whereas, in a quorum sensing system, individual particles are incapable of entering an oscillatory state due to the reaction kinetics. However, when a threshold population is reached oscillations occur.

To date all particles have been loaded with the same concentration of enzyme. Judiciously changing the enzyme concentration above and below the current level of 4 mg cm^{-3} would shift the midpoint of the threshold that has been observed. Decreasing the enzyme concentration would increase in number of particles required to observe a threshold response. Furthermore, it is thought that this would sharpen the threshold. With an increase in a particles enzyme concentration it is would be expected that the rate of acid production would also increase proportionally decreasing the number of particle required to observe a response. However, since the enzyme is physically entrapped within a particle substrate competition between the enzyme molecules may increase. Therefore, beyond a specific enzyme concentration a maximum activity may be observed. Use of particle clusters which have an increased enzyme concentration (to a level where an individual particle can reach an auto-catalytic state) could also be used to demonstrate another collective behaviour, synchronisation.

7.2.2.2 Spatial Studies

Simple modelling in chapter 6 (Figure 6-6; page 110) suggests that particles strongly interact when the distance between them is less than 2.11 mm, assuming that the diffusion parameters are uniform throughout the reaction. However, in tightly packed clusters show the pH to be significantly higher in the interstitial sights than in the alginate particles.

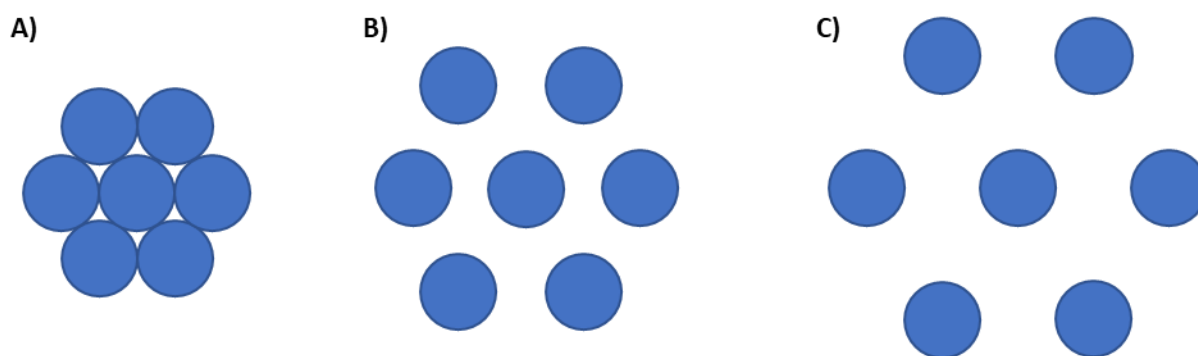


Figure 7-3. Clusters of 7 particles in a hexagonal arrangement where the interparticle distance is; A) 0; B) 0.5 x particle diameter; C) 1 x particle diameter.

A series of experiments would be carried out where the distance between the particles is varied (Figure 7-3). The interparticle distance would be varied between the 0 and 2.11 mm (the limit of the adjacent neighbour region). The interplay of particle interactions and distance could then be probed. Furthermore, decreasing the packing would aid diffusion decreasing acid pooling in the interstitial sights.

7.2.3 Delivering a response

Although a clear pH shift occurs when crossing a population threshold, the current GOx alginate particles present no pH switch induced response. There are a number of options available to achieve this final goal. From the facile such as the inclusion of pH responsive dye and increasing cluster size, resulting in a colorimetric response or oscillator behaviour respectively. Since the over arching theme of the thesis is to generate a drug delivery system a cargo-release or volumetric transition would be the ideal response to generate.

7.2.3.1 Colorimetric response

As previously described in section 7.2.1 either methyl red or chlorophenol red can simply be added to the GOx loaded alginate particles. Such particles could then form clusters in a glucose solution. As the pH of the cluster decreases the particles would undergo a colour change. Providing the dye is judiciously selected such that its pK_a is lower than the pH reached by small clusters. But higher than the pH reached by larger clusters a pK_a ($5.3 < pK_a < 6.5$; from Table 7), a quorum sensing response would be observed.

7.2.3.2 Cargo-release

In the present system of GOx loaded alginate particle a pH shift induced cargo release can not be induced. This can be overcome by either including a pH responsive carrier such as the degradable ketal-based block copolymer nanoparticles reported by De Geest et al.³³⁶ These nanoparticles are stable at a physiological pH, but degrade at around pH 5. Furthermore, these particles can encapsulate

either drugs such as paclitaxel or a rhodamine dye. As a proof of concept rhodamine loaded nanoparticles would be included in the alginate particle synthesis. Changing the filter set of the inverted microscope for one suitable for rhodamine (Nikon filter set G2-A) would enable observation of the dye release. It is hypothesised that a single particle in a glucose solution (initial pH 7.0) would not release the dye due to an insufficient shift in pH. However, clusters of 10 or more particles would cause the dye loaded nanoparticles to burst allowing the rhodamine dye to leach out.

Alternatively the particle disintegration method reported by Jagers and Bon could be employed.^{74,75} In this instance alginate particles would be loaded with urease and a dye such as Rhodamine. Placed in a solution of urea (initial pH 5.0) and EDTA, single particles would remain intact. However, clusters of particles would raise the pH to an extent that EDTA transitions into its Ca^{2+} chelating form, causing disintegration of the alginate particle and a burst release. A drawback of this method at present is the size of the alginate particles. Taylor et al⁷⁷ showed that 2 mm diameter alginate particles require very little urease (4-5 units cm^{-3} of Ca-alginate particle) for individual particles to exhibit a pH switch from 5.0 to 9.0. Since EDTA starts to chelate at $\text{pH} > 6.5$, low enzyme loading would be required. However, it was also shown that the degree of urease loading to observe a pH switch ($\text{pH} 5.0-9.0$) was inversely proportional to the particle diameter.⁷⁷ Therefore, the generation of smaller particles would enable a greater margin of error to achieve en masse particle disintegration.

7.2.3.3 Volumetric response

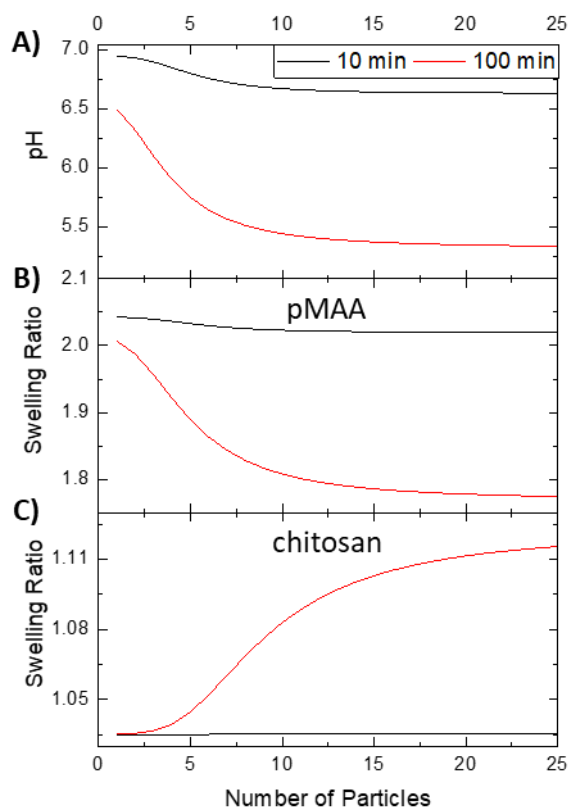


Figure 7-4 A) modelled quorum sensing response of GOx loaded alginate particles at 10 and 100 mins, using equation 6.3 and parameters given in Table 7. Theoretical quorum sensing response of GOx loaded pMAA (B) and chitosan (crosslinked with a 1:2 volumetric ratio of chitosan solution:GST; C) assuming; 2.11 mm particle diameter, enzyme loading 4.82 units cm^{-3} and no change in enzyme activity between polymers, nor change in activity with swelling of particle.

In chapter 5 pH responsive chitosan and PMAA particles were synthesised. It was proposed that such particles could be used as the polymeric body to encapsulate GOx. However, due to a number of reasons including a perceived lack of response in the transitional pH region and loss of enzyme activity either during synthesis or subsequent reactions, no further action was taken. Despite there only being a slight change in the size of the polymer particles a QS type volumetric response is hypothesised for pMAA and chitosan particles (see Figure 7-4). Both particles would have to be judiciously loaded with GOx, since they are much smaller than the alginate particles. Furthermore, the GOx will have to be immobilised within the polymer matrix since volumetric transitions are thought to aid the leaching of catalytic material.⁷²

7.2.3.3.1 Enzyme immobilisation

In this thesis glucose oxidase has been physically entrapped within a polymer matrix. To draw the conclusions already made it must be assumed that the enzyme is not diffusing out of the particle

tethering it to the particle. Furthermore, judicious selection of the polymer matrix has been shown to heighten enzymatic activity and tolerance to environmental stresses.³⁴² The enzyme creatine kinase was immobilised onto a silicate sol-gel, exhibiting a 100-fold increase in stability when exposed to high temperatures.³⁴³ However, activity and stability of the enzyme can decrease as well as the enzyme becoming less substrate specific. This is thought to be due to non-complementary surface chemistries of the enzyme and substrate, steric hindrances and or inappropriate microenvironments.^{324,325} Some enzymes like chloroperoxidase may exhibit enhanced stereoselectivity upon immobilisation³⁴⁴, whilst some lipases have been shown to switch from being (S)-selective to (R)-selective.³⁴⁵

One of the biggest drawbacks of chemical immobilisation is that it often requires the enzyme to be placed within a polymerisation which can expose it to free radicals and elevated temperatures which tends to denature the enzyme. Furthermore, altering the chemistry along the enzyme's backbone can kinetically lock it into a non-functioning conformer. It should also be noted that although the type of residue can be selected the location of binding cannot, as such, binding may sterically hinder the functional site of the enzyme.

7.2.3.4 Oscillatory Behaviour

In 2018 Bánsági and Taylor reported a model of urease loaded microparticles that demonstrated various quorum sensing induced responses including oscillatory behaviour.⁷³ In their model 100 μm particles loaded with urease ($500 \text{ units cm}^{-3}$) demonstrated oscillatory behaviour when in hexagonally packed clusters of 50-400 particles. Both these models and earlier ones were lead by experimental data collected from urease loaded alginate particles discussed earlier (see section 1.5).⁷⁷

8. References

1. Majhi, S., Bera, B. K., Ghosh, D. & Perc, M. Chimera states in neuronal networks: A review. *Phys. Life Rev.* (2018). doi:10.1016/j.plrev.2018.09.003
2. BUCK, J. SYNCHRONOUS RHYTHMIC FLASHING OF FIREFLIES .2. *Q. Rev. Biol.* **63**, 265–289 (1988).
3. Nealson, K. H. & Hastings, J. W. Bacterial bioluminescence: its control and ecological significance. *Microbiol. Rev.* **43**, 496–518 (1979).
4. Britton, M. & Sacks, L. *The SECOAS Project: development of a self-organising, wireless sensor network for environmental monitoring. 2nd International Workshop on Sensor and Actor Network Protocols and Applications, Boston* (2004).
5. Britton, M., Shum, V., Sacks, L. & Haddadi, H. A biologically-inspired approach to designing wireless sensor networks. in *Proceedings of the Second European Workshop on Wireless Sensor Networks, EWSN 2005* **2005**, 256–266 (IEEE, 2005).
6. Peysakhov, M. . M. D. & Regli, W. C. W. C. Ant inspired server population management in a service based computing environment. in *Swarm Intelligence Symposium, 2005. SIS 2005. Proceedings 2005 IEEE* 357–364 (IEEE, 2005).
7. Pratt, S. C. Quorum sensing by encounter rates in the ant *Temnothorax albipennis*. *Behav. Ecol.* **16**, 488–496 (2005).
8. Seeley, T., Visscher, P. & Passino, K. Group decision making in Honey Decision Bee Swarms: When 10,000 bees go house hunting, how do they cooperatively choose their new nesting site? *Am. Sci.* **94**, 220–230 (2006).
9. Miller, M. B. & Bassler, B. L. Quorum sensing in bacteria. *Annu. Rev. Microbiol.* **55**, 165–199 (2001).
10. Gonzalez, J. E., Marketon, M. M., González, J. E. & Marketon, M. M. Quorum sensing in nitrogen-fixing rhizobia. *Microbiol. Mol. Biol. Rev.* **67**, 574–592 (2003).
11. Perego, M. & Hoch, J. A. Cell-cell communication regulates the effects of protein aspartate phosphatases on the phosphorelay controlling development in *Bacillus subtilis*. *Proc. Natl. Acad. Sci. U. S. A.* **93**, 1549–53 (1996).
12. Hammer, B. K. & Bassler, B. L. Quorum sensing controls biofilm formation in *Vibrio cholerae*. *Mol. Microbiol.* **50**, 101–114 (2003).
13. Erickson, D. L. *et al.* *Pseudomonas aeruginosa* quorum-sensing systems may control virulence

- factor expression in the lungs of patients with cystic fibrosis. *Infect. Immun.* **70**, 1783–1790 (2002).
14. Quiñones, B., Dulla, G. & Lindow, S. E. Quorum Sensing Regulates Exopolysaccharide Production, Motility, and Virulence in *Pseudomonas syringae*. *Mol. Plant-Microbe Interact.* **18**, 682–693 (2005).
 15. Belousov, B. P. Sbornik Referatov po Radiatsionni Meditsine. *Medgiz, Moscow* **145**, (1958).
 16. Zhabotinsky, A. M. Periodical oxidation of malonic acid in solution (a study of the Belousov reaction kinetics). *Biofizika* **9**, 306–311 (1964).
 17. Epstein, I. R. & Pojman, J. A. *An introduction to nonlinear chemical dynamics: oscillations, waves, patterns, and chaos*. (Oxford University Press, 1998).
 18. FIELD, R. J., NOYES, R. M. & KOROS, E. OSCILLATIONS IN CHEMICAL SYSTEMS .2. THOROUGH ANALYSIS OF TEMPORAL OSCILLATION IN BROMATE-CERIUM-MALONIC ACID SYSTEM. *J. Am. Chem. Soc.* **94**, 8649- (1972).
 19. MAREK, M. & STUHL, I. SYNCHRONIZATION IN 2 INTERACTING OSCILLATORY SYSTEMS. *Biophys. Chem.* **3**, 241–248 (1975).
 20. Toiya, M., Vanag, V. K. & Epstein, I. R. Diffusively coupled chemical oscillators in a microfluidic assembly. *Angew. CHEMIE-INTERNATIONAL Ed.* **47**, 7753–7755 (2008).
 21. MASELKO, J., RECKLEY, J. S. & SHOWALTER, K. REGULAR AND IRREGULAR SPATIAL PATTERNS IN AN IMMOBILIZED-CATALYST BELOUSOV-ZHABOTINSKY REACTION. *J. Phys. Chem.* **93**, 2774–2780 (1989).
 22. MASELKO, J. & SHOWALTER, K. CHEMICAL WAVES ON SPHERICAL SURFACES. *Nature* **339**, 609–611 (1989).
 23. NISHIYAMA, N. & ETO, K. EXPERIMENTAL-STUDY ON 3 CHEMICAL OSCILLATORS COUPLED WITH TIME-DELAY. *J. Chem. Phys.* **100**, 6977–6978 (1994).
 24. MIYAKAWA, K., OKABE, T., MIZOGUCHI, M. & SAKAMOTO, F. SYNCHRONIZATION IN THE DISCRETE CHEMICAL OSCILLATION SYSTEM. *J. Chem. Phys.* **103**, 9621–9625 (1995).
 25. Toth, R. & Taylor, A. F. The tris(2,2'-bipyridyl)ruthenium-catalysed Belousov-Zhabotinsky reaction. *Prog. React. Kinet. Mech.* **31**, 59–115 (2006).
 26. Taylor, A. F., Tinsley, M. R., Wang, F., Huang, Z. & Showalter, K. Dynamical quorum sensing and

- synchronization in large populations of chemical oscillators. *Science (80-.)*. **323**, 614–617 (2009).
27. Aihara, R. & Yoshikawa, K. Size-dependent switching of the spatiotemporal structure between a traveling wave and global rhythm. *J. Phys. Chem. A* **105**, 8445–8448 (2001).
 28. Taylor, A. F., Tinsley, M. R., Wang, F. & Showalter, K. Phase Clusters in Large Populations of Chemical Oscillators. *Angew. CHEMIE-INTERNATIONAL Ed.* **50**, 10161–10164 (2011).
 29. Taylor, A. F., Tinsley, M. R. & Showalter, K. Insights into collective cell behaviour from populations of coupled chemical oscillators. *Phys. Chem. Chem. Phys.* **17**, 20047–20055 (2015).
 30. Yoshikawa, K., Aihara, R. & Agladze, K. Size-dependent Belousov-Zhabotinsky oscillation in small beads. *J. Phys. Chem. A* **102**, 7649–7652 (1998).
 31. Pikovsky, A., Rosenblum, M. & Kurths, J. *Synchronization: a universal concept in nonlinear sciences*. **12**, (Cambridge university press, 2003).
 32. ZHABOTINSKY, A. M., BUCHHOLTZ, F., KIYATKIN, A. B. & EPSTEIN, I. R. OSCILLATIONS AND WAVES IN METAL-ION-CATALYZED BROMATE OSCILLATING REACTIONS IN HIGHLY OXIDIZED STATES. *J. Phys. Chem.* **97**, 7578–7584 (1993).
 33. Glass, L. Synchronization and rhythmic processes in physiology. *Nature* **410**, 277–284 (2001).
 34. Lee, K. J., Cox, E. C. & Goldstein, R. E. Competing patterns of signaling activity in Dictyostelium discoideum. *Phys. Rev. Lett.* **76**, 1174–1177 (1996).
 35. Lauzeral, J., Halloy, J. & Goldbeter, A. Desynchronization of cells on the developmental path triggers the formation of spiral waves of cAMP during Dictyostelium aggregation. *Proc. Natl. Acad. Sci. U. S. A.* **94**, 9153–9158 (1997).
 36. WINFREE, A. T. SPIRAL WAVES OF CHEMICAL ACTIVITY. *Science (80-.)*. **175**, 634- (1972).
 37. Fukuda, H., Morimura, H. & Kai, S. Global synchronization in two-dimensional lattices of discrete Belousov-Zhabotinsky oscillators. *Phys. D-NONLINEAR Phenom.* **205**, 80–86 (2005).
 38. Tinsley, M. R., Taylor, A. F., Huang, Z., Wang, F. & Showalter, K. Dynamical quorum sensing and synchronization in collections of excitable and oscillatory catalytic particles. *Phys. D-NONLINEAR Phenom.* **239**, 785–790 (2010).
 39. Tinsley, M. R., Taylor, A. F., Huang, Z. & Showalter, K. Complex organizing centers in groups of oscillatory particles. *Phys. Chem. Chem. Phys.* **13**, 17802–17808 (2011).

40. Toth, R. & Taylor, A. F. Loss of coherence in a population of diffusively coupled oscillators. *J. Chem. Phys.* **125**, (2006).
41. Toth, R., Taylor, A. F. & Tinsley, M. R. Collective behavior of a population of chemically coupled oscillators. *J. Phys. Chem. B* **110**, 10170–10176 (2006).
42. WINFREE, A. T. BIOLOGICAL RHYTHMS AND BEHAVIOR OF POPULATIONS OF COUPLED OSCILLATORS. *J. Theor. Biol.* **16**, 15- (1967).
43. Kuramoto, Y. *Chemical oscillations, waves, and turbulence*. (Courier Corporation, 2003).
44. De Monte, S., d'Ovidio, F., Dano, S. & Sorensen, P. G. Dynamical quorum sensing: Population density encoded in cellular dynamics. *Proc. Natl. Acad. Sci. U. S. A.* **104**, 18377–18381 (2007).
45. Richard, P., Bakker, B. M., Teusink, B., vanDam, K. & Westerhoff, H. V. Acetaldehyde mediates the synchronization of sustained glycolytic oscillations in populations of yeast cells. *Eur. J. Biochem.* **235**, 238–241 (1996).
46. Miyakawa, K., Okabe, T. & Sakamoto, F. Irregular behaviors of two chemical oscillators with a diffusion coupling. *Phys. Rev. E* **55**, 2005–2008 (1997).
47. GOLOMB, D., HANSEL, D., SHRAIMAN, B. & SOMPOLINSKY, H. CLUSTERING IN GLOBALLY COUPLED PHASE OSCILLATORS. *Phys. Rev. A* **45**, 3516–3530 (1992).
48. HANSEL, D., MATO, G. & MEUNIER, C. CLUSTERING AND SLOW SWITCHING IN GLOBALLY COUPLED PHASE OSCILLATORS. *Phys. Rev. E* **48**, 3470–3477 (1993).
49. Vanag, V. K., Yang, L. F., Dolnik, M., Zhabotinsky, A. M. & Epstein, I. R. Oscillatory cluster patterns in a homogeneous chemical system with global feedback. *Nature* **406**, 389–391 (2000).
50. Kim, M. *et al.* Controlling chemical turbulence by global delayed feedback: Pattern formation in catalytic CO oxidation on Pt(110). *Science (80-.)*. **292**, 1357–1360 (2001).
51. ARONSON, D. G., ERMENTROUT, G. B. & KOPELL, N. AMPLITUDE RESPONSE OF COUPLED OSCILLATORS. *Phys. D* **41**, 403–449 (1990).
52. BARELI, K. ON THE STABILITY OF COUPLED CHEMICAL OSCILLATORS. *Phys. D* **14**, 242–252 (1985).
53. Nkomo, S., Tinsley, M. R. & Showalter, K. Chimera States in Populations of Nonlocally Coupled Chemical Oscillators. *Phys. Rev. Lett.* **110**, (2013).

54. Tinsley, M. R., Nkomo, S. & Showalter, K. Chimera and phase-cluster states in populations of coupled chemical oscillators. *Nat. Phys.* **8**, 662–665 (2012).
55. Yoshida, R. & Ueki, T. Evolution of self-oscillating polymer gels as autonomous polymer systems. *NPG Asia Mater.* **6**, e107-14 (2014).
56. RABAI, G., KUSTIN, K. & EPSTEIN, I. R. SYSTEMATIC DESIGN OF CHEMICAL OSCILLATORS .52. A SYSTEMATICALLY DESIGNED PH OSCILLATOR - THE HYDROGEN PEROXIDE-SULFITE-FERROCYANIDE REACTION IN A CONTINUOUS-FLOW STIRRED TANK REACTOR. *J. Am. Chem. Soc.* **111**, 3870–3874 (1989).
57. YOSHIDA, R., ICHIJO, H., HAKUTA, T. & YAMAGUCHI, T. SELF-OSCILLATING SWELLING AND DESWELLING OF POLYMER GELS. *Macromol. Rapid Commun.* **16**, 305–310 (1995).
58. Yoshida, R., Yamaguchi, T. & Ichijo, H. Novel oscillating swelling-deswelling dynamic behaviour for pH-sensitive polymer gels. *Mater. Sci. Eng. C-BIOMIMETIC Mater. SENSORS Syst.* **4**, 107–113 (1996).
59. Yoshida, R., Takahashi, T., Yamaguchi, T. & Ichijo, H. Self-oscillating gel. *J. Am. Chem. Soc.* **118**, 5134–5135 (1996).
60. Yoshida, R., Tanaka, M., Onodera, S., Yamaguchi, T. & Kokufuta, E. In-phase synchronization of chemical and mechanical oscillations in self-oscillating gels. *J. Phys. Chem. A* **104**, 7549–7555 (2000).
61. Suzuki, D., Sakai, T. & Yoshida, R. Self-flocculating/Self-dispersing oscillation of microgels. *Angew. CHEMIE-INTERNATIONAL Ed.* **47**, 917–920 (2008).
62. Suzuki, D. & Yoshida, R. Temporal control of self-oscillation for microgels by cross-linking network structure. *Macromolecules* **41**, 5830–5838 (2008).
63. Suzuki, D. & Yoshida, R. Effect of initial substrate concentration of the Belousov-Zhabotinsky reaction on self-oscillation for microgel system. *J. Phys. Chem. B* **112**, 12618–12624 (2008).
64. Suzuki, D. & Yoshida, R. Self-oscillating core/shell microgels: effect of a crosslinked nanoshell on autonomous oscillation of the core. *Polym. J.* **42**, 501–508 (2010).
65. Suzuki, D., Kobayashi, T., Yoshida, R. & Hirai, T. Soft actuators of organized self-oscillating microgels. *Soft Matter* **8**, 11447–11449 (2012).
66. Ueki, T., Shibayama, M. & Yoshida, R. Self-oscillating micelles. *Chem. Commun.* **49**, 6947–6949 (2013).

67. Moad, G., Chong, Y. K., Postma, A., Rizzardo, E. & Thang, S. H. Advances in RAFT polymerization: the synthesis of polymers with defined end-groups. *Polymer (Guildf)*. **46**, 8458–8468 (2005).
68. Donlon, L. & Novakovic, K. Oscillatory carbonylation using alkyne-functionalised poly(ethylene glycol). *Chem. Commun.* **50**, 15506–15508 (2014).
69. Isakova, A. & Novakovic, K. Pulsatile release from a flat self-oscillating chitosan macrogel. *J. Mater. Chem. B* **6**, 5003–5010 (2018).
70. Malashkevich, A. V, Bruk, L. G. & Temkin, O. N. New oscillating reaction in catalysis by metal complexes: A mechanism of alkyne oxidative carbonylation. *J. Phys. Chem. A* **101**, 9825–9827 (1997).
71. Khabibulin, V. R. *et al.* Mechanism of the oxidative carbonylation of terminal alkynes at the equivalent to C-H bond in solutions of palladium complexes. *Kinet. Catal.* **48**, 228–244 (2007).
72. Isakova, A., Parkes, G. E., Murdoch, B. J., Topham, P. D. & Novakovic, K. Combining polymer-bound catalyst with polymeric substrate for reproducible pH oscillations in palladium-catalysed oxidative carbonylation of alkynes. *Eur. Polym. J.* **109**, 537–543 (2018).
73. Bánsági Jr, T. & Taylor, A. F. Switches induced by quorum sensing in a model of enzyme-loaded microparticles. *J. R. Soc. Interface* **15**, 20170945 (2018).
74. Jagers, R. W. & Bon, S. A. F. Independent responsive behaviour and communication in hydrogel objects. *Mater. Horizons* **4**, 402–407 (2017).
75. Jagers, R. W. & Bon, S. A. F. Temporal and spatial programming in soft composite hydrogel objects. *J. Mater. Chem. B* **5**, 7491–7495 (2017).
76. Jagers, R. W. & Bon, S. A. F. Communication between hydrogel beads via chemical signalling. *J. Mater. Chem. B* **5**, 8681–8685 (2017).
77. Muzika, F., Bansagi, T., Schreiber, I., Schreiberova, L. & Taylor, A. F. A bistable switch in pH in urease-loaded alginate beads. *Chem. Commun.* **50**, 11107–11109 (2014).
78. Blandino, A., Macías, M. & Cantero, D. Glucose oxidase release from calcium alginate gel capsules. *Enzyme Microb. Technol.* **27**, 319–324 (2000).
79. Halder, A., Maiti, S. & Sa, B. Entrapment efficiency and release characteristics of polyethyleneimine-treated or-untreated calcium alginate beads loaded with propranolol–resin complex. *Int. J. Pharm.* **302**, 84–94 (2005).

80. Martinkova, L. & Křen, V. Nitrile- and amide-converting microbial enzymes: stereo-, regio- and chemoselectivity. *Biocatal. Biotransformation* **20**, 73–93 (2002).
81. Djordjevic, S. & Driscoll, P. C. Structural insight into substrate specificity and regulatory mechanisms of phosphoinositide 3-kinases. *Trends Biochem. Sci.* **27**, 426–432 (2002).
82. Chen, L. H. *et al.* 4-Oxalocrotonate tautomerase, an enzyme composed of 62 amino acid residues per monomer. *J. Biol. Chem.* **267**, 17716–17721 (1992).
83. Smith, S. The animal fatty acid synthase: one gene, one polypeptide, seven enzymes. *FASEB J.* **8**, 1248–1259 (1994).
84. Breslow, R. *Artificial enzymes*. (John Wiley & Sons, 2006).
85. Kawaguchi, H. Functional polymer microspheres. *Prog. Polym. Sci.* **25**, 1171–1210 (2000).
86. Katz, E. & Privman, V. Enzyme-based logic systems for information processing. *Chem. Soc. Rev.* **39**, 1835–1857 (2010).
87. Muzika, F. & Schreiber, I. Control of Turing patterns and their usage as sensors, memory arrays, and logic gates. *J. Chem. Phys.* **139**, 164108 (2013).
88. Webb, E. C. *Enzyme nomenclature 1992. Recommendations of the Nomenclature Committee of the International Union of Biochemistry and Molecular Biology on the Nomenclature and Classification of Enzymes*. (Academic Press, 1992).
89. Cornish-Bowden, A. *Fundamentals of enzyme kinetics*. **510**, (Wiley-Blackwell Weinheim, Germany, 2012).
90. Dixon, M. The effect of pH on the affinities of enzymes for substrates and inhibitors. *Biochem. J.* **55**, 161 (1953).
91. Lineweaver, H. & Burk, D. The determination of enzyme dissociation constants. *J. Am. Chem. Soc.* **56**, 658–666 (1934).
92. Caplan, S. R., Naparstek, A. & ZABUSKY, N. J. Chemical oscillations in a membrane. *Nature* **245**, 364 (1973).
93. Goldbeter, A. & Caplan, S. R. Oscillatory enzymes. *Annu. Rev. Biophys. Bioeng.* **5**, 449–476 (1976).
94. Svendsen, A. Lipase protein engineering. *Biochim. Biophys. Acta (BBA)/Protein Struct. Mol. Enzymol.* **1543**, 223–238 (2000).

95. Hasan, F., Shah, A. A. & Hameed, A. Industrial applications of microbial lipases. *Enzyme Microb. Technol.* **39**, 235–251 (2006).
96. Nelson, L. A., Foglia, T. A. & Marmer, W. N. Lipase-catalyzed production of biodiesel. *J. Am. Oil Chem. Soc.* **73**, 1191–1195 (1996).
97. Fukuda, H., Kondo, A. & Noda, H. Biodiesel fuel production by transesterification of oils. *J. Biosci. Bioeng.* **92**, 405–416 (2001).
98. Eaton, K. A., Brooks, C., Morgan, D. R. & Krakowka, S. Essential role of urease in pathogenesis of gastritis induced by *Helicobacter pylori* in gnotobiotic piglets. *Infect. Immun.* **59**, 2470–2475 (1991).
99. Wilson, R. & Turner, A. P. F. Glucose oxidase: an ideal enzyme. *Biosens. Bioelectron.* **7**, 165–185 (1992).
100. Wong, C. M., Wong, K. H. & Chen, X. D. Glucose oxidase: natural occurrence, function, properties and industrial applications. *Appl. Microbiol. Biotechnol.* **78**, 927–938 (2008).
101. White Jr, J. W., Subers, M. H. & Schepartz, A. I. The identification of inhibine, the antibacterial factor in honey, as hydrogen peroxide and its origin in a honey glucose-oxidase system. *Biochim. Biophys. Acta (BBA)-Specialized Sect. Enzymol. Subj.* **73**, 57–70 (1963).
102. Metzger, R. P., Wilcox, S. S. & Wick, A. N. Studies with rat liver glucose dehydrogenase. *J. Biol. Chem.* **239**, 1769–1772 (1964).
103. Metzger, R. P., Wilcox, S. S. & Wick, A. N. Subcellular distribution and properties of hepatic glucose dehydrogenases of selected vertebrates. *J. Biol. Chem.* **240**, 2767–2771 (1965).
104. Hauge, J. G. Glucose dehydrogenase of *Bacterium anitratum*: an enzyme with a novel prosthetic group. *J Biol Chem* **239**, 3630–3639 (1964).
105. Duine, J. A., Jzn, J. F. & Van der Meer, R. Different forms of quinoprotein aldose-(glucose-) dehydrogenase in *Acinetobacter calcoaceticus*. *Arch. Microbiol.* **131**, 27–31 (1982).
106. Volc, J., Denisova, N. P., Nerud, F. & Musilek, V. Glucose-2-oxidase activity in mycelial cultures of basidiomycetes. *Folia Microbiol. (Praha).* **30**, 141–147 (1985).
107. Janssen, F. W. & Ruelius, H. W. Carbohydrate oxidase, a novel enzyme from *Polyporus obtusus*: II. Specificity and characterization of reaction products. *Biochim. Biophys. Acta (BBA)-Enzymology* **167**, 501–510 (1968).

108. Kleppe, K. The effect of hydrogen peroxide on glucose oxidase from *Aspergillus niger*. *Biochemistry* **5**, 139–143 (1966).
109. Tang, Z., Du, X., Louie, R. F. & Kost, G. J. Effects of pH on glucose measurements with handheld glucose meters and a portable glucose analyzer for point-of-care testing. *Arch. Pathol. Lab. Med.* **124**, 577–582 (2000).
110. Kim, S.-H., Lee, S.-M., Kim, D.-U., Cui, J.-Z. & Kang, S.-W. Enzyme-based glucose biosensor using a dye couple system. *Dye. Pigment.* **49**, 103–108 (2001).
111. Chudobova, I., Vrbová, E., Kodíček, M., Janovcová, J. & Káš, J. Fibre optic biosensor for the determination of D-glucose based on absorption changes of immobilized glucose oxidase. *Anal. Chim. Acta* **319**, 103–110 (1996).
112. Santoni, T., Santianni, D., Manzoni, A., Zanardi, S. & Mascini, M. Enzyme electrode for glucose determination in whole blood. *Talanta* **44**, 1573–1580 (1997).
113. Cui, G. *et al.* Disposable amperometric glucose sensor electrode with enzyme-immobilized nitrocellulose strip. *Talanta* **54**, 1105–1111 (2001).
114. Vodopivec, M., Berovič, M., Jančar, J., Podgornik, A. & Štrancar, A. Application of Convective Interaction Media disks with immobilised glucose oxidase for on-line glucose measurements. *Anal. Chim. Acta* **407**, 105–110 (2000).
115. Harborn, U., Xie, B., Venkatesh, R. & Danielsson, B. Evaluation of a miniaturized thermal biosensor for the determination of glucose in whole blood. *Clin. Chim. acta* **267**, 225–237 (1997).
116. Crueger, A. & Crueger, W. Glucose transforming enzymes. in *Microbial enzymes and biotechnology* 177–226 (Springer, 1990).
117. Isaksen, A. & Adler-Nissen, J. Antioxidative effect of glucose oxidase and catalase in mayonnaises of different oxidative susceptibility. I. Product trials. *LWT-Food Sci. Technol.* **30**, 841–846 (1997).
118. Rasiah, I. A., Sutton, K. H., Low, F. L., Lin, H.-M. & Gerrard, J. A. Crosslinking of wheat dough proteins by glucose oxidase and the resulting effects on bread and croissants. *Food Chem.* **89**, 325–332 (2005).
119. Bonet, A. *et al.* Glucose oxidase effect on dough rheology and bread quality: a study from macroscopic to molecular level. *Food Chem.* **99**, 408–415 (2006).

120. Malherbe, D. F., Du Toit, M., Otero, R. R. C., Van Rensburg, P. & Pretorius, I. S. Expression of the *Aspergillus niger* glucose oxidase gene in *Saccharomyces cerevisiae* and its potential applications in wine production. *Appl. Microbiol. Biotechnol.* **61**, 502–511 (2003).
121. Pickering, G. J., Heatherbell, D. A. & Barnes, M. F. Optimising glucose conversion in the production of reduced alcohol wine using glucose oxidase. *Food Res. Int.* **31**, 685–692 (1998).
122. Dawson, R. M. C., Elliott, D. C., Elliott, W. H. & Jones, K. M. Carboxylic acids, alcohols, aldehydes, and ketones; pH, buffers, and physiological media. *Data Biochem. Res.* (1986).
123. Stoll, V. S. & Blanchard, J. S. [4] Buffers: Principles and practice. in *Methods in enzymology* **182**, 24–38 (Elsevier, 1990).
124. Gomes, B. P. F. A. *et al.* In vitro antimicrobial activity of several concentrations of sodium hypochlorite and chlorhexidine gluconate in the elimination of *Enterococcus faecalis*. *Int. Endod. J.* **34**, 424–428 (2001).
125. Nakao, K., Kiefner, A., Furumoto, K. & Harada, T. Production of gluconic acid with immobilized glucose oxidase in airlift reactors. *Chem. Eng. Sci.* **52**, 4127–4133 (1997).
126. Klein, J., Rosenberg, M., Markoš, J., Dolgoš, O. & Krošlák, M. Biotransformation of glucose to gluconic acid by *Aspergillus niger*—study of mass transfer in an airlift bioreactor. *Biochem. Eng. J.* **10**, 197–205 (2002).
127. Singh, N. B. Effect of gluconates on the hydration of cement. *Cem. Concr. Res.* **6**, 455–460 (1976).
128. Wedding, P. & Kantro, D. Influence of Water-Reducing Admixtures on Properties of Cement Paste—A Miniature Slump Test. *Cem. Concr. Aggregates* **2**, 95 (1980).
129. Tzanov, T., Costa, S. A., Gübitz, G. M. & Cavaco-Paulo, A. Hydrogen peroxide generation with immobilized glucose oxidase for textile bleaching. *J. Biotechnol.* **93**, 87–94 (2002).
130. Opwis, K., Knittel, D., Schollmeyer, E., Hoferichter, P. & Cordes, A. Simultaneous application of glucose oxidases and peroxidases in bleaching processes. *Eng. Life Sci.* **8**, 175–178 (2008).
131. Nakamura, S., Hayashi, S. & Koga, K. Effect of periodate oxidation on the structure and properties of glucose oxidase. *Biochim. Biophys. Acta (BBA)-Enzymology* **445**, 294–308 (1976).
132. Bourdillon, C., Bourgeois, J. P. & Thomas, D. Covalent linkage of glucose oxidase on modified glassy carbon electrodes. Kinetic phenomena. *J. Am. Chem. Soc.* **102**, 4231–4235 (1980).

133. O'Malley, J. J. & Weaver, J. L. Subunit structure of glucose oxidase from *Aspergillus niger*. *Biochemistry* **11**, 3527–3532 (1972).
134. Wellner, D. Flavoproteins. *Annu. Rev. Biochem.* **36**, 669–690 (1967).
135. Bentley, R. Glucose oxidase. *Enzym.* **7**, 567–586 (1963).
136. Coulthard, C. E. *et al.* Notatin: an anti-bacterial glucose-aerodehydrogenase from *Penicillium notatum* Westling. *Nature* **150**, 634 (1942).
137. Keilin, D. & Hartree, E. F. Properties of glucose oxidase (notatin): Addendum. Sedimentation and diffusion of glucose oxidase (notatin). *Biochem. J.* **42**, 221 (1948).
138. James, T. L., Edmondson, D. E. & Husain, M. Glucose oxidase contains a disubstituted phosphorus residue. Phosphorus-31 nuclear magnetic resonance studies of the flavin and nonflavin phosphate residues. *Biochemistry* **20**, 617–621 (1981).
139. Jones, M. N., Manley, P. & Wilkinson, A. The dissociation of glucose oxidase by sodium n-dodecyl sulphate. *Biochem. J.* **203**, 285–291 (1982).
140. Hayashi, S. & Nakamura, S. Multiple forms of glucose oxidase with different carbohydrate compositions. *Biochim. Biophys. Acta (BBA)-Enzymology* **657**, 40–51 (1981).
141. Voet, J. G. & Andersen, E. C. Electrostatic control of enzyme reactions: the mechanism of inhibition of glucose oxidase by putrescine. *Arch. Biochem. Biophys.* **233**, 88–92 (1984).
142. Adams Jr, E. C., Mast, R. L. & Free, A. H. Specificity of glucose oxidase. *Arch. Biochem. Biophys.* **91**, 230–234 (1960).
143. Gibson, Q. H., Swoboda, B. E. P. & Massey, V. Kinetics and mechanism of action of glucose oxidase. *J. Biol. Chem.* **239**, 3927–3934 (1964).
144. Rogers, M. J. & Brandt, K. G. Multiple inhibition analysis of *Aspergillus niger* glucose oxidase by D-glucal and halide ions. *Biochemistry* **10**, 4636–4641 (1971).
145. Weibel, M. K. & Bright, H. J. The glucose oxidase mechanism interpretation of the pH dependence. *J. Biol. Chem.* **246**, 2734–2744 (1971).
146. Szklarz, G. & Leonowicz, A. Cooperation between fungal laccase and glucose oxidase in the degradation of lignin derivatives. *Phytochemistry* **25**, 2537–2539 (1986).
147. Dixon, M. *EC web, Enzymes.* (1964).
148. Keilin, D. & Hartree, E. F. Specificity of glucose oxidase (notatin). *Biochem. J.* **50**, 331 (1952).

149. Pazur, J. H. & Kleppe, K. The oxidation of glucose and related compounds by glucose oxidase from *Aspergillus niger*. *Biochemistry* **3**, 578–583 (1964).
150. Stults, C. L. M., Wade, A. P. & Crouch, S. R. Immobilized enzyme kinetic study of D-glucose mutarotation by flow injection analysis. *Anal. Chem.* **59**, 2245–2247 (1987).
151. Sund, H. & Theorell, H. The Enzymes, Vol. 7. by Boyer, PD, Lardy, H. Myrback, K. London Acad. Press Ltd 25 (1963).
152. Chan, T. W. & Bruice, T. C. One and two electron transfer reactions of glucose oxidase. *J. Am. Chem. Soc.* **99**, 2387–2389 (1977).
153. Porter, D. J. T., Voet, J. G. & Bright, H. J. Direct evidence for carbanions and covalent N5-flavin-carbanion adducts as catalytic intermediates in the oxidation of nitroethane by d-amino acid oxidase. *J. Biol. Chem.* **248**, 4400–4416 (1973).
154. Porter, D. J. T., Voet, J. G. & Bright, H. J. Nitroalkanes as reductive substrates for flavoprotein oxidases. *Zeitschrift für Naturforsch. B* **27**, 1052–1053 (1972).
155. Nakanishi, Y., Ohashi, K. & Tsuge, H. Essential histidyl residues in glucose oxidase. Chemical modification of histidyl residues with diethylpyrocarbonate. *Agric. Biol. Chem.* **48**, 2951–2959 (1984).
156. Ramasamy, K., Kelley, R. L. & Reddy, C. A. Lack of lignin degradation by glucose oxidase-negative mutants of *Phanerochaete chrysosporium*. *Biochem. Biophys. Res. Commun.* **131**, 436–441 (1985).
157. Schepartz, A. I. & Subers, M. H. The glucose oxidase of honey I. Purification and some general properties of the enzyme. *Biochim. Biophys. Acta (BBA)-Specialized Sect. Enzymol. Subj.* **85**, 228–237 (1964).
158. Tse, P. H. S. & Gough, D. A. Time-dependent inactivation of immobilized glucose oxidase and catalase. *Biotechnol. Bioeng.* **29**, 705–713 (1987).
159. Bourdillon, C., Thomas, V. & Thomas, D. Electrochemical study of D-glucose oxidase autoinactivation. *Enzyme Microb. Technol.* **4**, 175–180 (1982).
160. Keilin, D. & Hartree, E. F. The use of glucose oxidase (notatin) for the determination of glucose in biological material and for the study of glucose-producing systems by manometric methods. *Biochem. J.* **42**, 230 (1948).
161. Kulys, J. J. & Čénas, N. K. Oxidation of glucose oxidase from *Penicillium vitale* by one-and two-

- electron acceptors. *Biochim. Biophys. Acta (BBA)-Protein Struct. Mol. Enzymol.* **744**, 57–63 (1983).
162. Schläpfer, P., Mindt, W. & Racine, P. H. Electrochemical measurement of glucose using various electron acceptors. *Clin. Chim. Acta* **57**, 283–289 (1974).
163. F. Gibbs Inteaz Alli, Catherine N. Mulligan, Bernard, S. K. Encapsulation in the food industry: a review. *Int. J. Food Sci. Nutr.* **50**, 213–224 (1999).
164. Paul, W. & Sharma, C. P. Chitosan and alginate wound dressings: a short review. *Trends Biomater Artif Organs* **18**, 18–23 (2004).
165. Byrom, D. *Biomaterials: novel materials from biological sources*. (Springer, 1991).
166. Smidsrød, O., Skja, G., SMIDSRØD, O. & SKJAKBRAEK, G. Alginate as immobilization matrix for cells. *TRENDS Biotechnol.* **8**, 71–78 (1990).
167. Skj, G. *et al.* Monomer sequence and acetylation pattern in some bacterial alginates. *Carbohydr. Res.* **154**, 239–250 (1986).
168. Haug, A., Larsen, B. & Smidsrod, O. Studies on the sequence of uronic acid residues in alginic acid. *Acta chem. scand* **21**, 691–704 (1967).
169. Braccini, I. & Pérez, S. Molecular basis of Ca²⁺-induced gelation in alginates and pectins: the egg-box model revisited. *Biomacromolecules* **2**, 1089–1096 (2001).
170. Wikström, J. *et al.* Alginate-based microencapsulation of retinal pigment epithelial cell line for cell therapy. *Biomaterials* **29**, 869–876 (2008).
171. Burns, M. A., Kvesitadze, G. I. & Graves, D. J. Dried calcium alginate/magnetite spheres: a new support for chromatographic separations and enzyme immobilization. *Biotechnol. Bioeng.* **27**, 137–145 (1985).
172. Romalde, J. L., Luzardo-Alvarez, A., Ravelo, C., Toranzo, A. E. & Blanco-Méndez, J. Oral immunization using alginate microparticles as a useful strategy for booster vaccination against fish lactococcosis. *Aquaculture* **236**, 119–129 (2004).
173. Kim, B. *et al.* Mucosal immune responses following oral immunization with rotavirus antigens encapsulated in alginate microspheres. *J. Control. release* **85**, 191–202 (2002).
174. Zhao, Y., Li, F., Carvajal, M. T. & Harris, M. T. Interactions between bovine serum albumin and alginate: an evaluation of alginate as protein carrier. *J. Colloid Interface Sci.* **332**, 345–353

- (2009).
175. A Chaudhari, S., R Kar, J. & S Singhal, R. Immobilization of proteins in alginate: functional properties and applications. *Curr. Org. Chem.* **19**, 1732–1754 (2015).
 176. Blandino, A., Macias, M. & Cantero, D. Immobilization of glucose oxidase within calcium alginate gel capsules. *Process Biochem.* **36**, 601–606 (2001).
 177. Dupuy, B., Arien, A. & Minnot, A. P. FT-IR of membranes made with alginate/polylysine complexes. Variations with the mannuronic or guluronic content of the polysaccharides. *Artif. Cells, Blood Substitutes, Biotechnol.* **22**, 71–82 (1994).
 178. Andresen, I. L., Skipnes, O., Smidsrod, O., Ostgaard, K. & Hemmer, P. C. Some biological functions of matrix components in benthic algae in relation to their chemistry and the composition of seawater. in *ACS Symposium Series-American Chemical Society (USA)* (1977).
 179. Martinsen, A., Skjåk-Bræk, G., Smidsrød, O., Zanetti, F. & Paoletti, S. Comparison of different methods for determination of molecular weight and molecular weight distribution of alginates. *Carbohydr. Polym.* **15**, 171–193 (1991).
 180. Espevik, T. *et al.* The involvement of CD14 in stimulation of cytokine production by uronic acid polymers. *Eur. J. Immunol.* **23**, 255–261 (1993).
 181. Zimmermann, U. *et al.* Production of mitogen-contamination free alginates with variable ratios of mannuronic acid to guluronic acid by free flow electrophoresis. *Electrophoresis* **13**, 269–274 (1992).
 182. Cole, D. R., Waterfall, M., McIntyre, M. & Baird, J. D. Microencapsulated islet grafts in the BB/E rat: a possible role for cytokines in graft failure. *Diabetologia* **35**, 231–237 (1992).
 183. De Vos, P. *et al.* Association between capsule diameter, adequacy of encapsulation, and survival of microencapsulated rat islet allografts¹. *Transplantation* **62**, 893–899 (1996).
 184. Mumper, R. J., Huffman, A. S., Puolakkainen, P. A., Bouchard, L. S. & Gombotz, W. R. Calcium-alginate beads for the oral delivery of transforming growth factor- β 1 (TGF- β 1): stabilization of TGF- β 1 by the addition of polyacrylic acid within acid-treated beads. *J. Control. Release* **30**, 241–251 (1994).
 185. Martinsen, A., Storrø, I. & Skjåk-Bræk, G. Alginate as immobilization material: III. Diffusional properties. *Biotechnol. Bioeng.* **39**, 186–194 (1992).
 186. Chen, S. C. *et al.* A novel pH-sensitive hydrogel composed of N,O-carboxymethyl chitosan and

- alginate cross-linked by genipin for protein drug delivery. *J. Control. Release* **96**, 285–300 (2004).
187. YOTSUYANAGI, T., OHKUBO, T., OHHASHI, T. & Ikeda, K. E. N. Calcium-induced gelation of alginic acid and pH-sensitive reswelling of dried gels. *Chem. Pharm. Bull.* **35**, 1555–1563 (1987).
 188. Åsberg, P. & Inganäs, O. Hydrogels of a conducting conjugated polymer as 3-D enzyme electrode. *Biosens. Bioelectron.* **19**, 199–207 (2003).
 189. Gray, C. J. & Dowsett, J. Retention of insulin in alginate gel beads. *Biotechnol. Bioeng.* **31**, 607–612 (1988).
 190. Chevalier, P., Cosentino, G. P., De La Noüe, J. & Rakhit, S. Comparative study on the diffusion of an IgG from various hydrogel beads. *Biotechnol. Tech.* **1**, 201–206 (1987).
 191. Hara, M. & Miyake, J. Calcium alginate gel-entrapped liposomes. *Mater. Sci. Eng. C* **17**, 101–105 (2001).
 192. Torre, M. L. *et al.* Formulation and characterization of calcium alginate beads containing ampicillin. *Pharm. Dev. Technol.* **3**, 193–198 (1998).
 193. Liu, P. & Krishnan, T. R. Alginate-pectin-poly-L-lysine particulate as a potential controlled release formulation. *J. Pharm. Pharmacol.* **51**, 141–149 (1999).
 194. Kulkarni, A. R., Soppimath, K. S., Aminabhavi, T. M., Dave, A. M. & Mehta, M. H. Glutaraldehyde crosslinked sodium alginate beads containing liquid pesticide for soil application. *J. Control. Release* **63**, 97–105 (2000).
 195. Kulkarni, A. R., Soppimath, K. S., Aralaguppi, M. I., Aminabhavi, T. M. & Rudzinski, W. E. Preparation of cross-linked sodium alginate microparticles using glutaraldehyde in methanol. *Drug Dev. Ind. Pharm.* **26**, 1121–1124 (2000).
 196. Chan, L. W. & Heng, P. W. S. Effects of aldehydes and methods of cross-linking on properties of calcium alginate microspheres prepared by emulsification. *Biomaterials* **23**, 1319–1326 (2002).
 197. Leonard, M., De Boisseson, M. R., Hubert, P., Dalencon, F. & Dellacherie, E. Hydrophobically modified alginate hydrogels as protein carriers with specific controlled release properties. *J. Control. release* **98**, 395–405 (2004).
 198. Bodmeier, R. & Wang, J. Microencapsulation of drugs with aqueous colloidal polymer dispersions. *J. Pharm. Sci.* **82**, 191–194 (1993).

199. Gursoy, A. *et al.* Preparation and tableting of dipyrnidamole alginate-Eudragit microspheres. *J. Microencapsul.* **15**, 621–628 (1998).
200. Sezer, A. D. & Akbuga, J. Release characteristics of chitosan treated alginate beads: I. Sustained release of a macromolecular drug from chitosan treated alginate beads. *J. Microencapsul.* **16**, 195–203 (1999).
201. Hari, P. R., Chandy, T. & Sharma, C. P. Chitosan/calcium–alginate beads for oral delivery of insulin. *J. Appl. Polym. Sci.* **59**, 1795–1801 (1996).
202. Polk, A., Amsden, B., De Yao, K., Peng, T. & Goosen, M. F. A. Controlled release of albumin from chitosan—alginate microcapsules. *J. Pharm. Sci.* **83**, 178–185 (1994).
203. Gåserød, O., Smidsrød, O. & Skjåk-Bræk, G. Microcapsules of alginate-chitosan—I: a quantitative study of the interaction between alginate and chitosan. *Biomaterials* **19**, 1815–1825 (1998).
204. Kim, H. J. *et al.* Polyelectrolyte complex composed of chitosan and sodium alginate for wound dressing application. *J. Biomater. Sci. Polym. Ed.* **10**, 543–56 (1999).
205. Mi, F. L., Shyu, S. S. & Peng, C. K. Characterization of ring-opening polymerization of genipin and pH-dependent cross-linking reactions between chitosan and genipin. *J. Polym. Sci. PART A-POLYMER Chem.* **43**, 1985–2000 (2005).
206. Berger, J. *et al.* Structure and interactions in covalently and ionically crosslinked chitosan hydrogels for biomedical applications. *Eur. J. Pharm. Biopharm.* **57**, 19–34 (2004).
207. Bhumkar, D. R. & Pokharkar, V. B. Studies on effect of pH on cross-linking of chitosan with sodium tripolyphosphate: A technical note. *AAPS PharmSciTech* **7**, E138–E143 (2006).
208. Ravi Kumar, M. N. . A review of chitin and chitosan applications. *React. Funct. Polym.* **46**, 1–27 (2000).
209. Aly, A. S. Self-dissolving chitosan, I - Preparation, characterization and evaluation for drug delivery system. *Angew. Makromol. CHEMIE* **259**, 13–18 (1998).
210. Yamada, K. *et al.* Chitosan based water-resistant adhesive. Analogy to mussel glue. *Biomacromolecules* **1**, 252–258 (2000).
211. Denkbaz, E. B., Seyyal, M. & Piskin, E. Implantable 5-fluorouracil loaded chitosan scaffolds prepared by wet spinning. *J. Memb. Sci.* **172**, 33–38 (2000).
212. Khalid, M. N., Ho, L., Agnely, F., Grossiord, J. L. & Couarraze, G. Swelling properties and

- mechanical characterization of a semi-interpenetrating chitosan/polyethylene oxide network - Comparison with a chitosan reference gel. *STP PHARMA Sci.* **9**, 359–364 (1999).
213. Patel, V. R. & Amiji, M. M. Preparation and characterization of freeze-dried chitosan-poly(ethylene oxide) hydrogels for site-specific antibiotic delivery in the stomach. *Pharm. Res.* **13**, 588–593 (1996).
 214. Monteiro, O. A. C. & Airoidi, C. Some studies of crosslinking chitosan-glutaraldehyde interaction in a homogeneous system. *Int. J. Biol. Macromol.* **26**, 119–128 (1999).
 215. Wang, L.-Y., Ma, G.-H. & Su, Z.-G. Preparation of uniform sized chitosan microspheres by membrane emulsification technique and application as a carrier of protein drug. *J. Control. Release* **106**, 62–75 (2005).
 216. Nwosu, C. J., Hurst, G. A. & Novakovic, K. Genipin Cross-Linked Chitosan-Polyvinylpyrrolidone Hydrogels: Influence of Composition and Postsynthesis Treatment on pH Responsive Behaviour. *Adv. Mater. Sci. Eng.* (2015). doi:10.1155/2015/621289
 217. Brooks, B. R. & Klammer, L. *Interaction of DNA with Bifunctional Aldehydes.* *European J. Biochem* **5**, (1968).
 218. Leuba, J. L. & Stossel, P. Chitosan and Other Polyamines: Antifungal Activity and Interaction with Biological Membranes. in *Chitin in Nature and Technology* 215–222 (Springer US, 1986). doi:10.1007/978-1-4613-2167-5_29
 219. Qin, C. *et al.* Water-solubility of chitosan and its antimicrobial activity. *Carbohydr. Polym.* **63**, 367–374 (2006).
 220. Bhattarai, N., Gunn, J. & Zhang, M. Chitosan-based hydrogels for controlled, localized drug delivery. *Adv. Drug Deliv. Rev.* **62**, 83–99 (2010).
 221. Gallaher, D. D. *et al.* A glucomannan and chitosan fiber supplement decreases plasma cholesterol and increases cholesterol excretion in overweight normocholesterolemic humans. *J. Am. Coll. Nutr.* **21**, 428–433 (2002).
 222. Lehr, C. M., Bouwstra, J. A., SCHACHT, E. H. & JUNGINGER, H. E. INVITRO EVALUATION OF MUCOADHESIVE PROPERTIES OF CHITOSAN AND SOME OTHER NATURAL POLYMERS. *Int. J. Pharm.* **78**, 43–48 (1992).
 223. Gherds, O., Jolliffe, I. G., Hampson, F. C., Dettmar, P. W. & Skjak-Brzk, G. international journal of pharmaceutics The enhancement of the bioadhesive properties of calcium alginate gel beads

- by coating with chitosan. *Int. J. Pharm.* **175**, 237–246 (1998).
224. Shimoda, J., Onishi, H. & Machida, Y. Bioadhesive characteristics of chitosan microspheres to the mucosa of rat small intestine. *Drug Dev. Ind. Pharm.* **27**, 567–576 (2001).
225. Illum, L., He, P. & Davis, S. S. In vitro evaluation of the mucoadhesive properties of chitosan microspheres. *Int. J. Pharm.* **166**, 75–88 (1998).
226. Fiebrig, I., Harding, S. E., Rowe, A. J., Hyman, S. C. & Davis, S. S. Transmission electron microscopy studies on pig gastric mucin and its interactions with chitosan. *Carbohydr. Polym.* **28**, 239–244 (1995).
227. Deacon, M. P. *et al.* Atomic force microscopy of gastric mucin and chitosan mucoadhesive systems. *Biochem. J.* **348**, 557–563 (2000).
228. Bernkop-Schnürch, A., Humenberger, C. & Valenta, C. Basic studies on bioadhesive delivery systems for peptide and protein drugs. *Int. J. Pharm.* **165**, 217–225 (1998).
229. Illum, L., Farraj, N. F., Davis, S. S. & Illum, Lisbeth; Farraj, Nidal F.; Davis, S. S. Chitosan as a Novel Nasal Delivery System for Peptide Drugs. *Pharm. Res.* **11**, 1186–1189 (1994).
230. Junginger, H. E. & Verhoef, J. C. Macromolecules as safe penetration enhancers for hydrophilic drugs - A fiction? *Pharm. Sci. Technol. Today* **1**, 370–376 (1998).
231. A.F. Kotze, H.L. Luessen, M. Thanou, J.C. Verhoef, A. G. de & Boer, H.E. Junginger, C.-M. L. Chitosan and chitosan derivatives as absorption enhancers for peptide drugs across mucosal epithelia. *Drugs Pharm. Sci.* **98**, 341–386 (1999).
232. Schipper, N. G. M. *et al.* Chitosans as absorption enhancers of poorly absorbable drugs. *Eur. J. Pharm. Sci.* **8**, 335–343 (1999).
233. Lehr, C. M. From sticky stuff to sweet receptors - achievements, limits and novel approaches to bioadhesion. in *European Journal of Drug Metabolism and Pharmacokinetics* **21**, 139–148 (1996).
234. Schnurch, A. B., Hornof, M. & Guggi, D. Thiolated chitosans, *Eur. J. Pharm Biopharm.* 9–17 (2004). doi:[https://doi.org/10.1016/S0939-6411\(03\)00147-4](https://doi.org/10.1016/S0939-6411(03)00147-4)
235. Cheng, G.-X. *et al.* Studies on dynamic behavior of water in crosslinked chitosan hydrogel. *J. Appl. Polym. Sci.* **67**, 983–988 (1998).
236. Chen, L., Tian, Z. & Du, Y. Synthesis and pH sensitivity of carboxymethyl chitosan-based

- polyampholyte hydrogels for protein carrier matrices. *Biomaterials* **25**, 3725–3732 (2004).
237. Cui, F. *et al.* Preparation, characterization, and oral delivery of insulin loaded carboxylated chitosan grafted poly (methyl methacrylate) nanoparticles. *Biomacromolecules* **10**, 1253–1258 (2009).
238. Chang, K. L. B. & Lin, J. Swelling behavior and the release of protein from chitosan-pectin composite particles. *Carbohydr. Polym.* **43**, 163–169 (2000).
239. Munjeri, O., Collett, J. H. & Fell, J. T. Amidated Pectin Hydrogel Beads for Colonic Drug Delivery- An in vitro Study. *Drug Deliv.* **4**, 207–211 (1997).
240. Tapia, C. *et al.* Comparative studies on polyelectrolyte complexes and mixtures of chitosan-alginate and chitosan-carrageenan as prolonged diltiazem clorhydrate release systems. *Eur. J. Pharm. Biopharm.* **57**, 65–75 (2004).
241. Tavel, M. & Domard, A. Collagen and its interactions with chitosan. *Biomaterials* **17**, 451–455 (1996).
242. Tonge, S. R. & Tighe, B. J. Responsive hydrophobically associating polymers: A review of structure and properties. *Advanced Drug Delivery Reviews* **53**, 109–122 (2001).
243. Philippova, O. E., Hourdet, D., Audebert, R. & Khokhlov, A. R. pH-responsive gels of hydrophobically modified poly(acrylic acid). *Macromolecules* **30**, 8278–8285 (1997).
244. Soutar, I. & Swanson, L. *Luminescence Studies of Polyelectrolyte Behavior in Solution. 3. Time-Resolved Fluorescence Anisotropy Measurements of the Conformational Behavior of Poly(methacrylic acid) in Dilute Aqueous Solutions*. *Macromolecules* **27**, (1994).
245. Serjeant, E. P. & Dempsey, B. *Ionisation constants of organic acids in aqueous solution.* **23**, (Pergamon, 1979).
246. Lee, M. J., Green, M. M., Mikeš, F. & Morawetz, H. NMR spectra of polyelectrolytes in poor solvents are consistent with the pearl necklace model of the chain molecules. *Macromolecules* **35**, 4216–4217 (2002).
247. Isihara, A. & Koyama, R. Theory of Dilute High-Polymer Solutions (the Pearl Necklace Model). *J. Chem. Phys.* **25**, 712–716 (1956).
248. Pecora, R. Spectral Distribution of Light Scattered from Flexible-Coil Macromolecules. *J. Chem. Phys.* **49**, 1032–1035 (1968).

249. Limbach, H. J. & Holm, C. Single-Chain Properties of Polyelectrolytes in Poor Solvent. *J. Phys. Chem. B* **107**, 8041–8055 (2003).
250. Ebdon, J. R. *et al.* Luminescence studies of hydrophobically modified, water-soluble polymers. I. Fluorescence anisotropy and spectroscopic investigations of the conformational behaviour of copolymers of acrylic acid and styrene or methyl methacrylate. *Can. J. Chem.* **73**, 1982–1994 (1995).
251. Katchalsky, A. & Michaeli, I. Polyelectrolyte gels in salt solutions. *J. Polym. Sci.* **15**, 69–86 (1955).
252. Leroux, J. C. *et al.* pH-sensitive nanoparticles: an effective means to improve the oral delivery of HIV-1 protease inhibitors in dogs. *Pharm. Res.* **13**, 485–7 (1996).
253. Caldorera-Moore, M., Vela Ramirez, J. E. & Peppas, N. A. Transport and delivery of interferon- α through epithelial tight junctions via pH-responsive poly(methacrylic acid-grafted-ethylene glycol) nanoparticles. *J. Drug Target.* **27**, 582–589 (2019).
254. Islam, M. S., Tan, J. P. K., Kwok, C. Y. & Tam, K. C. Drug release kinetics of pH-responsive microgels of different glass-transition temperatures. *J. Appl. Polym. Sci.* **136**, 47284 (2019).
255. Gehrke, S. H. & Lee, P. I. Hydrogels for drug delivery systems. *Drugs Pharm. Sci.* **41**, 333–392 (1990).
256. Gupta, P., Vermani, K. & Garg, S. *Hydrogels: From controlled release to pH-responsive drug delivery. Drug Discovery Today* **7**, 569–579 (Elsevier Current Trends, 2002).
257. Huang, J., Wan, S., Guo, M. & Yan, H. Preparation of narrow or mono-disperse crosslinked poly((meth)acrylic acid)/iron oxide magnetic microspheres. *J. Mater. Chem.* **16**, 4535 (2006).
258. Zhang, Y., Fang, Y., Wang, S. & Lin, S. Preparation of spherical nanostructured poly(methacrylic acid)/PbS composites by a microgel template method. *J. Colloid Interface Sci.* **272**, 321–325 (2004).
259. Jameela, S. R. & Jayakrishnan, A. *Glutaraldehyde cross-linked chitosan microspheres as a long acting biodegradable drug delivery vehicle: studies on the in tit..o release of mitoxantrone and in viva degradation of microspheres in rat muscle. Biomaterials* **16**, (1995).
260. Hurst, G. A. & Novakovic, K. A facile in situ morphological characterization of smart genipin-crosslinked chitosan–poly (vinyl pyrrolidone) hydrogels. *J. Mater. Res.* **28**, 2401–2408 (2013).
261. Odian, G. *Principles of Polymerization.* (John Wiley & Sons, Inc., 2004). doi:10.1002/047147875X

262. Pelton, R. H. & Chibante, P. Preparation of aqueous latices with N-isopropylacrylamide. *Colloids and Surfaces* **20**, 247–256 (1986).
263. Clarke, J. & Vincent, B. Stability of non-aqueous microgel dispersions in the presence of free polymer. *J. Chem. Soc. Faraday Trans. 1 Phys. Chem. Condens. Phases* **77**, 1831 (1981).
264. Lichti, G., Gilbert, R. G. & Napper, D. H. The mechanisms of latex particle formation and growth in the emulsion polymerization of styrene using the surfactant sodium dodecyl sulfate. *J. Polym. Sci. Polym. Chem. Ed.* **21**, 269–291 (1983).
265. Kobiasi, M. Al, Chua, B. Y., Tonkin, D., Jackson, D. C. & Mainwaring, D. E. Control of size dispersity of chitosan biopolymer microparticles and nanoparticles to influence vaccine trafficking and cell uptake. *J. Biomed. Mater. Res. Part A* **100A**, 1859–1867 (2012).
266. Chua, B. Y., Al Kobaisi, M., Zeng, W., Mainwaring, D. & Jackson, D. C. Chitosan Microparticles and Nanoparticles as Biocompatible Delivery Vehicles for Peptide and Protein-Based Immunocontraceptive Vaccines. *Mol. Pharm.* **9**, 81–90 (2012).
267. Zhou, J., Yao, H. & Ma, J. Recent advances in RAFT-mediated surfactant-free emulsion polymerization. *Polym. Chem.* **9**, 2532–2561 (2018).
268. Hoffman, A. S. Hydrogels for biomedical applications. *Adv. Drug Deliv. Rev.* **64**, 18–23 (2012).
269. Dai, S., Ravi, P. & Tam, K. C. pH-Responsive polymers: synthesis, properties and applications. *Soft Matter* **4**, 435–449 (2008).
270. Hu, J., Zhang, G., Ge, Z. & Liu, S. Stimuli-responsive tertiary amine methacrylate-based block copolymers: Synthesis, supramolecular self-assembly and functional applications. *Prog. Polym. Sci.* **39**, 1096–1143 (2014).
271. Felber, A. E., Dufresne, M.-H. & Leroux, J.-C. pH-sensitive vesicles, polymeric micelles, and nanospheres prepared with polycarboxylates. *Adv. Drug Deliv. Rev.* **64**, 979–992 (2012).
272. Kedar, U., Phutane, P., Shidhaye, S. & Kadam, V. Advances in polymeric micelles for drug delivery and tumor targeting. *NANOMEDICINE-NANOTECHNOLOGY Biol. Med.* **6**, 714–729 (2010).
273. Koetting, M. C., Peters, J. T., Steichen, S. D. & Peppas, N. A. Stimulus-responsive hydrogels: Theory, modern advances, and applications. *Mater. Sci. Eng. R-REPORTS* **93**, 1–49 (2015).
274. Mayer, A. B. R. Colloidal metal nanoparticles dispersed in amphiphilic polymers. *Polym. Adv. Technol.* **12**, 96–106 (2001).

275. Liu, H. *et al.* Dual-Responsive Surfaces Modified with Phenylboronic Acid-Containing Polymer Brush To Reversibly Capture and Release Cancer Cells. *J. Am. Chem. Soc.* **135**, 7603–7609 (2013).
276. Min, K. H. *et al.* Tumoral acidic pH-responsive MPEG-poly(beta-amino ester) polymeric micelles for cancer targeting therapy. *J. Control. RELEASE* **144**, 259–266 (2010).
277. Cui, J., Yan, Y., Wang, Y. & Caruso, F. Templated Assembly of pH-Labile Polymer-Drug Particles for Intracellular Drug Delivery. *Adv. Funct. Mater.* **22**, 4718–4723 (2012).
278. Walker, G. F. *et al.* Toward synthetic viruses: Endosomal pH-triggered deshielding of targeted polyplexes greatly enhances gene transfer in vitro and in vivo. *Mol. Ther.* **11**, 418–425 (2005).
279. Gu, Y. *et al.* Acetal-Linked Paclitaxel Prodrug Micellar Nanoparticles as a Versatile and Potent Platform for Cancer Therapy. *Biomacromolecules* **14**, 2772–2780 (2013).
280. Clochard, M. C. D., Rankin, S. & Brocchini, S. Synthesis of soluble polymers for medicine that degrade by intramolecular acid catalysis. *Macromol. Rapid Commun.* **21**, 853–859 (2000).
281. Ding, C., Gu, J., Qu, X. & Yang, Z. Preparation of Multifunctional Drug Carrier for Tumor-Specific Uptake and Enhanced Intracellular Delivery through the Conjugation of Weak Acid Labile Linker. *Bioconjug. Chem.* **20**, 1163–1170 (2009).
282. Ke, X. *et al.* pH-sensitive polycarbonate micelles for enhanced intracellular release of anticancer drugs: a strategy to circumvent multidrug resistance. *Polym. Chem.* **5**, 2621–2628 (2014).
283. Kabanov, A. V & Vinogradov, S. V. Nanogels as Pharmaceutical Carriers: Finite Networks of Infinite Capabilities. *Angew. CHEMIE-INTERNATIONAL Ed.* **48**, 5418–5429 (2009).
284. Vinogradov, S., Batrakova, E. & Kabanov, A. Poly(ethylene glycol)–polyethyleneimine NanoGel™ particles: novel drug delivery systems for antisense oligonucleotides. *Colloids Surfaces B Biointerfaces* **16**, 291–304 (1999).
285. Oh, N. M. *et al.* A self-organized 3-diethylaminopropyl-bearing glycol chitosan nanogel for tumor acidic pH targeting: In vitro evaluation. *COLLOIDS AND SURFACES B-BIOINTERFACES* **78**, 120–126 (2010).
286. Wu, W. *et al.* Multi-functional core-shell hybrid nanogels for pH-dependent magnetic manipulation, fluorescent pH-sensing, and drug delivery. *Biomaterials* **32**, 9876–9887 (2011).
287. Bergmeyer, H. U., Gawehn, K. & Grassl, M. *Methods of Enzymatic Analysis. Methods of*

- enzymatic analysis* (Academic Press, 1974).
288. Jakoby, W. B. & Wilchek, M. *Enzyme purification and related techniques*,. (Academic Press, 1971).
 289. Colowick, S. P. (Sidney P., San Pietro, A. G. & Kaplan, N. O. (Nathan O. *Photosynthesis and nitrogen fixation. Volume 24, Part B.* (Academic Press).
 290. Good, N. E. *et al.* Hydrogen Ion Buffers for Biological Research*. *Biochemistry* **5**, 467–477 (1966).
 291. Hu, G., Pojman, J. A., Scott, S. K., Wrobel, M. M. & Taylor, A. F. Base-Catalyzed Feedback in the Urea-Urease Reaction. doi:10.1021/jp106532d
 292. Brooke, D., Movahed, N. & Bothner, B. Universal buffers for use in biochemistry and biophysical experiments. *AIMS Biophys.* **2**, 336–342 (2015).
 293. McIlvaine, T. C. A buffer solution for colorimetric comparison. *J. Biol. Chem.* **49**, 183–186 (1921).
 294. Michaelis, L. Diethylbarbiturate buffer. *J. Biol. Chem.* **87**, 33–35 (1930).
 295. Britton, H. T. S. & Robinson, R. A. CXCVIII.—Universal buffer solutions and the dissociation constant of veronal. *J. Chem. Soc.* **0**, 1456–1462 (1931).
 296. Tabatabai, M. A. Soil Enzymes. in *Encyclopedia of Agrochemicals* (John Wiley & Sons, Inc., 2003). doi:10.1002/047126363X.agr354
 297. Gomori, G. [16] Preparation of buffers for use in enzyme studies. (1955).
 298. Walser, M. Ion association. VI. Interactions between calcium, magnesium, inorganic phosphate, citrate and protein in normal human plasma. *J. Clin. Invest.* **40**, 723–730 (1961).
 299. Monthony, J. F., Wallace, E. G. & Allen, D. M. A non-barbital buffer for immunoelectrophoresis and zone electrophoresis in agarose gels. *Clin. Chem.* **24**, 1825–1827 (1978).
 300. Hu, Y., Su, L. & Snow, E. T. Arsenic toxicity is enzyme specific and its affects on ligation are not caused by the direct inhibition of DNA repair enzymes. *Mutat. Res. Repair* **408**, 203–218 (1998).
 301. van den Berg, R., Peters, J. A. & van Bakkum, H. The structure and (local) stability constants of borate esters of mono- and di-saccharides as studied by ¹¹B and ¹³C NMR spectroscopy. *Carbohydr. Res.* **253**, 1–12 (1994).
 302. Ment, W. M. & Naviasky, H. S. Effect of maleic acid in compendial UV absorption assays for

- antihistamine maleate salts. *J. Pharm. Sci.* **63**, 1604–1609 (1974).
303. Osorio-Román, I. O., Ortega-Vásquez, V., Vargas C, V. & Aroca, R. F. Surface-enhanced spectra on D-gluconic acid coated silver nanoparticles. *Appl. Spectrosc.* **65**, 838–43 (2011).
304. Rungrodnimitchai, S., Phokhanusai, W. & Sungkhaho, N. *Preparation of Silica Gel from Rice Husk Ash Using Microwave Heating. Journal of Metals, Materials and Minerals* **19**, (2009).
305. Bowers, G. N., Kelley, M.-L. & McComb, R. B. Continuous Spectrophotometric Measurement of Serum Alkaline Phosphatase Activity. *Clin. Chem.* **13**, (1967).
306. Bollag, D. M., Rozycki, M. D. & Edelstein, S. J. *Protein methods.* (Wiley-Liss, 1996).
307. Marcotte, N. & Brouwer, A. M. Carboxy SNARF-4F as a Fluorescent pH Probe for Ensemble and Fluorescence Correlation Spectroscopies. (2005). doi:10.1021/JP0510138
308. Dubbin, P. N., Cody, S. H. & Williams, D. A. Intracellular pH mapping with SNARF-1 and confocal microscopy. II: pH gradients within single cultured cells. *Micron* **24**, 581–586 (1993).
309. Murtazina, R. *et al.* Tissue-specific regulation of sodium/proton exchanger isoform 3 activity in Na⁺/H⁺ exchanger regulatory factor 1 (NHERF1) null mice cAMP inhibition is differentially dependent on NHERF1 and exchange protein directly activated by cAMP in ileum versus proxi. *J. Biol. Chem.* **282**, 25141–25151 (2007).
310. Cope, S. J., Hibberd, S., Whetstone, J., MacRae, R. J. & Melia, C. D. Measurement and mapping of pH in hydrating pharmaceutical pellets using confocal laser scanning microscopy. *Pharm. Res.* **19**, 1554–1563 (2002).
311. Wieder, E. D., Hang, H. & Fox, M. H. Measurement of intracellular pH using flow cytometry with carboxy-SNARF-1. *Cytom. J. Int. Soc. Anal. Cytol.* **14**, 916–921 (1993).
312. Lyko, B., Hammershaimb, E. A., Nguitragool, W., Wellems, T. E. & Desai, S. A. A high-throughput method to detect Plasmodium falciparum clones in limiting dilution microplates. *Malar. J.* **11**, 124 (2012).
313. Whitaker, J. E., Haugland, R. P. & Prendergastt, F. G. *Spectral and Photophysical Studies of Benzo[c]xanthene Dyes: Dual Emission pH Sensors.* (1991).
314. Hunter, R. C. & Beveridge, T. J. Application of a pH-Sensitive Fluoroprobe (C-SNARF-4) for pH Microenvironment Analysis in Pseudomonas aeruginosa Biofilms. *Appl. Environ. Microbiol.* **71**, 2501–2510 (2005).

315. Gryniewicz, G., Poenie, M. & Tsien, R. Y. A new generation of Ca²⁺ indicators with greatly improved fluorescence properties. *J. Biol. Chem.* **260**, 3440–50 (1985).
316. Bottenus, D., Oh, Y.-J., Han, S. M. & Ivory, C. F. Experimentally and theoretically observed native pH shifts in a nanochannel array. *Lab Chip* **9**, 219–31 (2009).
317. Brasselet, S. & Moerner, W. E. Fluorescence Behavior of Single-Molecule pH-Sensors. *Single Mol.* **1**, 17–23 (2000).
318. Fu, Y., Collinson, M. M. & Higgins, D. A. Single-molecule spectroscopy studies of microenvironmental acidity in silicate thin films. *J. Am. Chem. Soc.* **126**, 13838–44 (2004).
319. Raimondo, J. V., Irkle, A., Wefelmeyer, W., Newey, S. E. & Akerman, C. J. Genetically encoded proton sensors reveal activity-dependent pH changes in neurons. *Front. Mol. Neurosci.* **5**, 68 (2012).
320. Arosio, D. *et al.* Simultaneous intracellular chloride and pH measurements using a GFP-based sensor. *Nat. Methods* **7**, 516–518 (2010).
321. MSDS - 248614. Available at: <https://www.sigmaaldrich.com/MSDS/MSDS/DisplayMSDSPage.do?country=GB&language=en&productNumber=248614&brand=SIGALD&PageToGoToURL=https%3A%2F%2Fwww.sigmaaldrich.com%2Fcatalog%2Fproduct%2Fsigald%2F248614%3Flang%3Den>. (Accessed: 4th July 2019)
322. Foss, A. C., Goto, T., Morishita, M. & Peppas, N. A. Development of acrylic-based copolymers for oral insulin delivery. *Eur. J. Pharm. Biopharm.* **57**, 163–169 (2004).
323. Wang, F. *et al.* Development and analytical application of a glucose biosensor based on glucose oxidase/O-(2-hydroxyl)propyl-3-trimethylammonium chitosan chloride nanoparticle-immobilized onion inner epidermis. *Biosens. Bioelectron.* **25**, 2238–2243 (2010).
324. Manzano, M. F. G. & Igarzabal, C. I. A. Immobilization of lipase from *Candida rugosa* on synthesized hydrogel for hydrolysis reaction. *J. Mol. Catal. B Enzym.* **72**, 28–35 (2011).
325. Martín, M. T., Plou, F. J., Alcalde, M. & Ballesteros, A. Immobilization on Eupergit C of cyclodextrin glucosyltransferase (CGTase) and properties of the immobilized biocatalyst. *J. Mol. Catal. B Enzym.* **21**, 299–308 (2003).
326. Wesley, D. J., Smith, R. M., Zimmerman, W. B. & Howse, J. R. Influence of Surface Wettability on Microbubble Formation. *Langmuir* **32**, 1269–1278 (2016).

327. Gregg, S. J. Hysteresis of the Contact Angle. *J. Chem. Phys.* **16**, 549–550 (1948).
328. Prüsse, U. *et al.* Comparison of different technologies for alginate beads production. *Chem. Pap.* **62**, 364–374 (2008).
329. Chan, E.-S., Lee, B.-B., Ravindra, P. & Poncelet, D. Prediction models for shape and size of calcium alginate macrobeads produced through extrusion–dripping method. *J. Colloid Interface Sci.* **338**, 63–72 (2009).
330. Lübbe, A. S., Alexiou, C. & Bergemann, C. Clinical Applications of Magnetic Drug Targeting. *J. Surg. Res.* **95**, 200–206 (2001).
331. Shinkai, M. Functional magnetic particles for medical application. *J. Biosci. Bioeng.* **94**, 606–613 (2002).
332. Longsworth, L. Diffusion in liquids and the Stokes–Einstein relation. *Electrochemistry in biology and medicine* 225–247 (1955).
333. Delgado, J. M. P. Q. Molecular Diffusion Coefficients of Organic Compounds in Water at Different Temperatures. *J. Phase Equilibria Diffus.* **28**, 427–432 (2007).
334. Telis, V. R. N., Telis-Romero, J., Mazzotti, H. B. & Gabas, A. L. International Journal of Food Properties Viscosity of Aqueous Carbohydrate Solutions at Different Temperatures and Concentrations. *Int. J. Food Prop.* **10**, 185–195 (2007).
335. Lynn, D. M., Amiji, M. M. & Langer, R. pH-Responsive Polymer Microspheres: Rapid Release of Encapsulated Material within the Range of Intracellular pH. *Angew. Chemie Int. Ed.* **40**, 1707–1710 (2001).
336. Louage, B. *et al.* Degradable Ketel-Based Block Copolymer Nanoparticles for Anticancer Drug Delivery: A Systematic Evaluation. *Biomacromolecules* **16**, 336–350 (2015).
337. Stenzel, M. H. Bioconjugation using thiols: old chemistry rediscovered to connect polymers with nature’s building blocks. (2012).
338. Migneault, I., Dartiguenave, C., Bertrand, M. J. & Waldron, K. C. Glutaraldehyde: behavior in aqueous solution, reaction with proteins, and application to enzyme crosslinking. *Biotechniques* **37**, 790–802 (2004).
339. Sung, H., Chang, W., Ma, C. & Lee, M. Crosslinking of biological tissues using genipin and/or carbodiimide. *J. Biomed. Mater. Res. Part A An Off. J. Soc. Biomater. Japanese Soc. Biomater. Aust. Soc. Biomater. Korean Soc. Biomater.* **64**, 427–438 (2003).

340. Husar, G. M., Anziano, D. J., Leuck, M. & Sebesta, D. P. Covalent modification and surface immobilization of nucleic acids via the Diels-Alder bioconjugation method. *Nucleosides, Nucleotides and Nucleic Acids* **20**, 559–566 (2001).
341. Marek, S. R. & Peppas, N. A. Insulin release dynamics from poly (diethylaminoethyl methacrylate) hydrogel systems. *AIChE J.* **59**, 3578–3585 (2013).
342. Cao, L. Immobilised enzymes: science or art? *Curr. Opin. Chem. Biol.* **9**, 217–226 (2005).
343. Dorothy T. Nguyen, Mark Smit, Bruce Dunn, and & Zink*, J. I. Stabilization of Creatine Kinase Encapsulated in Silicate Sol–Gel Materials and Unusual Temperature Effects on Its Activity. (2002). doi:10.1021/CM020398T
344. Aoun, S. & Baboulène, M. Regioselective bromohydroxylation of alkenes catalyzed by chloroperoxidase: Advantages of the immobilization of enzyme on talc. *J. Mol. Catal. B Enzym.* **4**, 101–109 (1998).
345. Palomo, J. M. *et al.* Modulation of the enantioselectivity of lipases via controlled immobilization and medium engineering: hydrolytic resolution of mandelic acid esters. *Enzyme Microb. Technol.* **31**, 775–783 (2002).

9. Appendices

9.1 Appendix: Aqueous Acid-Base Equilibria and Titrations

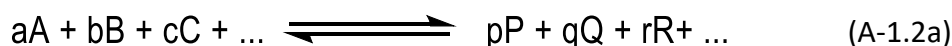
Although acids and bases have been known of for thousands of years they have only truly been understood since the 19th century. It was the work of Davy¹ in 1811 that showed hydrochloric acid did not contain oxygen, and it was the hydrogen rather than oxygen that imparted acidity. Over the following century the modern understanding of acidity continued to develop with von Liebig in 1838² introducing the concept of mobile, replaceable hydrogen. But it was Arrhenius who cemented the current concept of acidity as electrolytic dissociation, replacing von Liebig's hydrogen with a proton (H^+), which can dissociate from an acid and OH^- which can dissociate from a base. Such a definition also applies to H_2O which can dissociate to H_3O^+ and OH^- .

There are many ways to define acids and bases but the most appropriate for the body of work is that of Brønsted-Lowry who define acids as H^+ donors and bases as H^+ acceptors.³ Thereby, showing acids and bases to be complementary in nature since a proton-less acid is a base and a protonated base is an acid. As such acids and bases can be considered as conjugate acid-base pairs. This definition allows acids and bases to be independent of their solvent, therefore applying to solventless reactions like that of HCl and NH_3 vapours.

The concept of pH arises from the proton concentration in aqueous solutions varying from 10 M down to 10^{-17} M. Sorensen defined pH as the negative log of proton concentration (eq. (A-1.1)).² The logarithmic function allows this wide range of concentration to be encompassed and being a negative log makes the pH predominantly a positive value. Since it is only strong acids like HCl at high concentrations which have aqueous proton concentrations greater than 1 M. It is not just the convenience of the log scale that has made pH ubiquitous but also its proportional relationship with the electrode potential of a glass electrode, which remains the most facile and robust method of pH measurement for bulk solutions.

$$pH = -\log[H^+] \quad (A-1.1)$$

The mass action law underpins all chemical equilibria. It was first introduced by Goldberg and Waage before being refined by Horstmann and later Van't Hoff. The mass action law states that the rate of a chemical reaction is proportional to the product of the concentrations/activities of the reactants. For an equilibrium of chemical species:



$$K = \frac{[P]^p [Q]^q [R]^r}{[A]^a [B]^b [C]^c} \quad (\text{A-1.2b})$$

Where a, b, c, ... and p, q, r, ... are the associated stoichiometric coefficients. When the concentration of each species are denoted in the form of [N] the ratio of the product of the left hand side ($[A]^a[B]^b[C]^c$) and product of the right hand side ($[P]^p[Q]^q[R]^r$) at equilibrium is constant. Therefore, the equilibrium constant (K) for such a system is defined by equation (A-1.2b). Acid-base equilibria utilise dissociation constants. For a monoprotic acids (HA) such as hydrochloric acid or acetic acid exist in an equilibrium between its protonated and deprotonated states.



The point at which the equilibrium lies is dictated by the acid dissociation constant (K_a), where:

$$K_a = \frac{[\text{H}^+][\text{A}^-]}{[\text{HA}]} \quad (\text{A-1.4})$$

The acid dissociation constants for di- and triprotic acids like oxalic and citric acids respectively can be determined by treating the dissociation of the protons in a stepwise manner. For triprotics (H_3A):



Where the dissociation constants respectively are

$$K_{a1} = \frac{[\text{H}^+][\text{H}_2\text{A}^-]}{[\text{H}_3\text{A}]} \quad (\text{A-1.12})$$

$$K_{a2} = \frac{[H^+][HA^{2-}]}{[H_2A^-]} \quad (A-1.13)$$

$$K_{a3} = \frac{[H^+][A^{3-}]}{[HA^{2-}]} \quad (A-1.14)$$

9.1.1 Concentration fractions

When weak acids like gluconic and acetic acid are in solution only a fraction of the acid dissociates, as a result a solution of a weak monoprotic acid contains HA, A⁻, H⁺ and OH⁻. The hydroxide ions and a portion of the protons come from the aqueous solvent. For a solution of known volume and mass of weak acid the total analytical concentration (C) is the sum of all form the acid can take, which can be expressed as:

$$C = [HA] + [A^-] \quad (A-1.15)$$

The concentration fraction (α) of the protonated and deprotonated species can be denoted as:

$$\alpha_{HA} = \frac{[HA]}{C} \quad (A-1.16)$$

$$\alpha_{A^-} = \frac{[A^-]}{C} \quad (A-1.17)$$

Therefore,

$$\alpha_{HA} + \alpha_{A^-} = 1 \quad (A-1.18)$$

The subscript of HA and A⁻ are often replaced with 1 and 0 respectively where the integer indicate the number of dissociable protons. Combining the equation for total analytical concentration (eq. (A-1.15)) with the concentration fraction equation (eq. (A-1.16)) gives:

$$\alpha_1 = \frac{[HA]}{C} \quad (A-1.19)$$

$$\alpha_1 = \frac{[HA]}{[HA] + [A^-]} \quad (A-1.20)$$

From the acid dissociation constant (eq. (A-1.4)) [HA] can be substituted with $[H^+] \frac{[A^-]}{K_a}$

$$\alpha_1 = \frac{[H^+] \frac{[A^-]}{K_a}}{[H^+] \frac{[A^-]}{K_a} + [A^-]} \quad (\text{A-1.21})$$

Finally, the equation can be simplified with the cancelling of $[A^-]$

$$\alpha_1 = \frac{\left(\frac{[H^+]}{K_a}\right)}{\left(\frac{[H^+]}{K_a}\right) + 1} \quad (\text{A-1.22})$$

$$\alpha_1 = \frac{[H^+]}{[H^+] + K_a} \quad (\text{A-1.23})$$

Likewise, the concentration fraction of the deprotonated acid can be written as:

$$\begin{aligned} \alpha_0 &= \frac{[A^-]}{C} = \frac{[A^-]}{[HA] + [A^-]} = \frac{[A^-]}{[H^+] \frac{[A^-]}{K_a} + [A^-]} = \frac{1}{\frac{[H^+]}{K_a} + 1} \\ &= \frac{K_a}{[H^+] + K_a} \end{aligned} \quad (\text{A-1.24})$$

Concentration fractions are essential since they are explicit functions of $[H^+]$ and the acid dissociation constant(s) (K_a), whilst remaining independent of total analyte concentration. The concentration fractions of diprotic and triprotic acids can also be expressed in a similar manner. For triprotic acids:

$$\alpha_3 = \frac{[H^+]^3}{[H^+]^3 + [H^+]^2 K_{a1} + [H^+] K_{a1} K_{a2} + K_{a1} K_{a2} K_{a3}} \quad (\text{A-1.28})$$

$$\alpha_2 = \frac{[H^+]^2 K_{a1}}{[H^+]^3 + [H^+]^2 K_{a1} + [H^+] K_{a1} K_{a2} + K_{a1} K_{a2} K_{a3}} \quad (\text{A-1.29})$$

$$\alpha_1 = \frac{[H^+] K_{a1} K_{a2}}{[H^+]^3 + [H^+]^2 K_{a1} + [H^+] K_{a1} K_{a2} + K_{a1} K_{a2} K_{a3}} \quad (\text{A-1.30})$$

$$\alpha_0 = \frac{K_{a1} K_{a2} K_{a3}}{[H^+]^3 + [H^+]^2 K_{a1} + [H^+] K_{a1} K_{a2} + K_{a1} K_{a2} K_{a3}} \quad (\text{A-1.31})$$

Where $K_{a1} < K_{a2} < K_{a3}$

As with $[H^+]$ more usefully observed in the logarithmic form, concentration (C) observed in a logarithmic form ($\log(C)$) is also advantageous. It not only enables the concentration of all species to be viewed over a wide range of values but also gives rise to a plot formed of mostly linear segments with integer slopes.

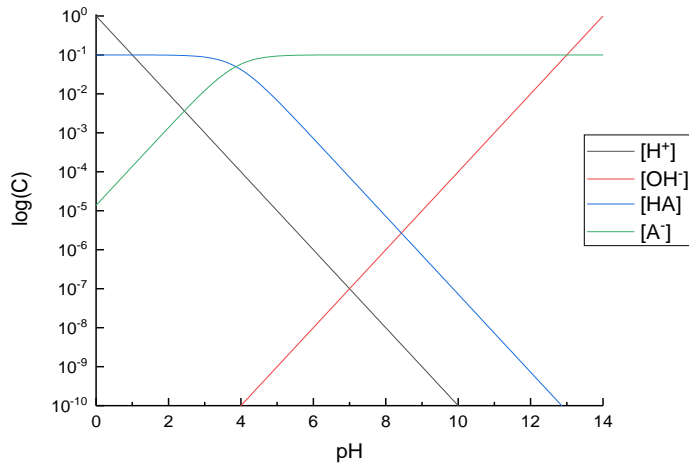


Figure 9-1 logarithmic concentration diagram as a function of pH for gluconic acid (0.1 molar) pK_a 3.86. ^{4,5}

For example the logarithmic concentration diagram of a monoprotic acid (such as gluconic acid at equilibrium) as a function of pH (see Figure 9-1) has 2 straight lines corresponding to $[H^+]$ and $[OH^-]$ whose slopes are -1 and 1 respectively assuming the self-ionisation of water (k_w) is 10^{-14} . The protonated form of gluconic acid (HA) and deprotonated form (A^-) share an asymptote where the pK_a is equal to the pH and $\log(c)$ is equal to the log of the total analytical concentration ($\log(C)$). The protonated form has two regions that are linear the first is when the pH is much less than the pK_a , where,

$$[HA] = C\alpha_1 = \frac{C[H^+]}{[H^+] + K_a} \quad (A-1.32)$$

As such $\log(c) = \log(C)$. The other linear portion occurs when the pH is much greater than the pK_a . When

$$[HA] = C\alpha_1 = \frac{C[H^+]}{K_a} \quad (A-1.33)$$

Which results in a slope of -1, since;

$$\log c = \log[H^+] + \log C - \log K_a = -pH + \log C - \log K_a \quad (A-1.34)$$

The deprotonated form is analogous to HA, when pH is much less than the pK_a ;

$$[A^-] = C\alpha_0 = \frac{CK_a}{[H^+] + K_a} \approx \frac{CK_a}{[H^+]} \quad (A-1.35)$$

When pH is much greater than the pK_a

$$[A^-] = C\alpha_0 = \frac{C[H^+]}{[H^+] + K_a} \approx C \quad (\text{A-1.36})$$

[HA] and [A⁻] intersect when the pH is equal to the pK_a

$$[A^-] = C\alpha_0 = \frac{C[H^+]}{[H^+] + K_a} = \frac{C}{2} \quad (\text{A-1.37})$$

$$[HA] = C\alpha_1 = \frac{C[H^+]}{[H^+] + K_a} = \frac{C}{2} \quad (\text{A-1.38})$$

Therefore;

$$\log c = \log C - \log 2 \approx \log C - 0.30 \quad (\text{A-1.39})$$

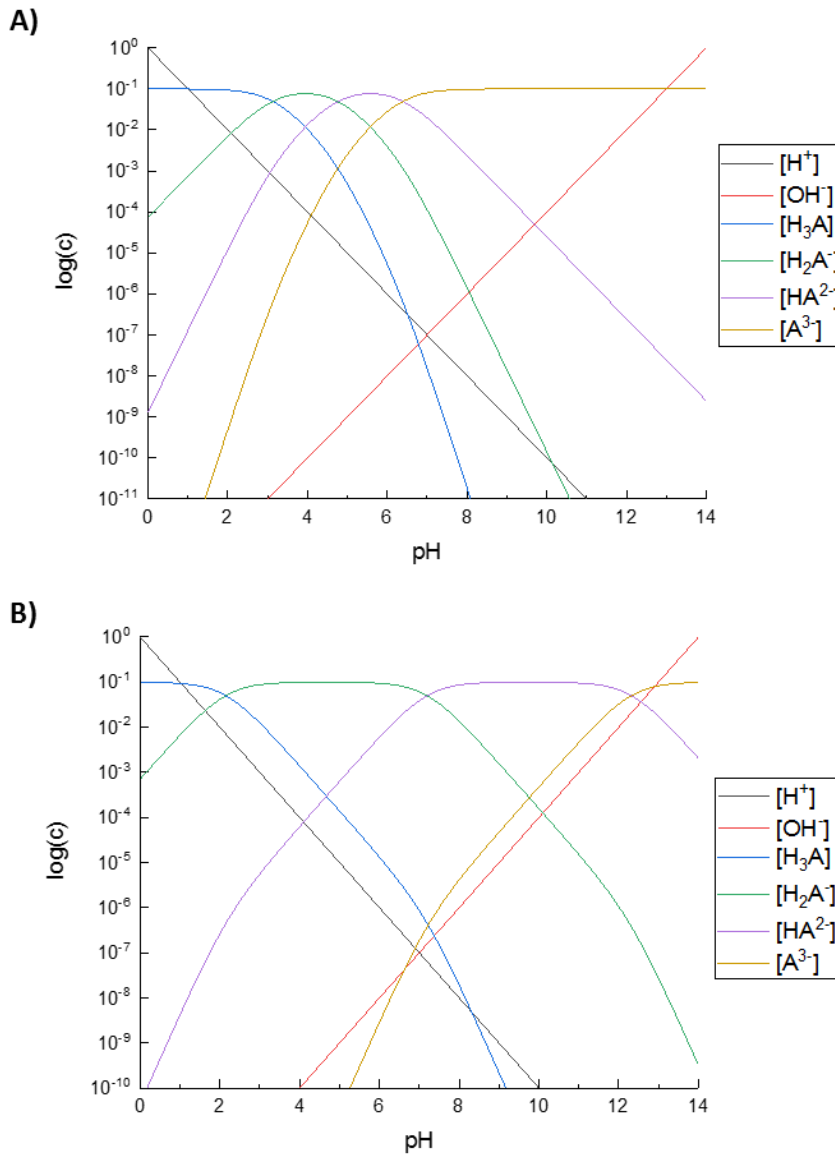


Figure 9-2. Logarithmic concentration diagrams of A) citric acid and B) phosphoric acid species. both are 0.1 molar

For triprotic acids like citric acid and phosphoric acid (Figure 9-2 A) and B) respectively) the logarithmic concentration diagram only has linear portion when the pH is either much less than pK_{a1} or much greater than pK_{a3} . Linear portions can also be observed in if the intermediate pK_a 's are sufficiently far apart as with phosphoric acid.

9.1.2 Titrations

Titrations are commonly used in both industry and research as they quantify the amount of a specific substance within a sample by chemically reacting it with a known amount of a suitable reagent. This results in an observable equivalence point i.e. a point at which the amount of substance is equal/proportional to the known amount of reagent. The concentration of the substance (s) can be expressed mathematically as

$$C_s = \frac{sC_t V_t}{V_s} \quad (\text{A-1.40})$$

Where C is the concentration and V is the volume, subscripts s and t indicate titrant and substance respectively. For the titration of an acid (a) with a base (b) or vice versa the subscript of s and t is often replaced with a or b. The progression curve of the titration of any acid by any base can be described by

$$\frac{V_b}{V_a} = \frac{F_a C_a - \Delta}{F_b C_b + \Delta} \quad (\text{A-1.41})$$

Where;

$$\Delta = [H^+] - [OH^-] = [H^+] - \frac{K_w}{[H^+]} \quad (\text{A-1.42})$$

The acid dissociation function (F_a) is the sum of all dissociated protons from the acid. As such for a strong monoprotic acid (hydrochloric acid) $F_a = 1$ since the acid fully dissociates at any pH. For a weak monoprotic acid (acetic acid):

$$F_a = \alpha_0 \quad (\text{A-1.43})$$

For a triprotic acid (phosphoric acid)

$$F_a = \alpha_2 + 2\alpha_1 + 3\alpha_0 \quad (\text{A-1.45})$$

Similarly, the base dissociation function is the sum of all partially or fully protonated forms of the base. Therefore, a strong monoprotic base's (sodium hydroxide) $F_b = 1$ and a weak base (sodium acetate) is:

$$F_b = \alpha_1 \quad (\text{A-1.46})$$

For the conjugate base to a triprotic acid (trisodium sodium)

$$F_b = \alpha_1 + 2\alpha_2 + 3\alpha_3 \quad (\text{A-1.47})$$

The progression curve describing the titration of an acid by a base (equation (A-1.41)) can be extended to the titration of any mixture of i acids with as mixture of j bases:

$$\frac{V_b}{V_a} = \frac{\sum_i F_{ai} C_{ai} - \Delta}{\sum_j F_{bj} C_{bj} + \Delta} \quad (\text{A-1.48})$$

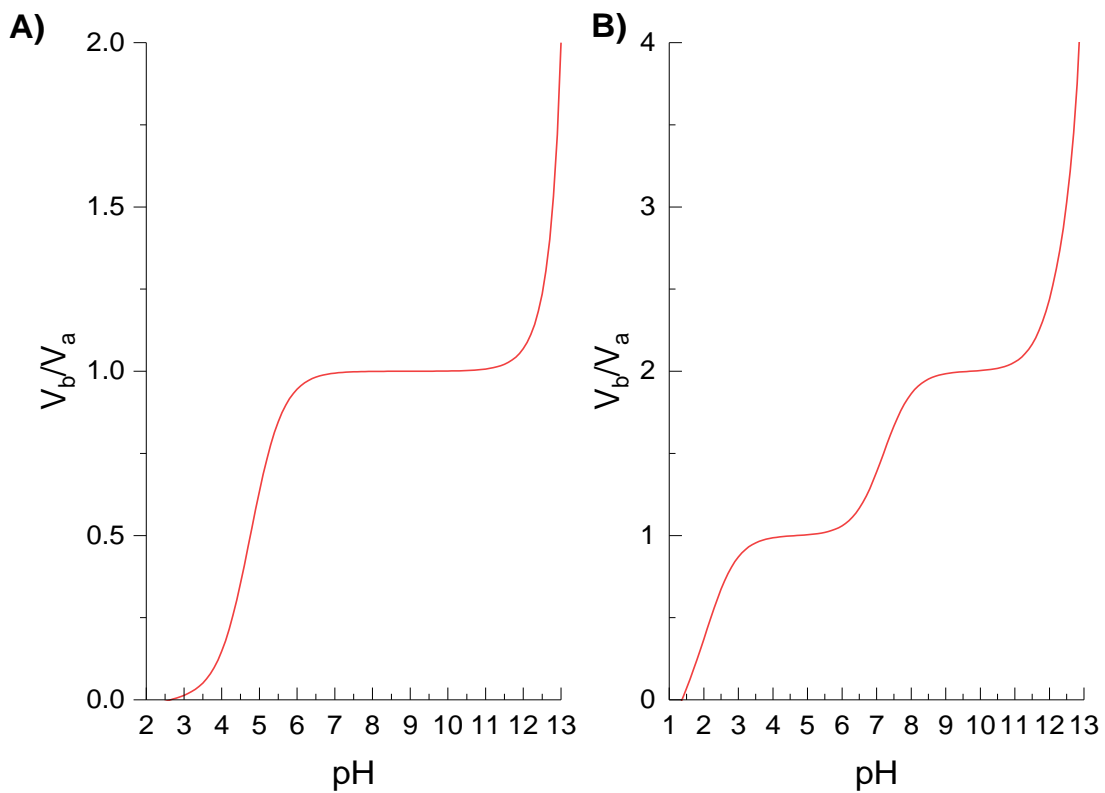


Figure 9-3 Progression curves generated from equation (A-1.48) for the titration of 0.3 M acid (A) acetic acid (pK_a 4.76)^{4,5}; B) phosphoric acid (pK_a s 2.15, 7.20 and 12.32)^{4,5} with 0.3 M NaOH (pK_a 13.8).⁶

Examples of such curves generated from this equation are shown in Figure 9-3. The progression of a titration of j bases by i acids is simply the inverse:

$$\frac{V_a}{V_b} = \frac{\sum_j F_{bj} C_{bj} + \Delta}{\sum_i F_{ai} C_{ai} - \Delta} \quad (\text{A-1.49})$$

9.1.2.1 Titration Error

In potentiometric titrations errors can occur via numerous aspects for example improper cell design, i.e. the placement of the stirrer, burette tip and sensing electrode. Errors can also arise from lags in the system and noise. Moreover, poorly calibrated equipment or systems can cause an overall offset due to drift, this can lead to significant errors. Potentiometric titration methods are often used to calculate proton concentration. Which is obtained from the pH measurement. Since pH and $[H^+]$ have a logarithmic relationship a small error in pH can produce a large error in $[H^+]$. It's important to note that titration errors can be minimised by using the appropriate experimental design, being extra vigilant and ensuring repeated precise calibration is performed. Such a calibration requires buffer solutions are of known pH accurate to two decimal places. Furthermore, the calibration should be carried out with three or more buffers, in order to obtain an accurate offset and gradient.

9.1.3 Buffers

Titration focus on the steep change in pH near the equivalence point. Whereas, buffers deal with the specific point where the pH change is small on the addition of a strong acid/base. In chemical systems especially those in living cells, maintaining the pH within narrow bounds is essential. Furthermore, all enzymes exhibit pH dependence. A shift in pH taking an enzyme outside of its normal pH range can dramatically decrease an enzymes activity, sometimes irreversibly (see section 1.7.4 Figure 1-11).

Buffer regions of a titration curve are those which exhibit only a small shift in pH as an acid or base is added. These regions often occur around the buffers dissociation constant ($pK_a \pm 1$). This buffer action is utilised by living organisms to stabilise pH. Furthermore, such pH stabilisation is a passive process.

9.1.4 Buffer Strength

Buffer action can be defined in terms of a titration curve. However, this means the property is defined and dependent upon 2 solutions, the sample and the titrant. A more useful definition is that it's dependent on the properties of a given solution, assuming the titrant is of infinite concentration and a strong acid/base. Such a definition was used by Van Slyke (1922) to define the buffer value (β) as:

$$\begin{aligned}\beta &= C_b \left(\frac{d(V_b/V_a)}{d \text{pH}} \right)_{C_b \rightarrow \infty} = -\ln(10) \times C_b \left[\frac{d(V_b/V_a)}{d(\ln[H^+])} \right]_{C_b \rightarrow \infty} \\ &= -\ln(10) \times C_b [H^+] \left[\frac{d(V_b/V_a)}{d[H^+]} \right]_{C_b \rightarrow \infty}\end{aligned}\tag{A-1.50}$$

Where the factor $-\ln(10) \approx 2.3$ is due to the conversion from $pH = -\log[H^+]$ to $\ln[H^+]$. Buffer strength (B ; also known as buffer capacity) simplifies the buffer equation to

$$B = \frac{\beta}{\ln(10)} = -C_b[H^+] \left[\frac{d(V_b/V_a)}{d[H^+]} \right]_{C_b \rightarrow \infty} \quad (\text{A-1.51})$$

Which only holds for the addition of base. Whereas,

$$B = \frac{\beta}{\ln(10)} = -C_a[H^+] \left[\frac{d(V_b/V_a)}{d[H^+]} \right]_{C_b \rightarrow \infty} \quad (\text{A-1.52})$$

Is applicable to for the addition of acid. Both result in a facile determination of buffer strength since there is no $\ln(10)$ factor to be considered. For strong acids and bases the buffer strength is simply defined as:

$$B = [H^+] + [OH^-] \quad (\text{A-1.53})$$

Therefore, for concentrated monoprotic acid/base B is for all practical purposes equal to its concentration C. For a single weak monoprotic acid/base of total analytical concentration (C)

$$B = [H^+] + \alpha_1 \alpha_0 C + [OH^-] \quad (\text{A-1.54})$$

And for a mixture of 2 or more such weak monoprotic acid/bases

$$B = [H^+] + \sum_i \alpha_{1i} \alpha_{0i} C_i + [OH^-] \quad (\text{A-1.55})$$

For a single diprotic weak acid or base

$$B = [H^+] + (\alpha_2 \alpha_1 + 4\alpha_2 \alpha_0 + \alpha_1 \alpha_0)C + [OH^-] \quad (\text{A-1.56})$$

For a single triprotic weak acid or base

$$B = [H^+] + (\alpha_3 \alpha_2 + 4\alpha_3 \alpha_1 + 9\alpha_3 \alpha_0 + \alpha_2 \alpha_1 + 4\alpha_2 \alpha_0 + \alpha_1 \alpha_0)C + [OH^-] \quad (\text{A-1.57})$$

Where the coefficients are the square of the index differences on the α : $4 = (3 - 1)^2$ etc.

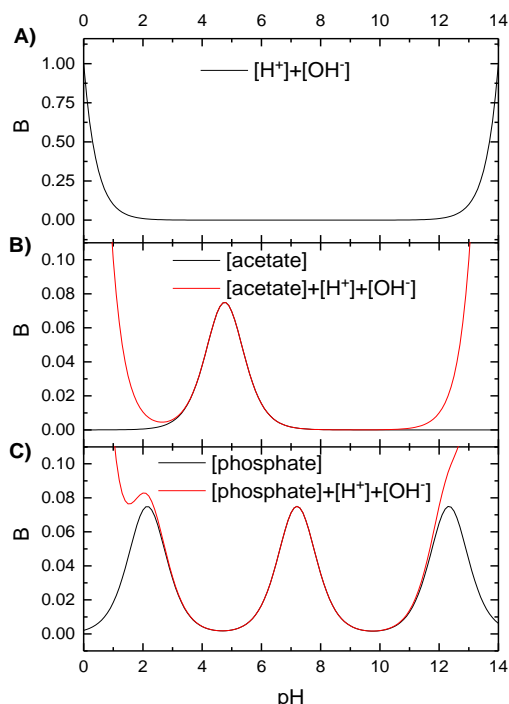


Figure 9-4 The buffer strength (B) as a function of pH of; A) water; B) acetic acid (0.3 M, pK_a 4.76)^{4,5} and its salts; C) phosphoric acid (0.3 M, $pK_{a1} = 2.15$, $pK_{a2} = 7.20$, $pK_{a3} = 12.33$)^{4,5} the pK_a s of which are well separated, however, two of the buffer regions overlap with those of water.

Examples of the application of the buffer strength equations are shown in Figure 9-4. The generalised buffer strength equation for mixtures of non-interchangeable species is expressed as

$$B = [H^+] + \sum_i C_i \sum_{j=1}^{j_{\max}} \sum_{k=1}^j (j-k)^2 \alpha_{ij} \alpha_{ik} + [OH^-] \quad (\text{A-1.58})$$

Where i is the number of non-interchangeable components.

9.1.5 Activity Effects

Dissociation constants like K_a and K_w are often treated as true constants. However, they are dependent on temperature and in principle pressure. An example is the dissociation of the second proton from phosphate (pK_{a2}) has a value of 7.20 under standard atmospheric conditions. Increasing the temperature to 37 °C lowers pK_{a2} to 7.16, whereas lowering the temperature to 4°C raises pK_{a2} to 7.26.⁷ It should be noted that not all acids/bases exhibit such a large shift dissociation constant and as a rule of thumb all constants can be considered approximately constant. Dilution does not have an effect on constants.

9.1.5.1 Ionic strength

Ionic strength was first observed Lewis and Randall (1921) when studying the activity coefficients of strong electrolytes. However, it was Debye and Huckle (1923) who described ionic strength in their setting out of the Debye-Huckle theory. Ionic strength is a measure of the ions in the solution where the ionic concentration of each species (c_i) is weighted by its valency (z_i):

$$I = \frac{1}{2} \sum_i z_i^2 c_i \quad (\text{A-1.59})$$

The factor of $\frac{1}{2}$ makes the ionic strength equal to the concentration of a single 1:1 electrolyte. By excluding non-charged species ionic strength is a reflection of the coulombic interactions. Furthermore, electroneutrality requires any macroscopic volume of electrolyte solution to contain an equivalent number of anions to cations. Individual ions can move relatively freely throughout the solution. However, ions of the same charge repel on another whilst opposites attract. As such the average cation-anion distance is smaller than the cation-cation/anion-anion distances. On average ions are coulombically attracted (lowering energy) by being in an electrolyte solution and more so at high ionic strength. This effect can be treated through a correlation term, the activity coefficient (f) and can be introduced in:

$$a = fc \quad (\text{A-1.60})$$

Where a =activity and c is concentration.

Activity corrections effect the value of an equilibrium constant since interionic attractions lower energetics of ions. Corrections have no effect on H^+ nor electron conditions since these are derived from mass and charge balance equations. Nor do they alter the equivalence volume (V_e) of a titration. However, it may slightly change the shape of the titration curve.

9.2 Appendix: Diffusion

Consider a solution where no external forces are at work and the system is at equilibrium (i.e. the solute is distributed evenly throughout). In such a system each molecule (i) present can be characterised by its chemical potential (μ_i ; or the solutes partial molal Gibb's free energy):

$$\mu_i = \bar{G}_i = \left(\frac{\partial G}{\partial n_i} \right)_{p,T,n_j} = \text{constant} \quad (\text{A-2.61 a})$$

$$d\mu_i = 0 \quad (\text{A-2.61 b})$$

Where G is the total Gibbs free energy of the system and n_i is the number of moles of solute i . When external forces are applied equation (A-2.61 a) must be altered accordingly to incorporate the force.

Let us take the earth's atmospheric composition as a function of altitude. To work with this system a gravitational element has to be introduced resulting in the gravito-chemical potential ($\tilde{\mu}_i$), which is defined by:

$$\tilde{\mu}_i = \mu_i + M_i \phi \quad (\text{A-2.62 a})$$

At equilibrium:

$$d\tilde{\mu}_i = d\mu_i + M_i d\phi = 0 \quad (\text{A-2.62 b})$$

Where ϕ is the gravitational potential ($= gh$) and M_i is the molar mass. Since chemical potential can be written as:

$$\begin{aligned} \mu_i &= \mu_i^\ominus + RT \ln a_i \\ &\cong \mu_i^\ominus + RT \ln c_i \end{aligned} \quad (\text{A-2.63})$$

Where R is the gas constant, T is the temperature, a_i is the activity of i and c_i is its concentration as a function of height. Assuming the system is ideal concentration (c_i) is determined to be:

$$d \ln c_i = - \frac{M_i g dH}{R T} \quad (\text{A-2.64})$$

For a colloidal system, gravitational forces are of greater significance than molecular solutions.⁸

9.2.1 Fick's Laws of Diffusion

When no external fields are present the chemical potential of a substance in a phase at equilibrium is constant. In contrast, if the μ_i is to vary between two points in the system then substance i will diffuse so to equalise the chemical potential throughout the system. Diffusion is directly proportional to the spatial gradient of μ_i (the driving force of diffusion). For a one-dimensional system this can be mathematically expressed as:

$$F_d = - \frac{d\mu_i}{dx} \quad (\text{A-2.65})$$

Where F_d is the driving force. Substitution of equation of (A-2.62a) into (A-2.65) gives:

$$F_d = - \frac{d}{dx} (\mu_i^\ominus + RT \ln [c_i \text{ mol}^{-1} \text{ L}]) \quad (\text{A-2.66 a})$$

$$= - \frac{RT}{c_i} \frac{dc_i}{dx} \quad (\text{A-2.66 b})$$

Since μ_i^\ominus is constant throughout the phase. Furthermore, molecular diffusion force can be written as:

$$f_d = - \frac{k_b T}{c_i} \frac{dc_i}{dx} \quad (\text{A-2.67})$$

Where k_b is the Boltzmann constant. When a particle is subjected to this “force” motion occurs. Such movement is perturbed by a viscous (drag) force (f_v), it is noteworthy that for a particle of smooth shape is proportional to the particle’s velocity:

$$f_v = Bu \quad (\text{A-2.68})$$

Where B is the frictional coefficient (from drag) and u is the particles initial velocity (m s^{-1}). f_v increases until it is equal to the diffusional force, when the particle reaches its terminal velocity (v). Therefore;

$$f_d = Bv \quad (\text{A-2.69})$$

A materials flux (flow) per unit area (J_i) is proportional to it diffusional velocity (v):

$$J_i = v c_i \quad (\text{A-2.70})$$

Material flux can be re-written to be Fick’s first law of diffusion:

$$J_i = -D \frac{dc}{dx} \quad (\text{A-2.71})$$

Where D is the diffusion coefficient and re-working of equation (271) and subsequently equations (A-2.70) and (A-2.69) respectively shows:

$$D = -\frac{J_i}{\left(\frac{dc}{dx}\right)} \quad (\text{A-2.72 a})$$

$$D = -\frac{v c}{\left(\frac{dc}{dx}\right)} \quad (\text{A-2.72 b})$$

$$D = -\frac{f_d c}{B\left(\frac{dc}{dx}\right)} \quad (\text{A-2.72 c})$$

Therefore, from equation (A-2.67) the diffusion coefficient is:

$$D = -\frac{k_b T}{B} \quad (\text{A-2.73 a})$$

$$D = -\frac{k_b T}{6 \pi \eta R_H} \quad (\text{A-2.73 b})$$

Equation (A-2.73 b) is the Stokes-Einstein equation, where η is the viscosity and R_H is the particle radius.

9.2.2 Time Dependent Diffusion Processes

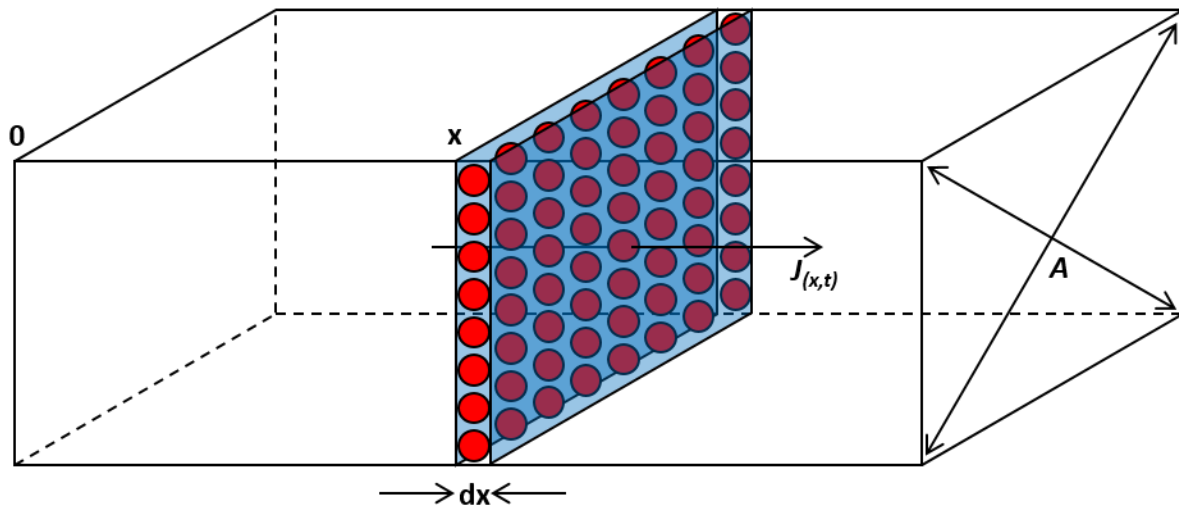


Figure 9-5 Schematic of diffusion in a plane showing flux (J) along the x -axis where A is the area of the yz plane.

Fick's first law is only applicable to a concentration gradient that is constant in time which only occurs under exceptional circumstances. More often the material (of a fixed amount) is initially limited to a region from which it diffuses away. Therefore, the concentration gradient has time dependence (see Figure 9-5).

For such a system the amount of material within a thin slab of the system between x and $(x + \delta x)$ is:

$$\frac{A\delta x \partial c_{(x,t)}}{\partial t} \quad (\text{A-2.74})$$

Which is equal to the difference between the influx ($J_{i(x,t)}$) and efflux ($J_{i(x+\delta x,t)}$) of matter. Therefore, the amount of material in the region of interest can be expressed as:

$$\frac{\partial c_{(x,t)}}{\partial t} = \frac{J_{(x,t)}A}{A\delta x} - \frac{J_{(x+\delta x,t)}A}{A\delta x} \quad (\text{A-2.75})$$

And substitution of equation (A-2.71) into (A-2.75) gives:

$$\frac{\partial c_{(x,t)}}{\partial t} = \frac{1}{\delta x} \left[-D \left(\frac{\partial c_{(x,t)}}{\partial x} \right)_x + D \left(\frac{\partial c}{\partial x} \right)_{x+\delta x} \right] \quad (\text{A-2.76 a})$$

$$\frac{\partial c_{(x,t)}}{\partial t} = \frac{D}{\delta x} \left[- \left(\frac{\partial c}{\partial x} \right)_x + \left(\frac{\partial c}{\partial x} \right)_x + \delta x \left(\frac{\partial^2 c}{\partial x^2} \right)_x \right]$$

$$\frac{\partial c}{\partial t} = D \frac{\partial^2 c}{\partial x^2} \quad (\text{A-2.76 b})$$

Equation (A-2.76 b) is also known as Fick's second law of diffusion. Such partial differentials can be solved using a variety of methods. There are three equations that are discussed here. These are diffusion from a plane, Diffusion from a point source and continuous diffusion from a point source.

9.2.3 Diffusion in a plane

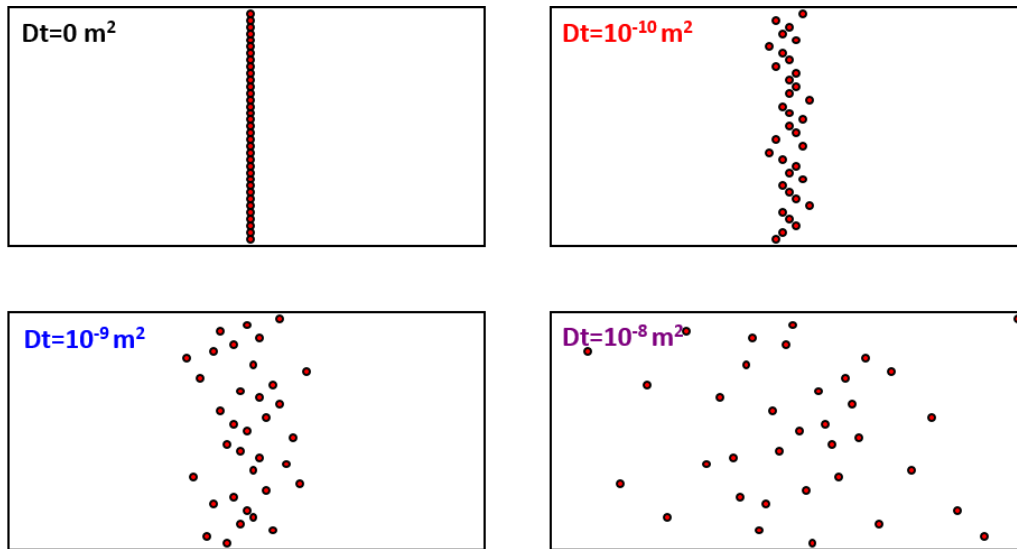


Figure 9-6 1 dimensional representation of diffusion from a plane source where each box is $2000 \mu\text{m}$ wide and the yz plane measures $1 \mu\text{m}^2$

The model for diffusion in a plane stipulates that initially all the solute molecules are confined to a thin strip of the system. This strip contains n_0 moles of solute; all of which can diffuse perpendicularly to the initial plane (see Figure 9-6).

It has been shown that the change in concentration as a function of time and distance is essentially a one-dimensional solution for “random walking” of particles:

$$c_{(x,t)} = \frac{n_0}{A} \left(\frac{\tau}{0.5\pi l^2 t} \right)^{\frac{1}{2}} \exp\left(-\frac{\tau x^2}{2l^2 t} \right) \quad (\text{A-2.77})$$

Where A is the cross-sectional area of the yz plane, l is the minimum measurable distance in the x axis and the time for the diffusion steps (τ) is:

$$\tau = \frac{l^2}{2D} \quad (\text{A-2.78})$$

Substitution of equation (A-2.78) into equation (A-2.77) give:

$$c_{(x,t)} = \frac{n_0}{A} \left(\frac{1}{4\pi Dt} \right)^{\frac{1}{2}} \exp\left(-\frac{x^2}{4Dt} \right) \quad (\text{A-2.79 a})$$

$$c_{(x,t)} = \frac{n_0}{A\sqrt{\pi Dt}} \exp\left(-\frac{x^2}{4Dt} \right) \quad (\text{A-2.79 b})$$

The exponential function must be dimensionless, therefore if x is given in metres Dt must have units of m^2 and as such the diffusion coefficient must have units of $m^2 s^{-1}$.

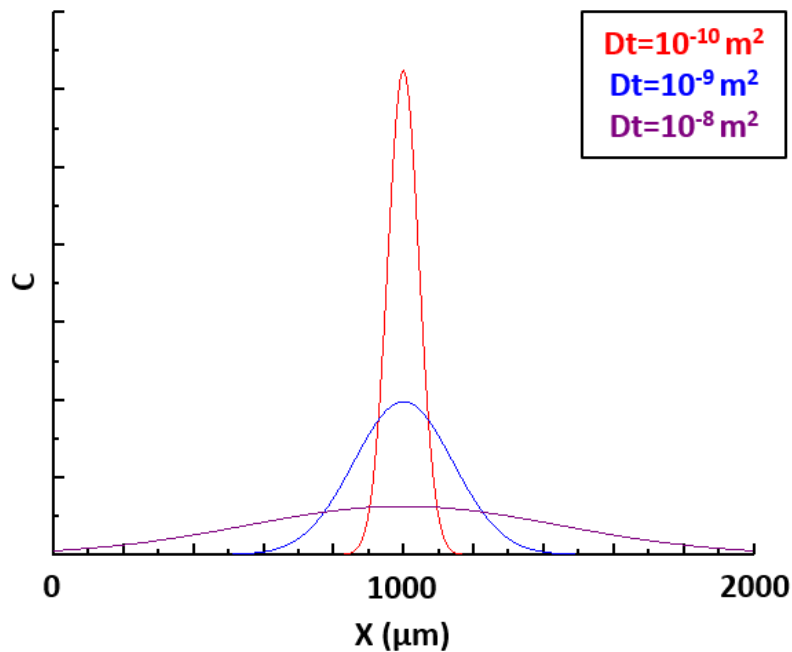


Figure 9-7 Graphical representation the variation of concentration with time and position when diffusing from a plane where each box is 2000 μm wide and the yz plane measures 1 μm^2

Figure 9-7 shows graphically shows that concentration distribution varies with time. As time increases the distribution of solute throughout the solvent tends to uniformity. The key limitation of the diffusion in a plane model is that all the particles only move perpendicularly to their initial plane. However, this model is of use when considering a quorum sensing system whose particle analogies can be drawn between diffusion in a plane and gravimetric aggregation of polymer particles. Therefore such a model could help when initially modelling aggregation of quorum sensing particles.

9.2.4 Diffusion from a point source

Diffusion from a point source is of greater use for modelling the release of not only the signalling molecules from quorum sensing particles but also the release of their cargo/tracer molecules. In the case diffusion from a point source the concentration of diffusing solute is considered to be spherically symmetric as such the concentration is dependent on the radius (r) from the point of origin rather than its distance from the original plane as previously discussed. The equation for diffusion in a sphere is given as:

$$c_{(r,t)} = \frac{n_0}{(4\pi Dt)^{\frac{3}{2}}} \exp\left(-\frac{r^2}{4Dt}\right) \quad (A-2.80)$$

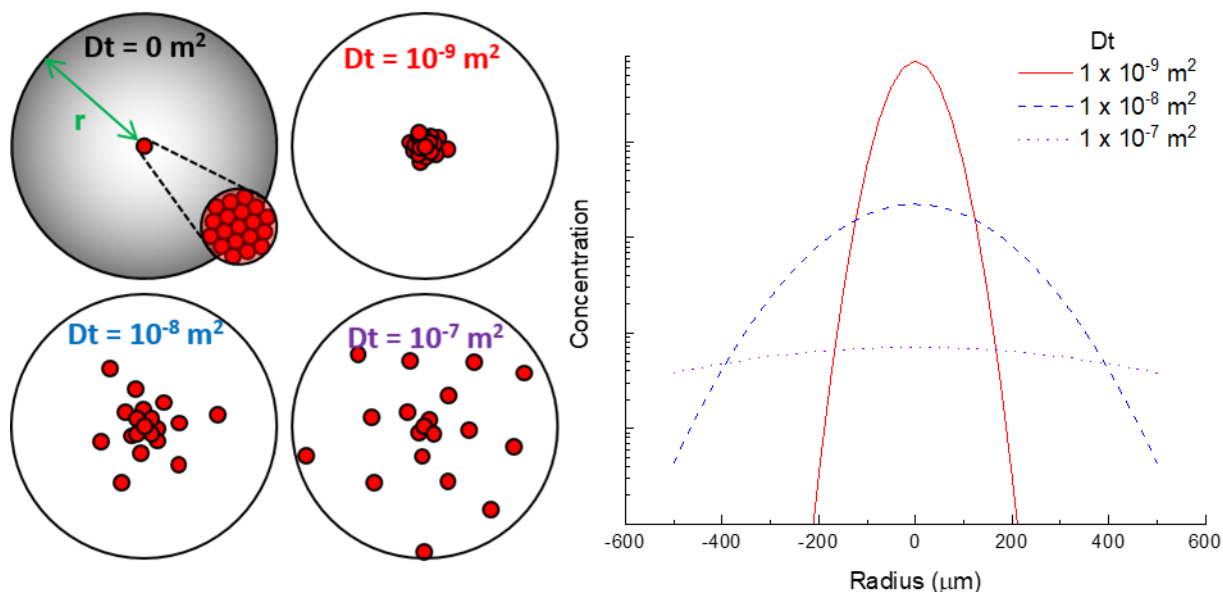


Figure 9-8 1) a 2D representation and 2) corresponding graphical representation of the diffusion of particles from a point source in a sphere with a radius of 500 microns showing that as time tends to infinity the concentration becomes constant throughout the system.

The pre-exponential denominator is raised to the power of $2/3$ to account for the 3 dimensional structure of the system. Figure 9-8 shows a simulation for 19 particles being released from a point source up to a radius of 500 μm . Common diffusion coefficients vary in order from 10^{-10} – $10^{-8} \text{ m}^2 \text{ s}^{-1}$.

Diffusion from a point source will be useful for when modelling and fitting data collected on cargo/tracer molecule release. However, in order to get to this stage in the synthetic quorum sensing system previously laid out a signal must be released which can be detected. It has already been discussed how a variety of enzyme could be used to do this. Such biocatalyst produce a product at a steady continuous rate. Therefore, the model for diffusion must be modified to take into account the continued production of solute which makes the concentration of solute at it source near constant.

9.2.5 Diffusion from a continuous source

The solution for diffusion from a point source which is continuously liberating the diffusing solute at a specific rate, is through the integration of equation (A-2.80) with respect to time t . Take a single synthetic quorum sensing particle that has been proposed earlier, due to its enzyme motifs continuously synthesises signal molecules at a specific rate (q). These molecules then diffuse from its source into an infinite volume. The concentration such a molecule at time t and at distance r from the particle is:

$$c_{(r,t)} = \frac{1}{8(\pi D)^{\frac{3}{2}}} \int_0^t q(t') \exp\left\{\frac{-r^2}{4D(t-t')}\right\} \frac{dt'}{(t-t')^{\frac{3}{2}}} \quad (\text{A-2.81})$$

From integration of equation (A-2.80) with respect to time. If q remains constant, then this can be re-written:

$$c_{(r,t)} = \frac{q}{4\pi Dr} \operatorname{erfc}\left(-\frac{r^2}{\sqrt{4Dt}}\right) \quad (\text{A-2.81})$$

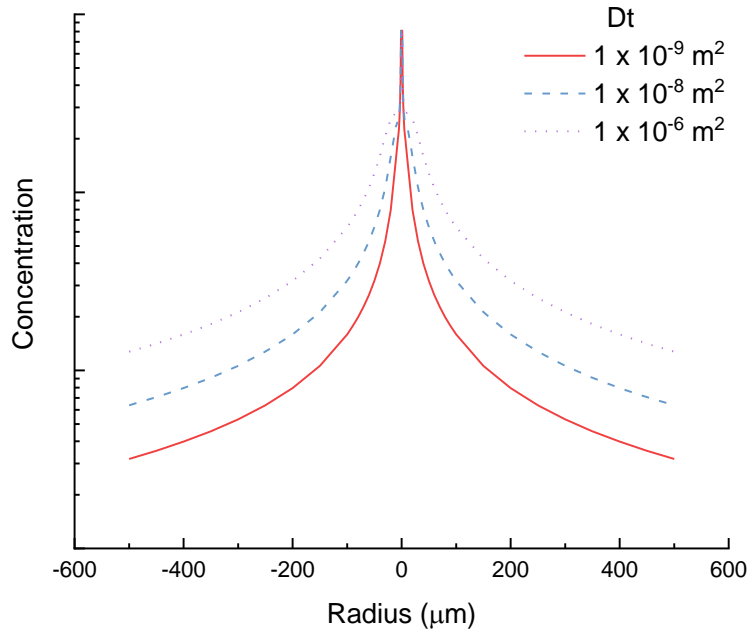


Figure 9-9 A model of continuous diffusion using equation A-2.81

9.3 Appendix: References

1. VIII. On a combination of oxymuriatic gas and oxygene gas. *Philos. Trans. R. Soc. London* **101**, 155–162 (1811).
2. De Levie, R. *Aqueous acid-base equilibria and titrations*. (Oxford University Press, 1999).
3. Kauffman, G. B. The Bronsted-Lowry acid base concept. *J. Chem. Educ.* **65**, 28 (1988).
4. Dawson, R. M. C., Elliott, D. C., Elliott, W. H. & Jones, K. M. Carboxylic acids, alcohols, aldehydes, and ketones; pH, buffers, and physiological media. *Data Biochem. Res.* (1986).
5. Stoll, V. S. & Blanchard, J. S. [4] Buffers: Principles and practice. in *Methods in enzymology* **182**, 24–38 (Elsevier, 1990).
6. Rungronmitchai, S., Phokhanusai, W. & Sungkhaho, N. *Preparation of Silica Gel from Rice*

- Husk Ash Using Microwave Heating. Journal of Metals, Materials and Minerals* **19**, (2009).
7. Good, N. E. *et al.* Hydrogen Ion Buffers for Biological Research*. *Biochemistry* **5**, 467–477 (1966).
 8. Perrin, J. Mouvement brownien et réalité moléculaire. *Ann. Chim. Phys.* **18**, (1909).